



2013

Hydraulic fracturing design for horizontal wells in the Bakken formation, Williston Basin

Hadi Jabbari
University of North Dakota

Follow this and additional works at: <https://commons.und.edu/theses>

 Part of the [Geology Commons](#)

Recommended Citation

Jabbari, Hadi, "Hydraulic fracturing design for horizontal wells in the Bakken formation, Williston Basin" (2013). *Theses and Dissertations*. 147.
<https://commons.und.edu/theses/147>

This Dissertation is brought to you for free and open access by the Theses, Dissertations, and Senior Projects at UND Scholarly Commons. It has been accepted for inclusion in Theses and Dissertations by an authorized administrator of UND Scholarly Commons. For more information, please contact zeinebyousif@library.und.edu.

HYDRAULIC FRACTURING DESIGN FOR HORIZONTAL
WELLS IN THE BAKKEN FORMATION, WILLISTON BASIN

by

HADI JABBARI

Bachelor of Science, Petroleum University of Technology, Iran, 2004

Master of Science, Sharif University of Technology, Iran, 2006

A Dissertation

Submitted to the Graduate Faculty

of the

University of North Dakota

In partial fulfillment of the requirements

for the degree of

Doctor of Philosophy

Grand Forks, North Dakota

May

2013

Copyright 2013 Hadi Jabbari

This dissertation, submitted by Hadi Jabbari in partial fulfillment of the requirements for the Degree of Doctor of Philosophy from the University of North Dakota, has been read by the Faculty Advisory Committee under whom the work has been done, and is hereby approved.



Dr. Richard LeFever (Committee Chair)



Dr. Steven A. Benson



Dr. Scott F. Korom

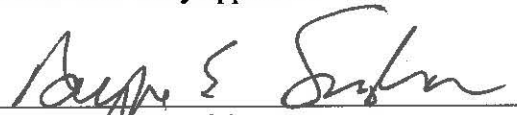


Dr. William Gosnold



Dr. Irina Smoliakova

This dissertation is being submitted by the appointed advisory committee as having met all of the requirements of the Graduate School at the University of North Dakota and is hereby approved.



Dr. Wayne E. Swisher
Dean of the Graduate School



April 23rd, 2013

Title Hydraulic Fracturing Design for Horizontal Wells in the Bakken
 Formation, Williston Basin.
Department Harold Hamm School of Geology and Geological Engineering
Degree Doctor of Philosophy

In presenting this dissertation in partial fulfillment of the requirements for a graduate degree from the University of North Dakota, I agree that the library of this University shall make it freely available for inspection. I further agree that permission for extensive copying for scholarly purposes may be granted by the professor who supervised my dissertation work or, in her/his absence, by the Chairperson of the department or the dean of the Graduate School. It is understood that any copying or publication or other use of this dissertation or part thereof for financial gain shall not be allowed without my written permission. It is also understood that due recognition shall be given to me and to the University of North Dakota in any scholarly use which may be made of any material in my dissertation.

Hadi Jabbari
04-23-2013

HYDRAULIC FRACTURING DESIGN FOR HORIZONTAL WELLS IN THE BAKKEN FORMATION, WILLISTON BASIN

by

HADI JABBARI

Submitted to the Graduate Faculty
Of the
University of North Dakota
In partial fulfillment of the requirements
for the degree of
Doctor of Philosophy

ABSTRACT

Unconventional hydrocarbon reservoirs have proved to be challenging in terms of reservoir characterization, predicting production potential, estimating ultimate recovery, and optimizing hydraulic fracture stimulations. The methods by which these resources are extracted use progressive, or unconventional, technologies. Today, through the use of hydraulic fracturing and horizontal drilling, extraordinary amounts of oil and natural gas from deep shale formations across the United States and around the world are being safely produced.

Performing a hydraulic fracture design requires modeling of fracture propagation and tracking the fluid front in the created fracture. In this dissertation, the roles of all effective parameters and properties on the design and performance of hydraulic fracturing in the Bakken Formation, Williston Basin, are examined.

To accomplish the above objectives, this dissertation is divided into four major sections that include: 1) basic principles of geology, lithology, and reservoir aspects of the Bakken Formation, 2) the fundamental concepts of hydraulic fracturing, 3) technology aspects are integrated into one cohesive unit to model and optimize the entire hydraulic fracture treatments, and 4) a comprehensive approach to the uncertainty assessment of the complex numerical simulations is described.

In this research by integrating reservoir and hydraulic fracture simulations, a robust workflow was used to evaluate several combinations of fracturing materials (i.e. fluids and proppants) and well/fracture parameters (i.e. lateral length, fracture spacing, and fracture half-length) to identify the best candidate(s) for well stimulation planning. Using an automated history matching procedure, the reservoir properties of the Bakken Formation were estimated that can be used in future reservoir simulation projects.

The fully 3D/FEM* fracture simulation showed that a fracturing treatment with injecting slickwater as the pad followed by crosslinked gel together with ceramic or resin-coated sand would guarantee that most proppants would stay within the Bakken Formation. The results from this research also suggest that in a Bakken well with a long lateral length (e.g. 10,000 ft), a fracturing strategy that leads to a relatively high fracture half-length (e.g. 1000 ft) with a high number of fractures (36 or more) would return an efficient balance between the operating charges, fracture treatment costs, drilling expenses, and the benefits earned from the incremental oil production. The pump schedule developed for the optimal fracture treatment, obtained from the fully-3D fracture modeling, would also guarantee fracture confinement within the Bakken Formation.

* Finite Element Method

DEDICATION

I would like to dedicate this work to my parents and my family to whom I cannot possibly express my gratitude for all that they have done for me. I would like to thank their endless love and encouragements all the way through. Without them, none of this would have been possible.

ACKNOWLEDGEMENTS

The work I have presented in this research represents the technical side of earning a PhD degree, for which I owe a great deal of thanks to several people. First, I would like to thank my advisor, Dr. Richard LeFever, for his guidance and support. I would also like to thank the members of my committee, Prof. Steven A. Benson, Dr. Scott F. Korom, Prof. William Gosnold, and Prof. Irina P. Smoliakova, who provided me with invaluable insights and support along the way as well as Prof. Joseph Hartman, the chair of *Harold Hamm School of Geology and Geological Engineering*.

I would specially like to acknowledge the following individuals: Prof. Steven A. Benson, the chair of the *UND Petroleum Engineering Department*, Scott Johnson, Shanna Corbett, Cassandra Olson, and Dr. Lance Yarbrough for all their help, kindness, and support throughout this research. I'd also like to thank Katie Sagstuen for all her help in the past four years.

Of course, obtaining a PhD requires more than just support and guidance from excellent technical experts. It also requires support from family and friends. There are so many people that have helped me in so many ways. In particular, I'd like to thank my best friend Mehdi Ostadhassan who would always help me out anytime I was having trouble with anything. I'd also like to thank one of my best friends ever Darin Buri who could always make me smile and for always being there whenever I needed anything.

Finally, I would like to thank the following sponsors for their financial support: US DOE through contract of DE-FC26-08NT0005643 (Bakken Geomechanics),

North Dakota Industry Commission (NDIC) together with five industrial sponsors (Denbury Resources Inc., Hess Corporation, Marathon Oil Company, St. Mary Land & Exploration Company, and Whiting Petroleum Corporation) under contract NDIC-G015-031, and North Dakota Department of Commerce (NDDC) through UND's Petroleum Research, Education and Entrepreneurship Center of Excellence (PREEC). I would also like to thank *NSI technology Inc.* and *Computer Modeling Group* for their software support.

Last but not least, I'd like to thank all my friends at the *UND Petroleum Engineering Department* and *Harold Hamm School of Geology and Geological Engineering*.

TABLE OF CONTENTS

LIST OF FIGURES	XV
LIST OF TABLES	XXI
CHAPTER	
I. INTRODUCTION	1
RESEARCH DESCRIPTION	1
OBJECTIVES AND MOTIVATIONS	2
METHODOLOGY	2
ANTICIPATED RESULTS	3
TECHNIQUES AND DISSERTATION OUTLINE	3
RESEARCH IMPACT	4
BACKGROUND	5
OVERVIEW OF THE BAKKEN FORMATION	6
OVERVIEW OF HYDRAULIC FRACTURING	12
II. HYDRAULIC FRACTURING CONCEPTS AND FUNDAMENTALS	16
INTRODUCTION	16
FRACTURE INITIATION AND PROPAGATION; ENERGY-BALANCE APPROACH	16
THE FUNDAMENTALS OF HYDRAULIC FRACTURE	20
<i>Hydraulic Fracture Size</i>	21
HYDRAULIC FRACTURE CONTAINMENT	22
HYDRAULIC FRACTURE GROWTH	23

TWO-DIMENSIONAL FRACTURE MODELS	26
<i>2D Fracture Models with Fluid Leakoff</i>	30
<i>Three-Dimensional Hydraulic Fracture Simulation</i>	31
FRACTURING FLUIDS AND ADDITIVES	34
<i>Fluid Rheological Models</i>	36
HYDRAULIC FRACTURE FLUID	38
<i>Water-Based Fluid</i>	39
<i>Linear Fracturing Fluids</i>	39
<i>Crosslinked Fracturing Fluids</i>	41
PROPPANT TRANSPORT IN HYDRAULIC FRACTURES	43
SLURRY	49
III. HYDRAULIC FRACTURING DESIGN METHODOLOGY	53
.....	
INTRODUCTION	55
DESIGN OF HYDRAULIC FRACTURING TREATMENT— RECIPE FOR SUCCESS.....	56
RESERVOIR SIMULATION— BAKKEN	57
THE BAKKEN FORMATIO PROPERTIES— WILLIAMS COUNTY	59
DYNAMIC MODELING AND SIMULATIONS	69
<i>Model Optimization and Validation</i>	70
Grid-Size Sensitivity Analysis	71
Numerical Tuning	73
Sensitivity Analysis of Reservoir Properties and Parameters	74
SAMPLING METHOD.....	75
HISTORY MATCHING	81
<i>History-Matching Procedure</i>	82
<i>History-Matching Results</i>	85
HYDRAULIC FRACTURING DESIGN OPTIMIZATION.....	91
<i>Optimal Treatment Materials</i>	92

HYDRAULIC FRACTURE SIMULATION	102
IV. UNCERTAINTY ASSESSMENT ASSOCIATED WITH PREDICTIONS	126
RSM FOR NPV CALCULATIONS USING MONTE CARLO SIMULATION	146
<i>ANOVA— Analysis of Variance</i>	155
UNCERTAINTY OF OIL PRICE IN THE NPV CALCULATIONS— ENGINEERING VS. POLITICS.....	172
<i>Anticipated value for a given investment</i>	176
V. CONCLUSIONS AND RECOMMENDATIONS.....	179
SUMMARY OF THE RESEARCH.....	179
CONCLUSIONS	181
FUTURE WORK.....	183
NOMENCLATURE	185
REFERENCES	187

List of Figures

Figure	page
1. Williston Basin stratigraphic column.....	7
2. Williston basin and its major structures in the USA portion.	9
3. Stratigraphy of the Bakken Formation.....	9
4. Structural cross section of Williston Basin.	10
5. Plot of core porosity versus permeability in sandstones and siltstones of the middle member of the Bakken Formation	11
6. Typical hydraulic fracturing treatment in petroleum industry	12
7. Idealization of unloaded region near crack flanks.	18
8. Idealization of the fracture energy balance.	19
9. Hydraulic Fracture Stimulation Process	21
10. Hydraulic fracture size	22
11. In-situ stress contrast.....	23
12. Hydraulic fracture growth; a) vertical fracture growth has stopped when stress contrast is large, b) limited upward fracture growth with medium stress contrast, and c) almost uncontrolled upward fracture growth when the stress contrast is so small.	24
13. Relationship between fracture containment and stress contrast.....	25
14. Schematic representation of linearly propagating fracture with laminar fluid flow according to Perkins and Kern model	27
15. Schematic representation of linearly propagating fracture with laminar fluid flow according to KGD model	28
16. Schematic representation of radially propagating fracture with laminar flow	29
17. Fracture geometry (a) P3D (cell approach) (d) Global 3D (parameterized).....	32
18. Fracture geometry of hydraulic fractures ranging from a single, planar fracture to out-of-plane fractures and complex fracture network	33
19. Fracture geometry models (a) PKN type (b) KGD type (c) Fully 3D (meshed).....	34
20. Different types of time-independent fluids	37

21.	Chemical structures of guar, HPG, HEC, CMHEC, and polyacrylamides	40
22.	Fluid leak-off from a longitudinal fracture during a fracturing treatment	43
23.	Fracture conductivity versus Fracture Closure Stress (FCS)	47
24.	Project area location in eastern Williams County, ND	59
25.	Lithofacies of the Bakken Formation.....	60
26.	Nesson State 41X-36H lateral stratigraphy	61
27.	Natural fracture data in the area understudy	62
28.	The distribution of natural fracture aperture (Well NS 41X-36H, Middle Bakken).....	63
29.	NS 41X-36H completed wellbore configuration	64
30.	Left: Side view of the hydraulic fracture geometry, Right: Plan view of the hydraulic fracture geometry (well NS 41X-36H)	64
31.	Map view of the induced fracture area (well NS 41X-36H).....	65
32.	Side view of the induced fracture area (well 41X-36H)	65
33.	NS 41X-36H daily-production plot	67
34.	NS 41X-36H daily-oil-production rate (extracted from Figure 33).....	67
35.	NS 41X-36H Cum-production plot.....	68
36.	Workflow of dynamic simulation	71
37.	Sensitivity analysis on grid size— Cum Oil Prod.....	72
38.	Sensitivity analysis on grid size— Cum GAS Prod.....	72
39.	Sensitivity analysis on grid size— Cum WTR Prod	73
40.	Numerical tuning of the reservoir model to improve run-time and solver failures.....	74
41.	Tornado plot of Cum_OIL (linear model t-ratios)	79
42.	Tornado plot of Cum_WTR (linear model t-ratios).....	79
43.	Tornado plot of Cum_OIL (reduced model).....	80
44.	Tornado plot of GlobalObj function (reduced model)	80
45.	Similarity between SRV and a shattered windshield	83
46.	History-matching algorithm.....	84
47.	Final history-matching iteration of 1467 jobs showing the convergence of the objective function (red dots represent the cases with the lowest error values).....	85

48.	Oil production rate history match	86
49.	Cumulative oil production history match-- oil production rate constraint.....	86
50.	Cumulative water production history match-- oil production rate constraint	87
51.	Relative permeability curves for matrix obtained from history matching— water-oil system	88
52.	Relative permeability curves for matrix obtained from history matching— gas-liquid system	88
53.	Relative permeability curves for natural fracture system obtained from history matching— water-oil system	89
54.	Relative permeability curves for natural fracture system obtained from history matching— gas-liquid system.....	89
55.	Relative permeability curves for hydraulic fractures— water-oil system.....	90
56.	Relative permeability curves for hydraulic fractures— gas-liquid system	90
57.	The algorithm of Latin hypercube plus Proxy Optimization	96
58.	Well and fracture spacing setup (top view)— 12 fracture stages	97
59.	NPV optimization of hydraulic fracture treatment— red dots are the optimal solutions (job-IDS 73 and 121)	97
60.	NPV optimization of hydraulic fracture treatment— red dots are the optimal solutions (job-IDS 40 and 149)	98
61.	NPV optimization of hydraulic fracture treatment— red dots are the optimal solutions (job-IDS 147 and 150)	98
62.	NPV comparisons for the cases with differing number of wells and different bottomhole flowing pressures	99
63.	CUM_OIL comparisons— optimal cases versus base case	100
64.	Cross plot of NPV versus Capital Cost.....	101
65.	Cross plot of NPV versus fracturing treatment scenarios	101
66.	Input parameters for fracture geometry modeling— Well 41X-36H.....	102
67.	Developed pump schedule using Nolte method— time is in min.....	105
68.	Width profile from fully-3D, FEM simulation	109
69.	Fracture conductivity profile at shut-in and at closure.....	111
70.	Fracture conductivity profile— at shut-in and at closure.....	112
71.	Cross section versus time – at closure	112

72.	Cross section of the created hydraulic fracture – at closure.....	112
73.	the fluid efficiency obtained from fully-3D simulation	113
74.	Summary plot for the optimal fracturing treatment— at closure	114
75.	Summary plot for the optimal fracturing treatment— at closure.....	115
76.	Average width of the fracture versus fracture penetration— at closure	115
77.	Absolute value of fluid pressure in the fracture — at closure.....	116
78.	Cumulative fluid loss in the fracture — at closure	116
79.	Fracture volume as the crack elongates — at closure	117
80.	Local net pressure at each point in the fracture — at closure	117
81.	Net pressure at each point in the fracture — at closure	117
82.	Proppant concentration along the created fracture (effective) — at closure.....	118
83.	Proppant coverage along the created fracture — at closure.....	118
84.	Temperature profile along the created fracture — at closure	118
85.	Shear rate profile as the crack propagates — at closure	119
86.	Viscosity of the fracturing fluid along the created fracture — at closure	119
87.	Width profile along the created fracture (effective, propped width) — at closure	119
88.	Width profile along the created fracture (total width) — at closure	120
89.	The ratio of fracture width to average proppant particle diameter — at closure	120
90.	The contour plot of horizontal velocity of proppant as the crack propagates	121
91.	The contour plot of vertical velocity of proppant as the crack propagates	122
92.	The contour plot of horizontal velocity of fracturing fluid as the crack propagates ...	123
93.	The contour plot of vertical velocity of fracturing fluid as the crack propagates	124
94.	Uniform probability density function (continuous)	131
95.	Uniform probability density function (discrete)	132
96.	Normal probability density function (courtesy of Wikipedia).....	133
97.	Lognormal probability density function (courtesy of Wikipedia)	134
98.	Beta probability density function (courtesy of Wikipedia).....	135
99.	Triangular probability density function	136

100.	Fitting a probability distribution function to PorMtrxMultiplier by history matching— Uniform Distribution Function fits the data	137
101.	Fitting a probability distribution function to PermMtrxMultiplier by history matching— Normal Distribution Function fits the data	138
102.	Fitting a probability distribution function to PorFracMultiplier by history matching— Fixed-value Distribution Function fits the data	138
103.	Fitting a probability distribution function to PermNatFrac by history matching— Lognormal Distribution Function fits the data.....	139
104.	Fitting a probability distribution function to KvKhRatio by history matching— Normal Distribution Function fits the data	139
105.	Fitting a probability distribution function to DI_NatFrac by history matching— Lognormal Distribution Function fits the data.....	140
106.	Fitting a probability distribution function to DJ_NatFrac by history matching— Normal Distribution Function fits the data	140
107.	Fitting a probability distribution function to DK_NatFrac by history matching— Triangular Distribution Function fits the data.....	141
108.	Fitting probability distribution functions to Rel.Perm.Table_Matrix by history matching.....	142
109.	Fitting probability distribution function to Rel.Perm.Table_NatFrac by history matching.....	143
110.	Fitting a probability distribution function to Swtr by history matching— Normal Distribution Function fits the data	144
111.	Fitting a probability distribution function to HFCase by history matching—Fixed-value Distribution Function fits the data	144
112.	Latin hypercube sampling.....	145
113.	The verification plot (actual vs. prediction)— linear model.....	147
114.	The verification plot (actual vs. prediction)— quadratic model	147
115.	Tornado plot of NPV function (reduced quadratic model)	148
116.	The verification plot (actual vs. prediction)— reduced quadratic model	149
117.	Monte Carlo results—unconditional distributions (PDF plot).....	158
118.	Monte Carlo results—unconditional distributions (CDF plot)	159
119.	Monte Carlo results for DI_Nfrac—conditional distributions (PDF plot).....	160
120.	Monte Carlo results for DI_Nfrac —conditional distributions (CDF plot)	160
121.	Monte Carlo results for DJ_Nfrac—conditional distributions (PDF plot).....	161

122.	Monte Carlo results for DJ_Nfrac —conditional distributions (CDF plot)	161
123.	Monte Carlo results for DK_Nfrac—conditional distributions (PDF plot)	162
124.	Monte Carlo results for DK_Nfrac —conditional distributions (CDF plot).....	162
125.	Monte Carlo results for PERM_Nfrac—conditional distributions (PDF plot)	163
126.	Monte Carlo results for PERM_Nfrac —conditional distributions (CDF plot).....	163
127.	Monte Carlo results for PERMtrxMULTPLR—conditional distributions (PDF plot)	164
128.	Monte Carlo results for PERMtrxMULTPLR —conditional distributions (CDF plot)	164
129.	Monte Carlo results for PorFracMULTPLR—conditional distributions (PDF plot)..	165
130.	Monte Carlo results for PorFracMULTPLR —conditional distributions (CDF plot)	165
131.	Monte Carlo results for REFINE_VAR—conditional distributions (PDF plot).....	166
132.	Monte Carlo results for REFINE_VAR —conditional distributions (CDF plot)	166
133.	Monte Carlo results for Swtr—conditional distributions (PDF plot).....	167
134.	Monte Carlo results for Swtr —conditional distributions (CDF plot)	167
135.	Cross plot of NPV versus fracturing treatment scenarios	168
136.	Cross plot of NPV versus DI_Nfrac	169
137.	Cross plot of NPV versus DJ_Nfrac	169
138.	Cross plot of NPV versus DK_Nfrac	170
139.	Cross plot of NPV versus PERM_Nfrac	170
140.	Cross plot of NPV versus PERMtrxMULTPLR.....	171
141.	Cross plot of NPV versus PorFracMULTPLR	171
142.	Cross plot of NPV versus Swtr	172
143.	Average annual world oil prices in six scenarios— prices are in WTI.....	173
144.	Average annual world oil prices in six scenarios— prices are in WTI (in step-function form)	173
145.	Conditional probability curves for six oil-price scenarios	175
146.	Joint probability curves for six oil-price scenarios	176
147.	Expected values of NPV for six oil-price scenarios.....	178

List of Tables

Table	Page
1. The properties of the Bakken Formation	10
2. Behavior of different proppants under closure stress.....	46
3. Cost and resistance to crushing for different proppant types.....	47
4. Input parameters-- Bakken reservoir model.....	60
5. Natural Fracture Data (Well 41X-36H, Middle Bakken).....	61
6. Hydraulic fracture simulation parameters.....	66
7. Parameters and properties examined in the Sensitivity Analysis & History Matching .	77
8. Comparison of different fracturing treatments—for each fracture stage	93
9. Cost of fracture treatment & completion used in the economic study.....	94
10. Other parameters used in the economic analysis.	94
11. Optimal fracture treatment cases—2-well completion plan.....	99
12. Formation layer data - multi-layer height growth.....	103
13. Developing proppant schedule using power-law method	104
14. Pumping schedule using Nolte method [1986].....	105
15. Proppant data— Ceramic 20/40.....	106
16. Fluid data— slickwater & crosslinked gel.....	106
17. Pipe friction data.....	106
18. The results of fully3D/FEM fracture simulation.....	108
19. The results from fully-3D fracture simulation—time history	109
20. The fracture geometry summary— at end of pumping schedule.....	110
21. Factors examined in the Uncertainty Assessment.....	129
22. Effect screening using normalized parameters (-1, +1)	150
23. Coefficients in terms of actual parameters.....	152

24.	The summary of fit.....	153
25.	ANOVA (Analysis of Variance).....	156
26.	The probability of occurrence of the oil price events (event B)	174

CHAPTER I

INTRODUCTION

Research Description

Hydraulic fracturing is the process of creating small cracks, or fractures, in underground formations to allow oil or natural gas to flow into the wellbore and thereby increasing production. Prior to initiating hydraulic fracturing, geoscientists and reservoir engineers model the characteristics of the hydrocarbon bearing rock formation, including its permeability, porosity and thickness. Today using this information, they design the hydraulic fracturing process to insure that the resulting fractures are within the target zone.

The Bakken Formation of Williston Basin is a tight layer of interbedded, naturally fractured low permeability black shale, siltstone, silty sandstone, and silty carbonate at about 10,000 ft depth [*Philipp et al.*, 2012]. It is believed that it would not produce economic quantities of hydrocarbons without hydraulic fracturing and horizontal drilling technologies. To fully unlock the potential of the Bakken Formation, we must confront challenges related to our knowledge of geology, geochemistry, geomechanics, fracture mechanics and reservoir engineering. With this in mind, a comprehensive study of the Bakken wells was conducted to develop systematic criteria to optimized horizontal drilling and hydraulic fracturing that has the potential to lead to successful development of the Bakken shale oil.

Successful completion of this project will provide a better insight into the design of hydraulic fractures, the reservoir response to fracturing operations, and more accurate prediction of fracture dimensions in the Bakken Formation. These are the keys to lowering the risk of horizontal drilling and hydraulic fracturing, and for increasing the recovery factor in the Bakken Formation, an unconventional shale play.

Objectives and Motivations

Since hydraulic fracturing is a complex phenomenon, analytical solutions to modeling the process are either unavailable or complex. This is particularly true when formulating the hydraulic fracture propagation in a complex geologic formation, or when modeling the rock-fluid interaction within the framework of poroelasticity. The main objective of this research is, therefore, to use available numerical simulation methods to describe the process of hydraulic fracturing design, to emphasize critical design factors that determine design effectiveness, and to investigate optimal treatment selection for horizontal wells of the Bakken Formation.

Methodology

This research is intended to enhance industry's understanding of the hydraulic fracturing of horizontal wells in the Bakken Formation, in order to improve oil recovery from this important domestic resource. The data used for the simulation tasks in this research have come from the following sources:

- 1) Structural and geomechanical properties:
 - Well log data,
 - Laboratory geomechanical tests on the cores (AutoLab 1500).
- 2) Well selection and data gathering:

- Literature review on geology and lithology,
 - Well log data.
- 3) Numerical modeling:
- Hydraulic fracture simulation,
 - Reservoir simulation.
- 4) Optimization:
- Integrating fracture/reservoir simulation,
 - Economic analysis,
 - Uncertainty assessment.

Anticipated Results

Using the reservoir information and the interpretation methods discussed above, we conducted an integrated study on fracture simulation, reservoir characterization, reservoir simulation, and hydraulic fracture optimization, from which the following results were obtained:

1. An integrated study on the role(s) of hydraulic fracturing in enhancing recovery from the Bakken Formation.
2. A thorough understanding of hydraulic fracture initiation and propagation in Bakken horizontal wells, and better design of drilling/completion for Bakken horizontal wells.

Techniques and Dissertation Outline

In this research the following topics are covered to help develop an integrated package for the successful hydraulic fracturing of horizontal wells in the Bakken Formation:

Chapter 1 is an introduction to the subject of this research and the essential information on the Bakken Formation, Williston Basin.

Chapter 2 is an overview of hydraulic fracturing technology.

In *chapter 3* an integrated study was conducted to thoroughly analyze the hydraulic fracture treatment in the study area located in Williams County, North Dakota. Topics include the basics of hydraulic fracturing process, stress issues, fracture geometry, and fluid and proppant selection. This chapter presents an integrated fracture/reservoir simulation to investigate the effects of various fracturing treatment parameters on both hydraulic fracture geometry/propagation and post-frac performance of the stimulated well. An economic optimization of hydraulic fracturing treatments was conducted in which series of discounted cash flow analysis for evaluating the financial performance of different treatment scenarios were considered.

Finally, in *chapter 4* an uncertainty assessment was conducted to support decision-making process in well stimulation planning in the Bakken Formation. This study helped us determine how to: a) use cash flow techniques applicable in economic evaluations, b) evaluate and choose investment opportunities, c) use models to weigh risk and uncertainties, and d) evaluate decision alternatives using predictive techniques.

Chapter 5 presents the conclusions and recommendations.

Research Impact

A more accurate simulation of hydraulic fracture propagation and post-frac performance of stimulated wells in the Bakken Formation would drastically improve our understanding hydraulic fracturing in Bakken horizontal wells. This has profound implications for hydrocarbon exploration because the production in such a tight formation is largely influenced by well/completion design. In fact, how much of the

Bakken oil is technically and economically recoverable may be determined by answering some key questions facing the industry:

- 1) How would the results of detailed reservoir characterization impact the hydraulic fracturing design?
- 2) What is the optimal completion design alternative among those which can be practiced?
- 3) What are the optimal horizontal well parameters?
- 4) What is the optimal fracturing treatment scenario (in terms of fracturing materials) for a set of known well/fracture parameters?

Background

The geological heterogeneity, in-situ stress, recovery mechanisms, and geomechanical parameters of the Bakken Formation have been studied by many researchers [*Breit et al.*, 1992; *LeFever and Helms*, 2006; *Lantz et al.*, 2007; *Besler et al.*, 2007; *Cox et al.*, 2008; *Dunek et al.*, 2009]. Based on their reservoir characterization results, they concluded that: a) horizontal well drilling with hydraulic fracturing is a required completion technology for producing oil in the Bakken Formation, b) well orientation is the essential factor to the success of hydraulic fracturing and wellbore stability during drilling and production, c) hydraulic fracture geometry and orientation (longitudinal, transverse or oblique) is fully controlled by the local in-situ stress field and geomechanical properties of the formation. More often than not, a longitudinal fracture in design becomes a transverse or skewed one in reality, d) in-situ stress field and geomechanical properties change from along the axis of those horizontal wells that extended several thousand feet, such as those in the Bakken Formation, e) knowing the in-situ stresses and the fundamental

geomechanical properties of the rock is the key to designing a successful horizontal well and the future hydraulic fracturing stimulation.

Overview of the Bakken Formation

The Williston Basin in central North America, with an area of 96,500 mi² and a maximum stratal thickness of 13,500 ft, stretches across the Canadian provinces of Manitoba and Saskatchewan and the U.S. states of Montana, North Dakota, and South Dakota [Philipp *et al.*, 2012]. The Bakken is one of the hydrocarbon producing formations in the Williston Basin, a sedimentary basin covering parts of three states and two provinces. The total layer of sediments in the basin can be up to 15,000 ft thick, and within that, the Bakken itself reaches a maximum thickness of about 150 ft, but is thinner in most areas. The depth to the top of the Bakken can vary from a few thousand feet in Canada to more than 10,000 feet in the deeper areas in North Dakota. In terms of geologic age, it was deposited during the upper Devonian and Lower Mississippian periods about 360 million years ago. The entire stratigraphic column for the Williston Basin is shown below. Figure 1 indicates 15 primary producing formations in the basin, including the Bakken.

The Bakken shale consists of three members, the upper, middle, and lower. The upper and lower members are similar, and can be characterized as gray or black organic-rich shale. The middle member is more like a conventional reservoir with siltstones, sandstones, dolostones, and limestones. The middle member has been a target for many horizontal wells, but more recently the upper and lower horizons are also being seen as important reservoirs [Dow, 1974; LeFever and Helms, 2006; Lantz *et al.*, 2007; Besler *et al.*, 2007].

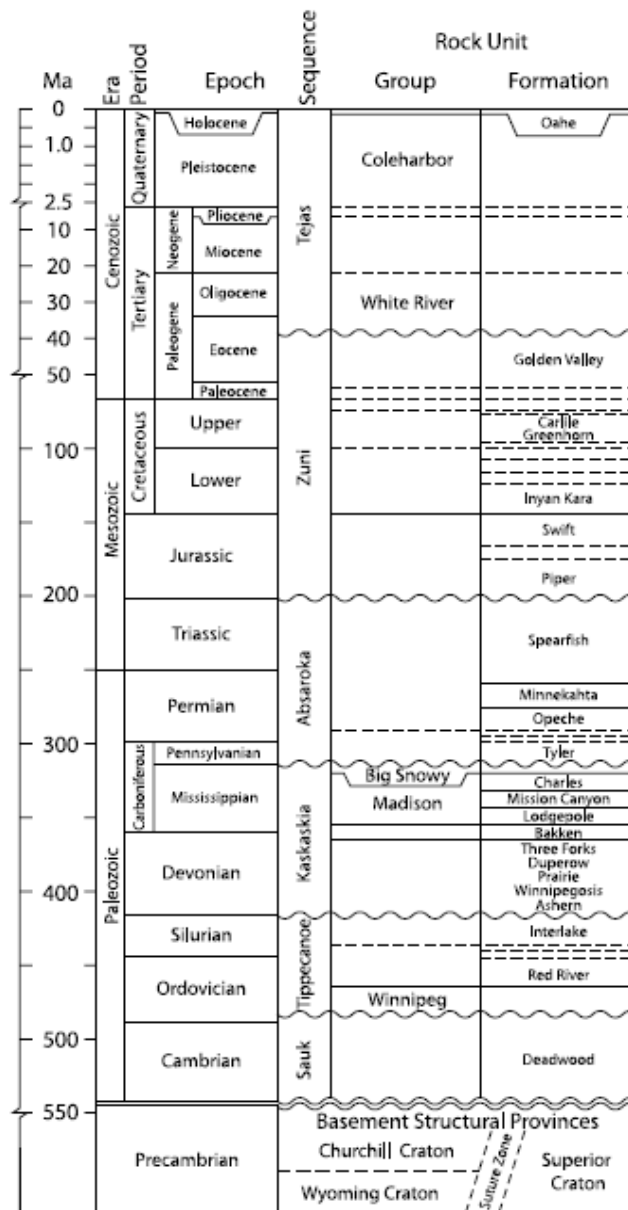


Figure 1. Williston Basin stratigraphic column [Philipp et al., 2012]

Horizontal drilling technology achieved commercial viability during the late 1980's. Its successful employment, particularly in the Bakken Shale of North Dakota and the Austin Chalk of Texas, has encouraged testing of it in many domestic geographic regions and geologic situations. Of the three major categories of horizontal drilling, short-, medium-, and long-radius, the medium-radius well has been most widely used and productive [Lantz et al., 2007; Besler et al., 2007; Cox et

al., 2008; *Dunek et al.*, 2009; *Lolon et al.*, 2009]. Achievable horizontal borehole length grew rapidly as familiarity with the technique increased; horizontal displacements have now been extended to over 8,000 feet [*NDIC*, 2013]. Some wells have featured multiple horizontal bores. Completion and production techniques have been modified for the horizontal environment, with more change required as the well radius decreases; the specific geologic environment and production history of the reservoir also determine the completion methods employed.

In shale reservoirs like the Bakken, natural fractures play a big role. These are natural cracks which have low porosity but can have permeabilities one to several orders of magnitude greater than the rock fabric or matrix. Most of the better wells in the Bakken have encountered abundant open natural fractures. The Mississippian-Devonian Bakken Petroleum System of the Williston Basin is characterized by low porosity (~6%) and permeability reservoirs (<0.0001 md), organic rich source rocks, and regional hydrocarbon charge. This unconventional play is the current focus of exploration and development activity by many operators. Estimates of oil generated from the petroleum system range from 10 to 400 billion barrels (1.6 to 63.9 billion m³) [*Dow*, 1974; *Schmoker and Hester*, 1983; *LeFever and Helms*, 2006; *Webster*, 1984; *Meissner and Banks*, 2000; *Flannery and Kraus*, 2006].

The Williston Basin is a large, intracratonic sedimentary basin that occupies parts of North Dakota, South Dakota, Saskatchewan, and Manitoba (Figure 2). The stratigraphic column for the Bakken Formation and the adjacent intervals are shown in Figure 3. The field is a recent giant discovery in the Middle Bakken. Horizontal drilling began in the field in 2000, and to date many horizontal wells have been drilled. The estimated ultimate recovery for the field is more than 4 billion barrels of oil. Horizontal drilling and fracture stimulation of the horizontal leg are key

technologies that enable a low permeability reservoir to produce. A detailed understanding of reservoir properties will aid in the exploration and discovery of other areas as well as successful design of development plans in the Bakken petroleum system, which is one of the major goals of this research project [LeFever and Helms, 2006; Webster, 1984; Meissner and Banks, 2000; Flannery and Kraus, 2006].

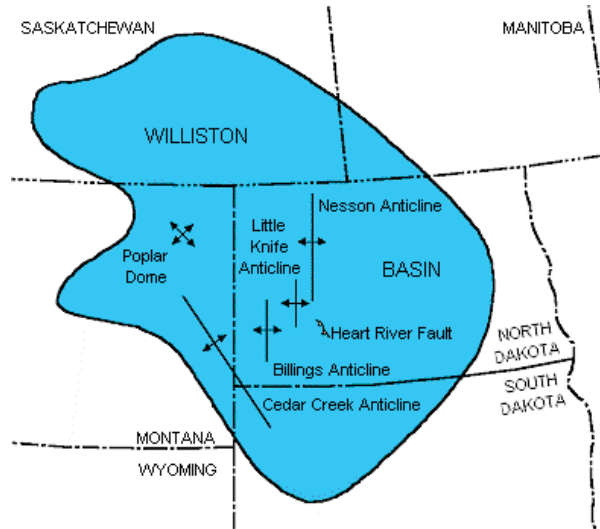


Figure 2. Williston basin and its major structures in the USA portion [Heck et al., 2002].

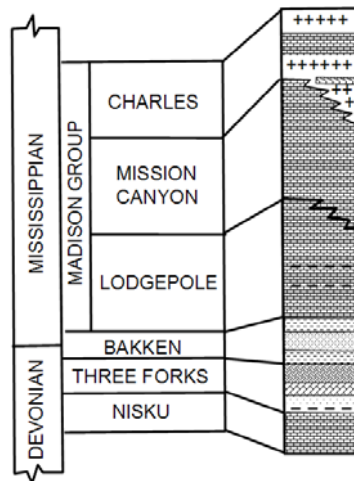


Figure 3. Stratigraphy of the Bakken Formation.

The three members of the Bakken are thin and converge towards the margins of the Williston Basin and have an onlapping relationship with the underlying Three

Forks (Figure 4). The petrophysical properties of the Bakken Formation over a study area in the Williston Basin are shown in Table 1.

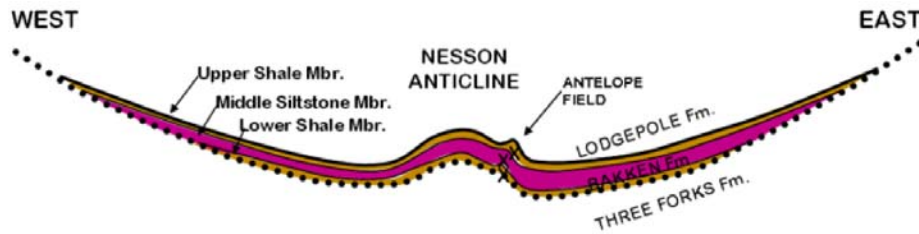


Figure 4. Structural cross section of Williston Basin.

Table 1. The properties of the Bakken Formation [Bohrer et al. 2008]

Member of the Bakken Formation	Upper	Middle	Lower
Measured Depth at Top, feet	11,160	11,260	11,310
Thickness, feet	18	41	19
Pay thickness, feet	18	14	19
Porosity (fraction)	0.07	0.12	0.07
Water saturation, S_w (fraction)	0.14	0.17	0.20
Oil saturation, S_o (fraction)	0.86	0.83	0.80
Reservoir Temperature, °F	168	170	171
FVF	1.4	1.4	1.4
GOR, ft ³ per Res.BBL	808	1026	591

FVF - Formation volume factor
 GOR - Gas-oil ratio

The measured permeability ranges from 0 to 20 millidarcies in the middle member and typically is very low, averaging 0.04 millidarcies (Figure 5). At any given depth, permeability in sandstones can vary markedly. It can also vary with the thermal maturity of the source shales. As burial depth increases, permeability in sandstones has been shown to decrease from a range of about 0.06 to 0.01 millidarcies, where the adjacent shales are immature, to a range of about ≤ 0.01 to 0.01 millidarcies where these shales are mature. This decrease in permeability is attributed to carbonate precipitation in response to the generation of CO₂ during kerogen maturation of the shales [Pitman et al., 2001].

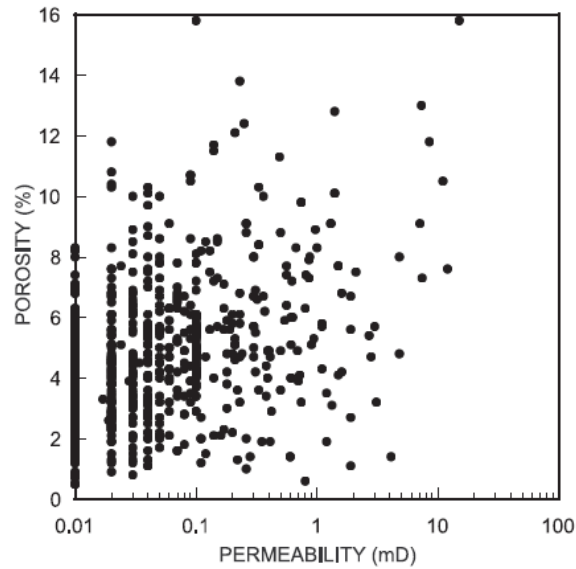


Figure 5. Plot of core porosity versus permeability in sandstones and siltstones of the middle member of the Bakken Formation [Pitman *et al.*, 2001].

As is clear from Figure 5, the permeability of the Bakken Formation is very low compared to conventional reservoirs. However, the presence of natural fractures in the tight Bakken reservoir enhances the reservoir quality [Murray, 1968; Meissner, 1978; Pitman *et al.*, 2001]. Three types of fractures are reported to occur in the Bakken: (1) structural related tectonic fractures, (2) stress-related regional fractures, and (3) expulsion fractures associated with overpressuring due to hydrocarbon generation [Druyff, 1991].

Two or more decades ago, recovery of oil from the Bakken Formation would have been considered in terms of primary recovery from minimally-stimulated vertical wells. Today, however, petroleum engineers think of the Bakken oil recovery in terms of the degree of fracturing stimulation in horizontal wells, optimal lateral length, and optimal number of horizontal wells drilled as well as optimal fracturing treatment materials (fracturing fluid plus proppant) that shape the success of well

stimulation in Bakken horizontal wells to a large degree [Cox *et al.*, 2008; Dunek *et al.*, 2009; Lolon *et al.*, 2009].

Overview of Hydraulic Fracturing

Hydraulic fracturing is a widely used technique to enhance oil and gas production. The technique was introduced to the petroleum industry in 1947 [Montgomery and Smith, 2010], and is now a standard operating procedure. By 1981, more than 800,000 hydro fracturing treatments had been performed and recorded [Gidley, 1990].

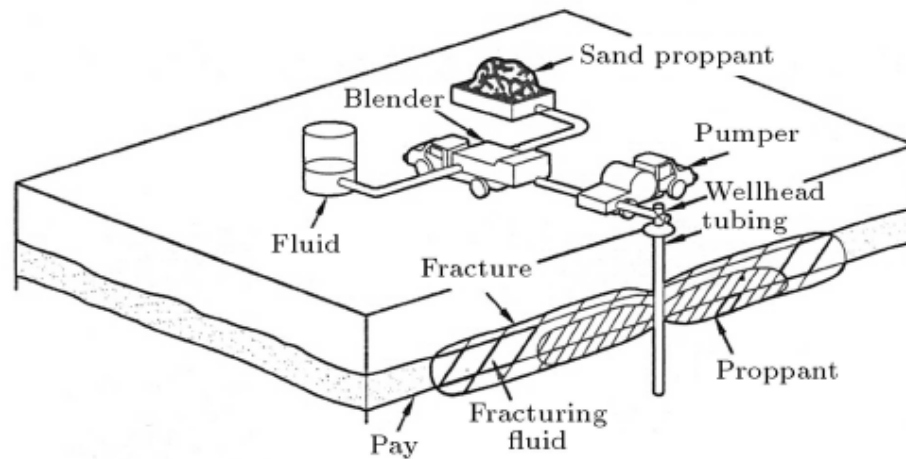


Figure 6. Typical hydraulic fracturing treatment in petroleum industry [Gidley, 1990]

Since its inception, hydraulic fracturing has developed from a simple low volume and low injection rate reservoir stimulation technique to a highly engineered and complex procedure that can be used for many purposes. Figure 6 depicts a typical hydraulic fracturing process in the petroleum industry. The procedure is as follows. First, a neat fluid, such as water (called “pad”), is pumped into the well at the desired depth (pay zone), to initiate the fracture and to establish its propagation. This is

followed by pumping slurry, which is a fluid mixed with a propping agent, such as sand (often called “proppant”). This slurry continues to extend the fracture and concurrently carries the proppant deep into the fracture.

After pumping, the injected fluid chemically breaks down to a lower viscosity and flows back out of the well, leaving a highly conductive propped fracture for oil and/or gas to easily flow from the extremities of the formation into the well. It is generally assumed that the induced fracture has two wings, which extend in opposite directions from the well and is oriented, more or less, in a vertical plane. Other fracture configurations, such as horizontal fractures, are also reported to occur, but they constitute a relatively low percentage of situations documented. Experience indicates that at a depth of below 600 meters, fractures are usually oriented vertically [Veatch *et al.*, 1989; Gidley, 1990]. The fracture pattern, however, may not be the same for different types of rock.

For decades, petroleum engineers have been developing models for simulating hydraulic fracturing in hydrocarbon reservoirs. In the early 1960's, the industry felt the need for a design tool for this fast growing technique. In response to this need, a number of two-dimensional (2D) models were developed for designing hydraulic fracturing treatments [Perkins and Kern, 1961; Geertsma and de Klerk, 1969]. This type of simple closed form solution has been used by the industry with some success; however, as the technology progressed from low volume/rate to high volume/rate treatments in more sophisticated and massive hydraulic fracturing projects, the industry demanded more rigorous design methods in order to minimize costs. In the last 20 years, a number of 2D and 3D numerical models have been developed.

The most common equations used in these numerical models are fluid flow equations, which are usually solved iteratively. Geomechanical aspects are

incorporated in the models, mostly in an uncoupled manner. Mainly vertical or horizontal planar fractures were considered, based on the 2D closed form solutions mentioned above. The degree of sophistication of these models varies considerably and their results cannot be validated with much confidence. The main problem in validating these models is that the configuration of the induced fracture is not really known; therefore, the results of the model are usually evaluated based on fluid injection pressure measurements and/or the production history of the well.

In a 3D fracture model, however, fracture width is calculated using 3D elasticity; i.e. the fracture width anywhere is a function of the pressure everywhere in the fracture [Warpinski *et al.*, 1982]. In a pseudo-3D (P3D) solution the combination of analytical and numerical routines will predict the fracture height and width. Fully 3D models, on the other hand, are complex numerical routines with extensive input data and high computation requirements. In a fully 3D model, the fracture height, width, length, and shape can all vary completely independently [Gidley, 1990].

CHAPTER II

HYDRAULIC FRACTURING CONCEPTS AND FUNDAMENTALS

Introduction

Hydraulic fracturing is a technique used by the oil and gas industry to increase a well's productivity by injecting water, sand and a mixture of often chemicals at very high pressures, fracturing the rock and creating fissures for the hydrocarbon to flow more freely out of the formation [Nijhuis, 2009]. Hydraulic fracturing includes a number of processes: fracture initiation, fracture propagation, fluid flow in the fracture, and fluid diffusion into the formation. A detailed study on each of these processes is beyond the objectives of this research. However, it is beneficial to review these processes to better understand the problems involved in the design of a hydraulic fracturing job.

Fracture Initiation and Propagation; Energy-Balance Approach

In dealing with the fracture initiation problem, we need to evaluate the critical level of applied loads corresponding to the inception of a hydraulic fracture. Using the concepts of deformation and stresses, one can decipher the criteria of fracture initiation and fracture propagation.

Griffith began his pioneering studies of fracture in glass just prior to 1920 in which he stated that in a stressed plate of elastic material containing a crack, the

potential energy decreases when the surface energy increases [Griffith, 1921]. He employed an energy-balance approach that became one of the most popular developments in material science [Collins, 1981; Roylance, 2001]. The strain energy per unit volume of stressed material is:

$$U^* = \frac{1}{V} \int f dx = \int \frac{f}{A} \frac{dx}{L} = \int \sigma d\varepsilon \quad (1)$$

If the material is linear elastic, which means $\sigma = E\varepsilon$ (E is Young's modulus and ν is strain), then the strain energy per unit volume is given by:

$$U^* = \frac{E\varepsilon^2}{2} = \frac{\sigma^2}{2E} \quad (2)$$

The region adjacent to a fracture around the wellbore will be unloaded once the crack has grown into the formation to a length x_f . Griffith used Inglis [1913] solution in calculating the stress concentrations around elliptical holes [Barsom, 1987; Perez, 2004], to compute just how much energy will be released from fracture growth. Figure 7 illustrates a simple way of visualizing this energy release. Two triangular regions near the crack flanks, of height x_f and length βx_f , as being completely unloaded, while the remaining rock formation continues to feel the effective stress σ_e . The total strain (potential) energy (U) released is then the strain energy per unit volume (U^*) times the volume in both triangular regions (the dimension normal to the plane is taken to be unity):

$$U = -\frac{\beta\sigma^2 x_f^2}{2E} \quad (3)$$

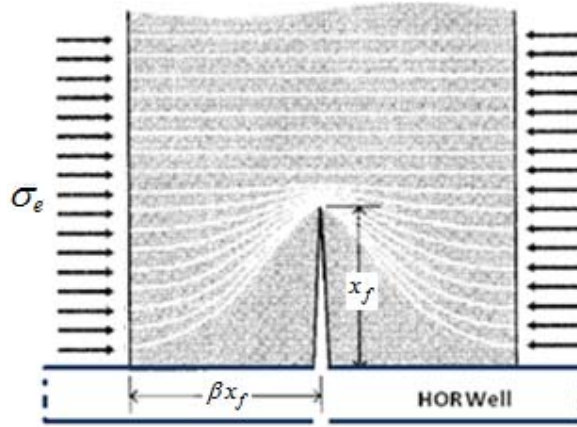


Figure 7. Idealization of unloaded region near crack flanks.

This strain energy is liberated by crack growth. But in forming the crack, bonds must be broken, and the requisite bond energy is in effect absorbed by the material. The surface energy (S) associated with a crack of length x_f (and unit thickness) is:

$$S = 2\gamma x_f \quad (4)$$

Where γ is the surface energy (joules/m²) and the factor 2 is needed since two crack surfaces have been formed. The total energy associated with the crack is then sum of the (positive energy) absorbed to create the new surfaces, plus (negative) strain energy liberated by allowing the regions near the crack flanks to become unloaded [Roylance, 2001] (Figure 8).

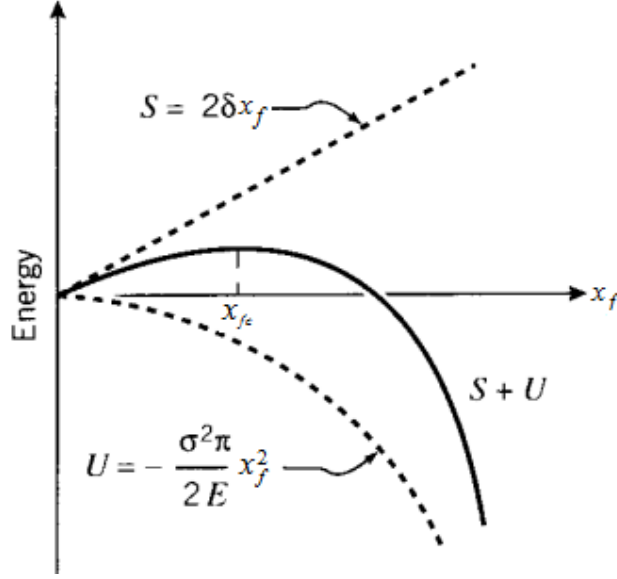


Figure 8. Idealization of the fracture energy balance.

As shown in Figure 7, a long horizontal well containing a crack is subjected to a uniform tensile load in the direction of the wellbore (x-axis), and perpendicular to the crack line along the y-axis. The question here is: *What is the external stress that will cause crack instability (crack propagation) value?*

Solution: Considering the configuration in Figure 7, the total potential energy of the system is given by [Perez, 2004]:

$$\begin{aligned}
 U &= U_o - U_{x_f} + U_\gamma \\
 &= U_o - \frac{\pi(1-\nu^2)\beta\sigma^2 x_f^2}{E} + 2(2x_f\beta\gamma_s)
 \end{aligned} \tag{5}$$

Where U_o is the potential energy of uncracked body, U_{x_f} is the elastic energy due to the presence of the crack, U_γ is the elastic-surface energy due to the formation of crack surfaces, $4x_f\beta$ is the total surface crack area, γ_s is the specific surface energy, and ν is Poisson's ratio (plain strain— biaxial stress state). The equilibrium condition of Eq.5 is defined by the first order derivative with respect to crack length. This

derivative is very useful because the critical crack size can be readily predicted. When

$dU/dx_f = 0$, the crack size and total surface energy are, respectively [Perez, 2004]:

$$x_f = \frac{(2\gamma_s)E}{\pi\beta\sigma^2} \quad (6)$$

$$2\gamma_s = \frac{\pi\beta x_f \sigma^2}{E} \quad (7)$$

Rearranging Eq.7 yields an important expression in linear elastic fracture mechanics (LEFM) [Perez, 2004]:

$$\sigma\sqrt{\pi x_f} = \sqrt{\frac{2\gamma_s E}{1-\nu^2}} \quad (8)$$

$$K_I = \sigma\sqrt{\pi x_f} \quad (9)$$

The parameter K_I is called the stress intensity factor which is the crack driving force and its critical value is a material property known as fracture toughness, which in turn, is the resistance force to crack extension.

The Fundamentals of Hydraulic Fractures

Generally speaking, hydraulic fracturing is used to increase the productivity index of a producing well, or injectivity index of an injection well. The productivity index refers to the total volume of fluid that can be produced for a specific drawdown pressure, and injectivity index refers to the amount of fluid that can be injected into a formation at a given pressure differential. A fracturing job usually consists of four main stages:

- a) Injecting a small quantity of fluid down the well known as “pre-pad” to fill up the well and to breakdown the formation. This stage is intended to initiate the fracture.

- b) A clean fluid known as “pad” is then pumped. The hydraulic pressure generated by pumping the pad causes the fracture to propagate into the formation.
- c) Next, a proppant-laden fluid (slurry) is pumped into the fracture.
- d) Finally, in the last and very important stage of the fracturing job the fluid should be broken so as to flow back to the surface and the well can cleanup.

Figure 9 demonstrates the stages of a hydraulic fracturing job.

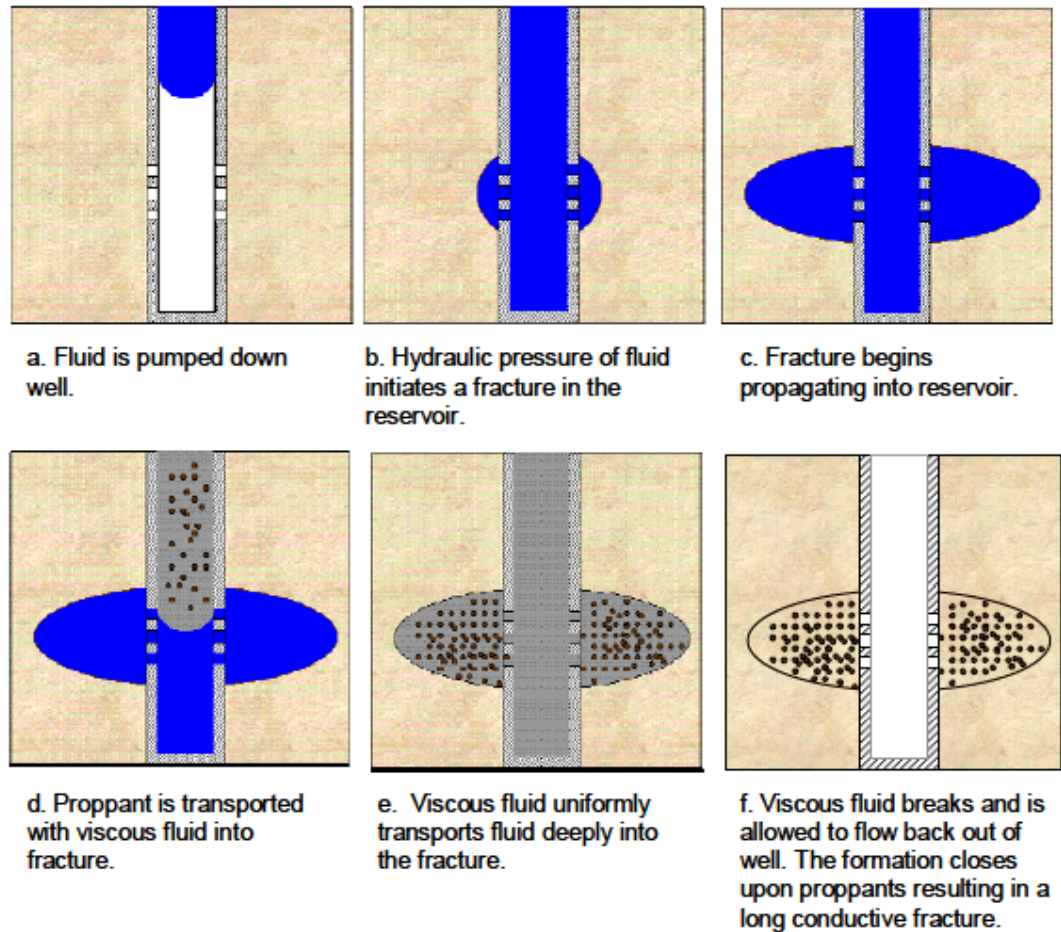


Figure 9. Hydraulic Fracture Stimulation Process [Tschirhart, 2005; Rajcopal, 2006]

Hydraulic Fracture Size

Larger hydraulic fractures will form if we use high volumes of fracturing fluid and proppant. However, uncontrolled growth of fractures is not intended from a

production point of view. Figure 10 shows how the maximum fracture size can be limited. In this specific case it is assumed that the fracture is initiated from the mid-point perforations and the fracture propagates radially. In practice, a fracture may propagate radially when the formation is homogeneous with a stress gradient equal to the hydrostatic head of the fracturing fluid.

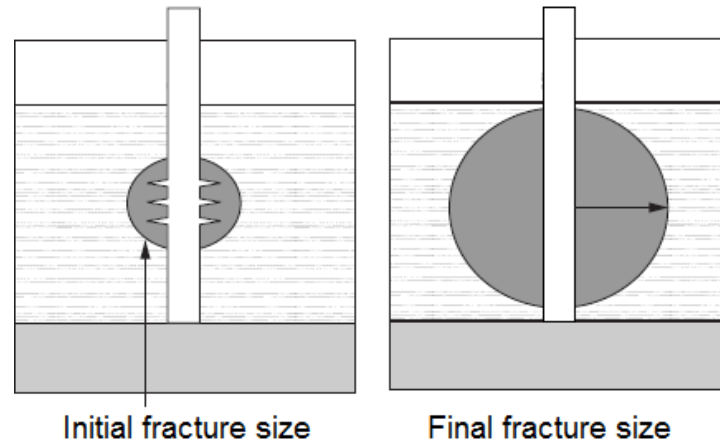


Figure 10. Hydraulic fracture size [*Courtesy of Prod Tech.*]

Hydraulic Fracture Containment

A successful hydraulic fracture job is such that the fracture does not contact undesired layers or it does not reach to unwanted fluids in a single-layer formation. A good hydraulic fracture design should guarantee that the fracture is contained within the pay zone, i.e. the upward/downward fracture growth will be retarded by the changes in formation property between the layers.

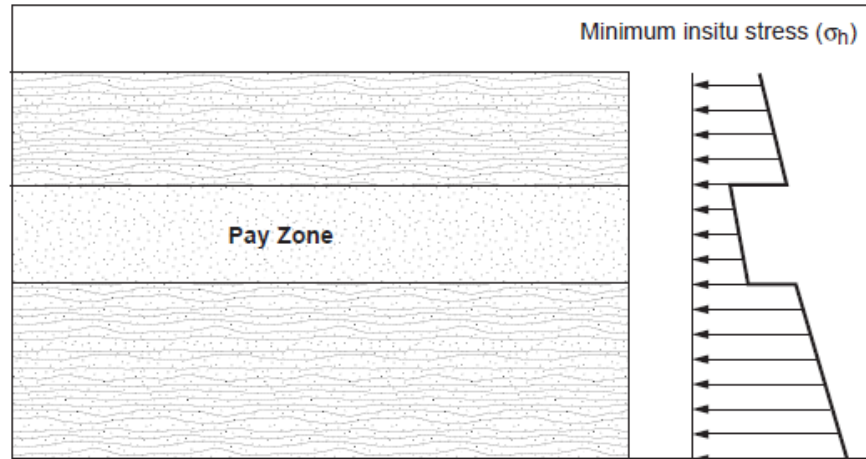


Figure 11. In-situ stress contrast [Courtesy of Prod Tech.]

The major formation properties that influence the fracture geometry and fracture growth are as follow [Gidley *et al*, 1990]:

- a) **Geomechanical parameters:** Sand layers have typically lower Poisson's ratio (but higher Young's modulus) than the bounding shale layers, which aids hydraulic fracture containment.
- b) **Critical fracture intensity factor:** Fracture propagation will become harder when fracture toughness is higher.
- c) **Fluid leakoff:** A hydraulic fracture will become blunt and thus no more propagation will occur when there is a high rate of the fluid loss from the fracture walls into the formation.

Hydraulic Fracture Growth

The minimum horizontal stress contrast and the thickness of the bounding layers are the key parameters that control the fracture containment. Figure 12 illustrates the effect of horizontal stress contrast on the vertical fracture growth. As is clear in the figure, the fracture grows initially in the pay zone until it reaches to the boundary.

Then, the fracture grows parallel to bedding and becomes more elongated— with higher stress contrasts the fracture grows horizontally [Gidley *et al*, 1990].

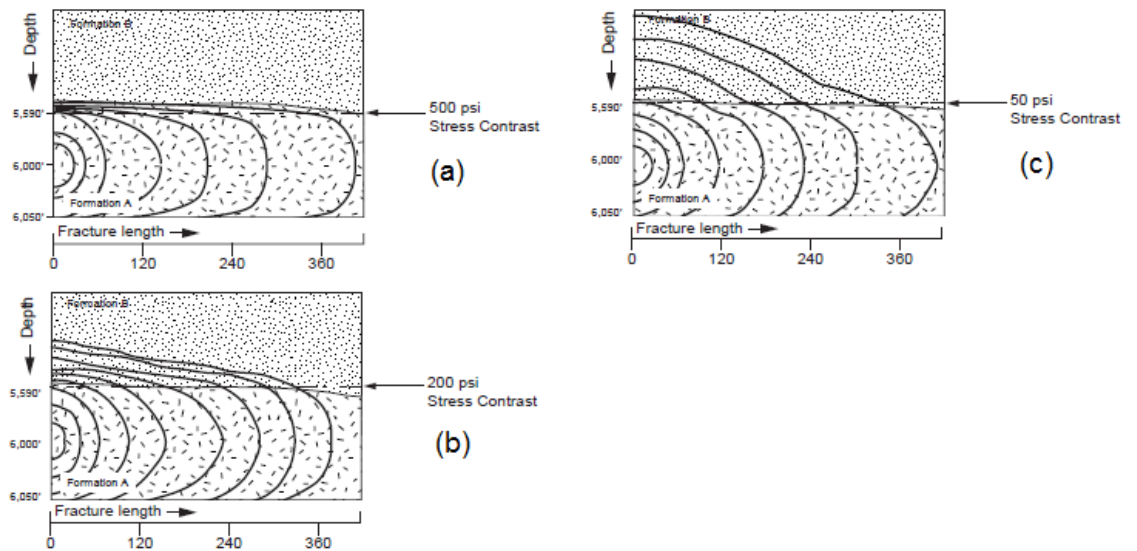


Figure 12. Hydraulic fracture growth; a) vertical fracture growth has stopped when stress contrast is large, b) limited upward fracture growth with medium stress contrast, and c) almost uncontrolled upward fracture growth when the stress contrast is so small [Courtesy of *Prod Tech.*].

Figure 13 explains what would happen when fracture containment is no longer effective due to the height of the upper barrier and the available in-situ stress contrast in the formation.

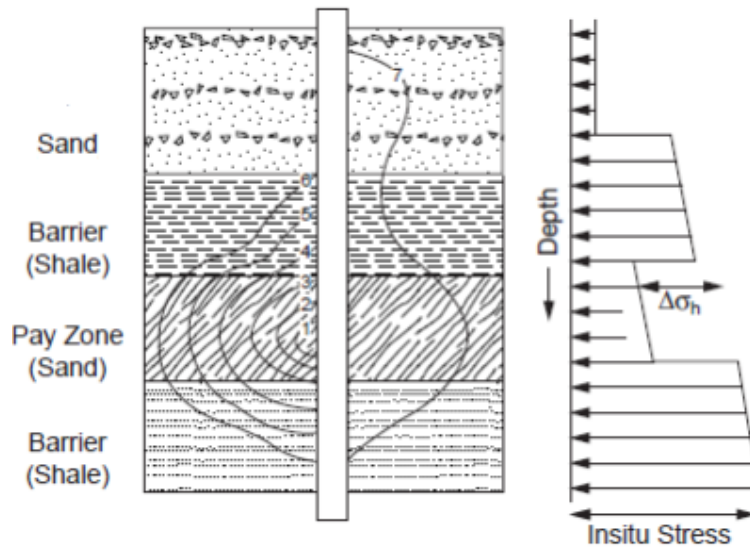


Figure 13. Relationship between fracture containment and stress contrast [Courtesy of *Prod Tech.*]

When the fracture breakthrough into the upper zone occurs, the fracture length in the pay zone will decrease. And, real time measurement (monitoring) of the fracture propagation (pressure), allows us to monitor the fracture containment. On the other hand, we should have knowledge of the fracture height when designing and executing a hydraulic fracture job. There are a number of measurement techniques used in the industry to measure the fracture height growth [Gidley *et al*, 1990]:

- 1) Temperature log that is run immediately after the fracture treatment.
- 2) Running a production log across the perforation interval to measure the flow profile.
- 3) Running a gamma ray log after removing the excess proppant from the wellbore. The proppants are given radioactive coating.
- 4) Using a formation microscanner or a borehole camera to observe the fractures in open-hole completions.

- 5) Meicroseismic. This involves triangulation of seismic events emitted from the propagating fracture tip. These seismic events are measured with geophones installed at the surface or in the wellbore.
- 6) Using tiltmeter at the surface to measure the surface topography due to propagation of the hydraulic fracture. Such changes indicate the length and orientation of the hydraulic fracture.

Two-Dimensional Fracture Models

Mathematical fracture propagation models have been introduced in the early 1960's, to relate injection rate, q , time of treatment, t , and fluid leakoff, q_ℓ , with fracture dimensions— i.e. width, w , height, h_f , and length, x_f [*Perkins and Kern*, 1961; *Barrenblatt*, 1962; *Geertsma and de Klerk*, 1969; *Nordgren*, 1972]. These models use two-dimensional, analytical equations where the fracture height is required to be input.

Two major models to describe hydraulically induced fracture propagation in rocks were emerged for design purposes [*Perkins and Kern*, 1961; *Geertsma and de Klerk*, 1969]. These models are called PK (after *Perkins and Kern*) and GDK (after *Geertsma and de Klerk*). An important forerunner to the GDK model is the work by Khristianovitch and Zheltov [1955] who introduced different equilibrium conditions [*Gidley et al*, 1990].

In the PK model for vertical elastic fracture the assumptions are: a) the fracture height is fixed and independent of fracture length, b) the pressure inside the fracture is constant over the cross sectional area, and c) the resistance to deformation prevails in

the vertical plane. They considered vertically limited fractures perpendicular to the direction of propagation (Figure 14).

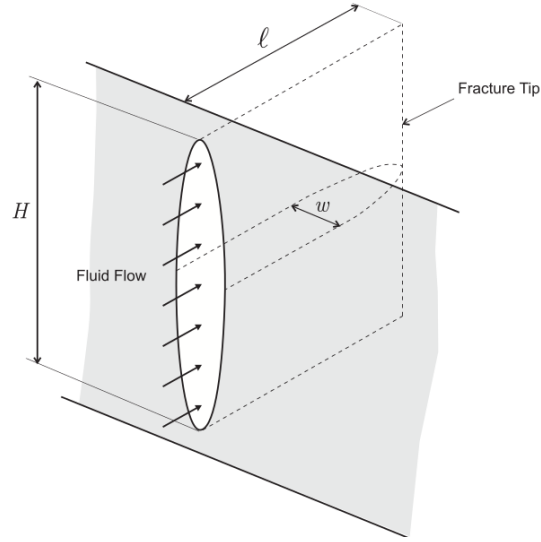


Figure 14. Schematic representation of linearly propagating fracture with laminar fluid flow according to Perkins and Kern model [Adachi *et al.*, 2007]

The width of the fracture is determined using the solution for a linear elastic, isotropic medium, subjected to an in-situ stress σ_h and constant fracture pressure p_f with the consideration of the assumptions above. The solution is [Gidley, 1990].

$$w(x) = \frac{(1-\nu)h\Delta p}{G} \sqrt{1 - \left(\frac{x}{x_f}\right)^2} \quad (10)$$

Where h and x_f are the fracture height and length, respectively, $\Delta p = p_f - \sigma_h$ is the net-pressure and G is the shear modulus. In this model the fracture opening is elliptical and maximum fracture width is given by:

$$w(x, t) = \frac{(1-\nu)h\Delta p(x, t)}{G} \quad (11)$$

Geertsma and de Klerk [1969] developed a model for vertical rectangular fracture propagation (Figure 15). The assumptions made in this model include: a) a fixed

fracture height is assumed, b) the resistance to deformation prevails in the horizontal plane only (as a result, fracture width does not depend on fracture height). The width of the fracture can be calculated by [Gidley, 1990]:

$$p(0,t) - p(x,t) = p_f - p = \frac{12\mu q_0}{h_f} \int_0^x \frac{dx}{w^3(x,t)} \quad (12)$$

Where q_0 is total injection rate, h_f is fracture height, p is fracturing fluid pressure along the fracture, p_f is fluid pressure at the wellbore, and $w(x,t)$ is the local fracture width.

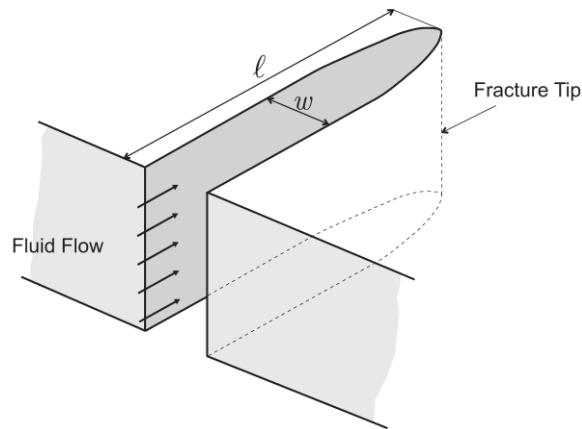


Figure 15. Schematic representation of linearly propagating fracture with laminar fluid flow according to KGD model [Adachi *et al.*, 2007]

The above equation is obtained from coupling solid mechanics of the rock and fluid flow analysis of the injected fluid. Both of the explained models assume that the fracture toughness at the tip of the fracture is negligible compared to the necessary pressure required to pump the fracturing fluid and oppose the in-situ stress. Hence, the fluid pumped at any stage of the fracturing job creates additional length instantly, regardless of the fluid pressure near the crack tip.

Daneshy [1973] modified the KGD model considering non-Newtonian fluids and different pressure distribution functions in the fracture. He further included the

proppant transport concepts into his model [Daneshy, 1978]. Whether these models are applicable or not can be determined by the match between the predicted and observed variation of pressure with time [Lehman et al., 2002; Guo et al., 2007]. In the PKN model [Nordgren, 1972] the pressure increases as fracture propagates, whereas in the KGD model the pressure decreases with time and fracture propagation.

A fracture would propagate radially when the injection interval is relatively smaller than the thickness of the formation. The modeling of radial fracture propagation by the PKN and GDK models differs only because of the hydraulic pressure distribution. The fluid pressure travels logarithmically from pressure p_0 at the entrance ($r = r_w$) as a result of viscous flow resistance [Gidley et al, 1990]:

$$p = p_0 - \frac{6q\mu}{\pi\bar{w}^3} \ln\left(\frac{r}{r_w}\right) \quad (13)$$

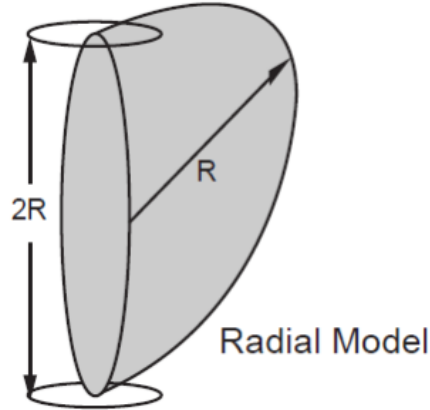


Figure 16. Schematic representation of radially propagating fracture with laminar flow
[Courtesy of Prod Tech.]

The width at the well, $w(0)$, of a radially propagating fracture is given by:

$$w(0) = C_7 \left(\frac{(1-\nu)\mu q_0 R}{G} \right)^{1/4} \quad (14)$$

Where the PK approach obtains a value of $C_7 = 1.4$ and the GDK approach, a value of 2.15.

2D Fracture Models with Fluid Leakoff

The basic elements to describe the fluid loss effect on fracture dimensions are from Carter's one-dimensional fluid loss equation. In Carter's model fracture height and width are assumed to be constant; only fracture length (x_f) is a variable. The fluid loss velocity function is then assumed to take the form:

$$v_\ell = \frac{K_\ell}{\sqrt{t - \tau}} \quad (15)$$

Where K_ℓ is the overall fluid-loss coefficient as measured in laboratory filtration tests and τ represents the time at which filtration starts. Using the concept of fluid-loss, Nordgren [1972] modified the PK model to account for the amount of fluid loss through the walls of a fracture:

$$\frac{\partial q}{\partial x} + \frac{\pi h_f}{4} \frac{\partial w}{\partial t} + q_\ell = 0 \quad (16)$$

Incorporating fluid leak-off into the PK model yields the following equation to approximate the fracture width [Nordgren, 1972; Gidley *et al*, 1990]:

$$w(0) = 4 \left(\frac{2}{\pi^3} \right)^{1/4} \left(\frac{(1 - \nu) \mu q_0^2}{G h_f K_\ell} \right)^{1/4} t^{1/8} \quad (17)$$

Where q_0 is the flow rate at fracture entrance. The GDK model, on the other hand, assumes that the fluid loss occurs with low loss coefficient and for small treatment times. The material balance is considered in the overall form as Carter did; thus, incorporating the fluid leakoff into GDK model yields [Gidley *et al*, 1990]:

$$w(0, t_p) = 2.27 \left(\frac{(1-\nu)\mu q_0 x_f}{G h_f} \right)^{1/4} \quad (18)$$

Where t_p represents the time when the pumps stop. As for a radially expanding fracture, it propagates usually during the early stages of the fracture growth (for small time), and one can use Eq.19 to relate the width at the fracture entrance and the radius R [Gidley *et al*, 1990].

$$w(0) \cong 2.15 \left(\frac{(1-\nu)\mu q_0 R}{G} \right)^{1/4} \quad (19)$$

Note that the computational models described above assume Newtonian fluid flow of the fracturing fluid during fracture propagation. However, most fracturing fluids exhibit non-Newtonian behavior in some way [Rajcopal, 2006].

Three-Dimensional Hydraulic Fracture Simulation

During the early period of hydraulic fracturing, simple models (2D) were developed to predict the dimensions of a hydraulic fracture based on rock and fluid properties, pumping parameters and in-situ stresses [Khristianovic and Zheltov, 1955; Geertsma and de Klerk, 1969; Perkins and Kern, 1961; Nordgren, 1972]. However, these 2D models are not applicable to simulate both vertical and lateral propagation (Figure 17). Therefore, pseudo 3D models were developed by removing the assumptions made in the 2D models that had considered constant and uniform height [Settari and Cleary, 1986; Morales, 1989; Economides and Demarchos, 2008; Pitakbunkate *et al.*, 2011]. The height in the pseudo-three dimensional (P3D) model is a function of both position along the fracture and time (Figure 17.(a) and (b)) [Cleary, 1994; Yang, 2011]. The main assumption in the P3D model is that fracture length is

much larger than fracture height, and the difference between P3D and 2D models is the addition of a vertical fluid flow component to the formalisms [Carter *et al.*, 1998]. Warpinski *et al* [1994] described the different fracture simulation models including P3D and 2D models.

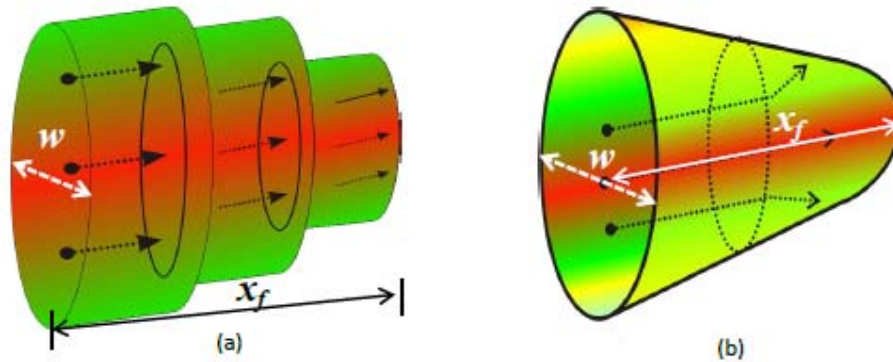


Figure 17. Fracture geometry (a) P3D (cell approach) (d) Global 3D (parameterized) [Yang, 2011]

The main disadvantage of the P3D model is that it cannot handle fractures with arbitrary shape and orientation. Hence, fully 3D models are required for this particular purpose [Clifton and Abou-Sayed, 1979; Ghassemi, 1996; Carter *et al.*, 1998]. Fully 3D models have been studied thoroughly in the literature; however, these are called planar-3D simulators since they cannot model out-of-plane fracture growth (Figure 18). Other planar-3D models (Figure 19) have been developed by Barree [1983], Morita *et al.* [1988], Advani *et al.* [1990], and Gu and Leung [1993].

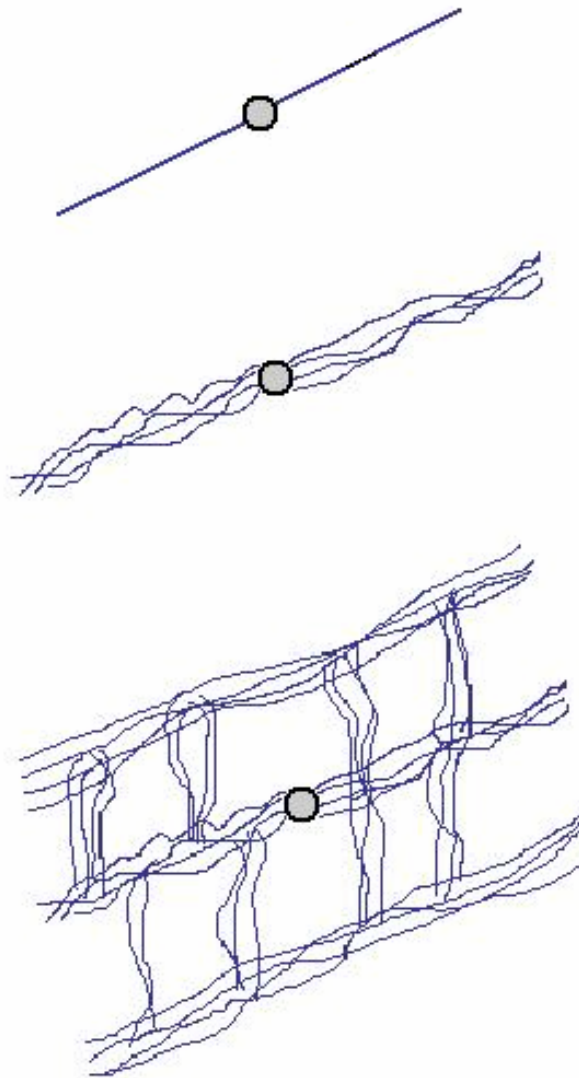


Figure 18. Fracture geometry of hydraulic fractures ranging from a single, planar fracture to out-of-plane fractures and complex fracture network

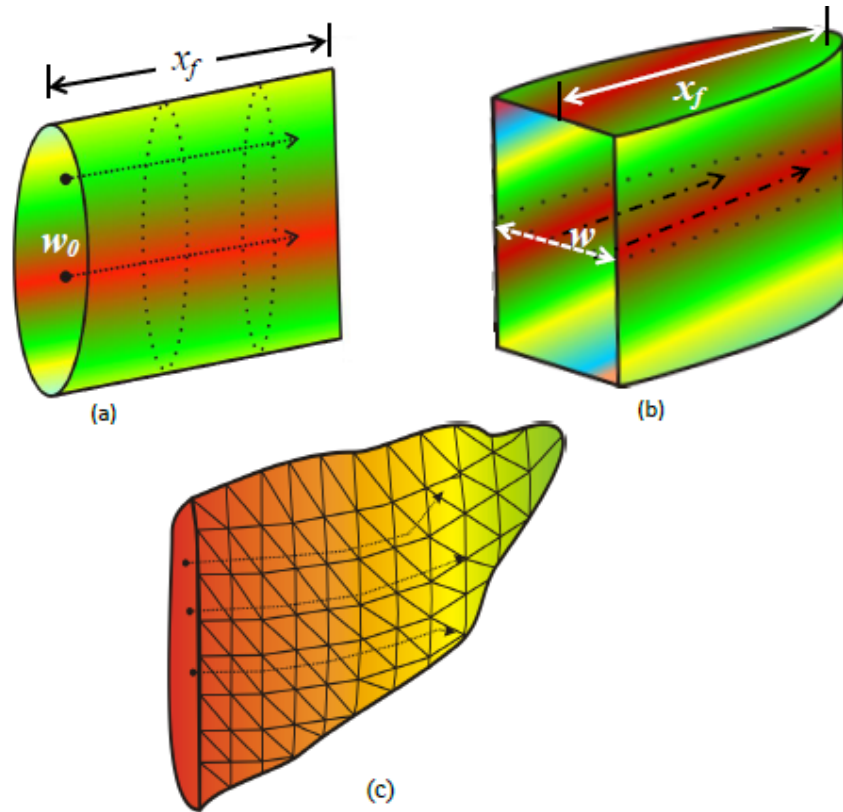


Figure 19. Fracture geometry models (a) PKN type (b) KGD type (c) Fully 3D (meshed)
[Yang, 2011]

On the other hand, Van Damme [1986] presented a fully 3D model in which the solid mechanics analysis is handled through the displacement discontinuity method (DDM). The main advantage of this model is that it allows out-of-plane propagation of the fracture that is not considered in the previous 3D models [Ghassemi, 1996; Kresse *et al.*, 2012].

Fracturing Fluids and Additives

Fracturing fluid is pumped into reservoir rock to create hydraulic fractures. To achieve successful stimulation, the fracturing fluid must have certain physical and chemical properties [Shah *et al.*, 1992; Woodroof *et al.*, 2003; Al-Ghazal *et al.*, 2013;

Rahim et al., 2013; Gomez and Patel, 2013; Che et al., 2013]. The functions of a fracturing fluid include: a) to initiate and propagate the fracture, b) to develop fracture width, c) to transport proppant throughout the length of the fracture, d) to flow back to the surface after the fracture treatment is finished that leaves a fracture with maximum permeability. To achieve the above, the characteristics of the fracturing fluid should be such that 1) fluid is stable with predictable rheology under surface and downhole treating conditions and treatment duration, 2) its pressure drop due to friction in tubing and flow lines is low, 3) provides fluid loss control, 4) it cleans and easily degrades to minimize formation damage to propped fracture. Generally speaking, a good fracturing fluid needs to be [*Gidley, 1990*]:

- compatible with the formation rock and fluids,
- capable of suspending proppants and transporting them deep into the fracture,
- capable to develop the necessary fracture width to accept proppants or to allow deep acid penetration,
- an efficient fluid; i.e. has low fluid loss,
- easy to remove from the formation,
- have low friction pressure,
- easy to be prepared and to perform in the field, and
- cost effective.

Compatibility of the fracturing fluid with the reservoir rock and fluid is one of the most critical characteristics. If the chemical nature of the fracturing fluid causes swelling of the naturally occurring clays in the formation, thereby plugging pore channels, the treatment will be a failure. If the fracturing fluid causes migration of fines and/or clays, the success of the treatment will be nullified [*Smith et al., 1964; Jones, 1964; Reed, 1972; Gidley et al., 1990; Rajcopal, 2006*].

Fluid Rheological Models

Rheology is the study of the deformation and flow of matters. Matters in this context can be solid, liquid, or gas. This term explains the relationship between force, deformation, and time and comes from the Greek word “Rheos” meaning to flow [Alkhatami, 2007]. The rheological characteristics of a fluid are important in evaluating the capability of the fluid to perform a specific function such as its ability to transport and suspend solid particles, reduce friction pressure, and control fluid loss.

Generally, fluids can be categorized into two groups: Newtonian fluids and non-Newtonian fluids. A Newtonian fluid is a fluid whose “shear-stress” versus “rate of shear” curve is linear and passes through the origin. A non-Newtonian fluid is one whose rheogram (shear stress versus shear rate) is non-linear or does not pass through the origin. Most fluids used in the petroleum industry are non-Newtonian fluids which can be classified into three groups [Chhabra and Richardson, 1999]:

- Inelastic fluids whose rate of shear is determined by the shear stress at that point (purely time-independent).
- More complex fluids whose relationship between shear stress and shear rate depends upon the duration of shearing and their kinematic history (time-dependent).
- Fluids that are partially elastic and recover after deformation (visco-elastic)

In Figure 20 different types of time-independent fluids are shown. The linear flow behavior (Newtonian fluids) is also included.

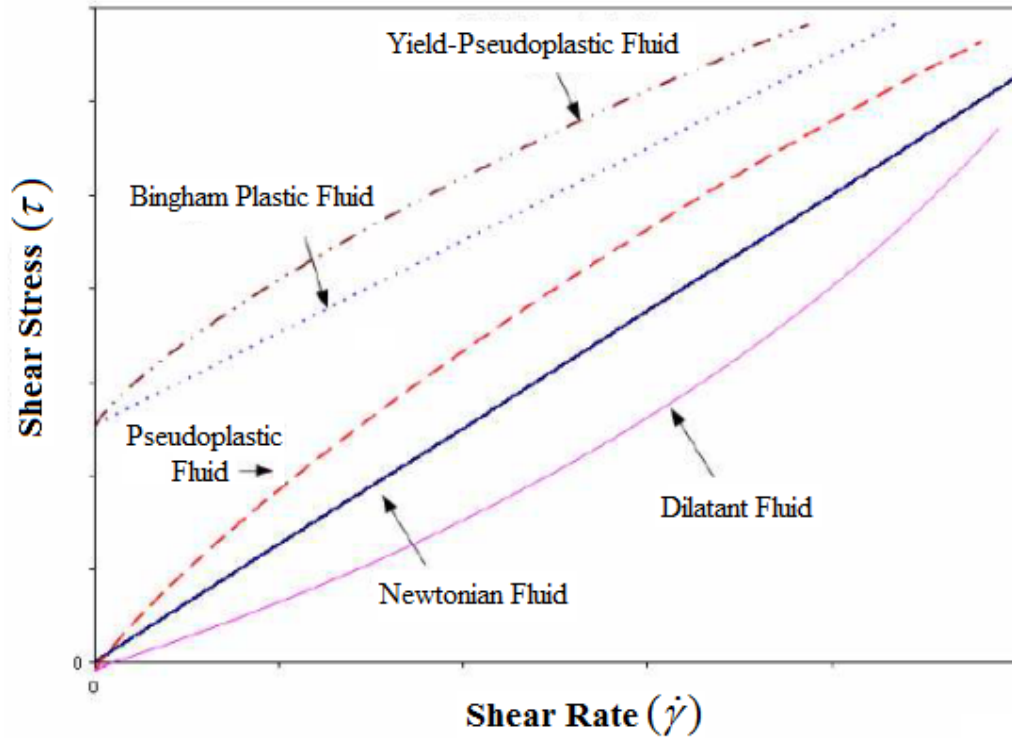


Figure 20. Different types of time-independent fluids [Youness, 2005]

The Bingham plastic model with its two parameters is a time-independent rheological model that accounts for the stress required to initiate fluid flow in viscous fluids. This initial stress that should be overcome for the fluid flow to occur is called “yield stress.” Once the initial stress (yield stress) is overcome, the fluid behaves similar to Newtonian fluids whose curve is shown by the linear relationship between the applied stress and the rate of shear. The Bingham plastic can be presented as follows:

$$\tau = \tau_0 + \mu_p \dot{\gamma} \quad (20)$$

Where τ is shear stress, τ_0 is yield stress, μ_p is plastic viscosity, and $\dot{\gamma}$ is shear rate. Another time-independent rheological model is the power law model which expresses a non-linear relationship between shear stress and shear rate that it seems to

better characterize the shear-thinning characteristics of drilling fluids. The power law model is given by [Dodge and Metzner, 1959; Vassilios, 2003].

$$\tau = k(\dot{\gamma})^n \quad (21)$$

Where n is the flow behavior index and k is the consistency index. In cases where $n < 1$ the fluid is termed as “pseudoplastic” or “shear thinning” since the apparent viscosity for such fluids decreases with increase in shear rate. When $n > 1$, the fluid is termed as “dilatant” or “shear thickening”. Obviously, $n = 1$ indicates that the fluid is Newtonian.

Another model was proposed by Herschel-Bulkley [1926] which is a simple generalization of the Bingham plastic model to define the non-linear flow behavior. In this model yield stress should be overcome for flow to occur, and the viscosity is shear rate dependent (Figure 20). Herschel-Bulkley model is given by:

$$\tau = \tau_0 + k(\dot{\gamma})^n \quad (22)$$

This model is widely used in the oil industry for the characterization of hydraulic fracturing fluids and drilling fluids.

Hydraulic Fracture Fluid

This section discusses the various fracturing fluids, including slickwater, linear gel, and crosslinked fracturing fluids. It is followed by a discussion of the additives necessary to achieve certain properties.

Water-Based Fluid

Water-based fracturing fluids are commonly used in the industry these days [Gupta and Pierce, 1998; Van Gijtenbeek *et al.*, 2006; Hassen *et al.*, 2012]. When compared to oil-based fluids, water-based fluids have some advantages:

- a) Water-based fluids are low cost.
- b) The hydrostatic head from water-based fluids is higher than that from oil-, gas-, and methanol-based fluids.
- c) Since water-based fluids are incombustible, they are safe.
- d) Easy to control its viscosity.

Water-based fluids were initially designed to create hydro-fractures by injecting low viscosity fracturing fluid composed of water, surfactants, clay stabilizing agents, and friction reducer materials [Mayerhofer and Meehan, 1998]. In the Bakken Formation water fracture treatments use slickwater as pad to create the initial fracture geometry, followed by linear gel or crosslinked gel [Hassen *et al.*, 2012].

Linear Fracturing Fluids

The need to thicken water to help transport proppant, to decrease fluid loss, and to increase fracture width was apparent to early investigators. The water viscosifier agents used in the early 60's were starch guar gum. Guar gum comes from a bean that thickens and viscosifies the mixture when added to water. Guar undergoes hydration upon contact with water. This unwinds the spiral molecular structure of guar, with water molecules attaching themselves to the polymer chain. This, in turn, leads to a viscous fluid by interaction of the polymer coils, one to another, in the water-based system. [Gidley *et al.*, 1990]

Other linear gels used as fracturing fluids are hydroxypropyl guar (HPG), hydroxyethyl cellulose (HEC), carboxymethyl HPG (CMHPG), xanthan gum, and in some rare cases polyacrilamides [Tiner, 1976; Chatterji and Borchardt, 1981; Ely, 1981; Gidley et al., 1990]. The structure of the viscosifier agents are shown in Figure 21.

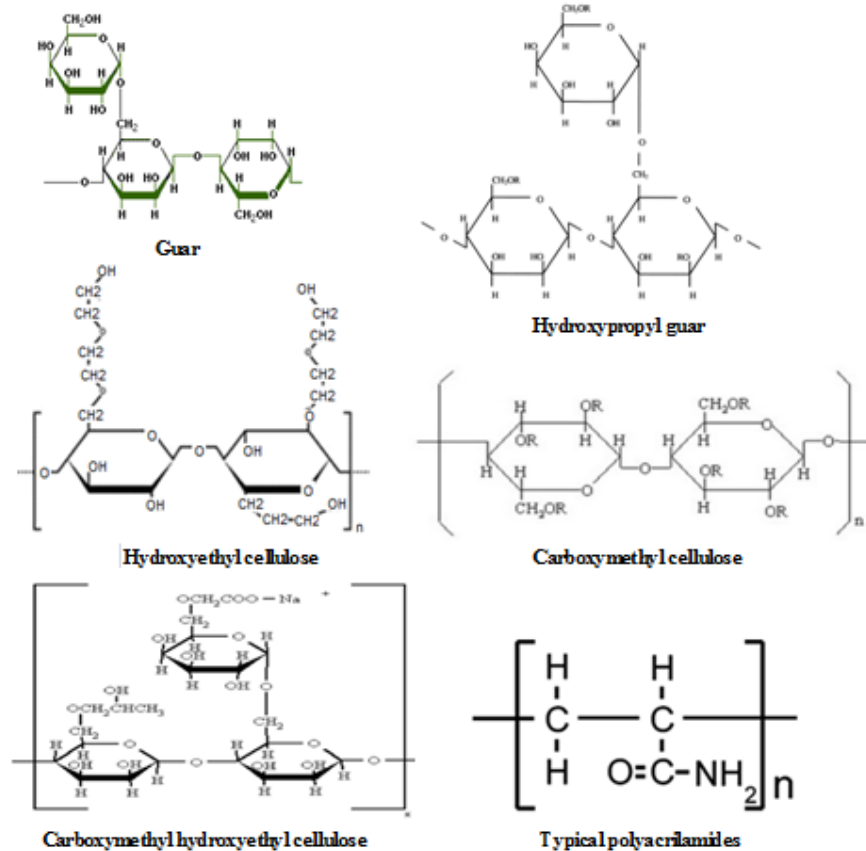


Figure 21. Chemical structures of guar, HPG, HEC, CMHEC, and polyacrilamides.

HPG, the most widely used viscosifier for water-based fracturing treatments, is obtained by the reaction of propylene oxide with the guar molecules, creating a more temperature-stable, and somewhat-higher-viscosity polymer. As noted in some research, 1-4% of HPG remains as insoluble product upon complete degradation of the polymer [White and Free, 1976; Almond, 1982; Pober et al., 1983; Volk et al., 1983].

Crosslinked Fracturing Fluids

Using the crosslinked gel was first proposed in the late 1960's [Wieland, 1971]. When using linear gel, the only means to increase viscosity is to increase the polymer concentration in the mixture. However, adding proppant and dispersing fluid-loss additives into such concentrated solutions of linear fluids is difficult [Grattoni *et al.*, 2001].

The development of crosslinked gel (for e.g. crosslinked HPG) has removed many of such problems especially when it is intended to operate hydraulic fracturing in deep, hot reservoirs, such as the Bakken Formation. The earliest crosslinkers were borates and antimony metal crosslinkers. In crosslinked fracture fluids the crosslinking reaction—where the molecular weight of the base polymer is substantially increased by tying together the various molecules of the polymer into a structure through metal or metal-chelate crosslinkers— helps increase the viscosity without the need for increasing the polymer concentration [Menjivar, 1986; Bartosek *et al.*, 1994; Romero-zeron *et al.*, 1994; Grattoni *et al.*, 2001; Nijenhuis, 2001].

The first crosslinked fluid was a guar gum system. The antimony system (a system that includes metallic elements, such as *Sb*) was a relatively-low-pH fracturing fluid. The borate fracture fluid was a high pH system, typically in the pH 10 range, while the antimony was approximately pH 3 to 5. The disadvantage of both antimony and borate systems in the early operations was that the fracturing treatments suffered in some cases with incomplete gel degradation. This incomplete degradation resulted in producing back very viscous gel that could possibly carry proppant back out of the fracture or even plug the fracture either temporarily or permanently [Nijenhuis, 2001].

In the 1980's the use of fracturing fluids with controlled crosslink time, or a delayed crosslink reaction, was examined. Crosslink time is simply defined as the time required observing a very large increase in viscosity as the fluid becomes rigid. Research work by Conway and Harris [1982] indicated that a delayed crosslink system allows better dispersion of the crosslinker, yields more viscosity, and improves fracturing fluid temperature stability. Another advantage of delayed crosslink system is lower pumping friction because of lower viscosity in the tubular goods [*Conway and Harris, 1982; Harris, 1985; Gidley et al., 1990*].

The major advantages of using a crosslinked gel versus a linear gel are: a) achieving much higher viscosity with crosslinked gel with a comparable gel loading, b) a crosslinked gel is more efficient from the fluid-loss point of view, c) a crosslinked gel has better proppant transport, d) a crosslinked gel has better temperature stability, and e) a crosslinked gel is more cost-effective than a linear fluid. For a formation which is deep and with high temperature (such as the Bakken Formation) if one requires high fracturing fluid viscosity, the ideal fracture fluid would be a zirconium or titanium delayed crosslinked system [*Harris, 1985; Gidley et al., 1990*].

Above all, an ideal fracturing fluid should be moderately efficient. This means that a high amount of the fluid should stay in the fracture and not be lost to the formation. Fluid efficiency is normally attained by combining high fluid viscosity with fluid-loss additives. The fracture volume is created by that portion of the injected pad that stays in the fracture and does not leak off into the formation (Figure 22). As is shown in this figure, fluid leak-off occurs linearly through the fracture faces, and can be defined by a parameter called “fluid loss coefficient” as:

$$\text{fluid loss coeff.} = \frac{\text{vol leaked - off}}{\text{area} \times \text{time}} \equiv \left[\frac{\text{length}}{\text{time}} \right] \quad (23)$$

This fluid loss coefficient is then used to determine the fluid efficiency:

$$\text{fluid efficiency} = \frac{\text{frac vol created}}{\text{total fluid pumped}} \quad (24)$$

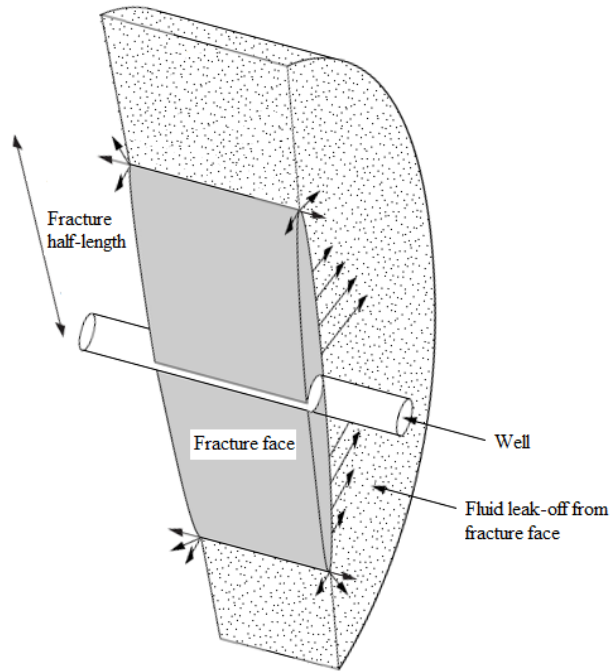


Figure 22. Fluid leak-off from a longitudinal fracture during a fracturing treatment

Proppant Transport in Hydraulic Fractures

The fluid pressure inside the created hydraulic fracture keeps it open during the fracturing treatment. The proppant mixed with the fracturing fluid keeps the fracture open when pump is shut off after the treatment. Actually, the success of a fracture treatment depends on three main factors: a) the propped length of the hydraulic fracture, b) the conductivity of the fracture, and c) the propped height of the fracture. Fracturing fluid and proppant characteristics together with the amount and their injection manner are the controlling parameters for the above factors.

The sequences of events in a hydraulic fracture treatment include: 1) injecting a fluid with low viscosity with no proppant for fracture initiation, which is called “pre-pad”, 2) injecting a fluid with relatively higher viscosity that does not contain any proppant in the fracture to help fracture propagation, and is called “pad”, 3) injecting slurry into the created fracture that is a mixture of proppant, fracturing fluid, and additives. The proppant concentration starts at lower values and increases as the treatment progresses. As the slurry moves inside the fracture, the proppant will move downward and settle depending on the viscosity of the fracturing fluid.

A propping agent moving inside the fracture is subjected to three forces: a) gravity force, b) buoyancy force, and c) drag force. Fluid and particle characteristics are the main controlling parameters for the proppant settlement process. According to Stoke’s law, the distribution of proppant (with spherical shape) inside the fracture depends on its settling velocity in the fracturing fluid [Gidley *et al.*, 1990]:

$$C_D = \frac{4}{3} \frac{\rho_p - \rho_f}{\rho_f} \frac{g d_p}{v_t^2} \quad (25)$$

Where C_D is the drag coefficient, g is gravity acceleration, d_p is particle diameter, v_t is terminal particle-settling velocity, and ρ_p and ρ_f are proppant and fluid densities, respectively.

Note that terminal velocity is the velocity of a single particle in an infinite medium. For non-Newtonian fluids, it is assumed that the fluid viscosity (μ_f) can be replaced with an apparent viscosity (μ_a) in Newtonian correlations for estimating the particle settling velocity. Some researchers such as Vassilios [2003] embraced this approach. The following equation is proposed for single particle settling velocity calculation for power-law fluids [Gidley *et al.*, 1990]:

$$v_t = \left[\frac{gd_p^{n+1}(\rho_p - \rho_f)}{18K(3)^{n-1}} \right]^{1/n} \quad (26)$$

Where n is flow-behavior index and K is flow-consistency index. For power-law fluids one can define the apparent viscosity (μ_a), corresponding to the viscosity of Newtonian fluids. The apparent viscosity can be calculated from

$$\mu_a = K(\dot{\gamma})^{n-1} \quad (27)$$

For Newtonian fluids, the drag coefficient can be obtained as follows:

$$C_D = \frac{24}{N_{Re(p)}} = \frac{2F_d}{A_p \rho_f v_t^2} \quad (28)$$

where,

$$N_{Re(p)} = \frac{d_p \rho_f v_t}{\mu_f} \quad (29)$$

Where $N_{Re(p)}$ is particle Reynolds number, μ_f is fluid viscosity, A_p is particle frontal area, and F_d is the Drag force. The settling velocity for Newtonian fluids is also given by Youness [2005]:

$$v_t = \frac{gd_p^2(\rho_p - \rho_f)}{18\mu_f} \quad (30)$$

The ideal proppant should be strong, resistant to crushing, resistant to corrosion, have a low density, and readily available at low cost [Holditch, 2011]. The proppant placed in the created hydraulic fracture is under the effective minimum in-situ stress (σ_{eh}) as fracturing fluid leaks off into the formation. This effective stress is also called fracture closing stress (FCS).

$$FCS = \sigma_{eh} = \sigma_h - p_f \quad (31)$$

Where σ_h is the minimum horizontal stress and p_f is the fluid pressure inside the fracture. A number of materials that best meet these desired traits are silica sand, resin-coated sand, and ceramic proppants.

Depending on the strength of the formation and the type of the proppant, different fracture closing state would result (Table 2). Table 2 shows how the resulting fracture conductivity is dependent on both the proppant type (quality of the material) and the formation rock properties.

Table 2. Behavior of different proppants under closure stress (*Courtesy of Prod. Tech.*)

		Sand Grains	Soft Proppants	Hard Proppants
Hard Rock	Closure Stress not Applied			
	Closure Stress Applied	Crushing 	Deformation 	Little Embedment

Soft Rock	Closure Stress not Applied			
	Closure Stress Applied	Crushing and Embedment 	Deformation 	Much Embedment and Embedment

The drawbacks of using a wrong type of proppant in the fracturing treatment would be: a) crushing of proppants under closure stress that results in reduced proppant conductivity, b) deformation of soft proppants which leads to reduced fracture width, and hence diminished fracture conductivity, and c) proppant

embedment in the fracture wall leads to further reduction of hydraulic fracture conductivity.

The available proppant types used in the industry are listed in Table 3, and the effect of fracture closure stress on the propped-hydraulic fracture is illustrated in Figure 23. It is clear from Figure 23 that the more rounded a proppant, the higher its conductivity. This means that a well rounded proppant has a better strength since the closure stress will be spread more evenly on the surface of the proppant, which in turn, yields a better fracture permeability.

Table 3. Cost and resistance to crushing for different proppant types (*Courtesy of Prod. Tech.*)

Proppant Type	Resistance to Crushing	Cost
Low quality sand (LQS)	Low	Low
High quality sand (Ottawa sand)	↓	↓
Resin-coated sand (RCS)		
Intermediate strength proppant (Ceramic)		
High strength proppant (Bauxite)	High	High

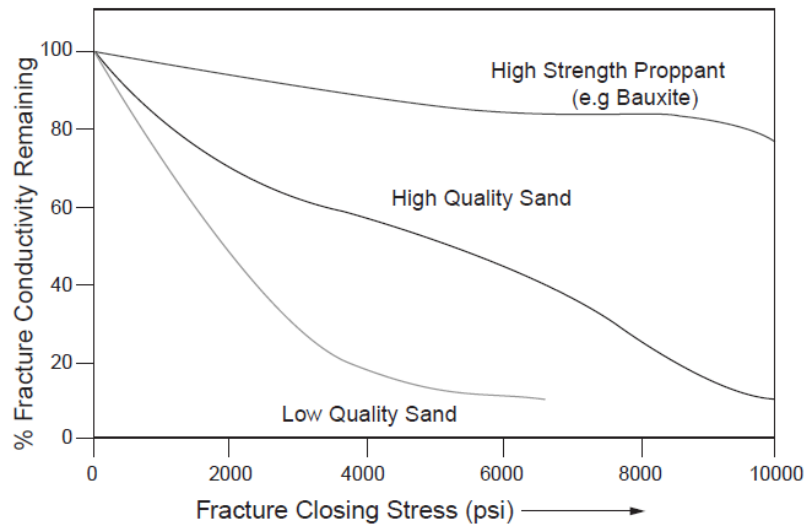


Figure 23. Fracture conductivity versus Fracture Closure Stress (FCS) (*Courtesy of Production Technology*)

From Figure 23, it can be inferred that: a) the low quality sand— especially when it is not well-rounded— will begin to crush at low closure stresses (less than 200 psi), b) the higher quality sand, such as Ottawa sand (well-rounded), shows a much higher stress resistance, and c) proppants with best quality, such as bauxite, shows negligible crushing from closure stress and hence a small amount of deformation.

Generally, sand is used for hydraulic fracturing shallow formations (for e.g. coal seam reservoirs). The best choice for a propping agent in a coal seam reservoir would be sand where the reservoir is relatively shallow. Resin-coated sand is used where more strength is required since it is much stronger than low quality sand. The resin in the proppant acts as a glue to form a consolidated sand pack in the fracture. This will help to avoid proppant flow back into the wellbore when the pumping is halted after the treatment. It is clearly more expensive than the regular sand. High quality proppants, such as ceramic and bauxite, are the strongest in the list above. Ceramic consists of sintered bauxite, intermediate strength proppant (ISP), and light weight proppants (LWP). These high quality proppants are usually used where the reservoir is deep (i.e. more than 8000 ft) and large values of fracture closure stresses are applied on the propping agent [*Phillips and Anderson, 1985; Montgomery and Steanson, 1985; Terracina et al., 2010; Raysoni and Weaver, 2012; Cohen et al., 2013*].

Once the characteristics of the proppants, the fracturing fluids, and the formation rock are well understood, one can use them for the design of hydraulic fracturing treatments.

Slurry

Slurry is defined as the mixture of fracturing fluid and proppant, and can be categorized into two groups: Newtonian and non-Newtonian slurry. There has been a great deal of research examining the increase in the viscosity of a Newtonian fluid when mixed with solid particles (proppant) [Einstein, 1956; Landel *et al.*, 1965; Thomas, 1965; Howard and Fast, 1970; Nicodemo *et al.*, 1974; Jeffrey and Acrivos, 1976; Faulkner and Schmidt, 1977; Hannah *et al.*, 1983; Acrivos, 1987; Fang *et al.*, 1997; Brannon *et al.*, 2005].

Einstein [1956] developed an early expression for calculating the slurry viscosity which was valid only for infinitely dilute particle concentrations:

$$\mu_s = \mu_o (1 + 2.5\phi_s) \quad (32)$$

Where μ_s and μ_o are the viscosities of slurry and carrier fluids, respectively. ϕ_s is the volume fraction of the solid phase.

Thomas [1965] presented an excellent correlation of slurry viscosity as a function of volume fraction of solids. This correlation is for Newtonian fluids; however, if the base fluid and the slurry are evaluated at the same velocity, the relationship will reasonably approximate the non-Newtonian, power law case [Hannah *et al.*, 1983]. The correlation is as follows:

$$\mu_r = 1 + 2.5\phi_s + 10.5\phi_s^2 + 0.00273 e^{(16.6\phi_s)} \quad (33)$$

Where μ_r is the relative viscosity of the highly solid concentrated slurry to the dilute one and ϕ_s (the volume fraction of solid) can be converted to oil field unit as follows:

$$\phi_s = \frac{C_p}{\rho_p + C_p} \quad (34)$$

Where C_p is the proppant concentration added in *lb/gal*, and ρ_p is the absolute density of proppant, in *lb/gal* as well.

Landel et al. [1965] developed an equation from the data of water with suspended glass beads and copper powder with the grain sizes ranging from 10 to 100 μm to meet the conditions of both infinite dilution and high solid concentrations. Their expression is given by:

$$\mu_r = \left(1 - \frac{\phi_s}{\phi_{s \max}}\right)^{-2.5} \quad (35)$$

Another expression for zero-shear relative viscosity of slurry was developed by Graham [1980] in that he assumed that hydrodynamic forces dominated the fluid flow around the particles interactions were also accounted for in his model:

$$\mu_r = 1 + 2.5\phi_s + \frac{2.5}{1 + h/a} \left[\frac{1}{h/a} - \frac{1}{h/a - 1} - \frac{1}{(h/a + 1)^2} \right] \quad (36)$$

Where h/a is the ratio of particle spacing to particle radius. For simple cubic packing

h/a is given by [Alkhatami, 2007]:

$$\frac{h}{a} = 2 \left[\frac{1 - (\phi_s / \phi_{s \max})^{2/3}}{(\phi_s / \phi_{s \max})^{1/3}} \right] \quad (37)$$

Frankel and Acrivos [1987] extended the previous research by developing a relationship for calculating the slurry viscosity when the solid load is relatively high

$(\phi_{s \max})$. The relative viscosity of the highly solid concentrated slurry to the more dilute one, and for spherical solid particles is given by [Shah, 1993]:

$$\mu_r = \frac{9}{8} \left(\frac{\phi_s / \phi_{s \max}}{1 - (\phi_s / \phi_{s \max})^{1/3}} \right) \quad (38)$$

Some authors believed that slurry viscosity can be a function of flow shear rate—even for Newtonian fluids [Nicodemo *et al.*, 1974; Jeffrey and Acrivos, 1976]. Correspondingly, it is even more likely to happen that the viscosity of non-Newtonian slurry is influenced by its shear rate.

Actually, slurries exhibit a Newtonian behavior at low volume fractions of solids but may exhibit non-Newtonian behavior at high solids concentrations [Ackermann and Shen, 1979; Satchwell *et al.*, 1988; Tsai *et al.*, 1989; Agarwal *et al.*, 1990; Dabak and Yucel, 1986]. This means that the viscosity equation must incorporate the shear-rate effect. Above a threshold volume fraction, the rheological behavior of many Newtonian slurries can be described by either a pseudoplastic-type model or Bingham plastic model [Shah, 1993]. The generalized equation for fracturing fluid rheology is given by [Baree and Conway, 1994; Alkhatami, 2007]:

$$\mu = \mu_o (1 - C_n)^{-a} \frac{\tan^{-1} \left(\left[\frac{\gamma}{\gamma_L} \right]^{n_o - 1} \right)}{\tan^{-1} \left(\left[\frac{\gamma}{\gamma_H} \right]^{n_o - 1} \right)} \quad (39)$$

Where n_o is the clean fluid power-law flow behavior index, γ_L is the adjustable parameter to match onset of deviation of low shear viscosity from the calculated power-law viscosity, γ_H is the adjustable parameter to match onset of deviation of

high shear viscosity from the calculated power-law viscosity, a is the slurry viscosity increase exponent, and C_n is equal to:

$$C_n = \frac{C_v}{C_{v \max}} \quad (40)$$

Where C_v is the volume fraction of solid and $C_{v \max}$ is the maximum volume fraction of solid.

CHAPTER III

HYDRAULIC FRACTURING DESIGN METHODOLOGY

Low permeability shale formations, such as the Bakken, require a large fracture network to enhance well productivity. Horizontal drilling and hydraulic fracturing play major roles in enhancing the hydrocarbon production from the Bakken Formation, Williston Basin. This chapter presents an integrated fracture/reservoir simulation, coupled with economic analysis to compare different fracture treatment scenarios for Bakken horizontal wells.

In this research, through a comprehensive fracture-simulation/reservoir-performance study, we have evaluated the main parameters controlling the fracture stimulation in horizontal wells. The main goal was to investigate opportunities to optimize hydraulic fracturing and production of horizontal Williston Basin Bakken Formation wells. The project area used in the investigation was located in Williams County, North Dakota. To design a successful hydraulic fracture treatment, four main tasks were carried out: First, a reservoir simulation to evaluate the response of the reservoir to fracture stimulation and to calibrate the reservoir model was performed using a two steps involving: a) sensitivity analysis (SA) to determine the significant well/reservoir properties and parameters and b) history matching (HM) the simulation results to the production data from a stimulated horizontal well in the study area.

Second, the amount of fracturing materials was estimated and preliminary pump schedules were developed based on selected design parameters including: fracture half-length, pump rate, and maximum proppant concentration. Next, design parameters screen was conducted using 2D fracture geometry solutions for fracture treatment parameters. An optimization task was then performed to identify optimal stimulation treatment(s) that together with optimal operating conditions would return a maximum value for the objective function (i.e. net present value or cumulative oil production).

As a next step, fully-3D hydraulic fracture modeling was utilized to perform implicit, coupled, finite difference/finite element solutions to basic conservation equations. The pump schedule— obtained from the scoping design— was changed in terms of the pad volume and proppant schedule for treatment optimization. The overall goal of such a schedule refinement was to place the right amount of proppant in the right place along the fracture, leading to fracture confinement in the Bakken Formation.

Finally, a comprehensive approach to the uncertainty assessment of the complex numerical simulations was performed which is applicable to support decision- and policy-making processes in well stimulation planning. The approach comprised of several steps to establish the assessment goals. A surrogate modeling technique along with Monte Carlo simulation was utilized for uncertainty assessment of the fracturing treatments planned by optimization task. Factor uncertainties were presented probabilistically, which were characterized by the principle of probability theory, and propagated via Monte Carlo simulation methodology.

Introduction

In recent years, there have been several studies on the simulation of horizontal wells in the Bakken Formation [Wiley *et al.*, 2004; Phillips *et al.*, 2007; Besler *et al.*, 2007; Lolon *et al.*, 2009; Zander *et al.*, 2011]. The main goal in the Bakken reservoir studies has been to simulate the production performance of the wells producing from the formation, and to come up with best scenarios for further field developments. Breit *et al.* [1992] used reservoir simulation to compare multi-well to single-well completions in the Bakken Formation. In their modeling, they considered a homogeneous layer with dual porosity and with an anisotropic permeability ratio of 4 to 1.

Lentz *et al.* [2007] described the benefits of re-fracture treatment in horizontal wells in the Middle Bakken Formation. They concluded that more perforations and diversion techniques would be attributed to the success of the treatments. Besler *et al.* [2007] studied the stimulation and operation of horizontal completions in the Middle Bakken Formation of North Dakota and Montana. They compared the production histories of the fractured horizontal wells to offset wells completed with other techniques to evaluate best industry practices.

Cox *et al.* [2008] investigated the production performance of Bakken wells, and by using reservoir simulation and pressure transient analysis, they evaluated the optimal economics in the early phase of Bakken development. Shanqiang *et al.* [2011], on the other hand, studied more complex fluid flow physics and stimulation practices in making long-term production forecasts for unconventional reservoirs. They proposed a probabilistic reservoir simulation workflow to provide realistic range of production forecast with application in the Bakken Formation.

Design of Hydraulic Fracturing Treatment— Recipe for Success

Hydraulic fracture stimulation is required for economic development of low permeability reservoirs, such as the Bakken Formation. This is because a highly conductive fracture results in a negative skin. At the same time, there is no single fracture treatment design that is best in all possible cases. The amount of knowledge about the treatment environment shapes the design process to a very large degree. When the area to be hydraulically fractured is new, there are generally a large number of potential uncertainties that may have effects on the production responses, such as static and dynamic parameters. As an example, Shanqiang et al. [2011] studied these uncertainties in the Bakken Formation through the use of a probabilistic reservoir simulation technique.

The best design depends very much on the environment in which the fracture treatment will be carried out. The characteristics that define the environment are: a) uncontrollable parameters, such as reservoir permeability, reservoir porosity, net sand thickness and areal extent, reservoir stress levels, reservoir temperature and pressure, reservoir fluid properties, barrier thicknesses, and adjacent barrier stress levels, and b) controllable parameters, such as wellbore casing, tubing and wellhead configurations, wellbore downhole equipment, lateral length, well spacing, perforation location and quantity (SPF^\dagger), fracturing fluid and proppant characteristics, and fracturing treatment rate and pumping schedule.

Carrying out a hydraulic fracturing job in horizontal wells is an expensive, complex undertaking. Hence, the volumes and types of the fracturing materials must be determined from a treatment optimization process. Basically, the main stages in the

[†] Shots per foot

creation of a propped hydraulic fracture include: a) the creation of an initial fracture of appropriate length and width by pumping fracture fluid called the pad. The most common fracturing fluids are water based, crosslinked, polymer solutions (or gels), which exhibit highly non-Newtonian rheological properties and appropriate fluid loss characteristics, b) the addition of proppant particles to the fracturing fluid at low concentrations, c) the increase of pump schedule proppant concentrations to compensate some of the proppant settled down due to greater particle density, d) the displacement of proppant slurry in the wellbore to the perforations at the end of the treatment when fluid injection ceases, and e) the continuation of fluid leak-off ending in fracture closure on proppant.

Conventional perception in designing a hydraulic fracture treatment for Bakken horizontal wells would suggest that successful stimulation requires creation of a long and highly conductive fracture. This means that we should pump a large volume of proppants and fluids at proper concentrations that are properly designed to transport the proppants deep into the hydraulic fracture. However, stimulation treatment plans are usually made through a comprehensive study including: a) goals descriptions (both short- and long-term), b) reservoir/fracture simulations, c) economic study (optimization), and d) uncertainty assessment [Allair, 2009; Mian, 2011].

Reservoir Simulation— Bakken

Using hydraulic fracture modeling and reservoir simulation, we investigated a hydraulic fracture treatment in the Bakken Formation. The main goal was to determine if the production performance of the stimulated well could be corrected to the type of the fracture fluid and proppants used. The results from this study can be used for future field development. Reservoir simulation was coupled with a

commercial hydraulic fracture simulator to create an expert system that could be used to design an efficient stimulation strategy for Bakken horizontal wells.

Reservoir simulation was used to perform four major tasks to provide insights into the optimization of hydraulic fracturing design. These tasks included: a) sensitivity analysis (SA) to determine how sensitive an objective function (an expression or single quantity) could be to different parameters and their ranges in values, b) history matching (HM) for calibrating the reservoir parameters conducted by an automated algorithm so that the simulation model could reproduce reservoir observations, c) optimization (OP) stage to come up with best scenarios for future hydraulic fracturing treatments, and d) uncertainty assessment (UA) to evaluate the impact of uncertainties on the objective function of optimal case(s).

The project area was located in section 36-T156N-R95W in eastern Williams County, North Dakota, on the eastern flank of the Nesson Anticline (Figure 24). The main goal in this research was to investigate opportunities to optimize the drilling, completion, and hydraulic fracturing treatments of horizontal wells in the Bakken Formation. In the area three horizontal wells were drilled and completed two of which were put on production and the middle well was used initially to deploy geophones for the microseismic monitoring of hydraulic fracture stimulation.

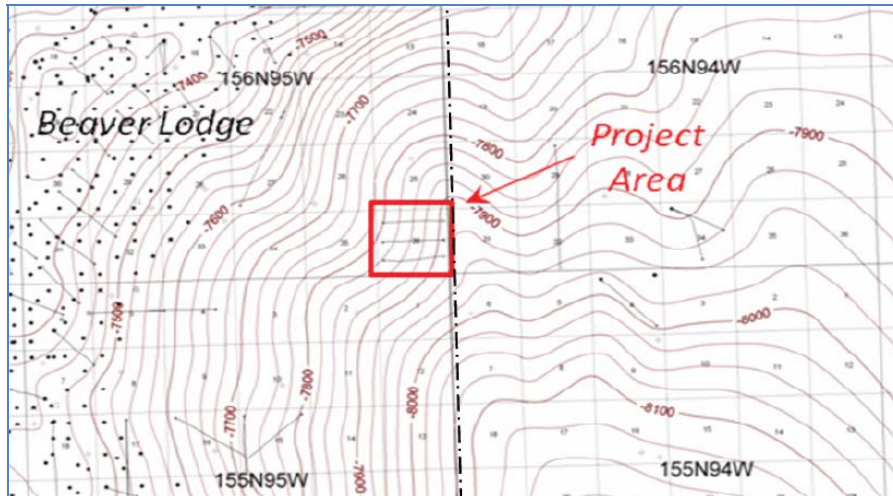


Figure 24. Project area location in eastern Williams County, ND [Courtesy of BRC[†]]

The Bakken Formatio Properties— Williams County

In the study area, the Bakken Formation consists of three members; an upper organic shale up to 25 ft thick, a middle silty carbonate and dolomitic/calcareous siltstone/sandstone up to 78 ft thick, and a lower organic shale up to 58 ft thick. The middle Bakken is composed of five lithofacies and varying in height [Heck *et al.*, 2002]. All five lithofacies are argillaceous rich and vary in regards to composition (Figure 25). Lithofacies 1, 4, and 5 enclose 2 and 3, which seems to contain the target zone of production [Gonzales and Callard, 2011].

[†] Bakken Research Consortium

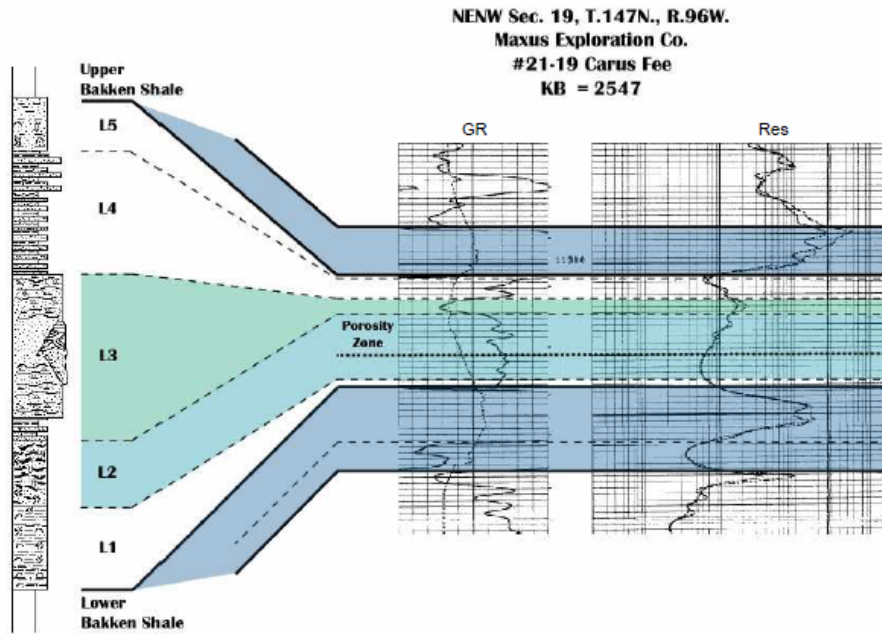


Figure 25. Lithofacies of the Bakken Formation [LeFever et al., 1991; Gonzales and Callard, 2011]

For reservoir characterization purposes, a number of studies were conducted on the wells by BRC including: taking cores from an interval of 10284-10466 ft (from the base of the Lodgepole Formation into the upper Three Forks Formation), analyzing the cores in the laboratory to measure porosity and permeability, and conducting detailed rock mechanics tests [Sturm and Gomez, 2009]. The properties of the Bakken Formation in the study area are shown in Table 4.

Table 4. Input parameters-- Bakken reservoir model [BRC, 2008]

Member of the Bakken Fm	Upper	Middle	Lower
Measured Depth at Top, ft	10,300	10,325	10,403
Thickness, ft	25	78	58
Matrix Porosity (%)	3.5-5.9	1.5-8.2	1.0-7.1
Matrix Permeability, md	0.00008- 0.00018	0.00017- 0.00373	0.00008- 0.00026
Reservoir Temperature, °F	250		
Res. Pressure (at datum), psi	6998	4600	7059
Water Saturation, S_w (fraction)	0.3	0.3	0.3
Acreage, ac	320		

Oil Gravity, °API	42
FVF, RBBL/STB	1.4
Rs, SCF/STB	700

Analysis of borehole image data indicated that both natural and induced fracturing would occur within the Middle Bakken [Sturm and Gomez, 2009]. FMI and logs run in the Nesson State wells also confirmed the presence of natural fractures in this area (Figures 26 and 27). These natural fractures appeared to be enhanced in specific lithofacies (brittle calcareous litologies) and by structural bending, but were limited in quantity (low fracture density) and were of very small aperture (Figure 28). Natural fracture parameters are listed in Table 5.

Table 5. Natural Fracture Data (Well 41X-36H, Middle Bakken) [Sturm and Gomez, 2009]

Fracture strike	NW-SE & NE-SW
Mean dip	>70°
Secondary Porosity (%)	0.0003-0.0005
NF Permeability, md	0.000001-0.001
NF Spacing (along lateral length), ft	87 - 266
Fracture aperture, inch	0.00002 – 0.00035
NF Orientation	NW-SE strike (σ_{hmin})
NF Dip	70°-90°
NF Status	All NFs are cemented along fracture faces.
NF extension	All NFs are bed-bound with height < 2f.t

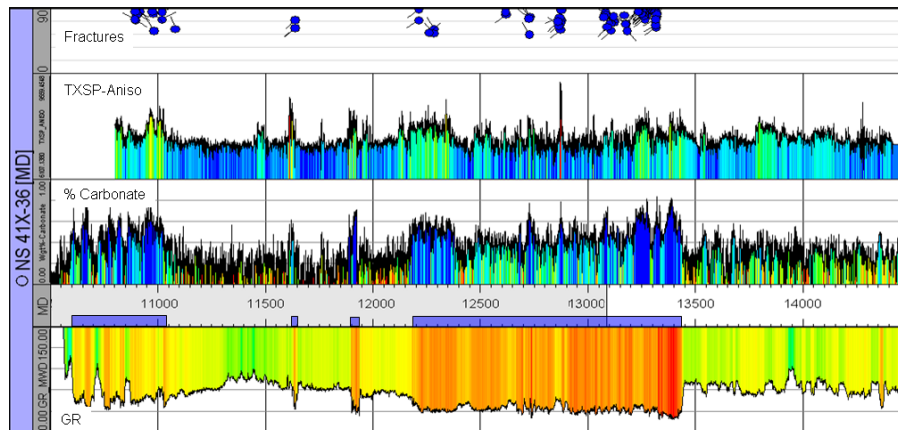


Figure 26. Nesson State 41X-36H lateral stratigraphy [Courtesy of Bakken Research Consortium]

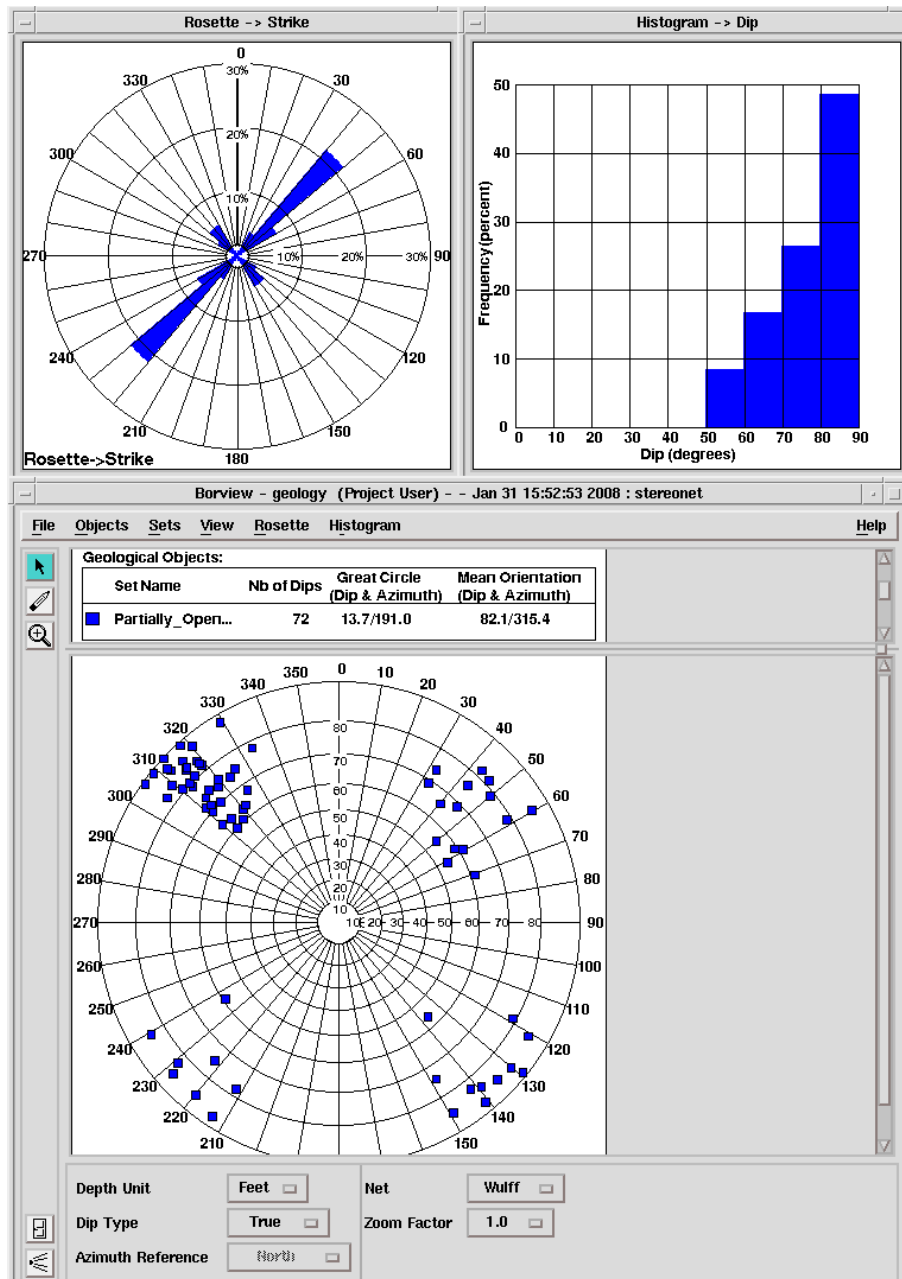


Figure 27. Natural fracture data in the study area [Sturm and Gomez, 2009]

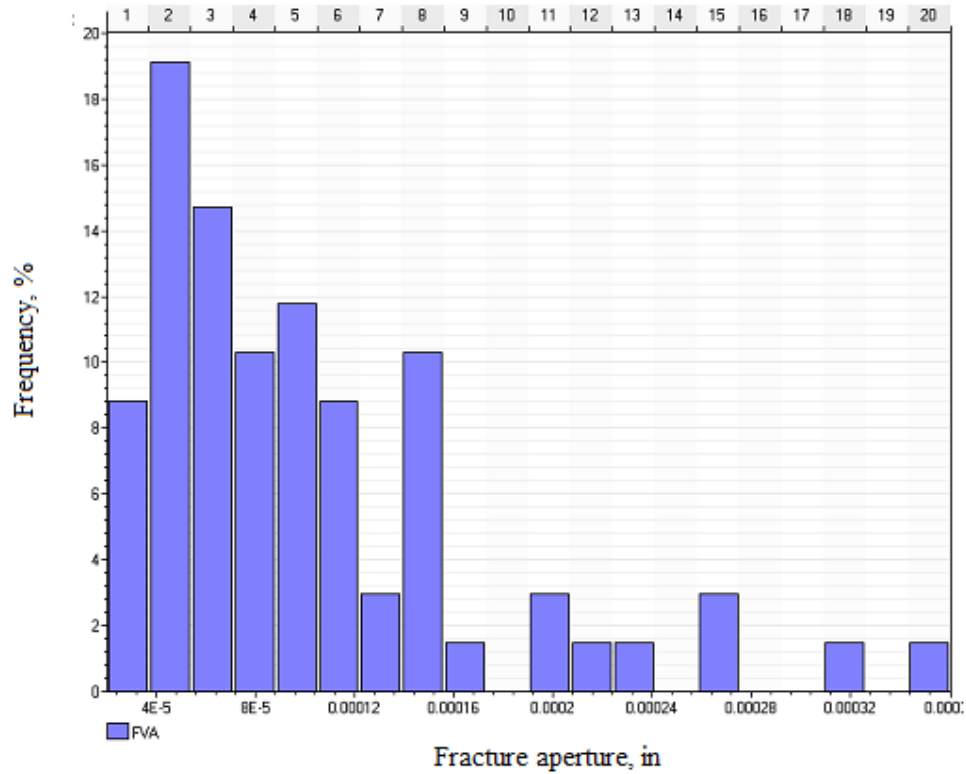


Figure 28. The distribution of natural fracture aperture (Well NS 41X-36H, Middle Bakken) [Sturm and Gomez, 2009]

In an effort to evaluate the reservoir response to hydraulic fracture treatment in Bakken horizontal wells, we have utilized reservoir simulation to generate the production profile for Well NS 41X-36H. We have used a dual porosity description for the purpose of reservoir simulation and history matching the production data.

A commercial fracture simulator was also used to estimate the created hydraulic fracture characteristics. The study well (NS 41x-36H) was completed with a pre-perforated 5" liner. The post completion wellbore construction is depicted in Figure 29 [BRC, 2008]. Note that the middle wellbore in the project area (Figure 24) was being used to conduct microseismic monitoring of the hydraulic fracture stimulation. Microseismic monitoring is a useful tool to provide accurate characterization of the locations, geometry, and dimensions of the hydraulic fracture system (Figure 29).

Single Lateral

As Drilled Well Construction Diagram

3.5 mi S of Tioga, ND on Hiway 40, 4 mi E on Hiway 2, 3 mi S on 102A Ave NW 1 mi E on 61st St NW, 1 mi S on 102 Ave NW, Well is on E side of rd

Nesson State 41X-36

Location: Sec 36 156N 95W
Footage: 200 FEL, 1140 FNL
Elev: Graded Pad 2369, KB 2390
Williams County, ND

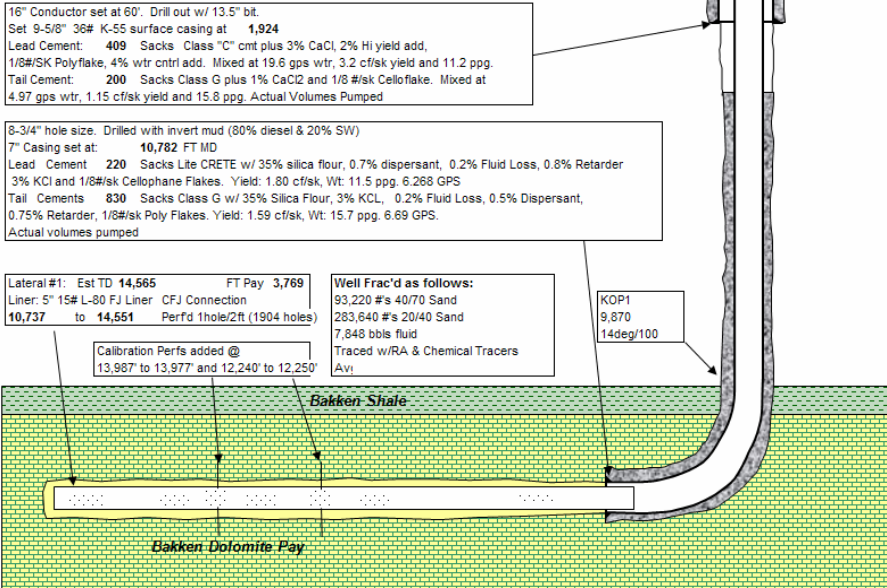


Figure 29. NS 41X-36H completed wellbore configuration (Courtesy of Headington Oil and BRC)

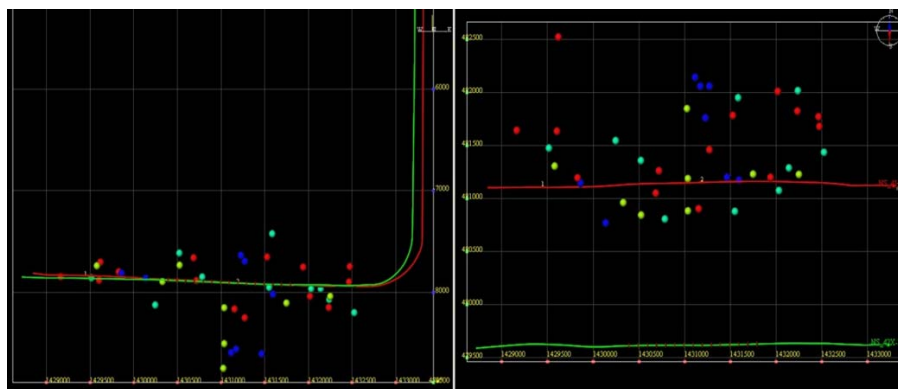


Figure 30. **Left:** Side view of the hydraulic fracture geometry, **Right:** Plan view of the hydraulic fracture geometry (well NS 41X-36H) (Courtesy of BRC)

Figure 31 also shows the estimation of stimulated reservoir area (SRA) while Figure 32 illustrates the stimulated-fracture-network height (SFNH) from the microseismic mapping data of Well NS 41X-36H, from which the SRV (a complex 3D structure) was approximated. While this method is not an analytically exact

calculation, it does provide a fast automated method to approximate a very complex 3D structure [Mayerhofer *et al.*, 2010]. Note that the hydraulic fractures have propagated in the direction of maximum principle horizontal stress which is NE-SW in this particular case [BRC, 2008].



Figure 31. Map view of the induced fracture area (well NS 41X-36H) (Courtesy of BRC)

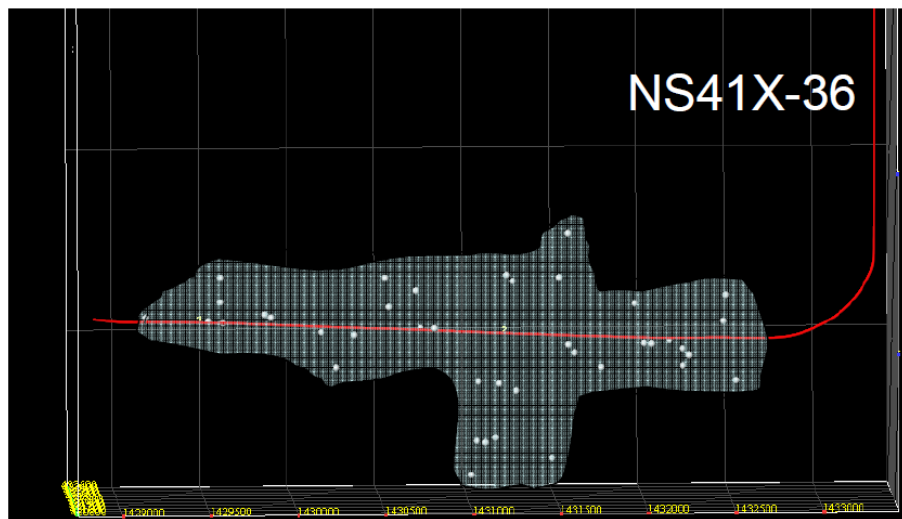


Figure 32. Side view of the induced fracture area (well 41X-36H) (Courtesy of BRC)

The stress state of the formation and the geomechanical properties as well as the properties of hydraulic fractures in the study area is shown in Table 6.

Table 6. Hydraulic fracture simulation parameters

Parameters	Values
Fracture Closure Gradient, psi/ft	0.7
Young's Modulus, MMpsi	
<i>Upper Bakken</i>	3
<i>Middle Bakken</i>	7.5
<i>Lower Bakken</i>	3
Poisson's Ratio	0.29
Stress Gradient, psi/ft	
<i>Upper Bakken</i>	0.8
<i>Middle Bakken</i>	0.7
<i>Lower Bakken</i>	0.8
σ_v , psi	11,000
σ_{hmin} , psi	7,000
σ_{Hmax} , psi	7,300
Hydraulic Fracture Data	
<i>HF treatment technique</i>	1-stage (pre-perforated liner)
<i>Avg. Height, ft</i>	120
<i>Fracture half-length (x_f), ft</i>	1,500-1,800
<i>Total proppant, lb</i>	377,000
<i>SRV, MM ft³</i>	2,925
<i>Total fracturing fluid, BBLs</i>	7,848
<i>Avg. propped width, inch</i>	0.105
<i>Avg. fracture conductivity, md-ft</i>	24

Figure 33 shows the daily production data for Well 41X-36H, Figure 34 illustrates the daily oil production rate used as the first well constraint in the simulation models, and Figure 35 represents the cumulative production data from the well used for history matching purposes.

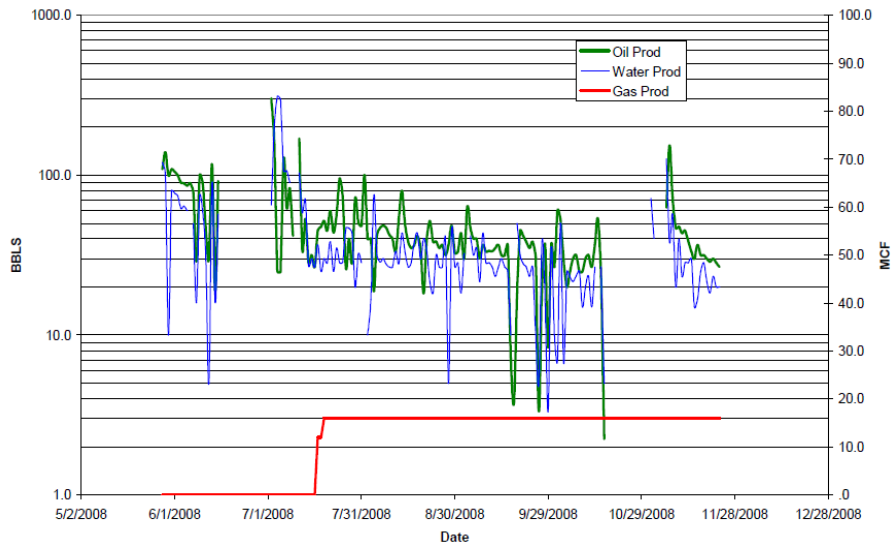


Figure 33. NS 41X-36H daily-production plot (Courtesy of BRC, 2008)

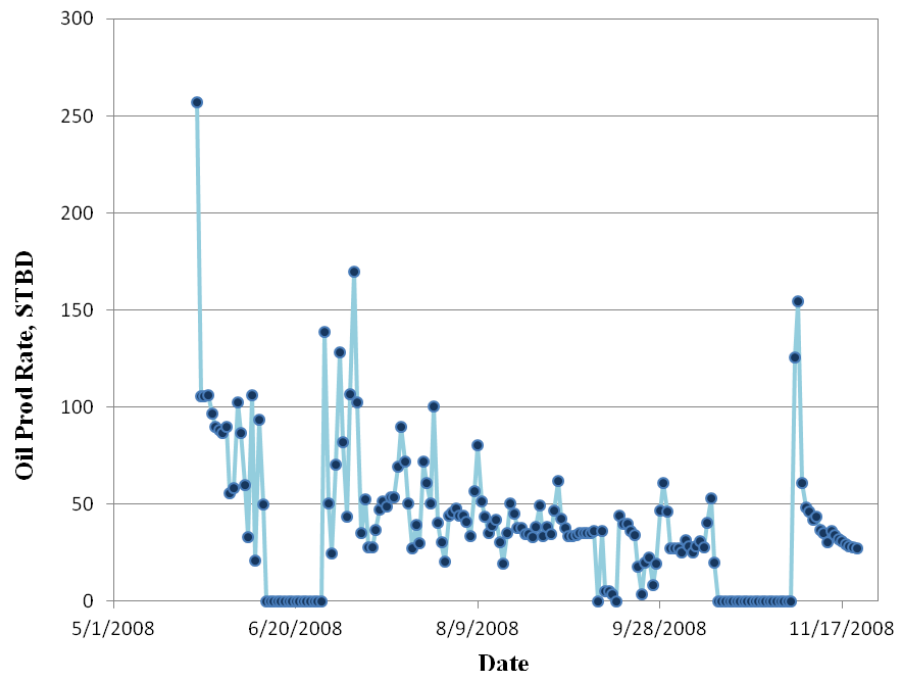


Figure 34. NS 41X-36H daily-oil-production rate (extracted from Figure 33)

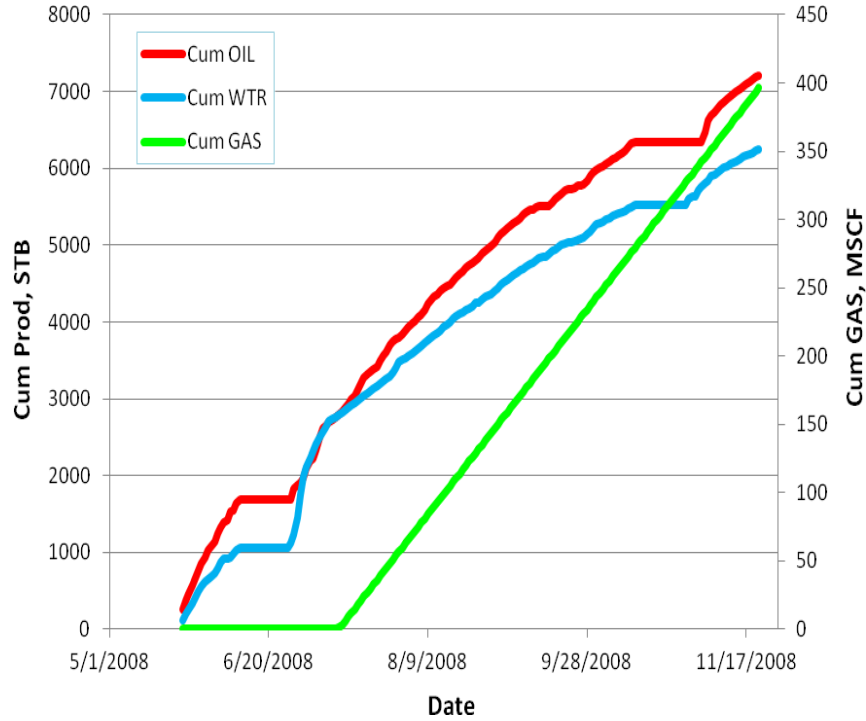


Figure 35. NS 41X-36H Cum-production plot

Based on experimental data, simplified models of relative permeability as a function of water saturation can be constructed. An often used approximation of relative permeability is the *Corey correlation* which is power-law in the water saturation [Brooks and Corey, 1964; Brooks and Corey, 1966]. The relative permeability curves were developed using Eqs.153-156 based on the definition of normalized water saturation value [Honarpour et al., 1986]. Note that there was no experimental data available for the relative permeability curves of the Bakken Formation. Hence, the end-point saturations were estimated from history matching the simulation results to historical data.

$$k_{rw} = k_{rwiro} \left(\frac{S_w - S_{wcrit}}{1 - S_{wcrit} - S_{oirw}} \right)^{n_w} \quad (41)$$

$$k_{row} = k_{rocw} \left(\frac{S_o - S_{orw}}{1 - S_{wcon} - S_{orw}} \right)^{n_{ow}} \quad (42)$$

$$k_{rog} = k_{rogcg} \left(\frac{S_l - S_{org} - S_{gcon}}{1 - S_{wcon} - S_{org} - S_{gcon}} \right)^{n_{og}} \quad (43)$$

$$k_{rg} = k_{rgcl} \left(\frac{S_g - S_{gcrit}}{1 - S_{gcrit} - S_{oirg} - S_{wcon}} \right)^{n_g} \quad (44)$$

Where k_{rocw} is k_{ro} at connate water, k_{rwiro} is k_{rw} at irreducible oil, k_{rogcg} is k_{rog} at connate gas, k_{rgcl} is k_{rg} at connate liquid, S_w is water saturation, S_{wcrit} is critical water saturation, S_{oirw} is irreducible oil for water-oil table, n_w is the exponent for calculating k_{rw} , S_{orw} is residual oil for water-oil table, S_{wcon} is connate water saturation, S_{org} is residual oil for water-oil table, n_{ow} is the exponent for calculating k_{row} , S_l is liquid saturation, S_{org} is residual oil for gas-liquid table, S_{gcon} is connate gas saturation, n_{og} is the exponent for calculating k_{rog} , and n_g is the exponent for calculating k_{rg} . Also, the linear relative permeability (X-curves) was considered for the grids containing the hydraulic fractures.

Dynamic Modeling and Simulations

The initial dynamic model (base case) was built using the data available in the literature. The base case was used to adjust the well/reservoir properties and parameters, and for history matching the reservoir simulation model to production history. The model was optimized through three steps before conducting history matching. The steps included: a) grid-size sensitivity analysis, b) numerical tuning, and c) properties/parameters sensitivity analysis. These calculations were made for

improving the numerical stability and run-time optimization. The validated and tuned model was then used for history matching and predictive simulations so as to achieve optimal fracturing treatments for Bakken horizontal wells.

Model Optimization and Validation

The optimization of dynamic model led to high-performance computations where we found a set of model specifications, for numerical keywords and structural assumptions, which returned minimal run-time and numerical failures. In history matching processes, on one hand, the range of parameter values and the number of parameter combinations may be too large for analysts to enumerate and test all possible scenarios, so they need a way to guide the search for good solutions. On the other hand, without model optimization, a simulation case may be too complex to be modeled. For this, the dynamic model was optimized and validated by using the dynamic modeling workflow depicted in Figure 36.

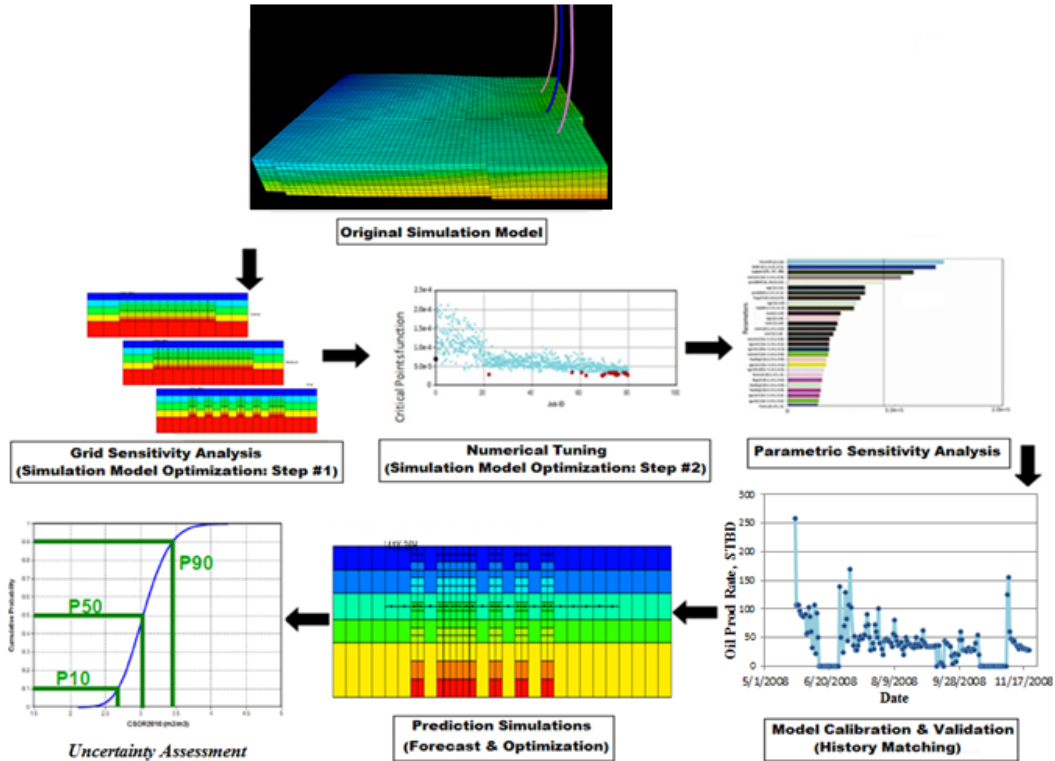


Figure 36. Workflow of dynamic simulation

Grid-Size Sensitivity Analysis

The grid size sensitivity is of prime concern in reaching reasonable grid size in any simulation study. It was intended to compare various grid sizes so that sufficiently large grid size could be determined. Three grid resolutions were examined: 100 by 100 ft, 200 by 200 ft, and 400 by 400 ft.

Fine grid: 100 × 100 ft; total 75,472 cells (includes refined cells)

Medium grid: 200 × 200 ft; total 30,200 cells (includes refined cells)

Coarse grid: 400 × 400 ft; total 9,760 cells (includes refined cells)

To examine the impact of grid size on reservoir performance, the cumulative production trends (*Cum_Oil*, *Cum_Gas*, and *Cum_WTR*) from the different cases were obtained and compared to each other (Figures 37-39).

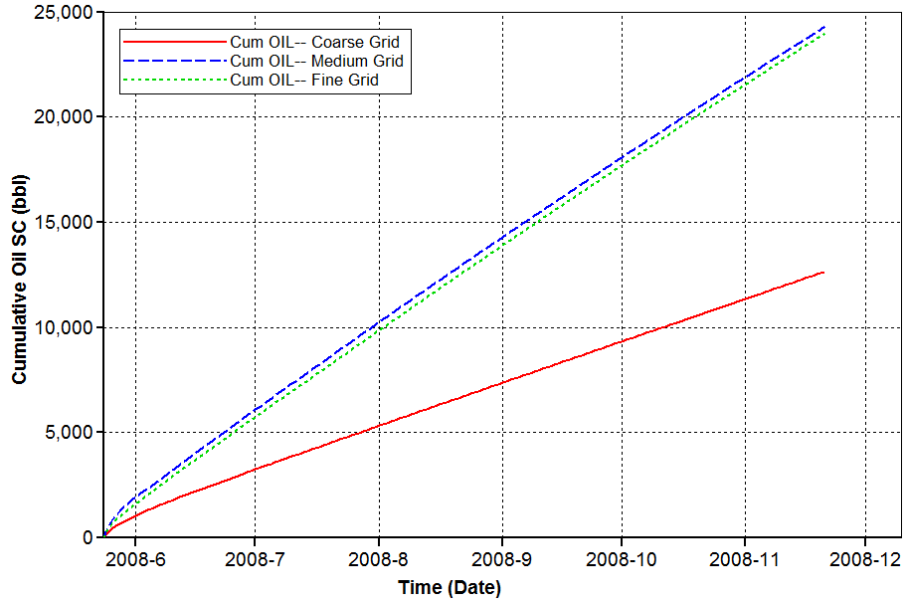


Figure 37. Sensitivity analysis on grid size— Cum Oil Prod

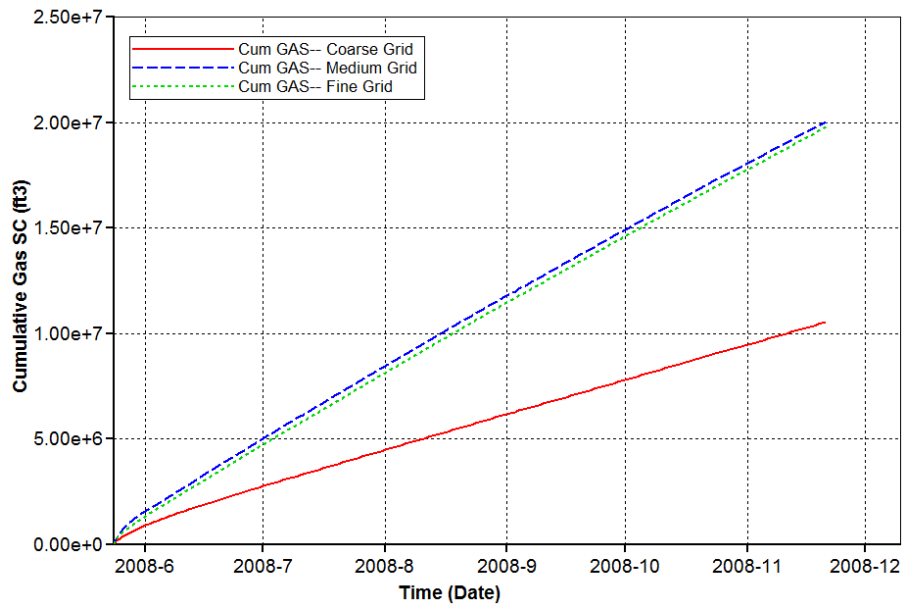


Figure 38. Sensitivity analysis on grid size— Cum GAS Prod

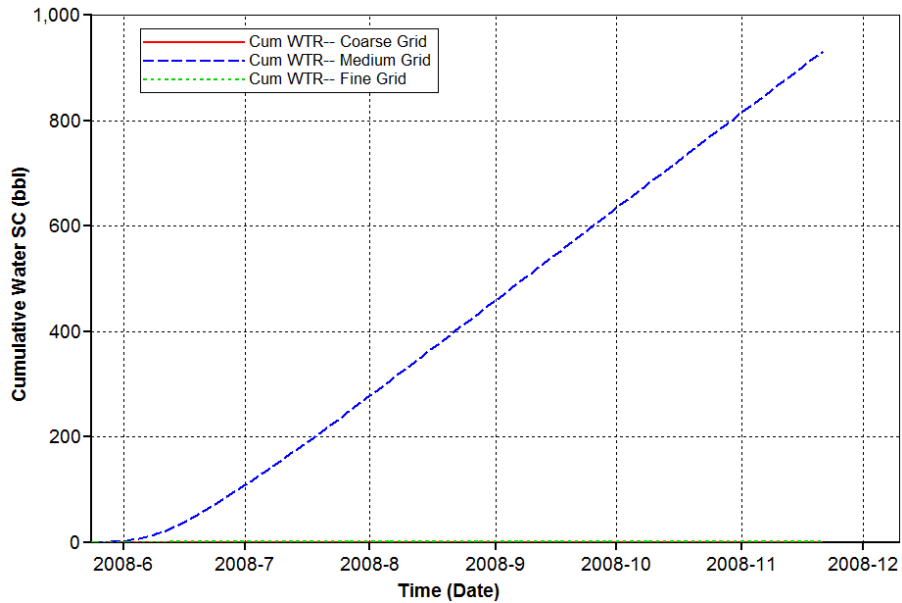


Figure 39. Sensitivity analysis on grid size— Cum WTR Prod

From these figures (37-39), it can be concluded that the medium grid size would yield adequate accuracy with regard to the cumulative production. The coarse grid size indicates under-prediction of recovery. Thus the 200×200 -ft grid resolution was chosen for further simulations in this project.

Numerical Tuning

The optimization of numerical settings was conducted to improve the run-time of the simulations. For the Bakken project, various numerical key words, such as *pressure change*, *saturation change*, and the *tolerance of convergence* over each time step were examined to tune the numerical settings in the simulation runs [Hutchinson, 1989; LeDimet et al., 1995; Griffith and Nichols, 1996]. The optimization of critical points used in the project included *material balance error*, *central processing unit time (CPU)*, and *solver failure percent*. The original run-time on a single job with 200×200 -ft grid resolution prior to the numerical tuning was almost 3.3 hours over an 8-

month simulation period (Figure 40). After numerical tuning, up to 69% reduction in the run-time was achieved.

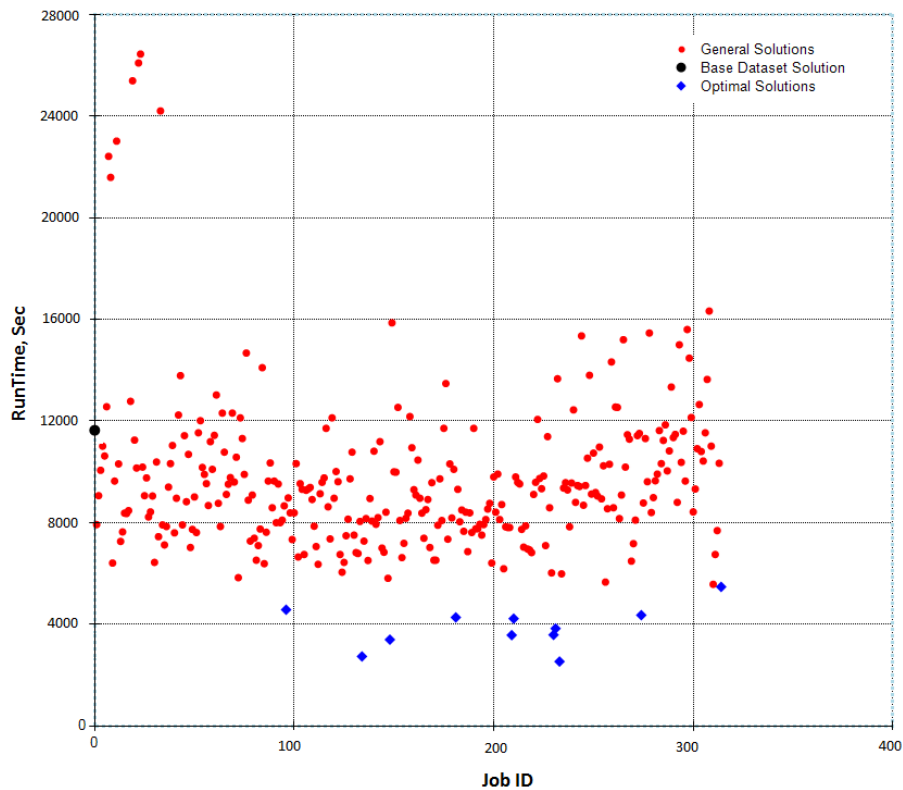


Figure 40. Numerical tuning of the reservoir model to improve run-time and solver failures

Sensitivity Analysis of the Reservoir Properties and Parameters

Sensitivity analysis is used to ascertain how a given model output depends upon the input parameters. This is an important method for tracking the significant parameters as well as a powerful tool for checking the reliability of the analyses [Saltelli *et al.*, 2004]. It will help reservoir modelers to achieve a better understanding of how different parameters influence the reservoir responses. The information from such analysis can later be used in other tasks, such as *History Matching*, *Optimization*, and *Uncertainty Assessment* as it helps determine which parameters to vary and to what degree.

A sensitivity analysis was conducted on the Bakken project. The parameters which were found significant were allowed to change over a realistic range during the history-matching process, which will be discussed later in this chapter. The ranges were selected based on the geology and the nature of the Bakken Formation that reflected close behavior of such an unconventional reservoir.

Sampling Method

For a given set of parameters and sample values, the parameter space is usually very large, and it would be too perplexing to select a reliable design (the set of job patterns). According to the theory of experimental design, an efficient design should have two characteristics to be acceptable [McKay *et al.*, 1979; Lawson and Erjavec, 2001; Cioppa, 2002;]:

- a) The input parameters should be approximately orthogonal. This means that in a design matrix, the correlation between the vectors of any pair of columns should be either zero or very small. An orthogonal design is very worthwhile in that it ensures independence among the coefficients in a regression model or Response Surface (RS). The correlation between two vectors $\vec{v} = (v_1, v_2, v_3, \dots)$ and $\vec{w} = (w_1, w_2, w_3, \dots)$ is given by the Orthogonality Index (*OI*) as below [Computer Modeling Group, 2012]:

$$OI = \frac{\sum_{i=1}^n [(v_i - \bar{v})(w_i - \bar{w})]}{\sqrt{\sum_{i=1}^n [(v_i - \bar{v})^2] \sum_{i=1}^n [(w_i - \bar{w})^2]}} \quad (45)$$

Where \bar{v} and \bar{w} are the averages of the two vectors. Generally, to ensure the accuracy of sensitivity analysis and uncertainty assessment results, the maximum pair-wise correlation of the design should be less than 0.15.

b) The sampling points (job patterns) should be evenly distributed in the parameter space. Or, in other words, the job patterns should represent all the possible job patterns (space-filling). The space-filling of the design in our simulation was assessed by the Euclidian minimum distance [Marie Deza and Deza, 2009] which is the minimum Euclidian distance of all design points (job patterns). This means that no two points are close to each other.

One common method to select a job pattern is random design, but its main disadvantage is that the interpretation of the results cannot be justified due to random confounding and the estimated coefficients can be biased [Cioppa, 2002]. To avoid such a problem of random design, we have used *Latin hypercube sampling* method proposed by Mckay et al. [1979], in that the input variables are considered to be random variables with known distribution functions. The parameters whose changes were examined in the sensitivity analysis are listed in Table 7. Each parameter was given a range of values over which it could vary.

Table 7. Parameters and properties examined in the Sensitivity Analysis & History Matching

Parameters	Base Value	Lower Level (-1)	Upper Level (+1)	History- Matched
PorMtrxMultiplier	1	0.5	10	10
PermMtrxMultiplier	1	0.5	10	10
PorFracMultiplier	1	0.5	10	10
PermNatFrac	0.001	0.00001	0.01	0.001
KvKhRatio	0.1	0.01	0.5	0.1
CPor_Mtrx	1.00E-06	2.00E-06	8.00E-06	8.00E-06
CPor_NatFrac	5.00E-06	1.00E-06	1.00E-05	2.00E-06
DI_NatFrac	200	100	1000	1000
DJ_NatFrac	200	100	1000	500
DK_NatFrac	50	20	500	185
Rel. Perm. Table -- Matrix				
swcon	0.1	0.05	0.2	0.1
swcrit	0.3	0.25	0.45	0.3
soirw	0.1	0.05	0.25	0.10
sorw	0.25	0.25	0.45	0.25
soirg	0.1	0.05	0.25	0.1
sorg	0.4	0.25	0.45	0.4
sgcon	0	0	0.02	0
sgcrit	0	0.01	0.06	0
krocw	1	0.3	1	1
krwiro	0.3	0.2	0.7	0.6
kgcl	1	0.4	1	0.9
krogcg	1	0.3	1	1
nw	2	1	3	1
no	3	2	5	3
nog	2	1	3	2
ng	2	1	3	2
Rel. Perm. Table – Nat. Frac.				
sgconf	0	0	0.01	0
sgcritf	0	0.01	0.06	0.06
sorgf	0.4	0.25	0.45	0.35
soirgf	0.1	0.05	0.25	0.15
sorwf	0.25	0.25	0.45	0.3
soirwf	0.1	0.05	0.25	0.1
swcritf	0.3	0.25	0.45	0.40
swconf	0.1	0.05	0.25	0.05
kgclf	1	0.4	1	0.90
krogcgf	1	0.3	1	0.90
krwirof	0.3	0.2	0.7	0.55
krocwf	1	0.3	1	0.9
nwf	1.5	1	2	2
nof	1.5	1	2	1.5
nogf	1.5	1	2	2
ngf	1.5	1	2	1.5
Swtr(i)	0.2	0.3	0.4	0.37
Hyd. Frac. Cond. (kfw), md-ft	22	22	500	22
SRV, million cu ft	2900	2000	3500	3200
Fracture spacing, ft	300	100	300	300
Fracture half-length	1500	1000	2000	1500

The results from 2300 simulation runs were collected and were investigated to screen the parameters (factors) which appeared to have significant effects on the response (objective function). The statistical significance of each effect and interaction was judged by comparing its signal-to-noise t-ratio, t_E (or t_{n-1}), to the critical t-value, denoted by $t_{\alpha/2}^*$. When the population standard deviation (σ) is unknown (i.e. small samples, or small n), we can replace it by an estimate, s_p , then the quantity in Eq.46 follows the *Student's T-distribution* with $n-1$ degrees of freedom (for n runs) [Lawson and Erjavec, 2001].

$$t_{n-1, \alpha/2} = \frac{\bar{Y} - \mu_o}{s_p / \sqrt{n}} \quad (46)$$

Note that the significance level (α), which is left to the investigator, was considered to be 5% as reasonable accuracy was required. Finally, we used a Tornado chart of the effects to determine the magnitude and the importance of the effects on the cumulative oil and cumulative water production. The chart displays the value of the effects. Any effect that extends past critical value is potentially important (Figures 41 and 42). From such sensitivity analysis, the significant parameters were found as listed in Table 7. The tornado plots in Figures 43 and 44 show only the significant parameters obtained from the *t-test*.

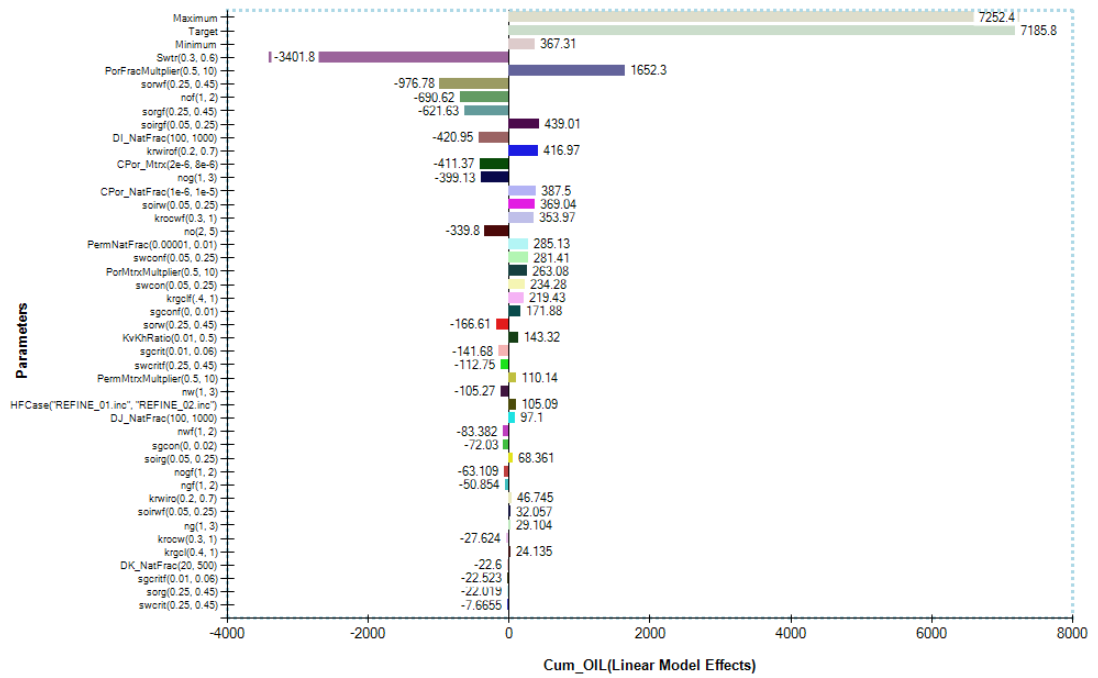


Figure 41. Tornado plot of Cum_OIL (linear model t-ratios)

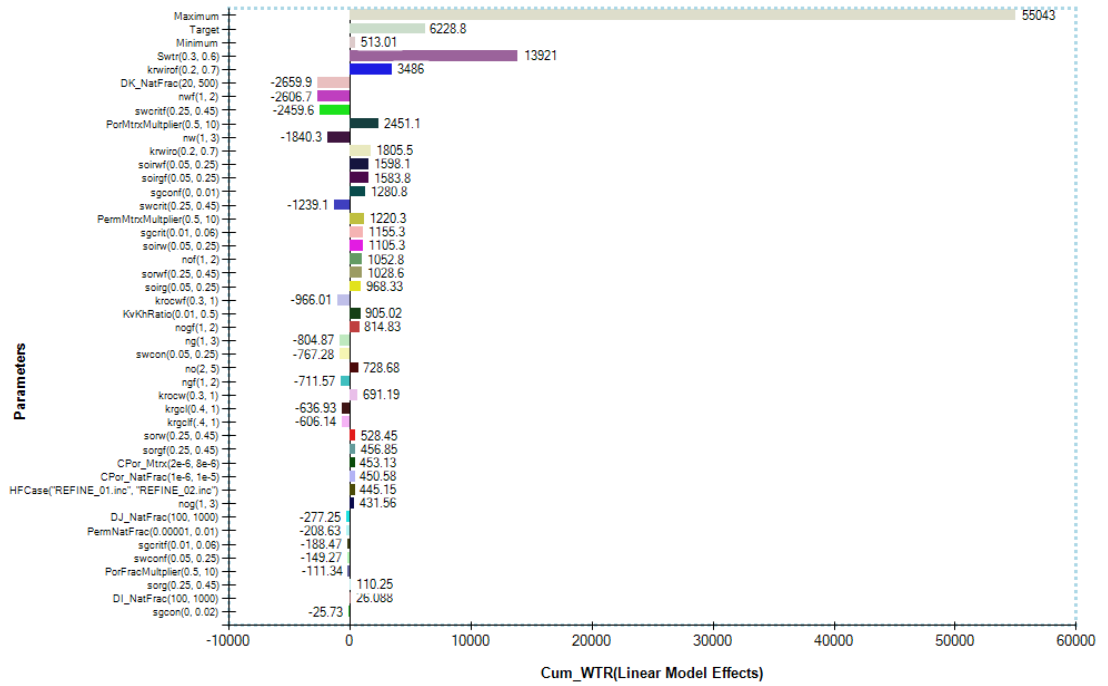


Figure 42. Tornado plot of Cum_WTR (linear model t-ratios)

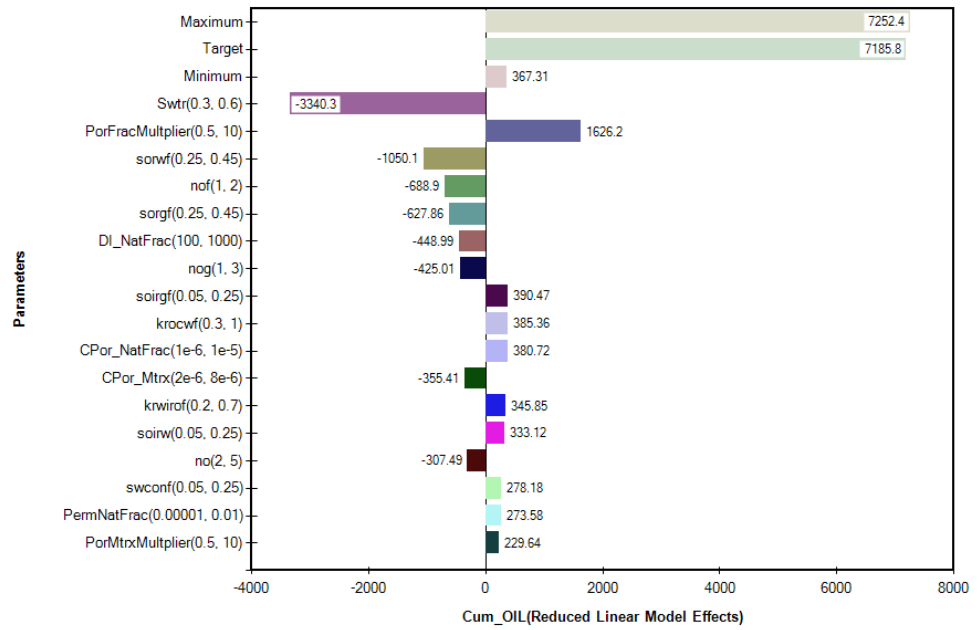


Figure 43. Tornado plot of Cum_OIL (reduced model)

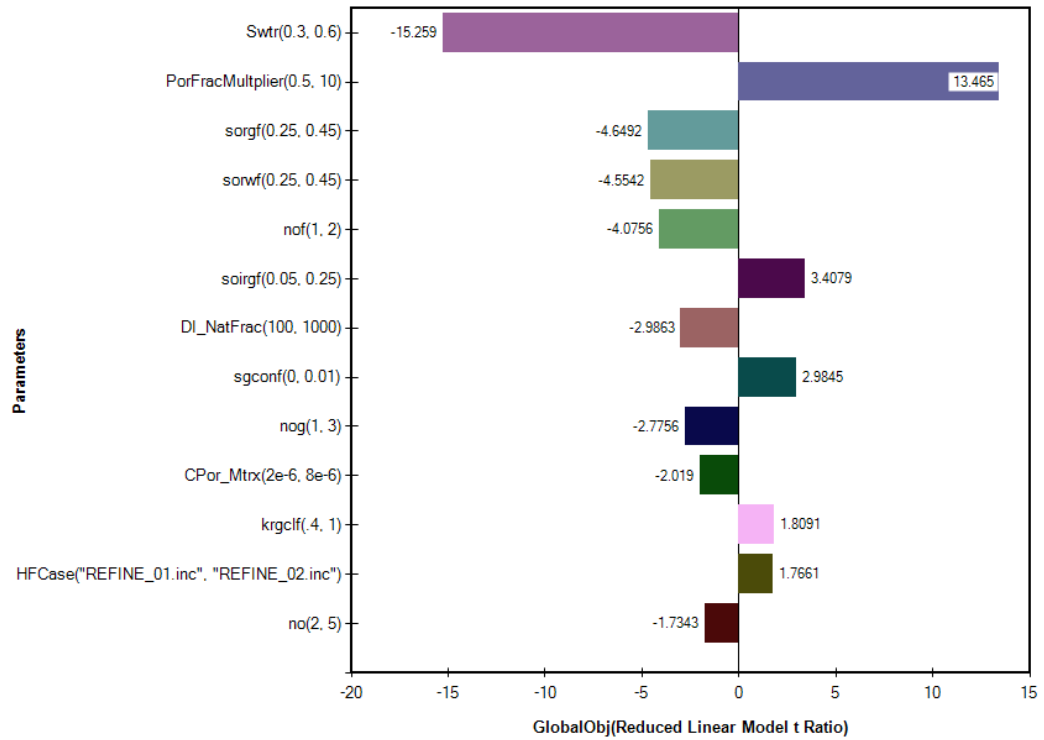


Figure 44. Tornado plot of GlobalObj function (reduced model)

History Matching

As a well-examined technique, history matching is a method of adjusting, or tuning, reservoir characteristics (properties) to match historical field data through an iterative trial-and-error process. The sensitivity analysis above helped us to find the significant parameters, as shown in Table 7. These parameters were then altered over realistic ranges in order to achieve a close match between the simulation results and field data. On the other hand, the insignificant parameters were set to constant values which were figured from the available data.

In the history matching process implemented in this study a global objective function was used to measure the relative difference between historical data and simulation results. In such a function the well variables are accounted for by means of a root-mean-squared error method (RMSE). Small values of objective function correspond to small differences between historical data and simulation results that is the main goal of history matching effort. The global objective function is given by Yang et al. [2007]:

$$E_g = \frac{1}{\sum_{p=1}^{N(w)} W_{w,p}} \sum_{p=1}^{N(w)} \sqrt{\frac{\sum_{t=1}^{T(w,p)} (R_{w,p,t}^s - R_{w,p,t}^m)^2}{T(w,p)}} \times W_{w,p} \times 100\% \quad (47)$$

Where, subscripts w , p , and t are well, production data, and time, respectively, $N_{(w)}$ is the total production data from well 1 to w , $W_{w,p}$ is weight, $T(w, p)$ is the total of time step, $R_{w,p,t}^s$ represents simulation results while $R_{w,p,t}^m$ is measured historical data, $\Delta R_{w,p}^m$ is the measured maximum change for well w and production data p , and $E_{w,p}^m$ is measurement error. The global objective function in Eq.47 was used for history

matching only *Cum_OIL* and *Cum_WTR* data of Well 41X-36H. By forcing the well to produce at historic oil rates the reservoir model was matched to the production history. The results are shown in Table 7.

History-Matching Procedure

To accomplish the history match of Well 41X-36H data, the cumulative oil production and the cumulative water production were compared to the observed field data. The concept of stimulated reservoir volume (SRV) was employed by assuming that a complex network of fractures would be created around the wellbore in such a shaly formation— through opening the micro-fissures/micro-fractures (natural fractures), and/or through the shear slippages of natural fractures within weak zones [Fisher *et al.*, 2004; Mayerhofer *et al.*, 2010].

This type of complex fracture network may look like a shattered windshield (Figure 45). Such a complex fracture network in many shaly formations are envisioned to be similar to that in a shattered glass, forming a series of flow paths reaching out a few hundred feet from the wellbore as confirmed by microseismic monitoring of the fracture treatments [King, 2012]. The microseismic events are created mainly as a result of shear slippages induced by altered stresses near the tip of the fractures (Figure 18), and shear slippages related to leakoff-induced pore-pressure changes. Since in tight shale reservoirs (the Bakken) the diffusivity-related pore-pressure changes would not move far from the actual fracture planes, the cloud of microseismic could be approximately equivalent to the actual fracture network size [Mayerhofer *et al.*, 2010].



Figure 45. Similarity between SRV and a shattered windshield [King, 2012]

The size of a complex fracture network can be estimated as the 3D volume of the microseismic-event cloud. It is important to note that the SRV is just the reservoir volume affected by the stimulation. Along with SRV, fracture spacing and conductivity within a given SRV are important as well [Mayerhofer *et al.*, 2010]. In this study, history matching was used to calibrate the reservoir model by way of an automated algorithm so that the reservoir observations were close enough to the calculated values. The value of SRV estimated from the history matching procedure is given in Table 7.

In the history matching process an automatic procedure was utilized to adjust the well/reservoir properties and to calibrate the reservoir model. Each simulation run generated a new set of input parameters which was evaluated for a next iteration [Landa and Guyaguler, 2003]. Figure 46 demonstrates the steps of the history matching procedure. The procedure repeats until the difference between historical data and simulation results become negligible that is figured by the global objective function error, given by Eq.47.

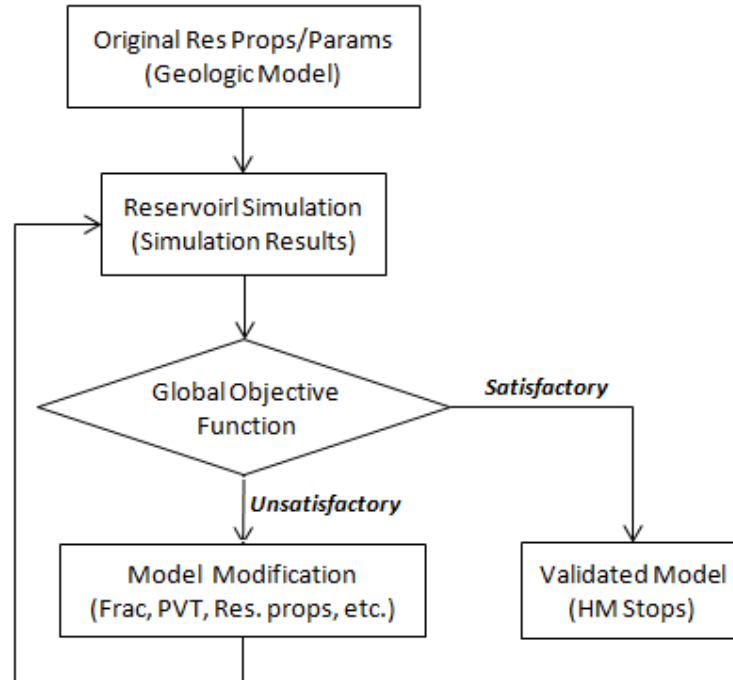


Figure 46. History-matching algorithm

In this procedure, sensitivity coefficients were used to construct a response surface or a proxy model, honoring the exact data values for the simulated combinations of the parameters. Response surfaces were constructed by the method of ordinary kriging to approximately reproduce costly reservoir simulation outcomes, which were actually utilized as surrogates or proxies to full simulations. The kriging method is a geostatistical estimator that infers the value of a parameter (random field) at an unobserved (un-simulated) location [Deutsch and Journel, 1998]. Experimental design was used to produce the most informative response surface given a limited number of actual simulation runs. In fact, the response surfaces were used to generate data for the numerical simulator at un-simulated points.

In most of the applications of response surfaces in reservoir engineering, the response surface is some form of a polynomial. However, the choice of the function to construct the response surface and the location of the sample points are critical in

obtaining a good proxy model for our study. For this, the ordinary kriging algorithm was used to construct the proxy model due to these features: a) kriging is data-exact, b) kriging can represent multi-dimensional data, c) it can handle irregular data, and d) it can be numerically constrained the gradient of data [Landa and Guyaguler, 2003].

History-Matching Results

Final history matching plot in Figure 47 shows the convergence of the objective function after 1467 iterations. Indeed, the small variation in the values of red dots, shown in Figure 47, indicates that the reservoir model can represent the actual reservoir case.

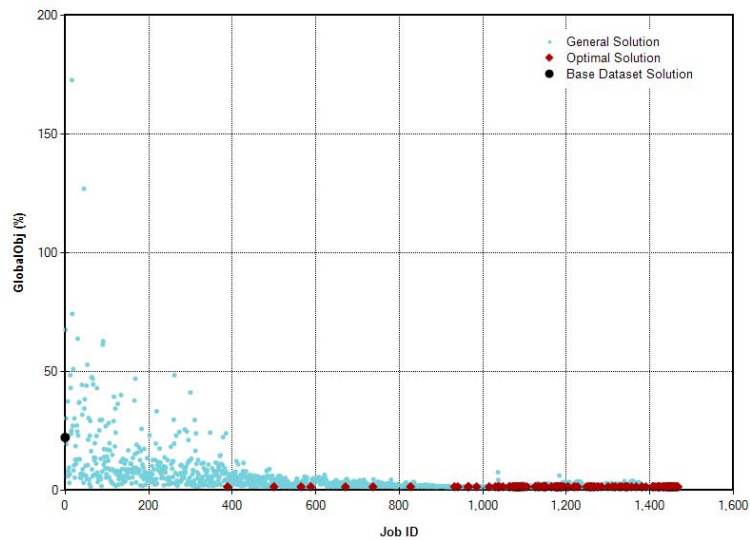


Figure 47. Final history-matching iteration of 1467 jobs showing the convergence of the objective function (red dots represent the cases with the lowest error values)

Using the history matching approach shown in Figure 46, the well/reservoir parameters for the studied sector of the Bakken Formation were estimated, as shown

in the far right-hand column of Table 7. As depicted in Figures 48, 49, and 50, reasonable matches were obtained for *OIL_PROD*, *Cum_OIL* and *Cum_WTR* trends.

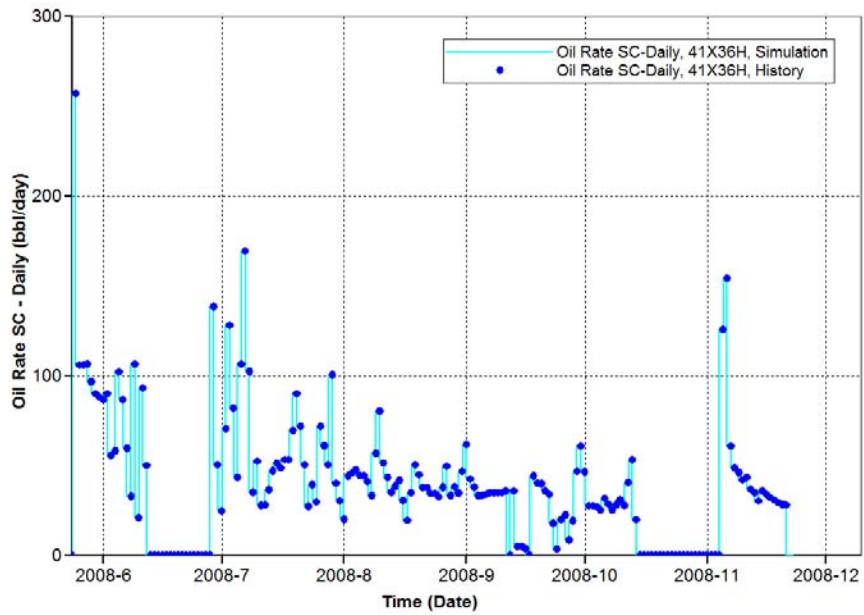


Figure 48. Oil production rate history match

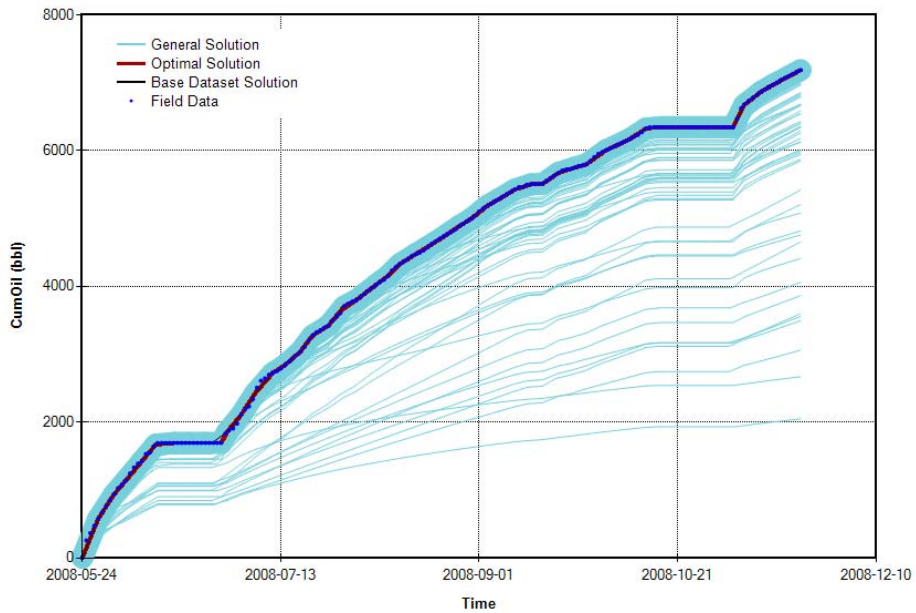


Figure 49. Cumulative oil production history match-- oil production rate constraint

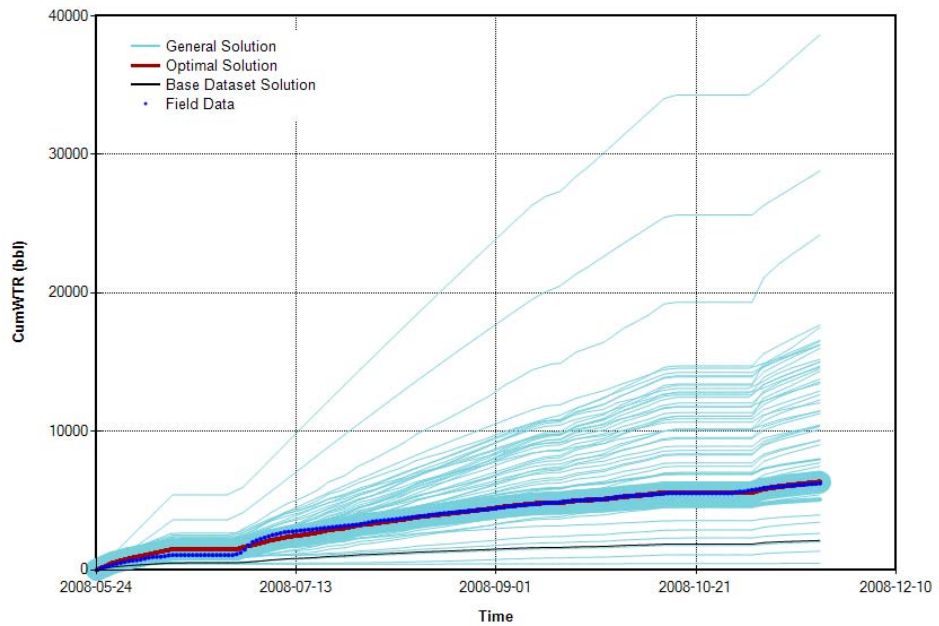


Figure 50. Cumulative water production history match-- oil production rate constraint

The reservoir description obtained from the above history-match process was then utilized to forecast production performance— for the purpose of optimizing the hydraulic fracturing treatments in Bakken wells. Also, the relative permeability curves— estimated from history matching— for matrix, natural fracture system, and hydraulic fractures are demonstrated in Figures 51-56.

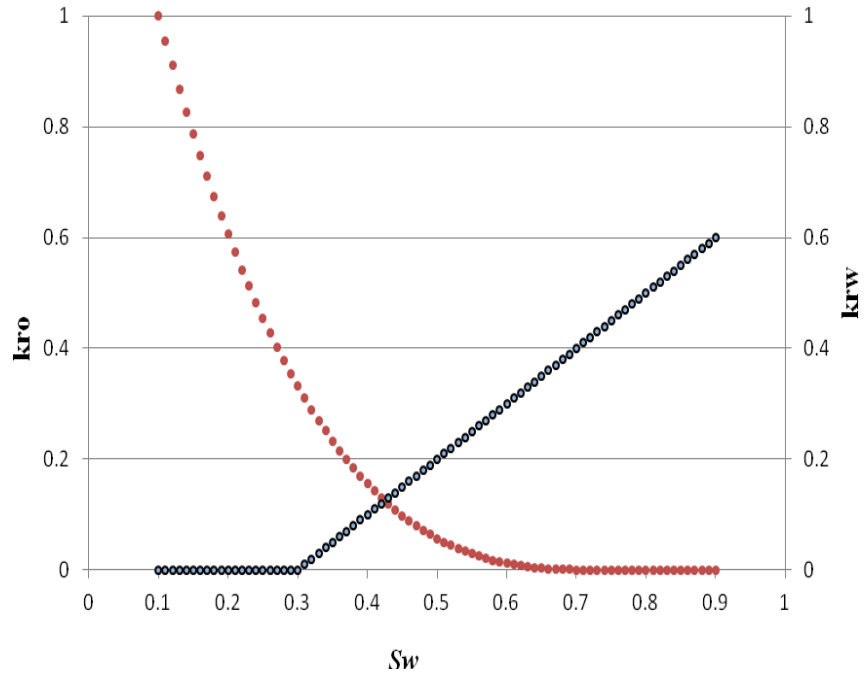


Figure 51. Relative permeability curves for matrix— water-oil system

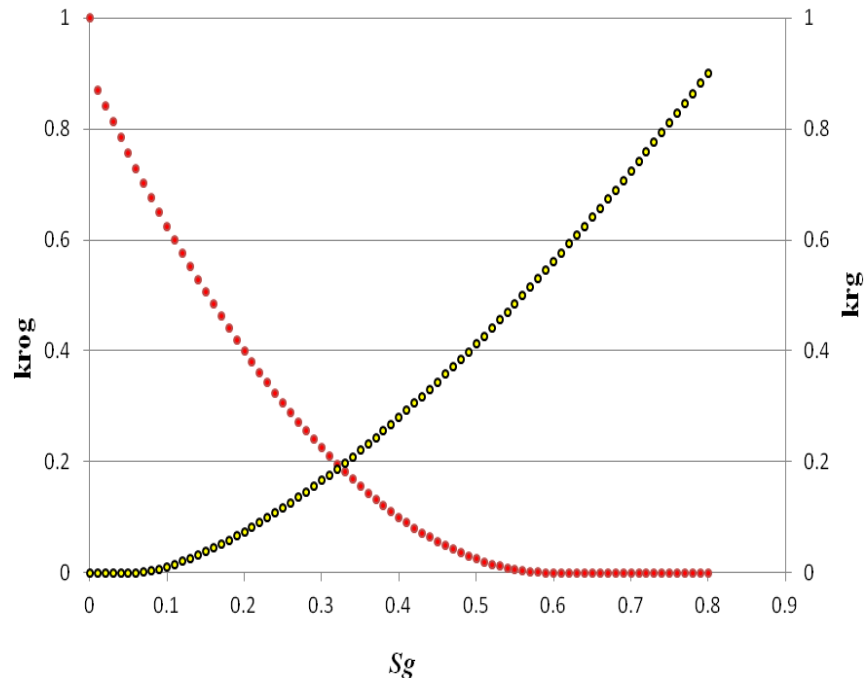


Figure 52. Relative permeability curves for matrix— gas-liquid system

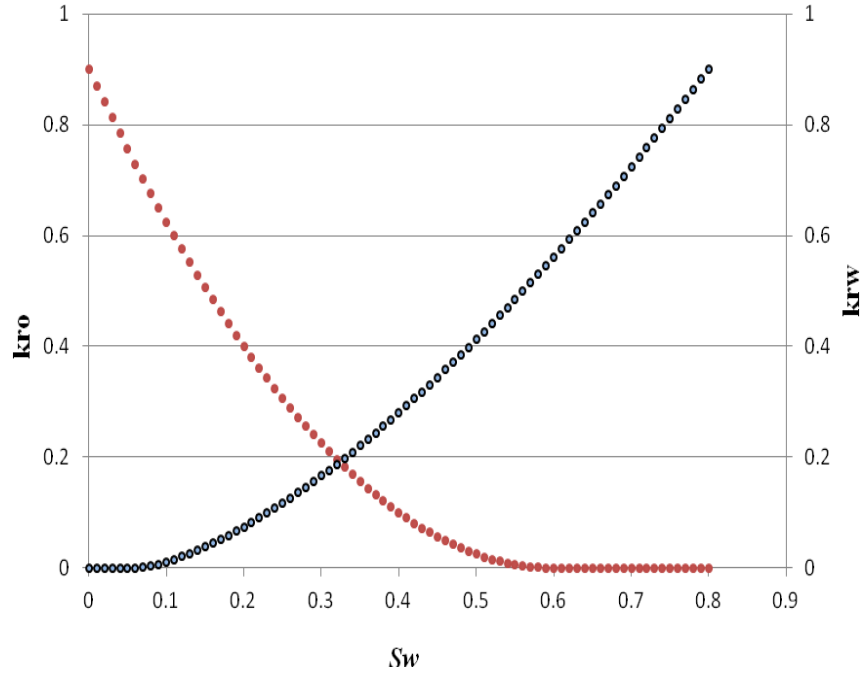


Figure 53. Relative permeability curves for natural fracture system— water-oil system

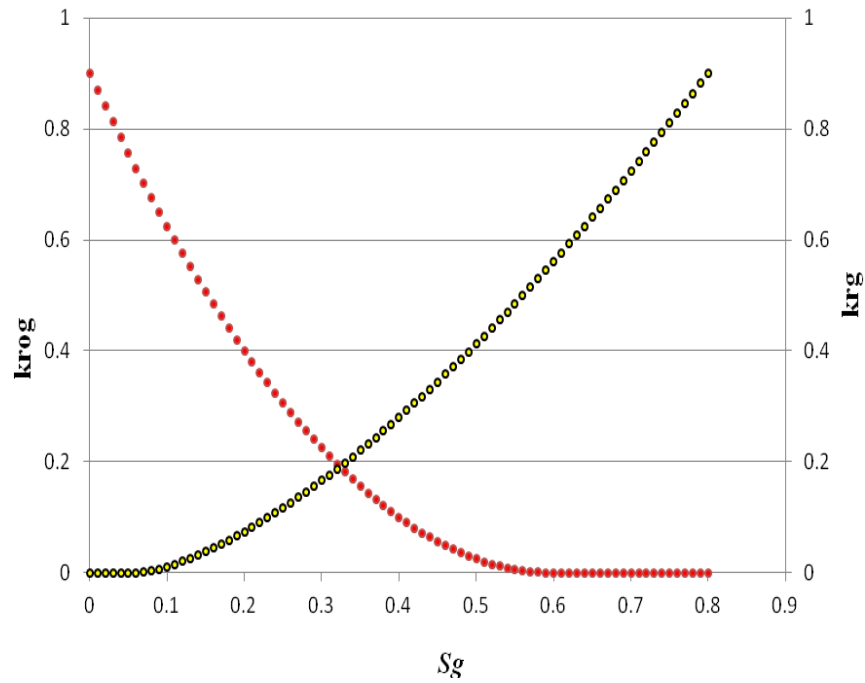


Figure 54. Relative permeability curves for natural fracture system— gas-liquid system

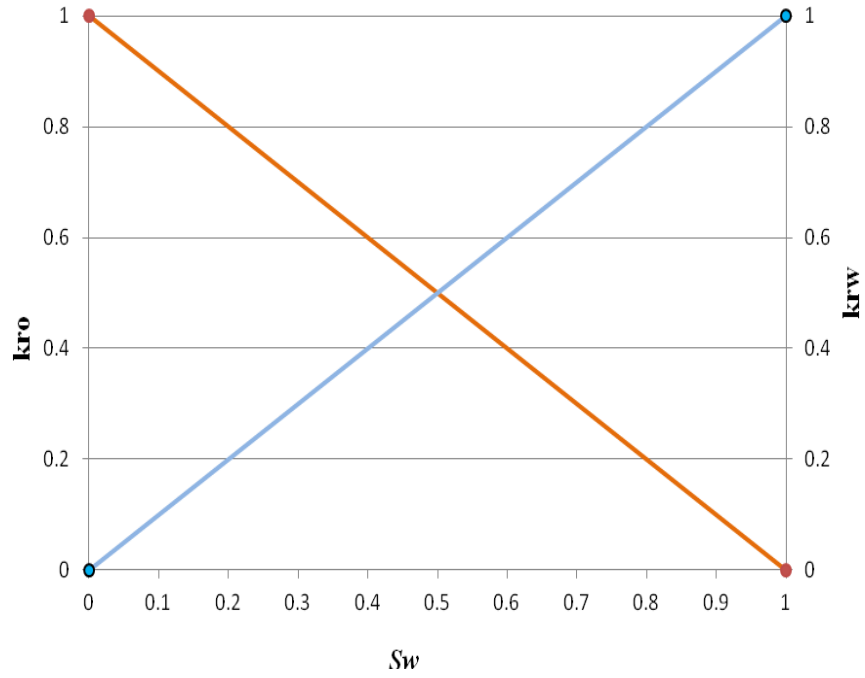


Figure 55. Relative permeability curves for hydraulic fractures— water-oil system

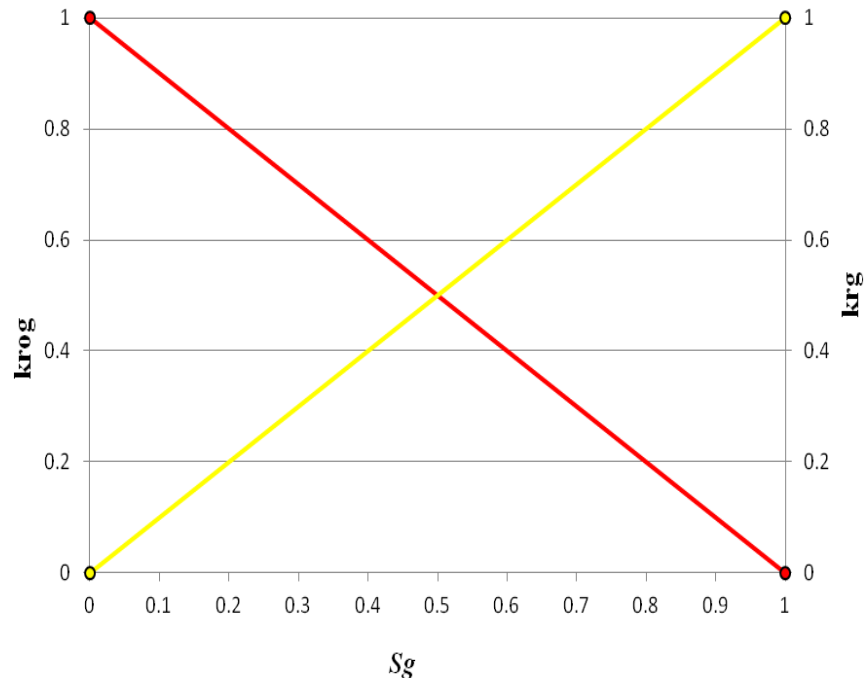


Figure 56. Relative permeability curves for hydraulic fractures— gas-liquid system

Hydraulic Fracturing Design Optimization

In fact, there is no single fracture treatment design that is best in all possible cases. While in vertical wells the primary way to increase fracture network-size and production rate is executing larger fracture treatments, in horizontal wells other optimization opportunities are provided owing to the geometry of such type of wells, such as longer laterals and more stimulation stages [Wiley *et al.*, 2004; Mayerhofer *et al.*, 2010; Zander *et al.*, 2011].

Mayerhofer *et al.* [2006] presented reservoir simulation studies in which they investigated the impact of different fracture-network properties. They showed that well production can be enhanced by long effective fractures, forming large networks inside a tight formation. The challenge in designing a successful hydraulic fracture treatment for Bakken horizontal wells lies in understanding the practical and physical limitations of what is possible in terms of fracture-network size (SRV) and hydraulic fracture parameters, at reasonable operational costs. The following key parameters may be addressed in the design optimization of hydraulic fracturing treatments for Bakken horizontal wells:

- a) Fracturing fluid properties (fluid rheology, injection rate, and fluid leakoff),
- b) Proppant properties (proppant type and size),
- c) Horizontal well parameters (spacing and number of wells),
- d) Fracture properties (SRV, fracture spacing, conductivity, and half-length), and
- e) Economic optimization (NPV).

In hydraulic fracturing optimization two important notions should be considered:

- a) there is no fundamental difference between hydraulic fracturing in high-permeability and low-permeability reservoirs (i.e. only the fracturing execution issues

need to be figured out), and b) for any fracturing materials (proppant and fluid) there exists only one optimal fracture geometry that would give us optimal production rate [Wiley *et al.*, 2004; Marongiu-Porcu, 2009; Mayerhofer *et al.*, 2010; Zander *et al.*, 2011].

Optimal Treatment Materials

We have examined hydraulic fracturing designs for a Bakken horizontal well with a 10,000-*ft* lateral drilled inside a 1280-acre drainage area. The goal of the design was to consider all the plausible combinations of fluids and proppants to find the best candidates of treatment materials. Improper fracturing design can result in fractures that are too narrow that may cause proppant bridging and screenout or too wide that can allow too much proppant settling. In this study we have done a comparative study for selected proppants, pads, and fracturing fluids to determine the best combination(s) for carrying out the stimulation job for Bakken horizontal wells.

The first step was to use 2D fracture simulation method (PKN model in this case) to quickly perform the sensitivity analysis, preliminary designs, and calculating the fracturing material sizes prior to performing fully-3D fracture modeling. Table 8 shows the results of the scoping calculations that were carried out for 27 combinations of the candidate fracturing materials.

Table 8. Comparison of different fracturing treatments—for each fracture stage

NO.	Cases	xf	kfw (md-ft)	Vf_total (M-Gal)	mp (M-lbs)	HHP	Material Cost (\$)
1		500	261	11.3	32.3	9164	\$338,463
2	Slickwater 20/40 Ottawa Sand	1000	260	22.6	64.4	9101	\$341,038
3		1500	297	38.2	110.3	9204	\$351,700
4		500	1039	11.3	32.3	9168	\$344,745
5	Slickwater 16/30 RC Sand	1000	1035	22.7	64.3	9104	\$353,362
6		1500	1183	38.4	110.2	9208	\$372,789
7		500	824	10.8	32.3	9130	\$345,901
8	Slickwater 20/40 Ceramic	1000	828	21.9	64.9	9075	\$357,612
9		1500	946	37.1	111.3	9175	\$380,716
10		500	157	7.4	19.4	8814	\$325,526
11	50# Linear HPG 20/40 Ottawa Sand	1000	197	17.9	48.6	8925	\$336,430
12		1500	225	30.2	83.4	9003	\$347,381
13		500	623	7.4	19.3	8816	\$329,253
14	50# Linear HPG 16/30 RC Sand	1000	782	18	48.6	8928	\$345,805
15		1500	894	30.3	83.3	9006	\$363,337
16		500	498	7.2	19.5	8798	\$330,156
17	50# Linear HPG 20/40 Ceramic	1000	626	17.4	49.1	8906	\$348,895
18		1500	715	29.3	84.1	8981	\$369,083
19		500	261	11.3	32.3	9164	\$342,870
20	30# XLink Gel 20/40 Ottawa Sand	1000	319	27	78.9	9339	\$362,368
21		1500	359	45.1	133.2	9459	\$381,940
22		500	1039	11.3	32.3	9168	\$349,152
23	30# XLink Gel 16/30 RC Sand	1000	1271	27.1	78.9	9344	\$377,589
24		1500	1430	45.3	133.2	9465	\$407,562
25		500	824	10.8	32.3	9130	\$350,113
26	30# XLink Gel 20/40 Ceramic	1000	1008	26	79	9298	\$381,737
27		1500	1134	43.4	133.4	9413	\$415,491

The financial analysis was conducted to evaluate the costs and benefits associated with each hydraulic fracturing design. The expenses considered for fracturing job economic analysis and gross treatment sizing were restricted to four major components: a) fluid cost, b) proppant cost, c) pumping charges, and d) gross equipment charges. Therefore, the job cost is the sum of all these expenses. The treatment costs per fracture stage are shown in Table 9. All cost values used are general averages based on personal communications with some companies operating in Western North Dakota.

Table 9. Cost of fracture treatment & completion used in the economic study.

Components	Cost
Fixed Cost	\$400,000
Drilling & Completion	
Lateral length=4500 ft	\$5,500,000
Lateral length=10000 ft	\$8,500,000
Proppants	
Ottawa Sand	\$0.09-0.12/lb
Resin-Coated Sand	\$0.25-0.31/lb
Ceramic	\$0.32-0.39/lb
Fluid	
Slickwater	\$0.09/gal
Linear HPG	\$0.32/gal
Xlinked Gel	\$0.48/gal
Pumping charges	\$36.40/HHP Includes all pump EQP

Other parameters used in the economic analysis are shown in Table 10.

Table 10. Other parameters used in the economic analysis.

Parameter	Value
Oil Price, \$/STB	96
Water disposal/process, \$/STB	-3
Monthly Operational Cost, \$	-7,900
Operational Expenses (f_o)	0.2 of annual revenue
Interest Rate (i)	10%
Royalty (f_r)	3/16 of annual revenue

An optimization task was then conducted to identify optimal stimulation plan (fracture treatment design), drilling and completion plans, and operating conditions (flowing bottomhole pressure) that would yield maximum value for the objective function, being net present value (NPV) in this study. Equation 48 gives the equivalent net present value (NPV) of a future value at n equal consequent intervals of time, Δt , from present time with the constant interest rate i per interval prevalent during the total time, $n \Delta t$. Note that interest rate is an identifiable measure of the earning power of money and is defined as an extra amount of money paid to the lender for the use of money during a specified period of time [Ardalan, 2000].

$$NPV = \sum_{n=1}^N \frac{R_n}{(1+i)^n} - Cost \quad (48)$$

Where R_n , the expected revenue earned in each interval of time Δt , is given by [Marongiu-Porcu et al., 2008]:

$$R_n = V_H \$_H (1 - f_r)(1 - f_o)(1 - f_t) \quad (49)$$

Where V_H is the cumulative volume of hydrocarbons produced in the reference year, $\$_H$ is the unitary revenue for the produced hydrocarbon, f_r is the fraction of gross cash flow due to the lease owners and/or to the foreign nation governments as royalties, f_o is the fraction of gross cash flow to be allocated as operative expenditures, and f_t is the fraction of grow cash flow due as taxes in the relative fiscal regime.

In the optimization task we used the history matched reservoir model to forecast the reservoir response to different hydraulic fracturing strategies. The main goal was to determine the best completion and fracture treatment(s), and optimal drawdown pressure that would yield the highest profit from the well stimulation plan(s). The well was operated at bottomhole pressures of 1000, 1500, and 2000 psi during a 5-year time period. The NPV was made up of three terms: a) the value of the oil produced—being \$96/STB, b) the cost for water disposal/processing— being \$3/STB, and c) the capital expenses (CapEX) (Table 9). The annual interest rate for calculating the discounted NPV used in this study was considered as 10%.

The method of “*Latin hypercube plus proxy optimization*” (LHPO) was used to find the optimal treatment scenario(s). This method consists of four main steps: a)

constructing combinations of the input parameter values to obtain the maximum information from the minimum number of simulation runs (Latin hypercube design), b) building an empirical proxy model by using the data from Latin hypercube design runs (proxy model), c) conducting a proxy-based optimization, and d) validation of the optimal solution obtained from the proxy by iterative simulation runs. A flow chart of *LHPO* algorithm is shown in Figure 57.

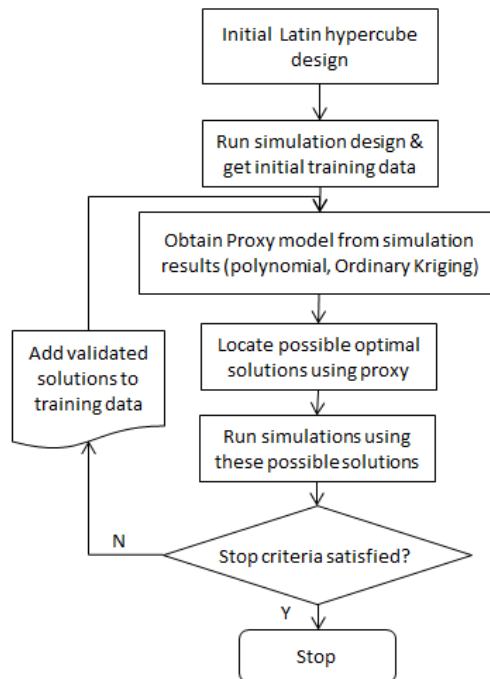


Figure 57. The algorithm of Latin hypercube plus Proxy Optimization [*Computer Modeling Group*, 2012]

Figure 58 shows the well and fracture spacing configurations. A total of three well scenarios were considered for the optimization. Scenario w_1 had one lateral, scenario w_2 had two laterals, and scenario w_3 had three laterals, each of which was 10,000 *ft* long. All these scenarios were completed with 12, 18, and 36 fracture stages.

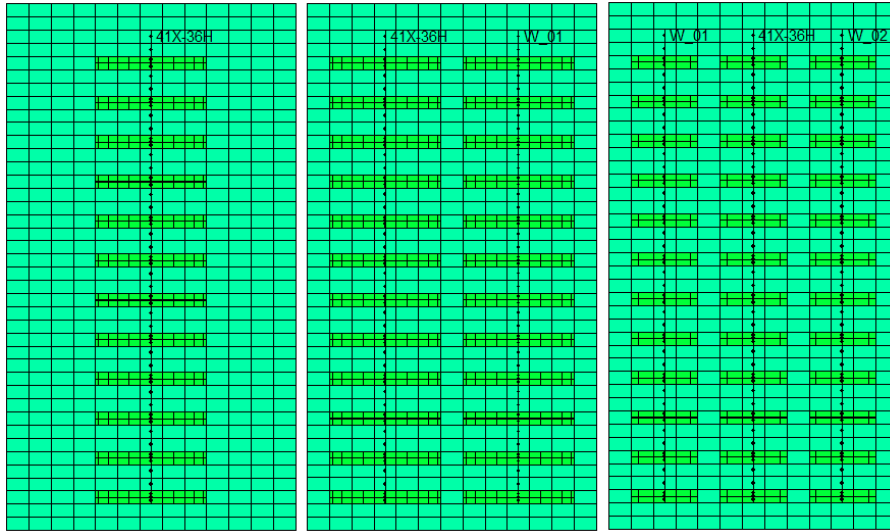


Figure 58. Well and fracture spacing setup (top view)— 12 fracture stages

Figures 59-62 show the results of the NPV calculations using the *Latin hypercube* algorithm, with three different bottomhole flowing pressures.

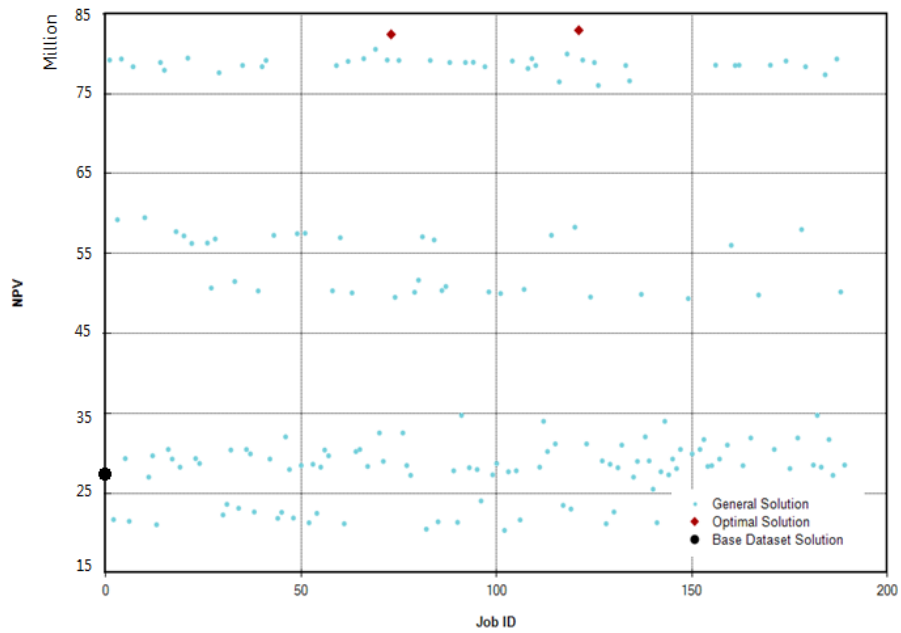


Figure 59. NPV optimization of hydraulic fracture treatment with $p_{wf} = 1000 \text{ psi}$ — red dots are the optimal solutions (job-IDS 73 and 121)

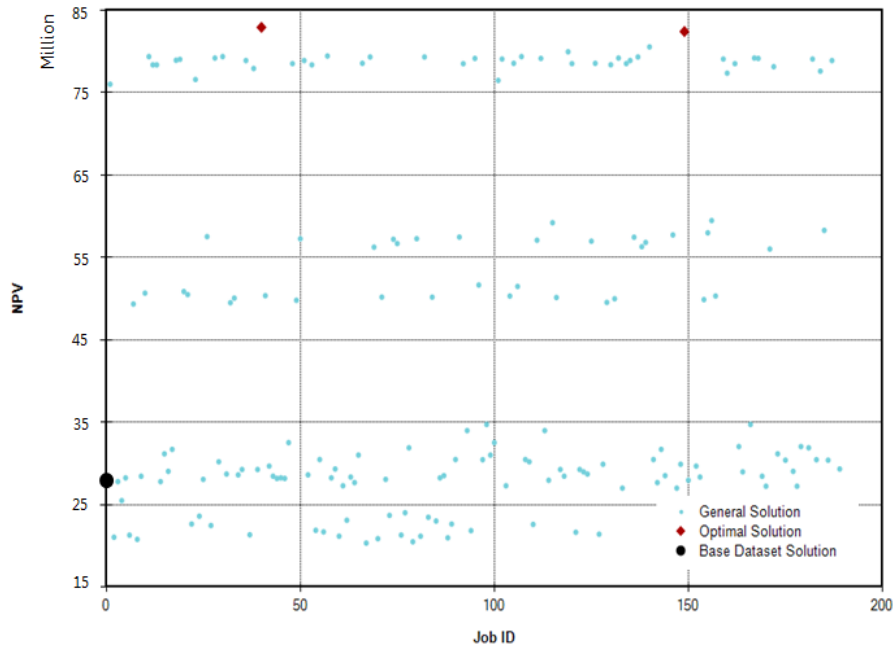


Figure 60. NPV optimization of hydraulic fracture treatment with $p_{wf} = 1500 \text{ psi}$ — red dots are the optimal solutions (job-IDS 40 and 149)

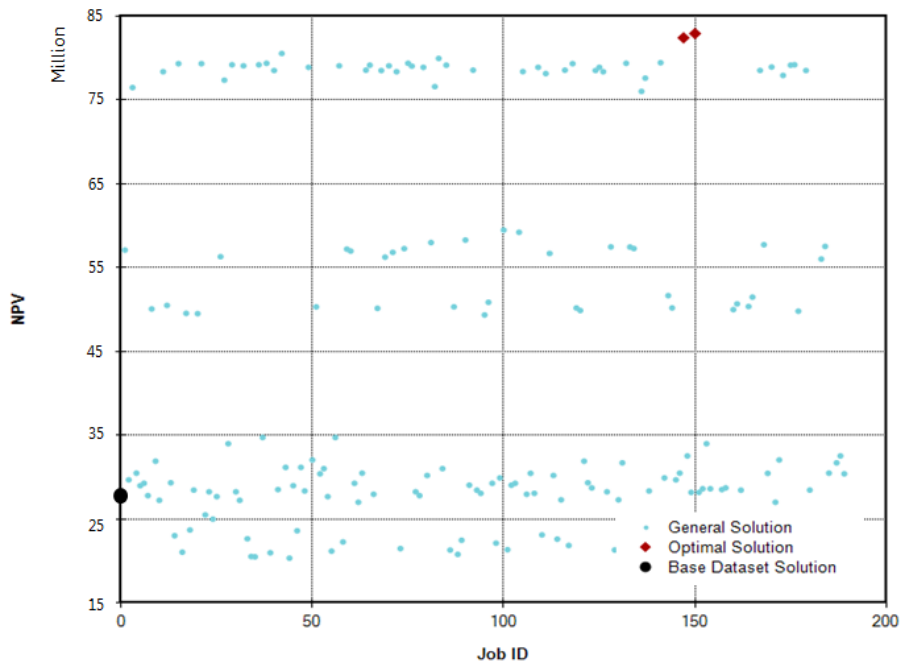


Figure 61. NPV optimization of hydraulic fracture treatment with $p_{wf} = 2000 \text{ psi}$ — red dots are the optimal solutions (job-IDS 147 and 150)

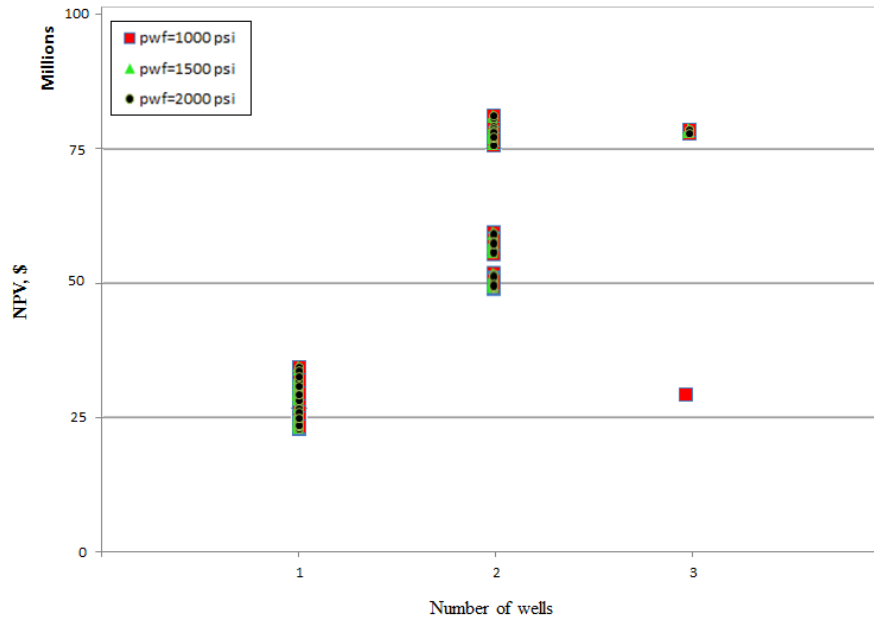


Figure 62. NPV comparisons for the cases with differing number of wells and different bottomhole flowing pressures

It took the iterative procedure 567 (=3*189) runs to optimize the NPV from 17 million to almost 84 million USD. The comparison figures above show that the job-IDs 40, 73, 121, 147, 149, and 150 with the specifications shown in Table 11, outperformed all other treatment cases. Figure 62 also shows how a change in flowing bottomhole pressure would change the wells performance.

Table 11. Optimal fracture treatment cases—2-well completion plan

Job ID	Bottomhole pressure, (psi)	Xf, (ft)	Fracture conductivity, (md-ft)	Fracturing fluid Type	Proppant Type	Number of stages
40	1500		1008		Ceramic	
73	1000		1271		RC Sand	
121	1000	1000	1008	Xlinked gel	Ceramic	36
147	2000		1271		RC Sand	
149	1500		1271		RC Sand	
150	2000		1008		Ceramic	

Table 11 shows that the two-well completion plan with using crosslinked gel and either resin-coated sand or ceramic, as treatment materials, appeared to be the best case scenarios owing to higher cumulative oil produced in the 5-year time period

(Figure 63). Note that the majority of the data from Bakken show more fractures propagating in a transverse direction [Besler *et al.*, 2007]. Hence, the fluid flow should be improved by means of wider fractures, cleaner fluids, or better proppants. One of the major problems some operators in Western North Dakota encountered was the proppant flowback and they had to overflush their treatments to reduce the proppant flowback. This would result in loss of fracture width near the wellbore. However, with ceramic proppants, no proppant flowback was observed and therefore, there was no need to overdisplace the treatments [Lolon *et al.*, 2009].

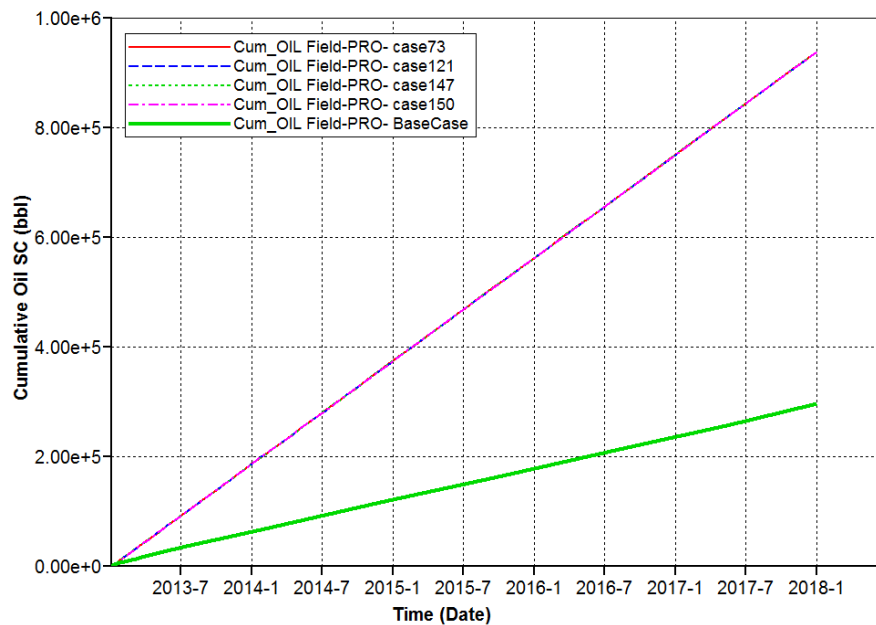


Figure 63. *CUM_OIL* comparisons— optimal cases versus base case

The cross plots in Figures 64 and 65 show the results of post-process analysis of the optimization task. Figure 64 shows the relationship between NPVs and capital cost (investment). This figure shows that we would make higher profits if we invested on better fracturing materials, which is what we expect to see in optimal cases. On the other hand, Figure 65 shows the cross plot of NPVs versus different hydraulic fracture

treatments. As is depicted only two cases turned out to be the optimal fracturing treatments.

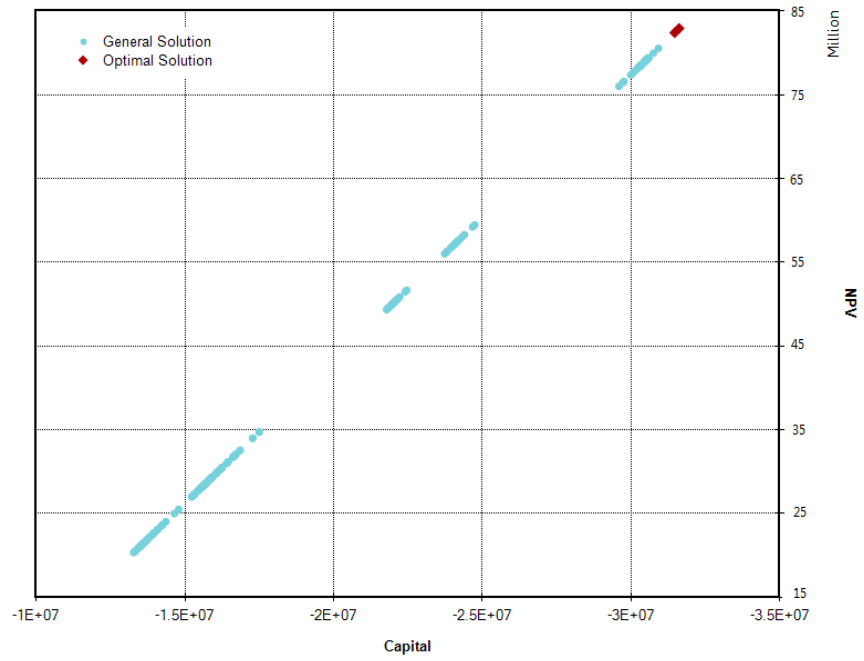


Figure 64. Cross plot of NPV versus Capital Cost

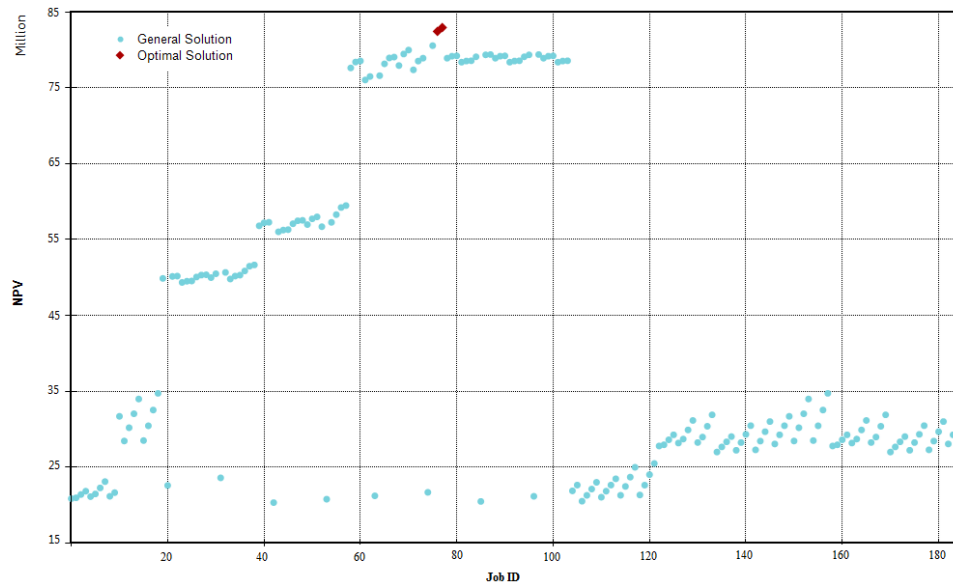


Figure 65. Cross plot of NPV versus fracturing treatment scenarios

Hydraulic Fracture Simulation

The optimal fracture treatment materials were determined by integrating fracture modeling (PKN model) with reservoir simulation, discussed above. As a next step, 3D fracture simulation was performed to model the created hydraulic fracture so as to find the best pump schedule. Figure 66 shows a log style illustration of the major data that were input into the fracture model as compared to depth in the study area. The geologic model is comprised of five layers with differing stresses, permeabilities, and moduli. They are: Lodgepole, Upper Bakken, Middle Bakken, Lower Bakken, and Three Forks.

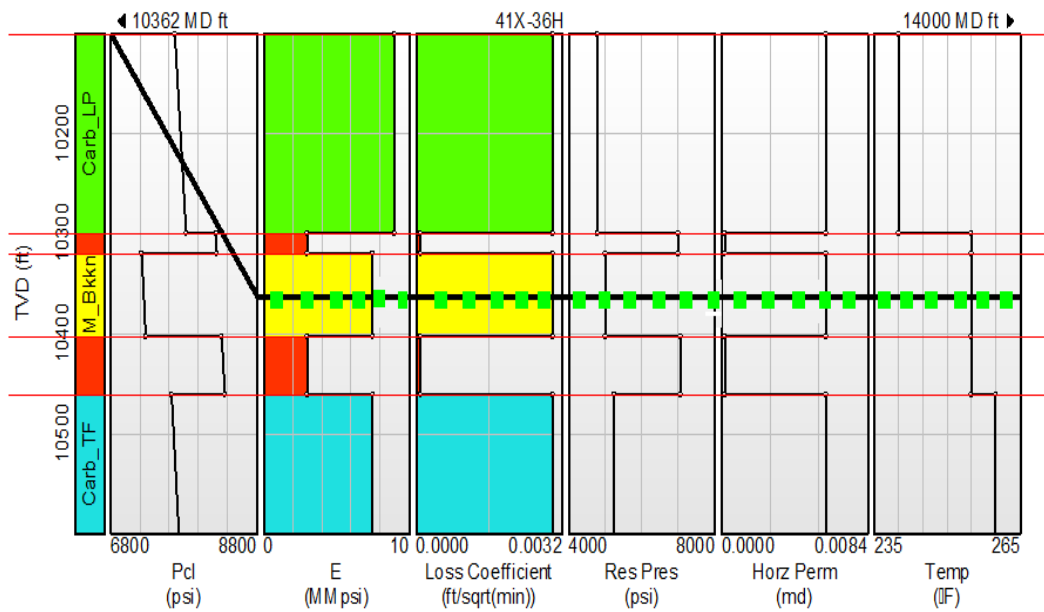


Figure 66. Input parameters for fracture geometry modeling— Well 41X-36H

The multi-layer model shown in Figure 66 was intended for detailed final fracture treatment design. The data of the layers used in the fracture simulations are shown in Table 12.

Table 12. Formation layer data - multi-layer height growth

Depth (ft)		Thickness	Stress (psi)		Gradient Modulus	Toughness	Loss Coef.
Top	Bottom	(ft)	Top	Bottom	(psi/ft)	(MMpsi)	psi*sqrt(in)
					(ft/sqrt(min))		
10200	10300	100	7752	7828	0.76	9.0	2000
10300	10325	25	8240	8260	0.80	3.0	1807
10325	10403	78	7227	7282	0.70	7.5	2500
10403	10461	58	8322	8368	0.80	3.0	1600
10461			7845		0.75	7.5	2000
<i>FORMATION:</i>						Permeability (md)	0.003
<i>TEMPERATURE:</i>						Bottom Hole (°F)	255
<i>PRESSURE:</i>						Reservoir Pressure (psi)	4600
						Closure Pressure (psi)	7255
<i>DEPTH:</i>						Well Depth (ft), TVD	10364

Since the estimation of fracture geometry plays a major role in evaluating the completion plans, a commercial hydraulic fracture simulator was used to help estimate the created fracture geometry and its characteristics. To evaluate the success of a fracture treatment in a horizontal well, the production response of the well to the presence of hydraulic fractures should be investigated. First, we need to know the fracture geometry and fracture conductivity. This information comes from fracture geometry models that range from simple hand calculation procedures (2D models) to complex 3D models (pseudo-3D or fully 3D) that must be run on powerful computers.

Fluid injected at the beginning of the fracturing job (pad) initiates and opens up the fracture. The pad provides the necessary extra fluid that is leaked off into the formation during a treatment. It also generates sufficient fracture length and width to place the proppant. If the pad volume was too small, the treatment would screen out. If the pad volume was too large, we would waste money, the fracture height would grow into the unwanted zones (i.e. the Lodgepole), and the fracture would not close as rapidly as it would with a smaller pad volume.

After pumping the specified volume of pad, the proppant concentration is ramped up step-by-step as the slurry is being injected. If proppant prematurely bridges in the fracture during the pumping, the treating pressure will rise rapidly to the technical

constraint due to a situation called screen-out. For calculating the ramped proppant schedule material balance method was used, such as the power-law method of Nolte [1986]. The power-law method is explained thoroughly by Economides et al. [2002] (Table 13).

Table 13. Developing proppant schedule using power-law method [Economides et al., 2002]

a) Calculation of the exponent of proppant concentration curve:	$\varepsilon = \frac{1 - \eta_e}{1 + \eta_e}$
b) Calculation of pad volume and pad pumping time:	$V_{pad} = \varepsilon V_i \quad , \quad t_{pad} = \varepsilon t_i$
c) Mass per unit of injected slurry volume:	$c = c_e \left(\frac{t - t_{pad}}{t_e + t_{pad}} \right)^\varepsilon$
d) Converting the concentration from mass per slurry volume into mass added per unit volume of base fluid (c_a):	$c_a = \frac{c}{1 - \frac{c}{\rho_p}}$

In an ideal pump schedule, the proppant schedule should be designed such that a uniform proppant concentration is obtained in the fracture and a minimum pad volume is used that the optimal proppant schedule makes use of that minimum pad to place the desired fracture half-length (X_{f_Design}). In the end, the pump schedule designed for the selected treatment scenario (optimal treatment case) was developed as shown in Figure 67 with the details presented in Table 14. Obviously, a pump schedule may vary based on the fracturing treatment materials, and/or based on the desired fracture half-length and fracture conductivity. Additionally, Tables 15 and 16 present the characteristics of the fluid and proppant used for the treatment.

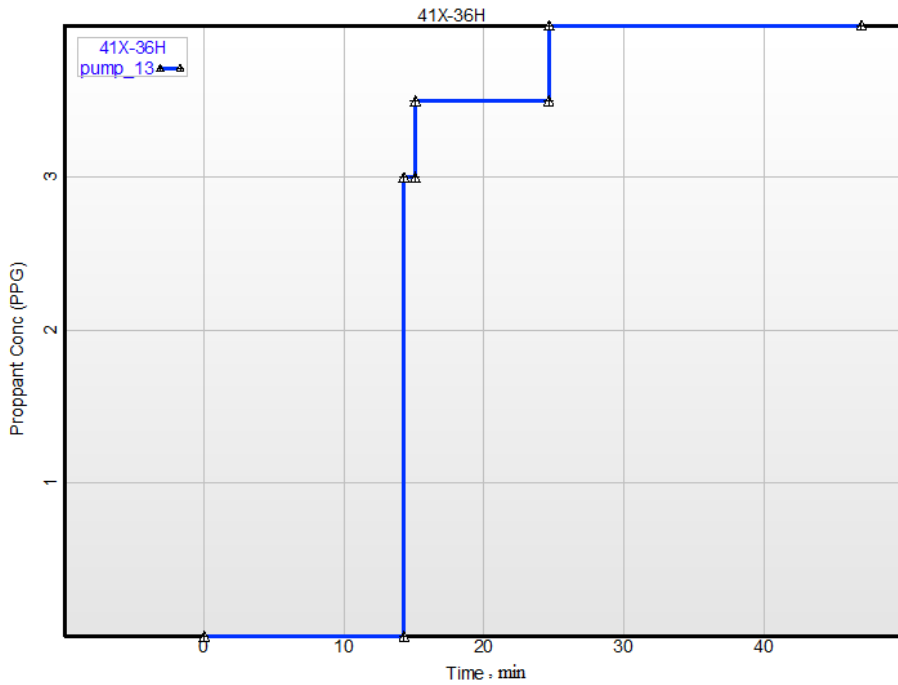


Figure 67. Developed pump schedule using Nolte method.

Table 14. Pumping schedule using Nolte method [1986]

Slurry Vol (M-Gal)	Fluid Vol (M-Gal)	Conc. (PPG)		Rate (BPM)	Fluid Type	Prop Type	Cum Proppant (M-lbs)	Pump Time (min)
		Start	End					
6.00	6.00	0.0	0.0	10	Slickwater	-	0.0	14.3
0.32	0.29	3.0	3.0	10	Xlinked Gel	40/70 Sand	0.6	0.8
4.04	3.62	3.5	3.5	10	Xlinked Gel	20/40 Ceramic	3.5	9.6
9.38	8.31	4.0	4.0	10	Xlinked Gel	20/40 Ceramic	10.6	22.3
Total Slurry, M-Gal				19.7	Total Fluid			18.2
Total Proppant, M-lb				46.8	Avg. Conc			2.6
Total Pump Time, min				47.0	Pad %			30.4

“M” is a Roman for thousand.

Table 15. Proppant data (Courtesy of NSI Tech., 2012)

<i>Ceramic 20/40</i>							
		Specific Gravity				3.70	
		Damage Factor (1.0 = No Damage)					0.85
	Stress, psi	0	2000	4000	8000	16000	
	K_rW @ 2 lb/sq ft (md-ft)	7300	7100	6400	4800	2200	
<i>RC Sand 16/30</i>							
		Specific Gravity				2.55	
		Damage Factor (1.0 = No Damage)					0.80
	Stress, psi	0	2000	4000	8000	16000	
	K_rW @ 2 lb/sq ft (md-ft)	11800	10800	8900	5500	1500	

Table 16. Fluid data (Courtesy of NSI Tech., 2012)

<i>Slickwater</i>								
				Specific Gravity:				1.04
	Data	@ Wellbore	@ FormTmp	1.0 hr	2.0 hr	4.0 hr	8.0 hr	
	vis(cp @ 170 1/sec)	188.0	123.0	88.0	67.0	35.0	14.0	
	non-Newtonian n'	0.46	0.53	0.58	0.61	0.64	0.67	
	K(lb/sec/ft²)x1000	0.06	0.03	0.02	0.01	0.00	0.00	
<i>30# X-linked gel</i>								
				Specific Gravity:				1.04
	Data	@ Wellbore	@ FormTmp	2.0 hr	3.7 hr	5.2 hr	6.6 hr	
	vis(cp @ 170 1/sec)	500.0	400.9	226.0	124.8	83.2	54.1	
	non-Newtonian n'	0.72	0.72	0.72	0.72	0.72	0.72	
	K(lb/sec/ft²)x1000	0.04	0.03	0.02	0.01	0.01	0.00	

The downhole friction versus rate for the simulated hydraulic fracture treatment (optimal case) is shown in Table 17.

Table 17. Pipe friction data

Q (BPM)	dP/dL (psi/100ft)
5	9
10	18
20	40
50	180

Using fully-3D modeling with the developed pump schedule, the fracture dimensions and fracture conductivities were calculated. Then, these parameters were evaluated to make sure that the job would not yield a fracture that could grow

upwards into the Lodgepole Formation. Table 18 contains the details of the treatment design and the results from the fully-3D fracture simulations. Note that in the 3D modeling we have used finite element method (FEM) for calculating the fracture width and fracture propagation. Generally, for cases where formation layers have differing values for modulus, FEM needs to be used for fracture width/propagation calculations. FEM should probably be used in any case where modulus values in different layers differ by a factor of 2 or more [NSI Tech., 2012].

Note that the basic theory of fluid loss from a hydraulic fracture has been employed based on 1-D fluid loss (also called Carter fluid loss [Gidley, 1990]), which is valid for matrix fluid loss as long as the lateral propagation (height and length) is rapid compared to the rate of fluid leakoff normal to the fracture. If the hydraulic fracture intersects with existing natural fractures, then these natural fissures may begin to open under the high pressure associated with the injected fluid. This can dramatically increase the rate of fluid loss. The natural fractures will begin to open when the net pressure inside the fracture begins to exceed a critical value ($P_{netCrit.}$). As the net pressure rises above this critical level, the rate of fluid loss then becomes proportional to the product of natural fracture density and $(P_{net} - P_{netCrit.})$ cubed. The critical net pressure can be obtained by analyzing the Nolte-Smith log-log plot of net treating pressure versus time [Kim and Wang, 2011]. Since this type of data for the study well was not available, the extra fluid loss due to natural fractures was considered by increasing the leak-off coefficient to some degree.

Also, in our calculations we checked the results to make sure that the three major constraints considered in the execution of the hydraulic fracture treatments were met. They are: a) a limit of 1000 psi was considered for the net-pressure that can influence the surface treating pressure (#HHP), and can have an effect on the fracture height

growth (unwanted fracture growth into the Lodgepole), b) fracture width limit that should be at least 3 times the proppant diameter in order to prevent the proppant bridging and involuntary screenout, and c) the injection time that has to be less than 24 hours. As is clear from the calculations in Table 18, these constraints hold in our simulation study.

Table 18. The results of fully3D/FEM fracture simulation

Half Length	'Hydraulic' Length (ft)	1091.8
	Propped length (ft)	870.0
PRESSURE:	Max Net Pressure (psi)	1213.0
	Final Net Pressure (psi)	755.0
	Surface Pres-End of Pad (psi)	7116.0
	Surface Pres-Start of Flush (psi)	5621.1
	Surface Pres-End of Job (psi)	6656.9
	Maximum Hydraulic horsepower	1779.0
TIME:	Max Exposure to Form. Temp. (min)	45.3
	Time to Close	12.0
RATE:	Fluid Loss Rate during pad (BPM)	0.17
EFFICIENCY:	At end of pumping schedule	0.96
	Average In Situ Conc.(lb/ft ²)	0.2
PROPPANT:	Average Conductivity (md-ft)	556.3
	Fcd (KfW/KXf)	213.15
HEIGHT:	Max Fracture Height (ft)	150.2
WIDTH:	Avg width at end of pumping (in)	0.14
VOLUMES:	Total Fluid Volume (M-Gal)	18.2
	Total Proppant Volume (M-Lbs)	46.8

Figure 68 shows the width profile calculated from the fully-3D, FEM simulation.

It shows that the created fracture is well confined within the Bakken Formation.

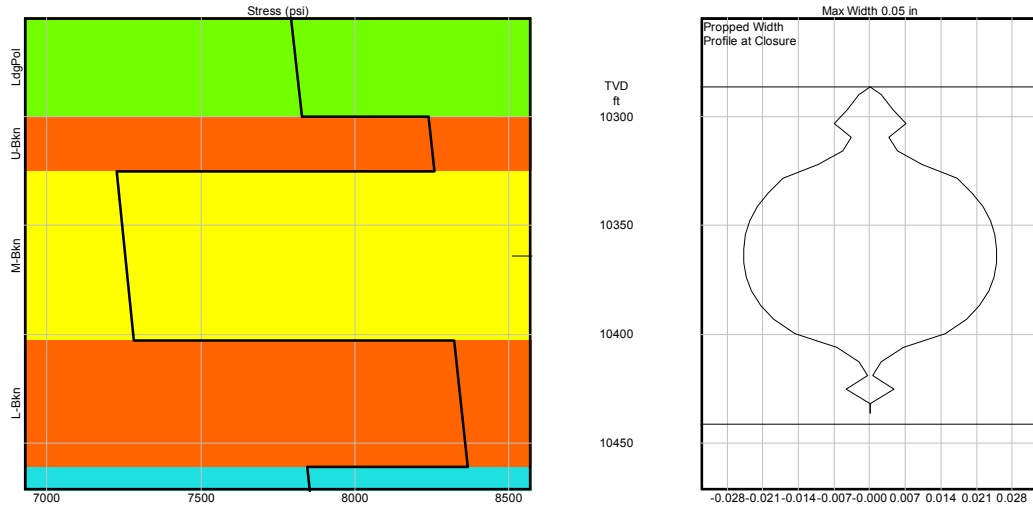


Figure 68. Width profile from fully-3D, FEM simulation

As is clear from this figure, the fracture height is nearly equal to the thickness of the pay zone. Generally, it is believed that in-situ stress differences (in the vertical stress profile) are the major controlling factor of fracture height confinement [Warpinski *et al.*, 1994]. The results from the fully-3D fracture simulation, performed by finite difference solutions for fracture geometry are shown in Table 19 and Table 20.

Table 19. The results from fully-3D fracture simulation—time history

Time (min)	Pen (ft)	Pres (psi)	Rate (BPM)	Prop (PPG)	SI Vol (M-Gal)	Efficiency	Loss (BPM)	Hght (ft)	W-Avg (in)
0.7	30.0	1213	10.00	0.0	0.3	1.00	0.6	60	0.16
3.1	134.8	426	10.00	0.0	1.3	1.00	0.2	88	0.10
5.5	213.0	468	10.00	0.0	2.3	1.00	0.3	88	0.10
7.9	276.5	498	10.00	0.0	3.3	0.99	0.3	90	0.11
10.3	338.9	515	10.00	0.0	4.3	0.99	0.3	92	0.12
12.6	394.5	534	10.00	0.0	5.3	0.98	0.3	92	0.12
14.3	431.9	548	10.00	0.0	6.0	0.98	0.4	92	0.13
15.0	451.6	553	10.00	3.0	6.3	0.98	0.4	92	0.13
15.1	452.1	554	10.00	3.5	6.3	0.98	0.4	92	0.13
17.5	505.4	590	10.00	3.5	7.3	0.98	0.4	95	0.13
19.9	553.5	612	10.00	3.5	8.4	0.98	0.4	103	0.13
22.3	603.2	631	10.00	3.5	9.4	0.97	0.4	106	0.13
24.6	642.2	660	10.00	3.5	10.4	0.97	0.4	112	0.14
24.7	643.3	660	10.00	4.0	10.4	0.97	0.4	113	0.14
27.1	684.7	675	10.00	4.0	11.4	0.97	0.5	137	0.14
29.6	725.6	695	10.00	4.0	12.4	0.97	0.5	137	0.14
32.0	763.1	707	10.00	4.0	13.5	0.97	0.5	140	0.14
34.4	800.3	715	10.00	4.0	14.5	0.97	0.5	143	0.14

36.8	838.9	727	10.00	4.0	15.5	0.96	0.5	143	0.14
39.2	872.9	735	10.00	4.0	16.5	0.96	0.5	145	0.14
41.6	904.2	743	10.00	4.0	17.5	0.96	0.5	148	0.14
44.1	938.8	748	10.00	4.0	18.5	0.96	0.5	150	0.14
46.5	969.5	754	10.00	4.0	19.5	0.96	0.6	150	0.14
47.0	975.5	755	10.00	4.0	19.7	0.96	0.5	150	0.14
49.4	1006.0	688	0.00	4.0	19.7	0.96	0.5	150	0.14
52.3	1035.5	661	0.00	4.0	19.7	0.96	0.5	150	0.13
56.0	1078.2	636	0.00	4.0	19.7	0.95	0.6	150	0.13
59.0	1091.8	619	0.00	4.0	19.7	0.95	0.5	150	0.13

Table 20. The fracture geometry summary— at end of pumping schedule

Distance (ft)	Pressure (psi)	W-Avg (in)	Q (BPM)	Sh-Rate (1/sec)	Total	Hght (ft)			Bank Fraction	Prop (PSF)
						Up	Down	Prop		
15	746	0.21	5.0	13	150	71	72	143	0.00	0.03
45	732	0.20	4.9	15	150	71	72	143	0.00	0.02
75	718	0.19	4.7	16	150	71	72	143	0.00	0.02
105	704	0.19	4.6	17	143	71	65	143	0.00	0.02
135	691	0.18	4.5	18	143	71	65	136	0.00	0.02
165	676	0.17	4.3	19	143	71	65	136	0.00	0.02
195	661	0.16	4.2	20	143	71	65	129	0.00	0.02
225	646	0.16	4.0	21	137	71	59	122	0.00	0.02
255	630	0.15	3.8	22	137	71	59	103	0.00	0.02
285	613	0.14	3.7	24	137	71	59	103	0.00	0.02
315	596	0.14	3.6	26	131	71	53	103	0.00	0.02
345	579	0.13	3.4	28	128	68	53	103	0.00	0.01
375	561	0.13	3.3	34	127	68	53	97	0.00	0.01
405	544	0.16	3.2	27	106	46	53	91	0.00	0.01
435	531	0.15	2.7	25	99	46	46	91	0.00	0.01
465	518	0.16	2.6	27	92	40	46	91	0.00	0.01
495	505	0.15	2.6	28	92	40	46	91	0.00	0.01
525	493	0.15	2.5	30	92	40	46	84	0.00	0.01
555	480	0.14	2.5	31	92	40	46	78	0.00	0.01
585	468	0.13	2.4	33	92	40	46	78	0.00	0.01
615	455	0.13	2.3	35	88	40	42	72	0.00	0.00
645	442	0.13	2.3	37	88	40	42	72	0.00	0.00
675	429	0.13	2.2	39	82	33	42	65	0.00	0.00
705	415	0.12	2.1	41	82	33	42	59	0.00	0.00
735	401	0.12	2.0	43	82	33	42	52	0.00	0.00
765	386	0.11	1.9	45	82	33	42	0	0.00	0.00
795	370	0.11	1.9	48	82	33	42	0	0.00	0.00
825	354	0.10	1.8	51	82	33	42	0	0.00	0.00
855	335	0.09	1.7	55	82	33	42	0	0.00	0.00
885	315	0.09	1.6	60	79	33	39	0	0.00	0.00
915	291	0.08	1.4	62	79	33	39	0	0.00	0.00
945	261	0.06	1.1	79	78	33	39	0	0.00	0.00
975	189	0.03	0.6	132	78	33	39	0	0.00	0.00

Figure 69 illustrates the trend of fracture conductivity versus fracture penetration. Once pumping stops and the fluid has leaked-off into the formation, the fracture faces close on proppants. Figure 69 shows that upon fracture closure a uniformly packed fracture would be created with almost 700 to 750 md-ft conductivity. It also shows that the fracture created by hybrid fracture treatment (slickwater plus crosslinked gel) would be well conductive and better confined within the Bakken.

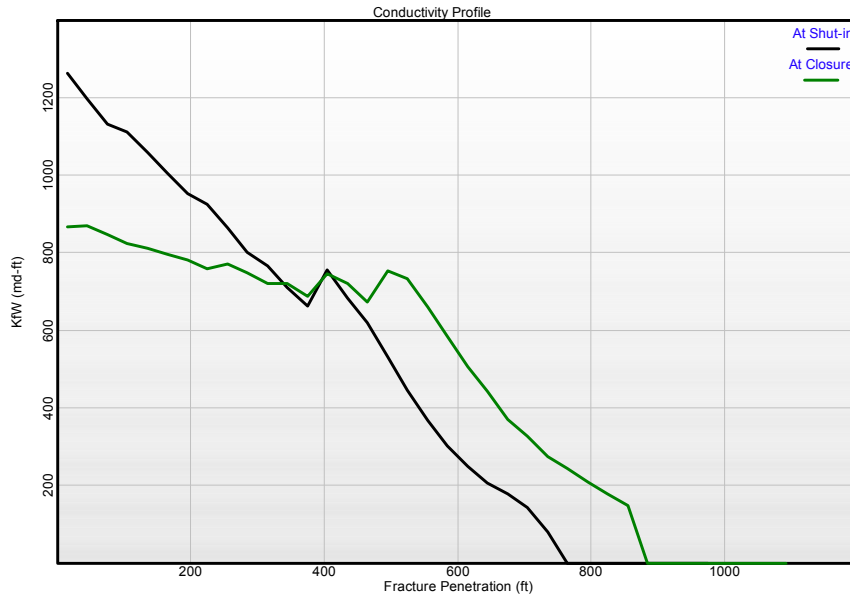


Figure 69. Fracture conductivity profile at shut-in and at closure

Figure 70 shows the proppant coverage versus fracture penetration. The final in-situ proppant concentration is shown in this figure, where it is clear that a relatively good proppant distribution (due to uniformity) was obtained from the hybrid fracture treatment.

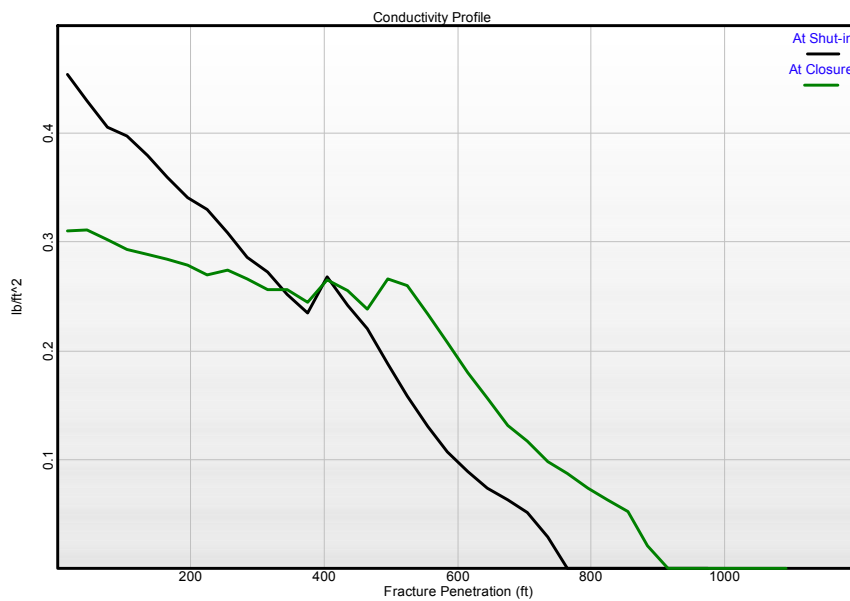


Figure 70. Fracture conductivity profile— at shut-in and at closure

Figure 71 depicts the crack-front positions at successive stages of crack growth.

Other results from the fully-3D/FEM fracture simulations are shown in Figures 72-93.

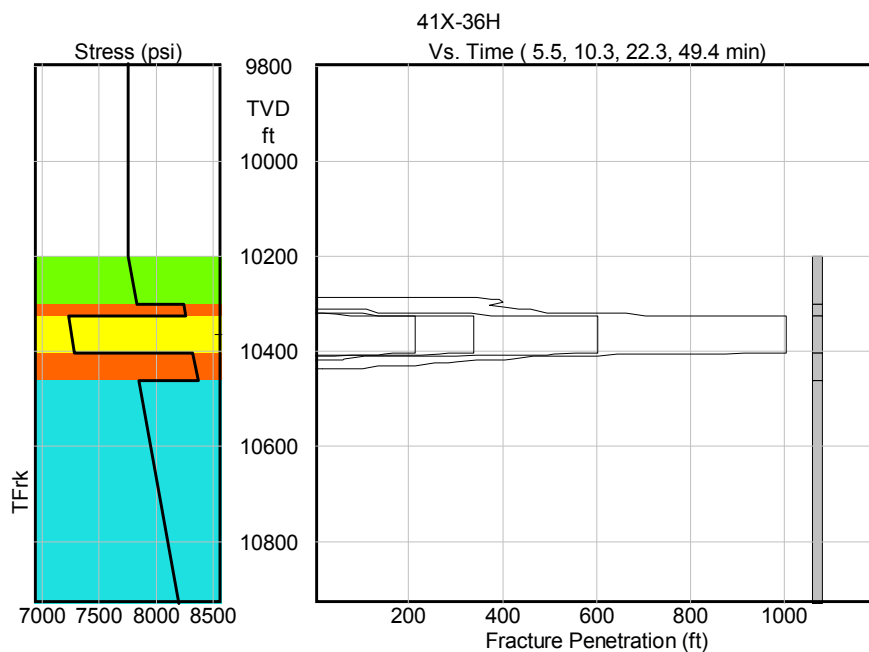


Figure 71. Propagation of fracture tip

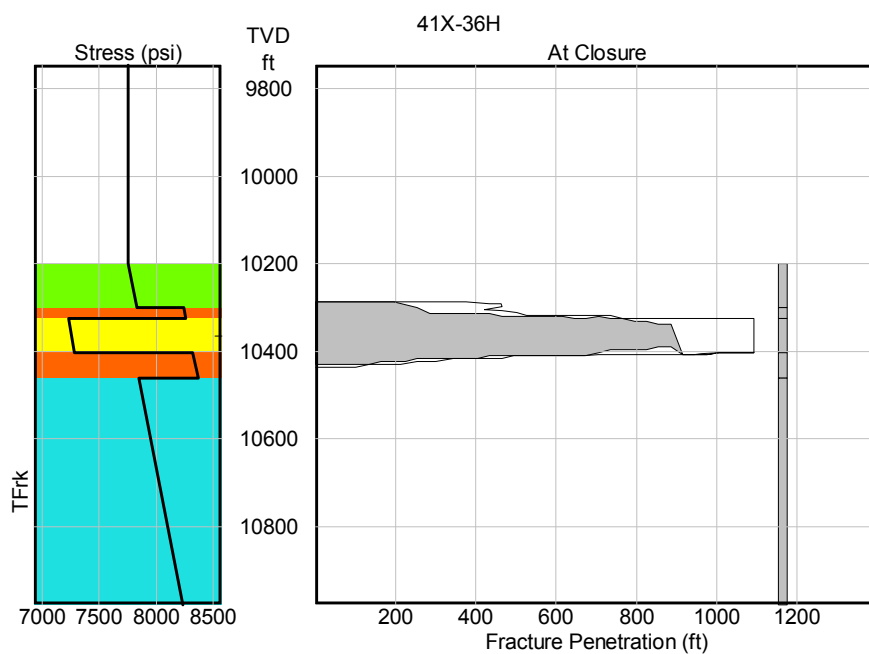


Figure 72. Cross section of the created hydraulic fracture – at closure

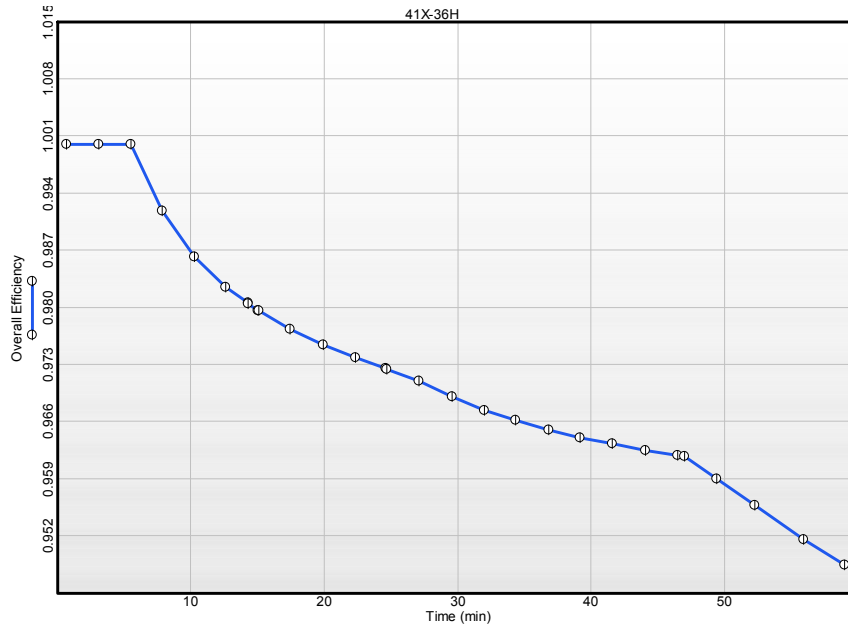


Figure 73. Fluid efficiency obtained from fully-3D simulation

In fact, the fracture volume is created by that portion of the fracturing fluid that does not leak-off into the formation. Hence, the fluid loss coefficient controls the created fracture geometry. This fluid loss coefficient determines the fluid efficiency, which is defined as:

$$\text{fluid efficiency} = \frac{\text{volume of fracture created}}{\text{total fracture fluid volume pumped}} \quad (50)$$

The best estimate of the fluid efficiency when designing a fracturing treatment for a specific well would be measuring the fluid efficiency in the laboratory or during a mini-frac test [Gidley, 1990].

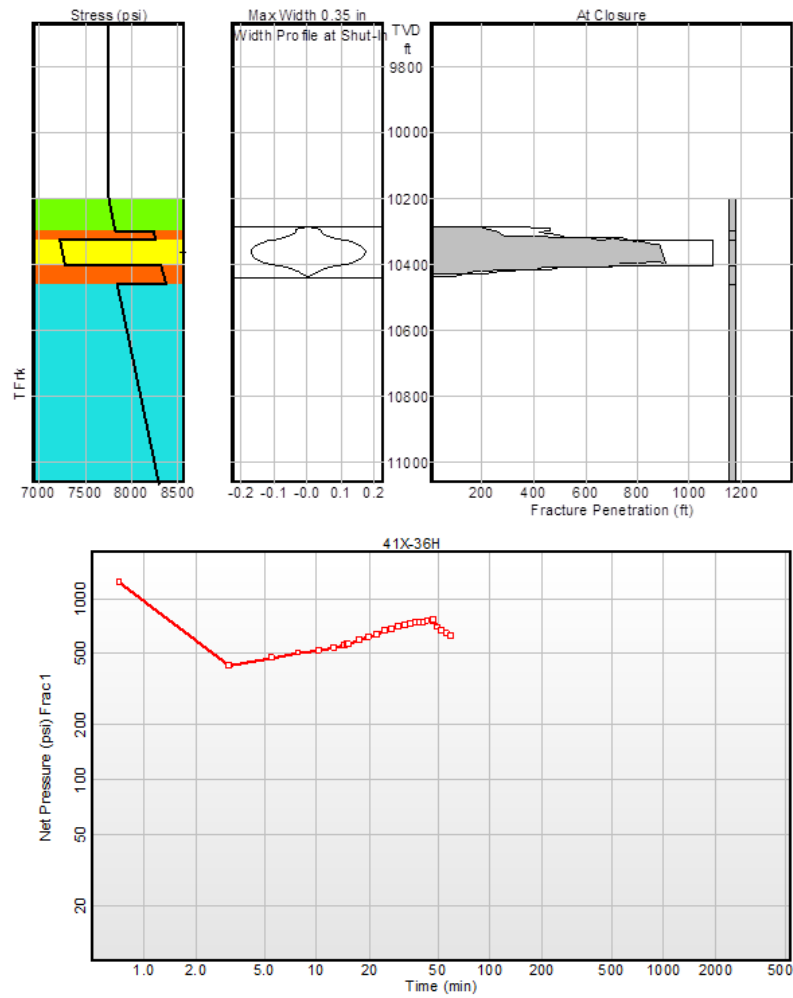


Figure 74. Summary plot for the optimal fracturing treatment— at closure

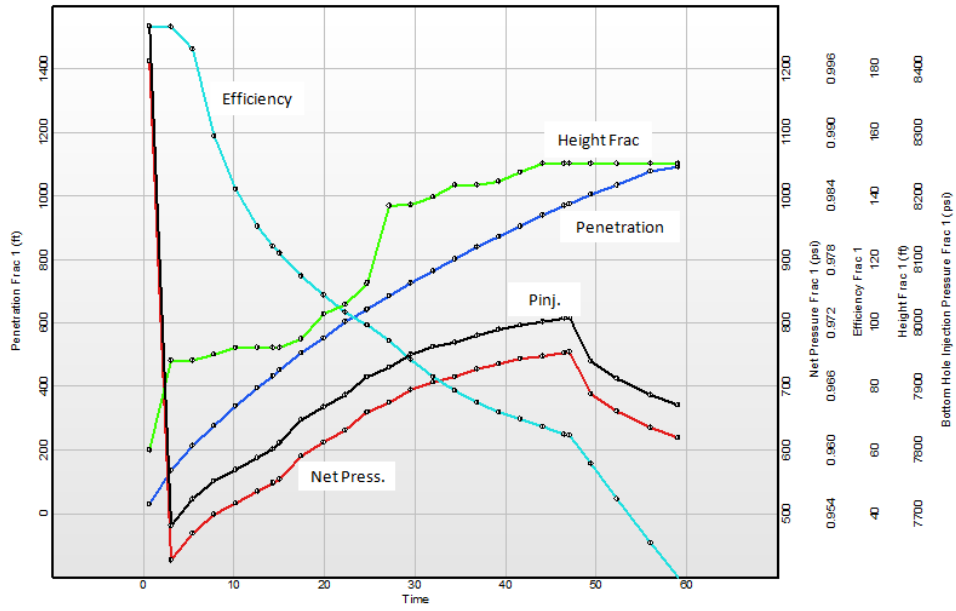


Figure 75. Summary plot for the optimal fracturing treatment— at closure

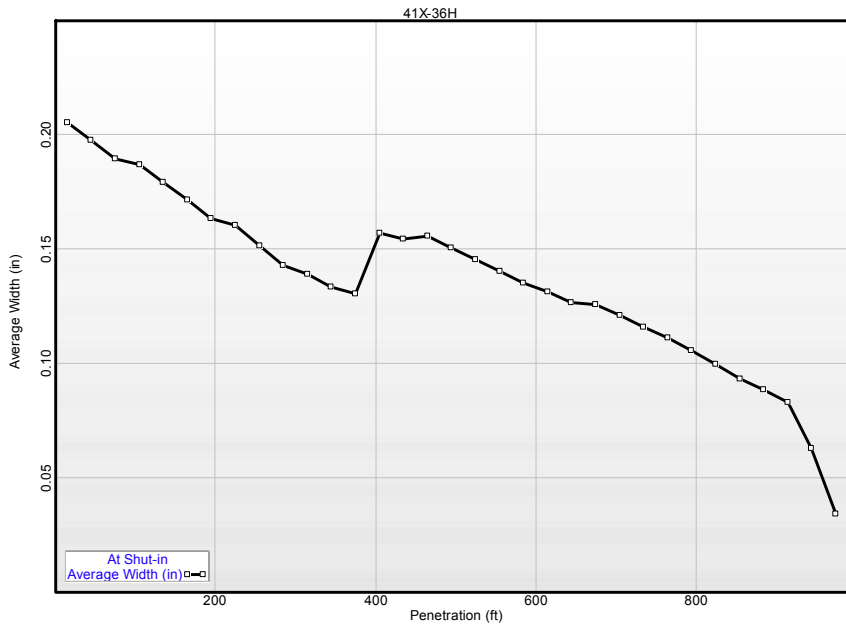


Figure 76. Average width of the fracture versus fracture penetration— at closure

The fully-3D/FEM modeling and simulation allow detailed contouring of the hydraulic fracture parameters. The parameters for which contour plots were prepared include: fluid pressure inside the fracture, cumulative fluid loss, fracture volume, local net pressure, net pressure (the difference between pressure in the fracture and closure

stress), proppant coverage, temperature, shear rate, and fluid viscosity along the fracture, fracture width profile (effective and total), the ratio of fracture width to proppant particle diameter, and the distribution of fluid velocity and proppant velocity at each point in the fracture, as illustrated in Figures 77 to 93.

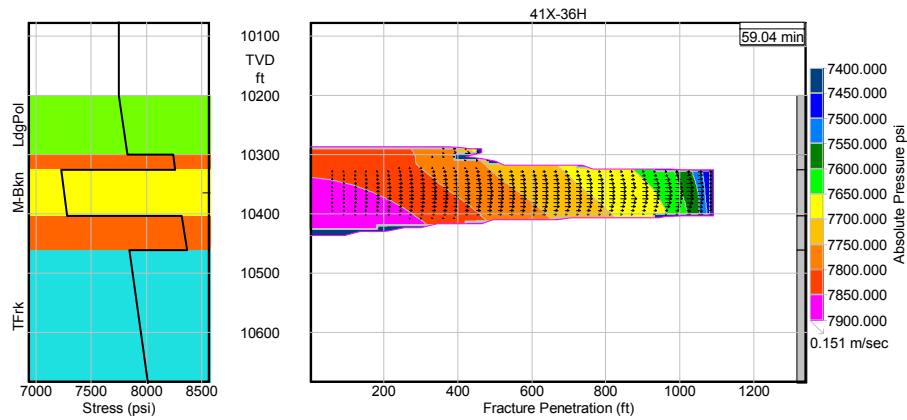


Figure 77. Absolute value of fluid pressure in the fracture — at closure

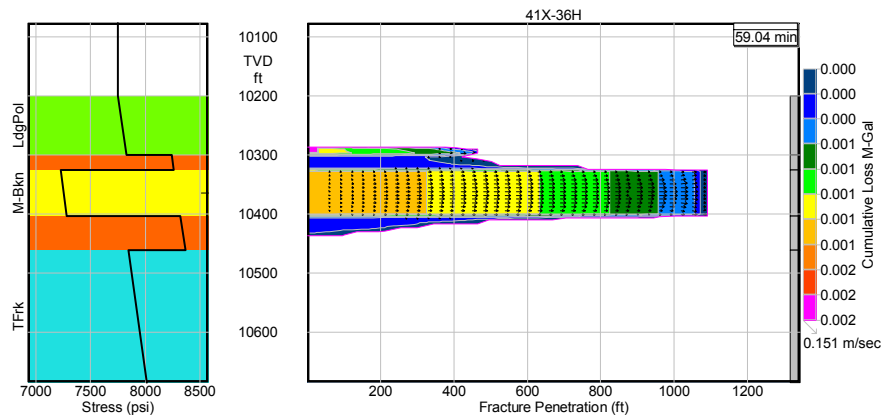


Figure 78. Cumulative fluid loss in the fracture — at closure

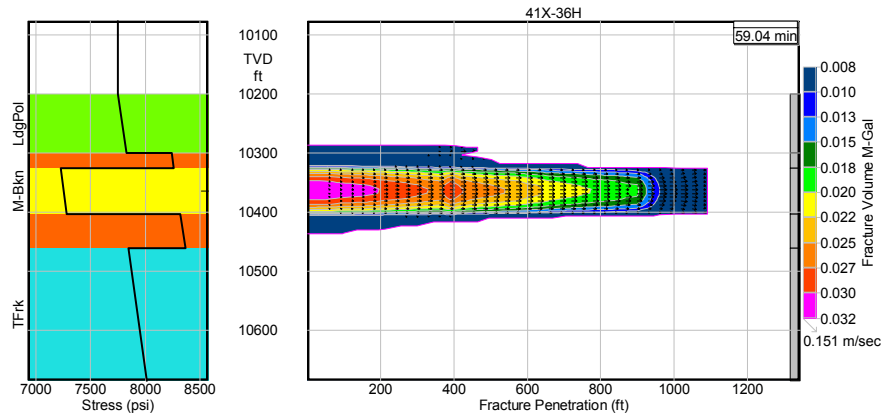


Figure 79. Fracture volume as the crack elongates — at closure

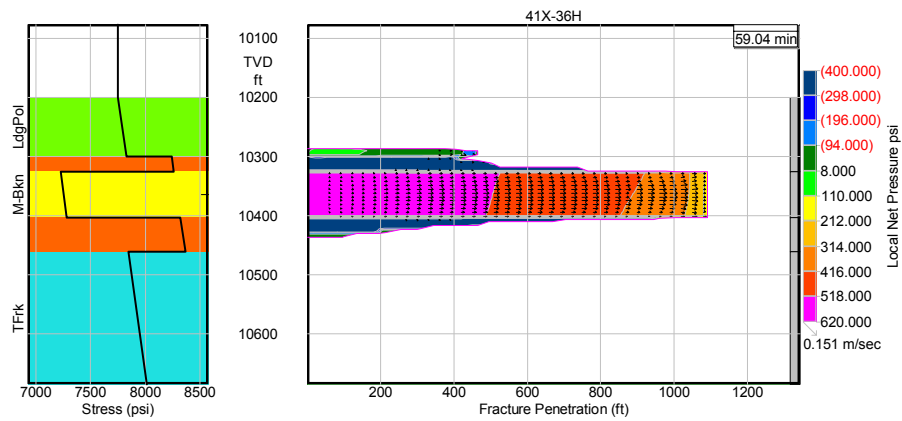


Figure 80. Local net pressure at each point in the fracture — at closure

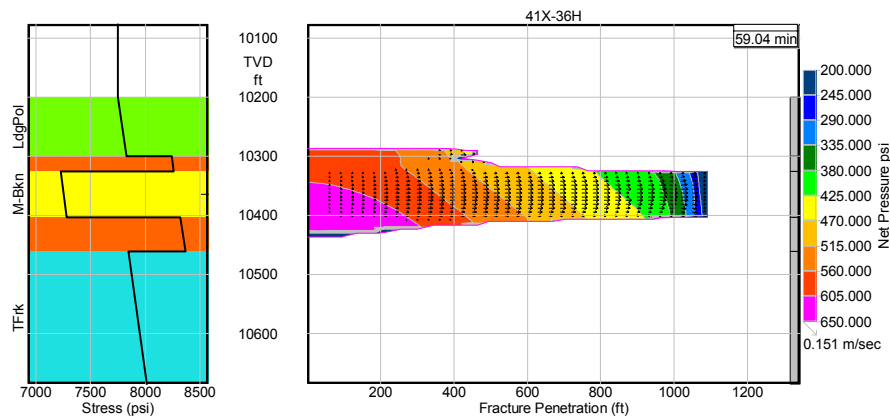


Figure 81. Net pressure at each point in the fracture — at closure

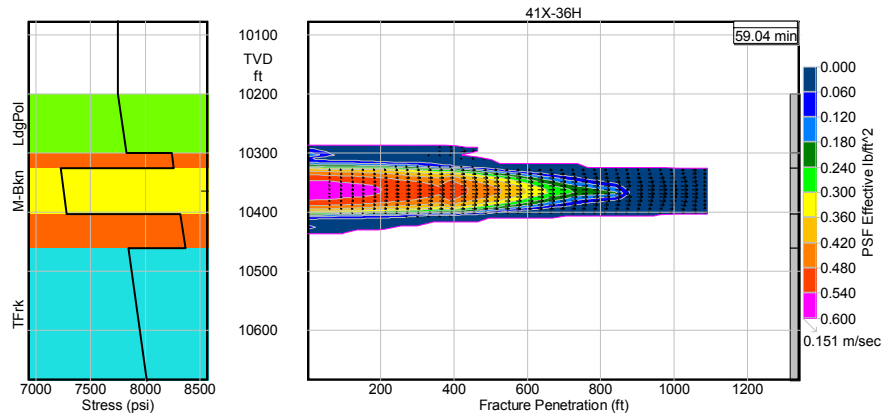


Figure 82. Proppant concentration along the created fracture (effective) — at closure

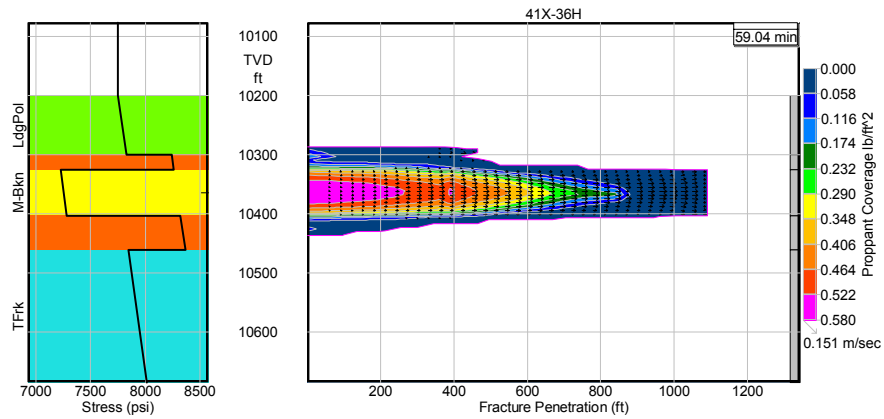


Figure 83. Proppant coverage along the created fracture — at closure

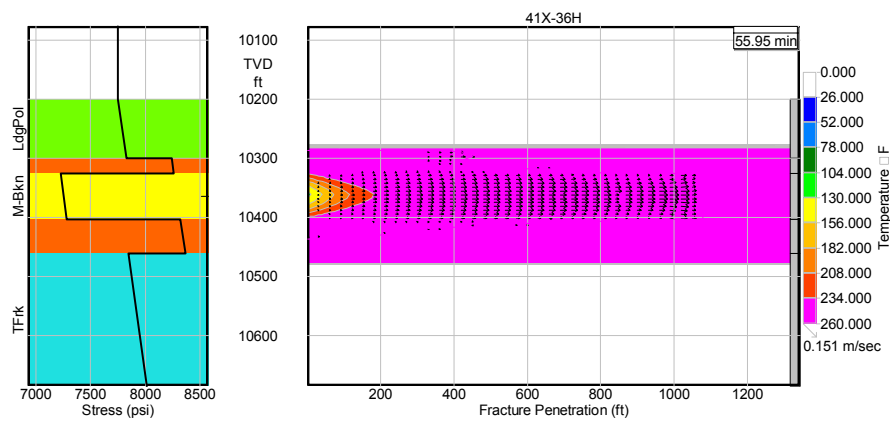


Figure 84. Temperature profile along the created fracture — at closure

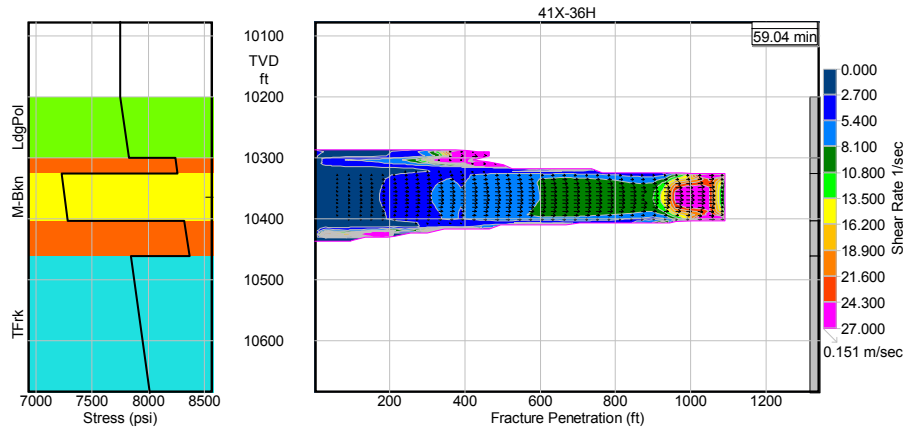


Figure 85. Shear rate profile as the crack propagates — at closure

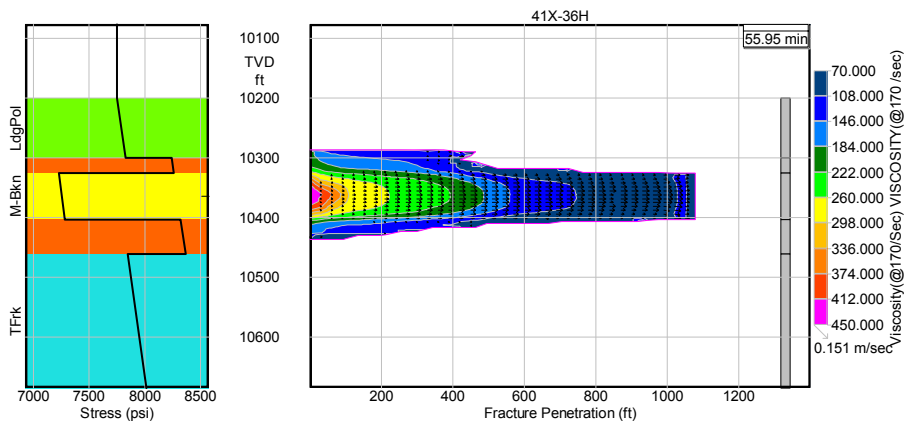


Figure 86. Viscosity of the fracturing fluid along the created fracture — at closure

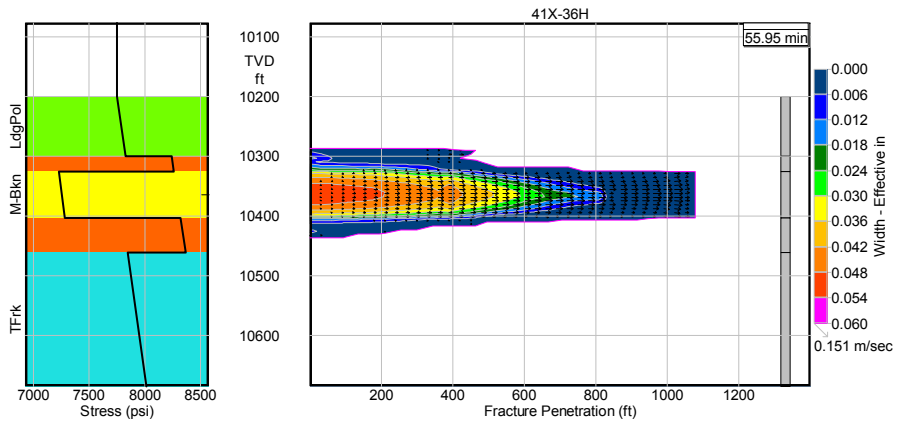


Figure 87. Width profile along the created fracture (effective, propped width) — at closure

Note that the effective fracture width is always less than the total width because some of the propped fracture width is lost due to embedment, crushing, or gel filter cake (compare Figures 88 and 89).

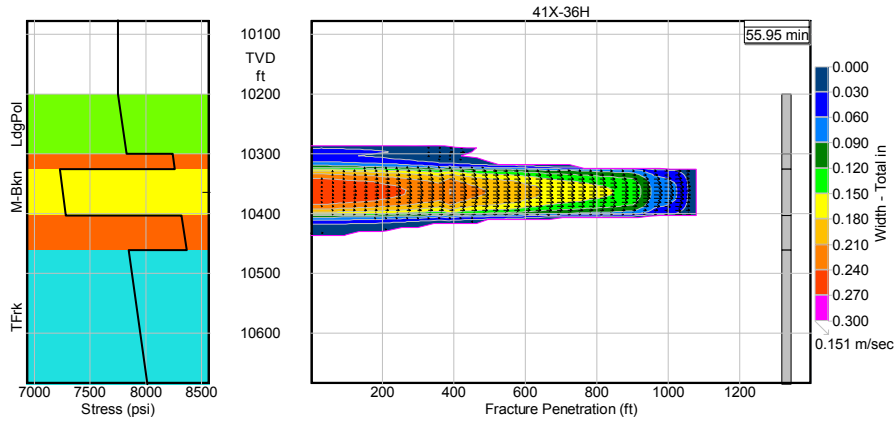


Figure 88. Width profile along the created fracture (total width) — at closure

Proppant mesh size impacts fracture length and width. The proppants can be “bridged out” if the fracture width decreases to less than three times the size of the diameter of the proppant particles [Gidley, 1990]. As proppants are deposited in a fracture, they can resist further fluid flow or the flow of other proppants, inhibiting further growth of the fracture. Proppant bridging calculations were made to make sure that the condition above (proppant constraint) would hold during the treatment (Figure 89).

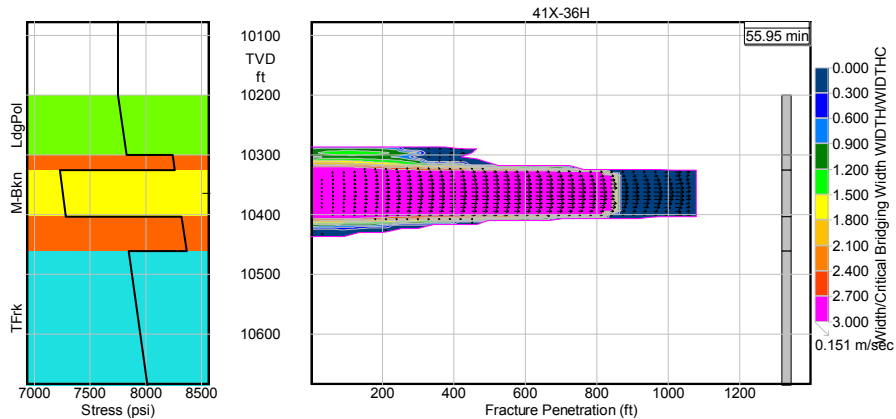


Figure 89. The ratio of fracture width to average proppant particle diameter — at closure

Figures 90 and 91 also illustrate the contour plots of proppant-velocity vector in the x-, and y-directions. These figures depict the elements of proppant-velocity as the crack-front advances along the “x” and “y” axes. Furthermore, Figures 92 and 93 depict the fluid-velocity distributions (in both x- and y-directions) as the crack propagates.

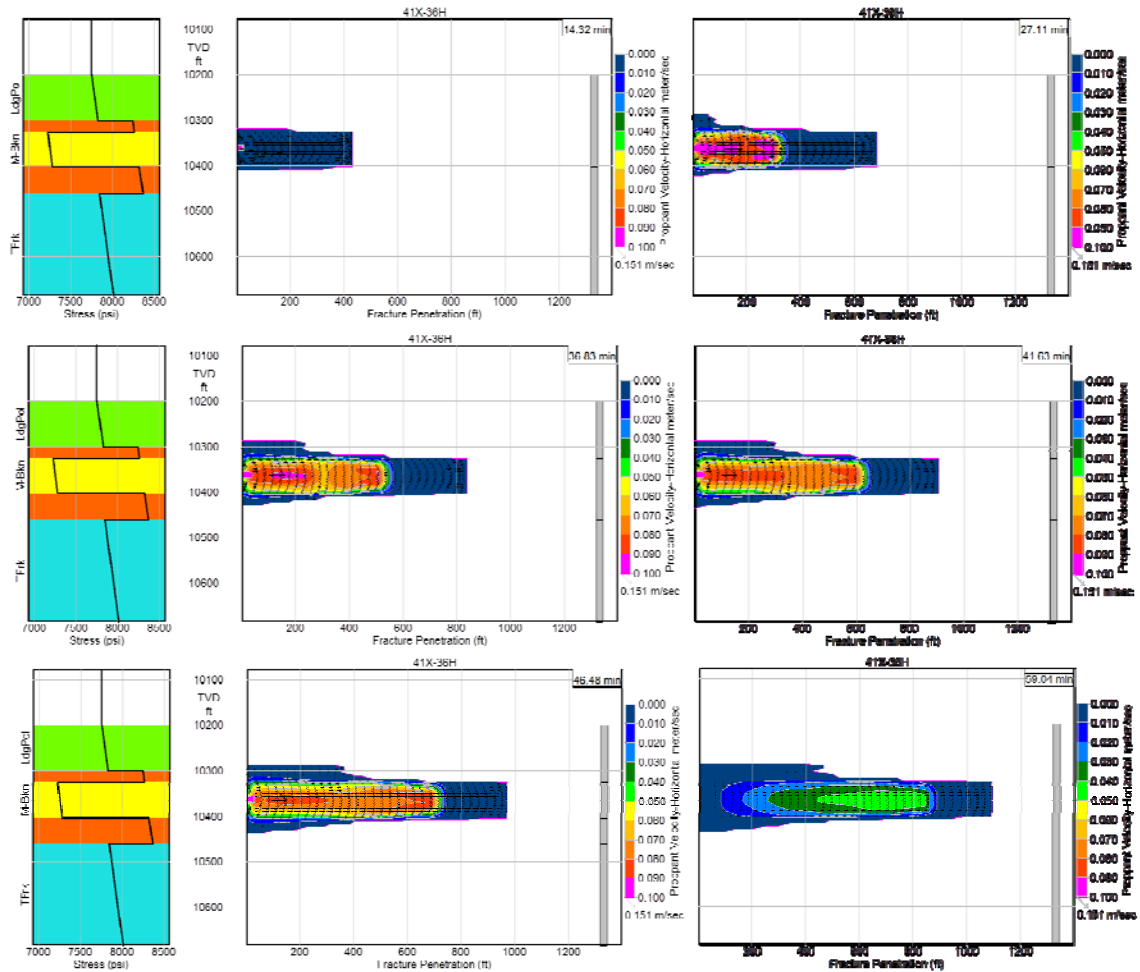


Figure 90. The contour plot of horizontal velocity of proppant as the crack propagates

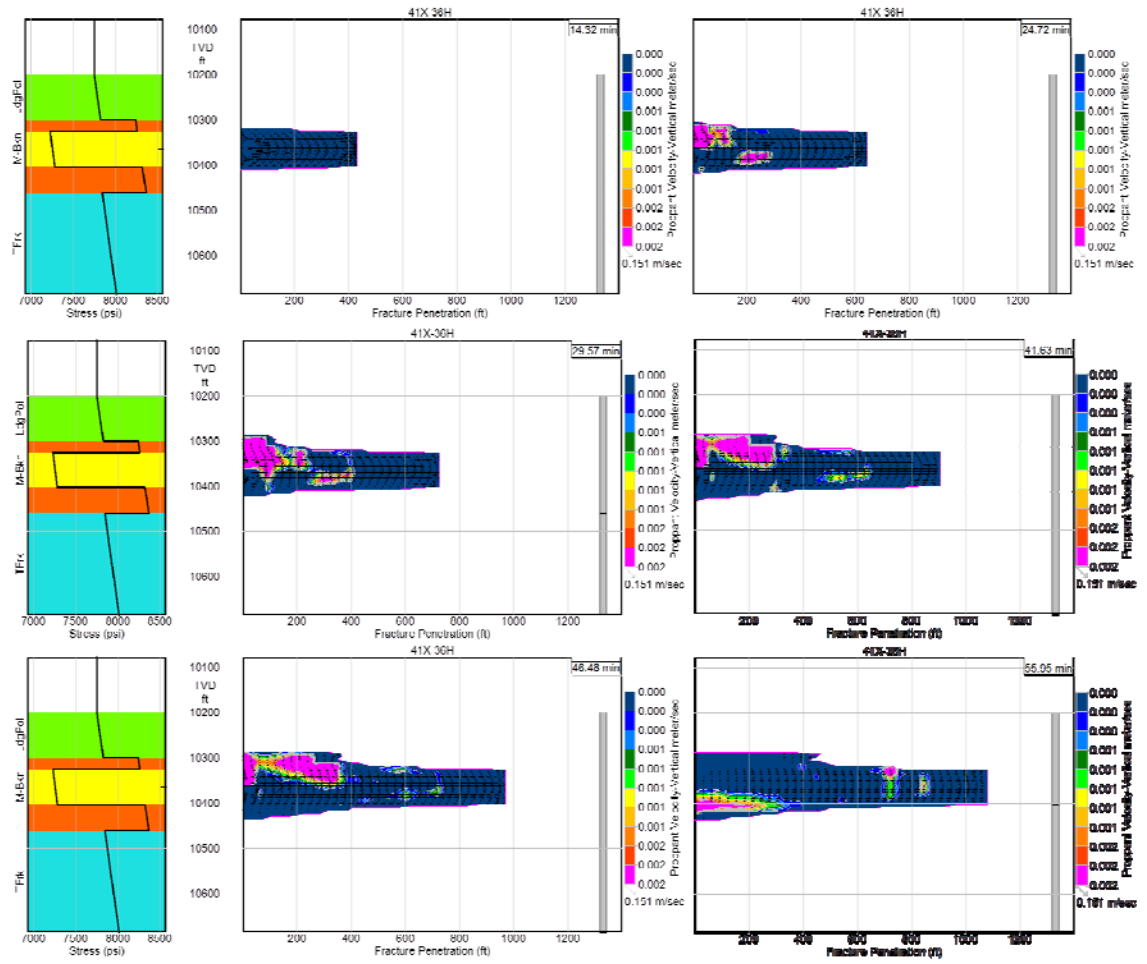


Figure 91. The contour plot of vertical velocity of proppant as the crack propagates

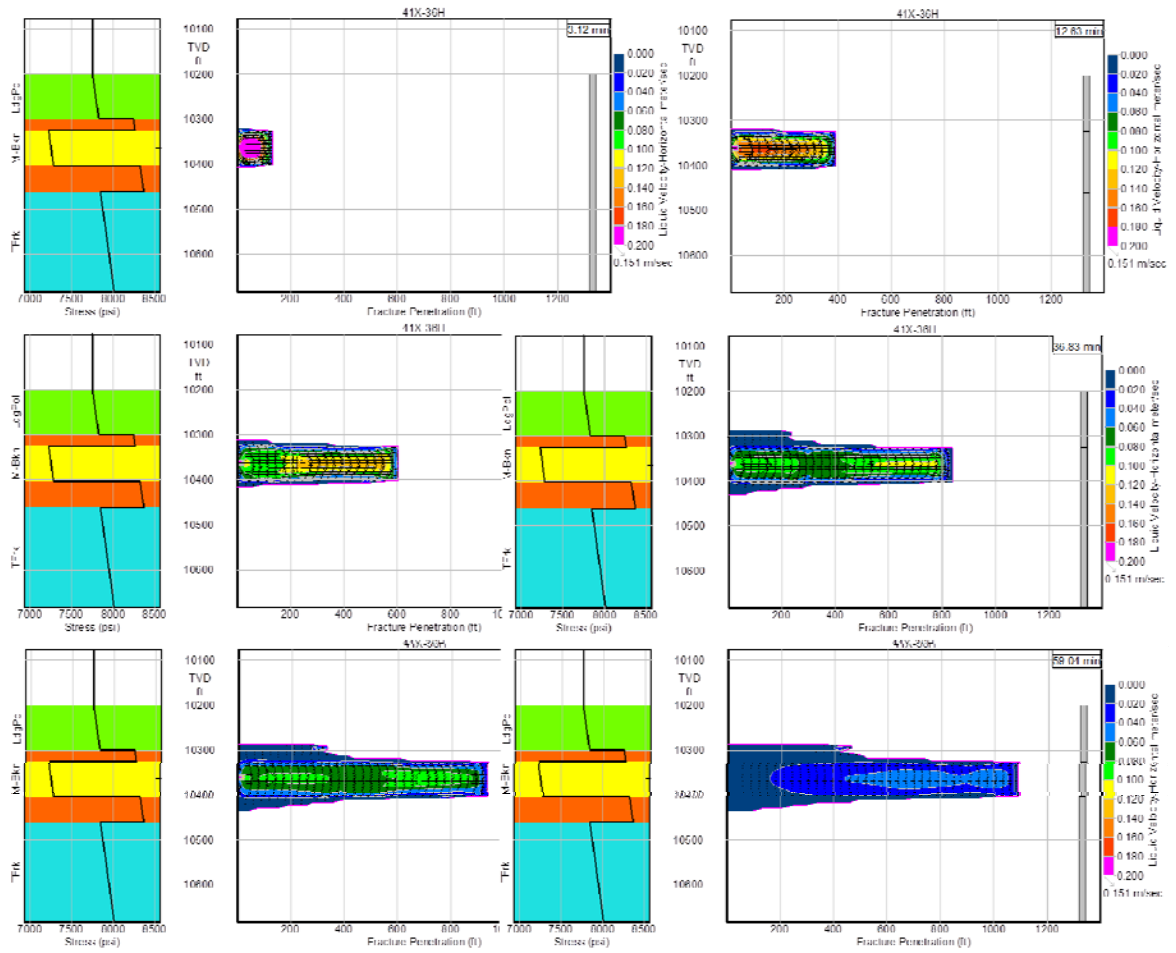


Figure 92. The contour plot of horizontal velocity of fracturing fluid as the crack propagates

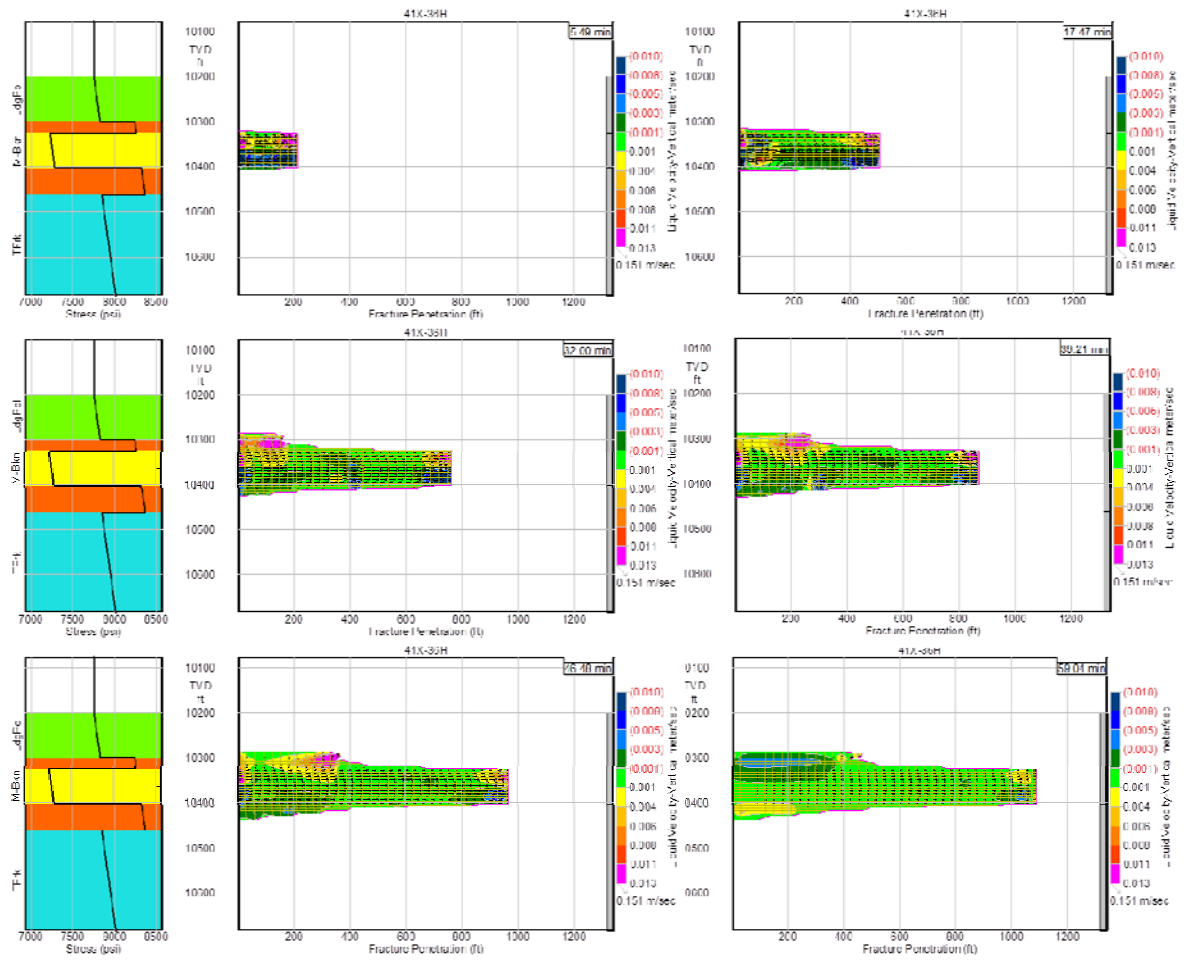


Figure 93. The contour plot of vertical velocity of fracturing fluid as the crack propagates

CHAPTER IV

UNCERTAINTY ASSESSMENT ASSOCIATED WITH PREDICTIONS AND SIMULATIONS

Numerical simulation models that are used for well stimulation planning are usually complex and are prone to error. These models have many factors that generally contain uncertainty, which lead to uncertainty in the model outputs. Uncertainty assessment can describe such uncertainties in model results. It is critical to the future development plans that uncertainty be properly assessed [*Cacuci*, 2003; *Marais et al.*, 2008; *Saltelli et al.*, 2008].

In this section we present an approach to the uncertainty assessment of the simulation models used for the design optimization of hydraulic fracturing in the Bakken Formation. The use of numerical simulation in petroleum engineering, and the presence of uncertainty in all aspects of design and modeling, may lead to questions such as: *What confidence do we have in model results? What are the limits in terms of applicability of model results?* Uncertainty assessment together with sensitivity analysis can provide the answers to such questions.

There are several methods of representing uncertainty, such as probability method, possibility method, Dempster Shafer evidence theory, and interval analysis [*Zadeh*, 1965; *Kalos and Whitlock*, 1986; *Manno*, 1999; *Ayyub and Klir*, 2006; *Dubois*, 2006; *Allaire*, 2009]. In this research, probabilistic approach with Latin

hypercube sampling (i.e. random variables with known distribution functions) was used.

The uncertainty assessment for the Bakken project was conducted using the following seven-step procedure:

- 1) ***Describing assessment goals:*** The goals of the uncertainty assessment for the designed fracturing treatments are: a) unveiling modeling errors, b) identifying important factors, c) rendering research priorities, and d) defending the simulation results in the face of criticism.
- 2) ***Describing assumptions and constraints:*** In an uncertainty assessment task three values for each parameter are required; low, middle, and high. The “low” should represent a value near the lower limit of practical values, the “high” should represent a value near the upper limit of practical values, and the “middle” should be a value in the range between the “low” and the “high”.
- 3) ***Describing parameters and outputs:*** The uncertainty assessment begins with the definition of factor distributions— usually reservoir variables. Uncertainty assessment uses simulation results to develop response surface (RS) for the objective functions, being NPV in this study. Factors and outputs used for the uncertainty assessment are shown in Table 21.
- 4) ***Classifying factor uncertainty:*** The uncertainties in the simulations can be classified into two types; a) *aleatory*, which arises through natural randomness, or, b) *epistemic*, which arises through imperfect knowledge [Ang and Tang, 2007; Allaire, 2009]. Note that aleatory uncertainty is irreducible (unless changing the sampling method), whereas epistemic uncertainty can be reduced either by increasing model fidelity (through

more accurate reservoir modeling) or by performing additional measurements (i.e. well logs, well tests, etc.). It is more likely that we have epistemic uncertainty in our simulations because we have used *Latin hypercube* as the sampling method. In an effort to reduce epistemic uncertainty propagation error in the modeling process, new models were developed which took into consideration the geomechanical behavior of naturally fractured reservoirs (NFRs). The models described the relationships between geomechanical parameters and fracture aperture, which can be important in stress-sensitive NFRs. Such relationships among the key parameters can be used for conducting more accurate reservoir characterization to reduce the epistemic uncertainties [Jabbari and Zeng, 2011; Jabbari et al., 2011a; Jabbari et al., 2011b; Jabbari et al., 2012].

- 5) **Conducting uncertainty analysis:** Performing the uncertainty assessment can lead to answering the key question: “*How do uncertainties in the simulation model, from parameters, propagate to uncertainties in the results?*”
- 6) **Conducting sensitivity analysis:** The main purpose of conducting a sensitivity analysis is to meet the goals of the uncertainty assessment by answering two key questions: a) which parameters contribute to variability in model outputs? and b) which factors should be considered for further research to reduce variability in model outputs?
- 7) **Presenting the results:** The visual presentation of quantitative information, such as the results of sensitivity and uncertainty analyses can be used in support of decision- and policy-making, though the results are not in the form of an evaluated decision-rule or utility function.

That being said, the main goals of our calculations are to establish a *probabilistic modeling* for assessing uncertainties in the simulation results, to develop proxy models for approximating the output at un-simulated points, and to demonstrate the results from the calculations with probability distribution curves.

Table 21. Factors examined in the Uncertainty Assessment

Parameters	Probability Distribution Function	Uncertainty Type
PorMtrxMultiplier	Uniform	
PermMtrxMultiplier	Normal	
PorFracMultiplier	Fixed-value	
PermNatFrac	Lognormal	
KvKhRatio	Normal	
DI_NatFrac	Lognormal	
DJ_NatFrac	Normal	
DK_NatFrac	Triangular	
Rel. Perm. Table – Matrix		
Soirw	Uniform	
Krocw	Uniform	
Krgcl	Uniform	
Krwiro	Triangular	
no	Normal	
nw	Uniform	epistemic
Rel. Perm. Table – Nat. Frac.		
Sgconf	Uniform	
Sgcrit	Lognormal	
Soirgf	Normal	
Sorgf	Lognormal	
Sorwf	Normal	
Swconf	Lognormal	
Krgclf	Normal	
Krocwf	Lognormal	
Krwirof	Triangular	
Swtr(i)	Normal	
Hyd. Frac. Cond. (kfw), md-ft	Fixed-value	
Hyd. Fracture Spacing, ft	Fixed-value	

In the simulation models, the input parameters are replaced by appropriate probability distributions rather than single values. The parameter whose value cannot be set with certainty is called a random variable (Table 21). Accordingly, the output value (either *Cum_OIL* or *NPV*) will be a probability distribution rather than a single value. The steps of the method include: a) using the simulation model via random sampling, such as Latin hyper cube, to obtain information, b) using a deterministic

model to combine the variables of the model, c) repeating the process several times, and d) analyzing the probabilistic outputs in order to make it possible to evaluate alternative courses of action [Mian, 2011]. Monte Carlo simulation was used in this study to conduct such analyses.

Monte Carlo simulation

Monte Carlo method is a broad class of computational algorithms that rely on random sampling to obtain numerical results. They are often used in physics and mathematical problems and are most suited to be applied when it is impossible to obtain a closed-form expression or infeasible to apply a deterministic algorithm. Monte Carlo methods are mainly used in three distinct problems: optimization, numerical integration and generation of samples from a probability distribution [Anderson, 1986; Mian, 2011]. The steps in a Monte Carlo simulation are as follows:

- 1) Defining the problem,
- 2) Assessing the input parameters through a sensitivity analysis,
- 3) Developing the probability distributions for the significant parameters. The probability distributions can be of standard forms, such as normal and lognormal, or they may be of empirical forms, such as rectangular/uniform and triangular, or more complicated shapes. Each of these distributions are explained in more details below:

Uniform Probability Distribution:

A uniform distribution is defined by two values, a and b , such that $a < b$. A random variable X with such a distribution is uniformly distributed on the interval $[a, b]$ with the following probability distribution function:

$$f(X) = \begin{cases} \frac{1}{b-a} & \text{for } b \leq X \leq a \\ 0 & \text{otherwise} \end{cases} \quad (51)$$

Figure 94 shows the general form of a uniform distribution.

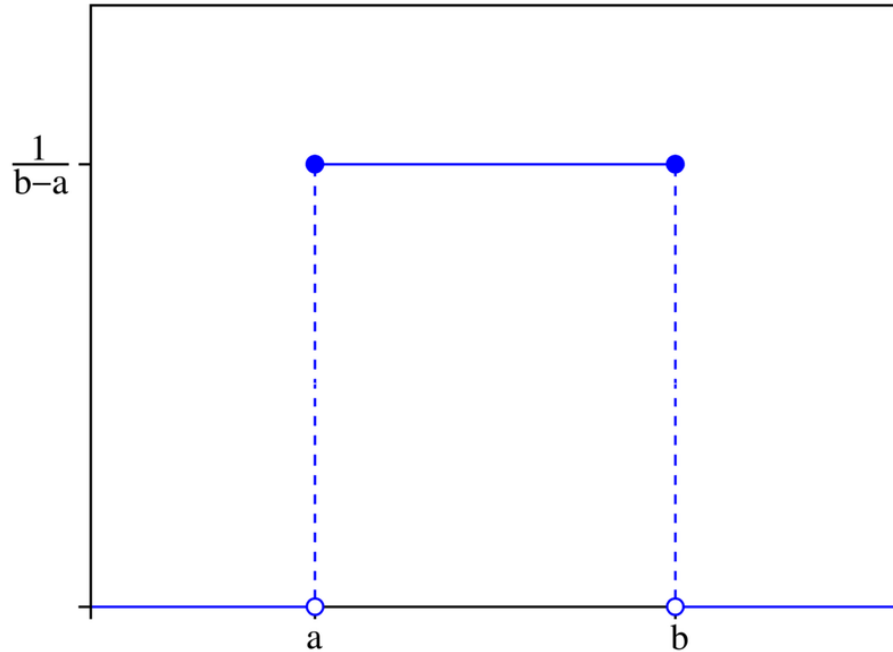


Figure 94. Uniform probability density function (continuous)

It can also be in the form of a discrete uniform distribution such that all values of a finite set of possible values have equal probability (Figure 95).

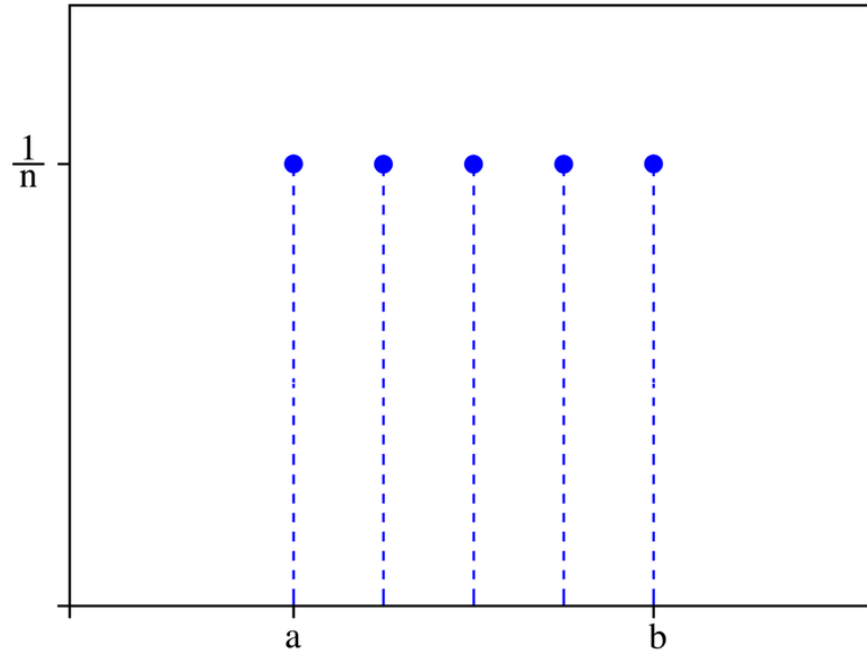


Figure 95. Uniform probability density function (discrete)

Normal Probability Distribution:

A normal distribution, or Gaussian distribution, is typically defined by a mean, μ , and variance, σ^2 . A random variable X with such a distribution is normally distributed on the interval $(-\infty, \infty)$ with the following probability distribution function:

$$f(X|\mu, \sigma^2) = \frac{1}{\sigma\sqrt{2\pi}} \exp\left[-\frac{1}{2}\left(\frac{X-\mu}{\sigma}\right)^2\right] \quad (52)$$

Figure 96 shows the general form of a normal distribution.

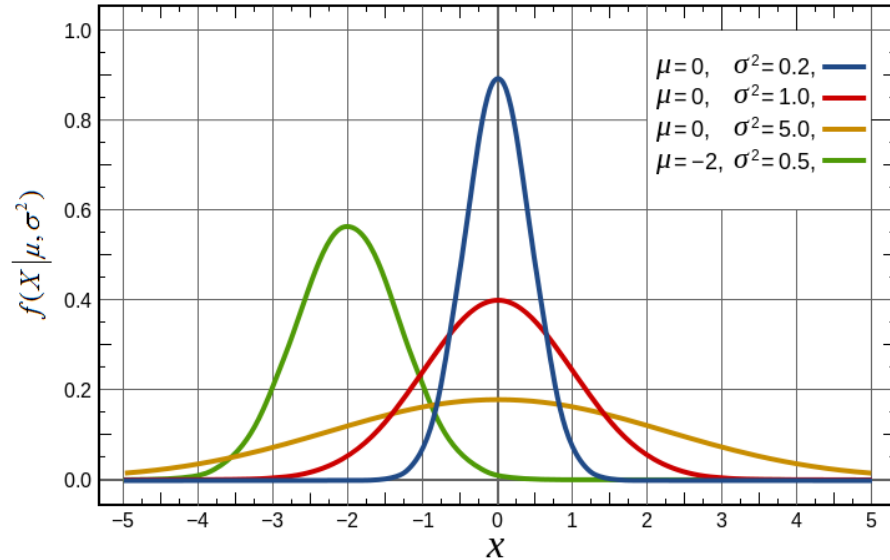


Figure 96. Normal probability density function (*courtesy of Wikipedia*)

Lognormal Probability Distribution:

Another useful distribution, based on the normal distribution, is the lognormal distribution. This type of distribution is widely used in environmental engineering and economics to represent the distribution of returns on investments, insurance claims, and many oil and gas related problems. Core permeability and formation thickness may be represented by the lognormal distributions [Mian, 2011]. In probability theory, a log-normal distribution is a continuous probability distribution of a random variable whose logarithm is normally distributed. If X is a random variable with a normal distribution, then $Y = \exp(X)$ has a log-normal distribution; likewise, if Y is log-normally distributed, then $X = \ln(Y)$ has a normal distribution. A random variable which is log-normally distributed takes only positive real values. The lognormal probability distribution is given by:

$$f(X|\mu, \sigma^2) = \frac{1}{\sigma X \sqrt{2\pi}} \exp\left[-\frac{1}{2}\left(\frac{\ln X - \mu}{\sigma}\right)^2\right] \quad (53)$$

The general form of a lognormal distribution is shown in Figure 97.

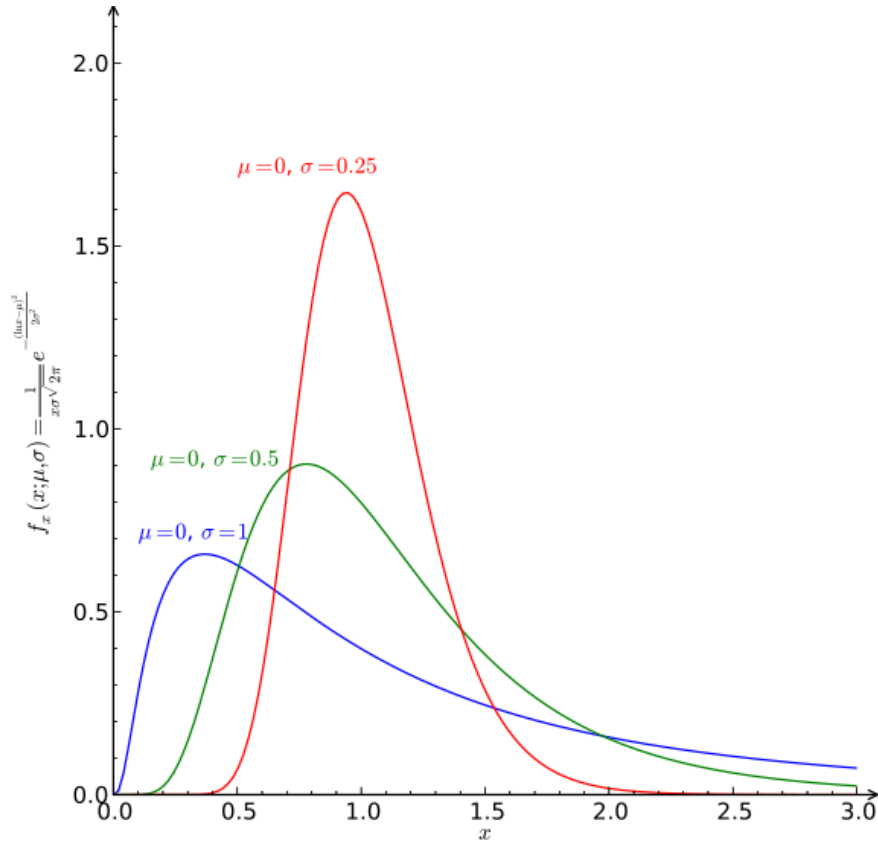


Figure 97. Lognormal probability density function (*courtesy of Wikipedia*)

Beta Probability Distribution:

A beta distribution is defined for the interval $[0,1]$ with two parameters, α and β , that define the shape of the distribution. The probability distribution function is given by:

$$f(X|\alpha, \beta) = \begin{cases} \frac{\Gamma(\alpha + \beta)}{\Gamma(\alpha)\Gamma(\beta)} X^{\alpha-1} (1-X)^{\beta-1} & \text{for } 0 \leq X \leq 1 \\ 0 & \text{otherwise} \end{cases} \quad (54)$$

Where $\Gamma(x)$ is the gamma function, which is defined as:

$$\Gamma(x) = \int_0^{\infty} x^{\alpha-1} e^{-x} dx \quad (55)$$

The general form of a beta distribution for some values of α, β is shown in Figure 98.

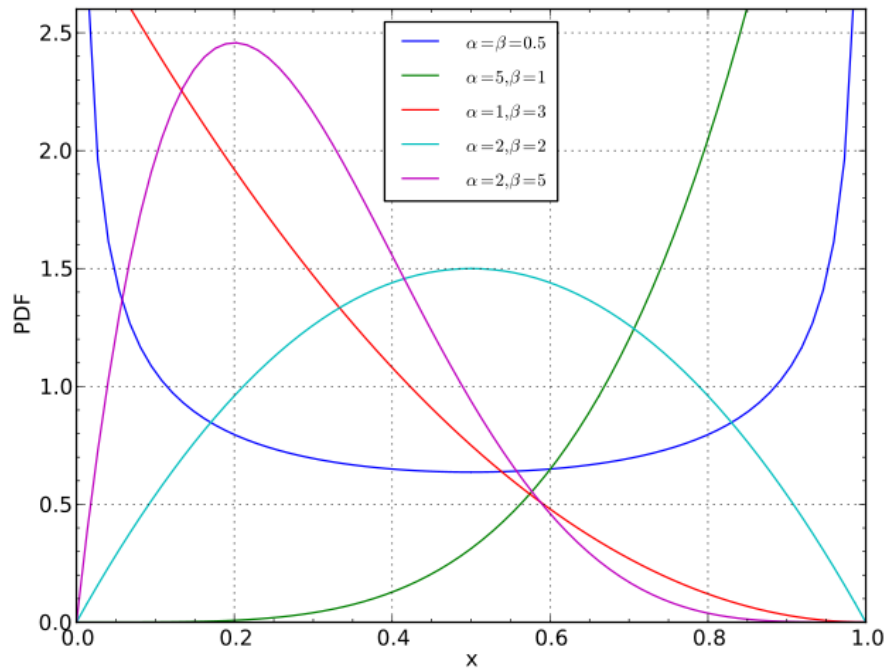


Figure 98. Beta probability density function (*courtesy of Wikipedia*)

The beta distribution is a useful distribution in the sense that its shape parameters give it a lot of flexibility and it is defined on a finite interval rather than on $(-\infty, \infty)$. However, as can be seen from the definition of its probability density function, a beta distribution is complex in that the parameters of the distribution do not have obvious interpretations. For this reason, it is common in modeling for decision- and policy-making to use a triangular distribution as a proxy for a beta distribution [Williams, 1992; Johnson, 1997; Allaire, 2009].

Triangular Probability Distribution:

In probability theory and statistics, the triangular distribution is a continuous probability distribution with lower limit a , upper limit b and mode c , where $a < b$ and $a < c < b$. The probability density function is given by:

$$f(X|a,b,c) = \begin{cases} \frac{2(X-a)}{(b-a)(c-a)} & \text{for } a \leq X < c \\ \frac{2(b-X)}{(b-a)(b-c)} & \text{for } c \leq X \leq b \\ 0 & \text{otherwise} \end{cases} \quad (56)$$

The triangular distribution is a more understandable means for quantifying uncertainty than a beta distribution in the sense that the role of the parameters in this family of distributions is transparent. The general form of a triangular distribution is shown in Figure 99.

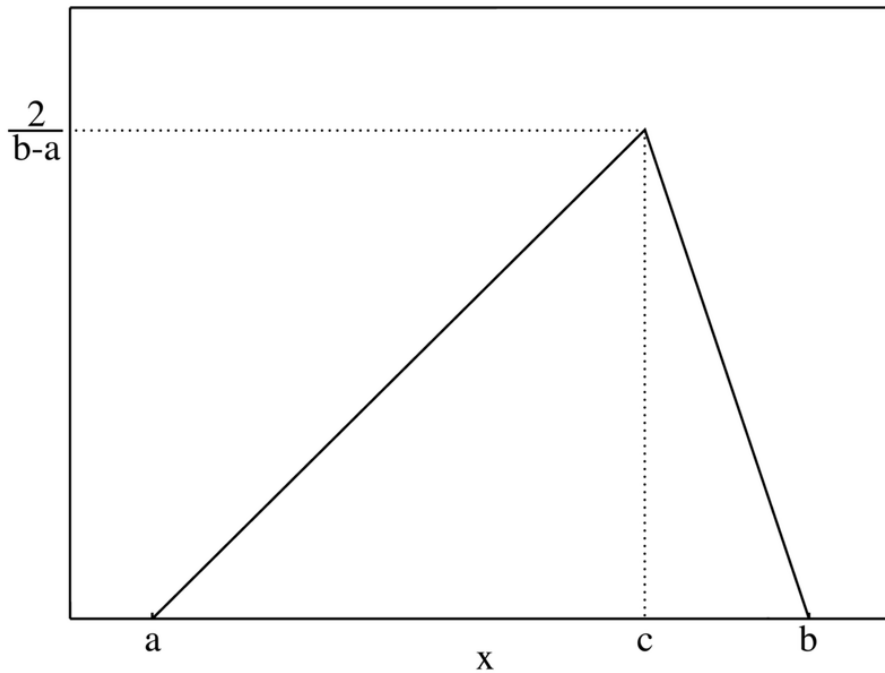


Figure 99. Triangular probability density function

The mean and standard deviation of a triangular distribution are calculated using the following equations [Mian, 2011]:

$$\bar{X} = \frac{X_{low} + X_{middle} + X_{high}}{3} \quad (57)$$

$$s = \sqrt{\frac{(X_{high} - X_{low})(X_{high}^2 - X_{high}X_{low}) - X_{middle}X_{high}(X_{high} - X_{middle}) - X_{low}X_{middle}(X_{middle} - X_{low})}{18(X_{high} - X_{low})}} \quad (58)$$

The assessment of the probability functions can be based on fitting one of the above theoretical distributions to available data from the history matching and sensitivity analysis, or it can be based on analyst experience. In Figs.100 to 111 the histograms resulting from the history matching and randomly sampling from original distributions are shown. In the absence of specific knowledge about the form of probability distributions, however, it seems reasonable in most cases to assume normal or lognormal distribution, especially when dealing with various geological distributions [Mian, 2011]. Generally, permeability distributions of reservoirs fit lognormal curves, unlike porosity, which most frequently falls into the category of normal distributions [Tiab, 2012].

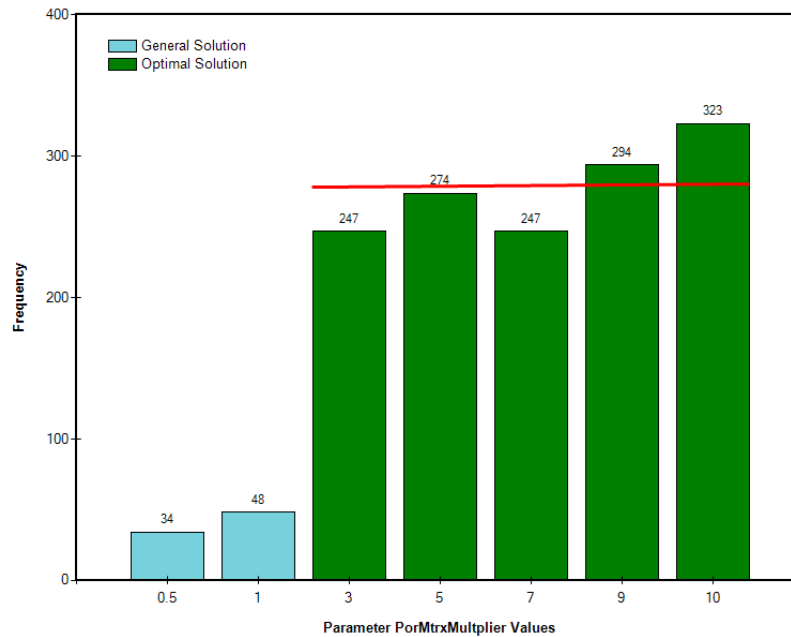


Figure 100. Fitting a probability distribution function to *PorMtrxMultiplier* by history matching—Uniform Distribution Function fits the data.

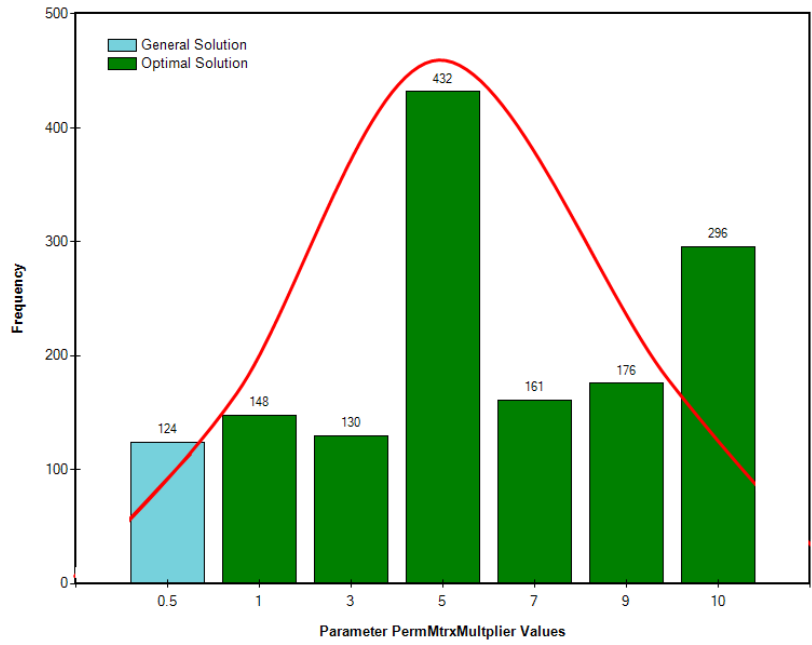


Figure 101. Fitting a probability distribution function to *PermMtrxMultiplier* by history matching—Normal Distribution Function fits the data.

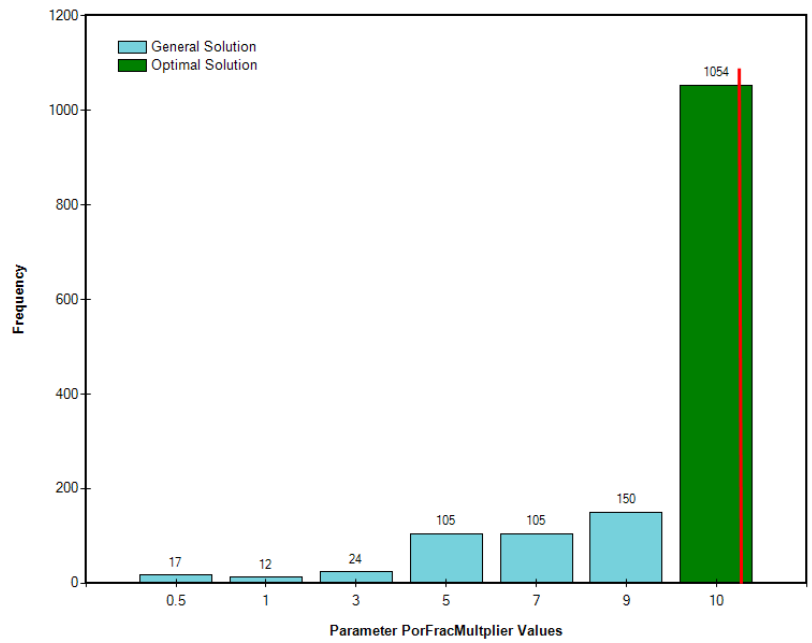


Figure 102. Fitting a probability distribution function to *PorFracMultiplier* by history matching—Fixed-value Distribution Function fits the data.

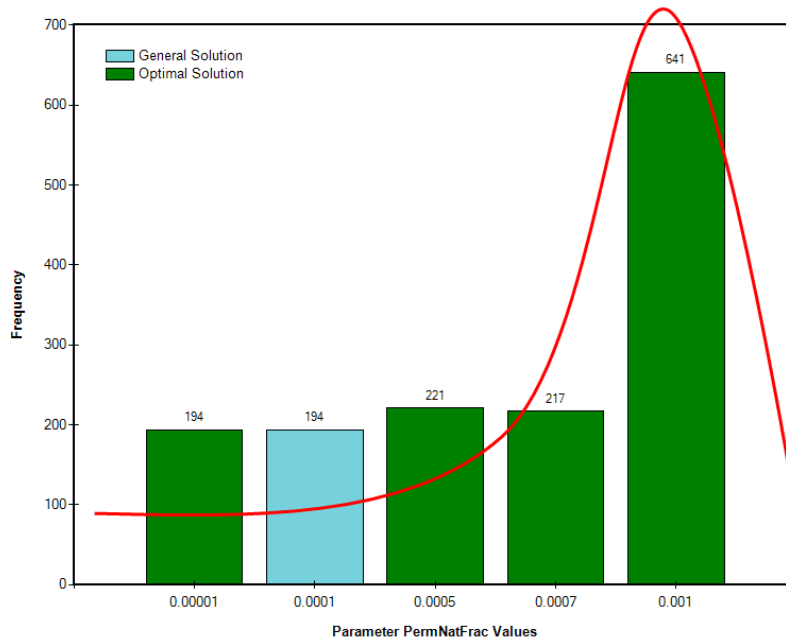


Figure 103. Fitting a probability distribution function to *PermNatFrac* by history matching—
Lognormal Distribution Function fits the data.

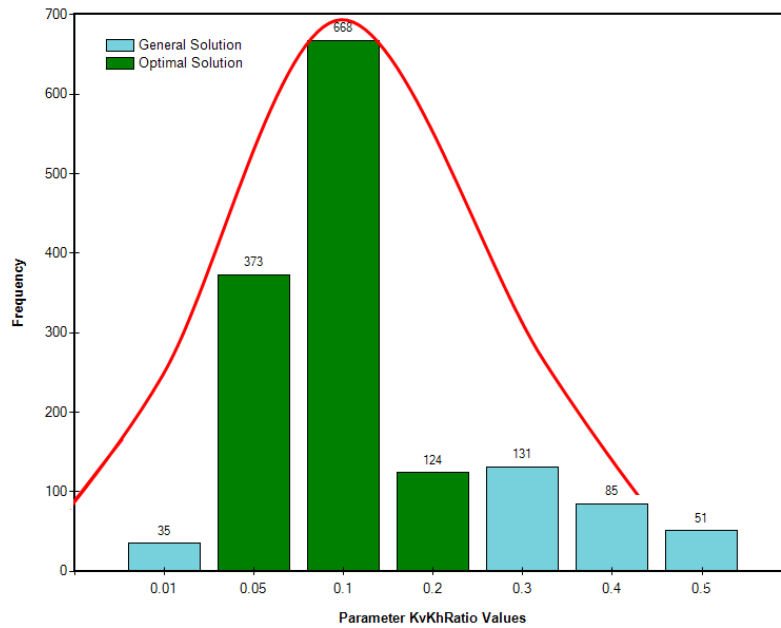


Figure 104. Fitting a probability distribution function to *KvKhRatio* by history matching—
Normal Distribution Function fits the data.

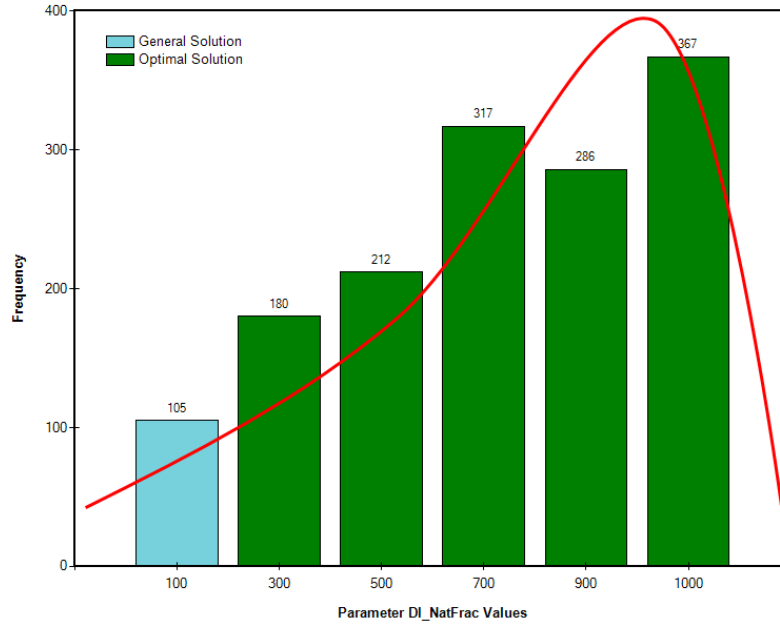


Figure 105. Fitting a probability distribution function to *DI_NatFrac* by history matching—
Lognormal Distribution Function fits the data.

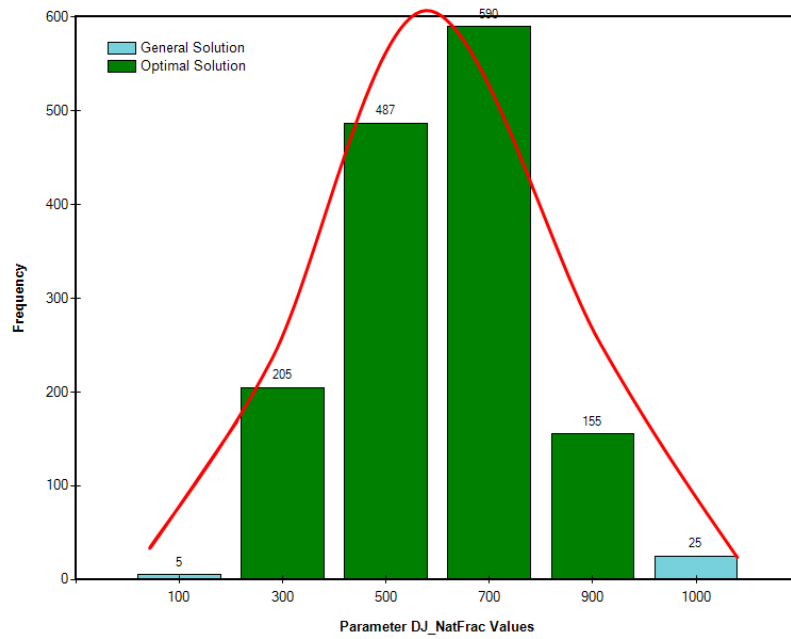


Figure 106. Fitting a probability distribution function to *DJ_NatFrac* by history matching—
Normal Distribution Function fits the data.

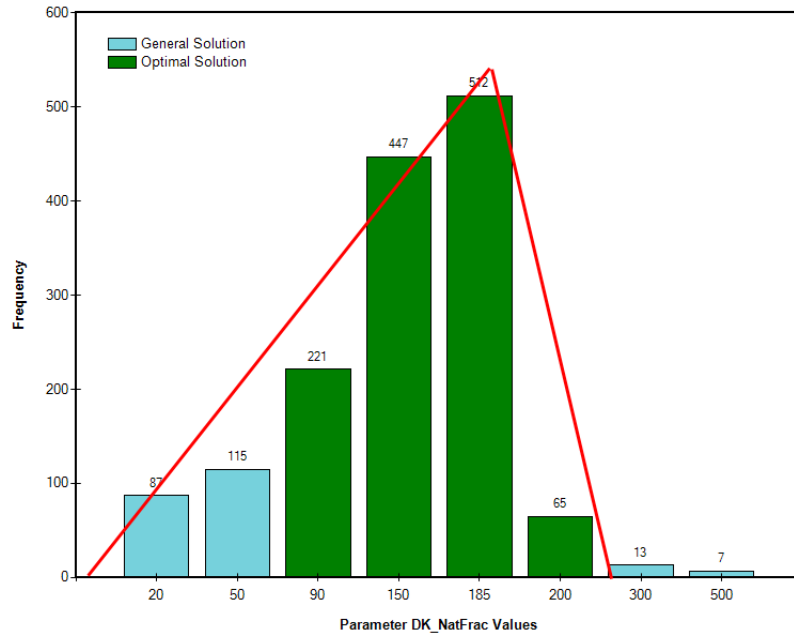


Figure 107. Fitting a probability distribution function to $DK_NatFrac$ by history matching—
 Triangular Distribution Function fits the data.

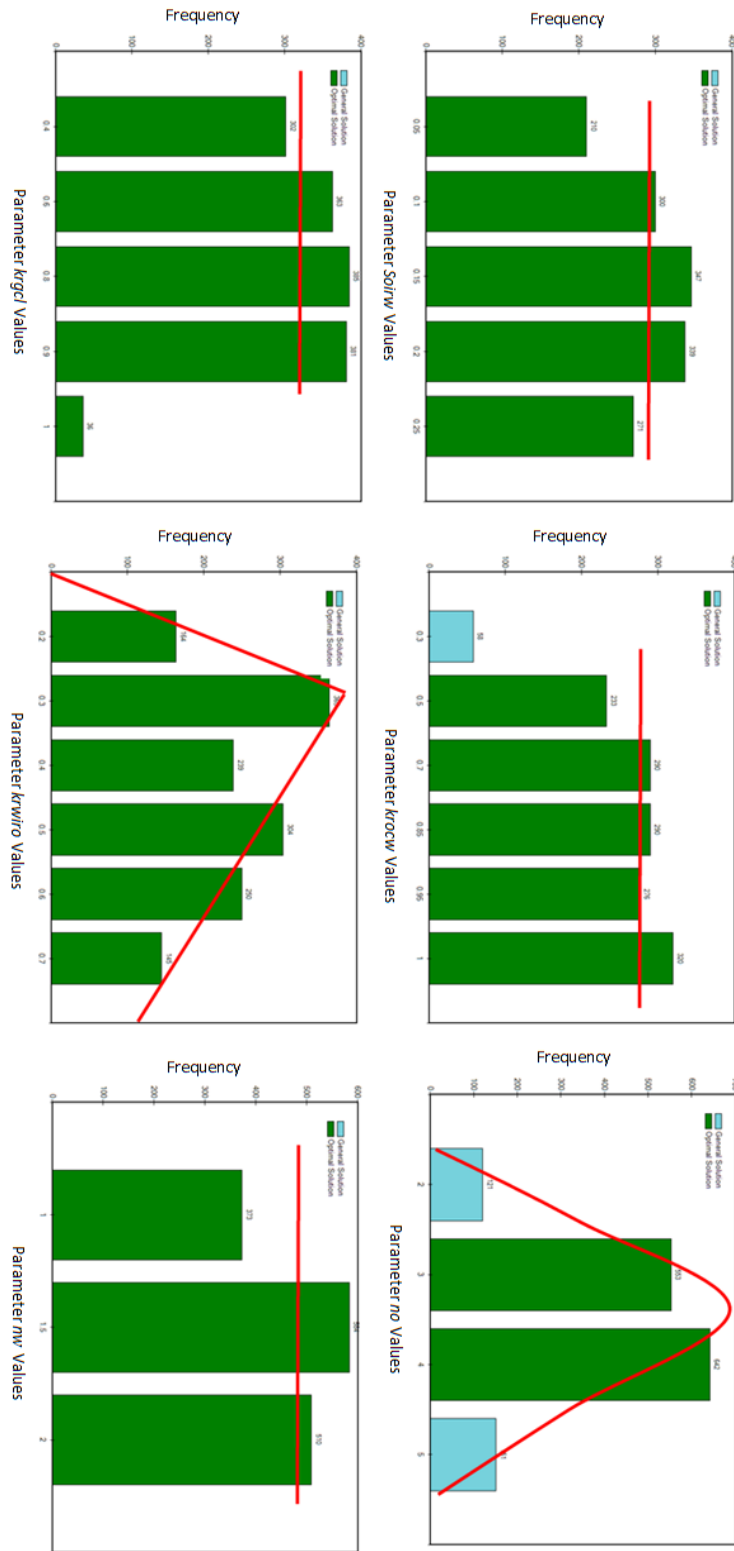


Figure 108. Fitting probability distribution functions to *Rel.Perm.Table_Matrix* by history matching

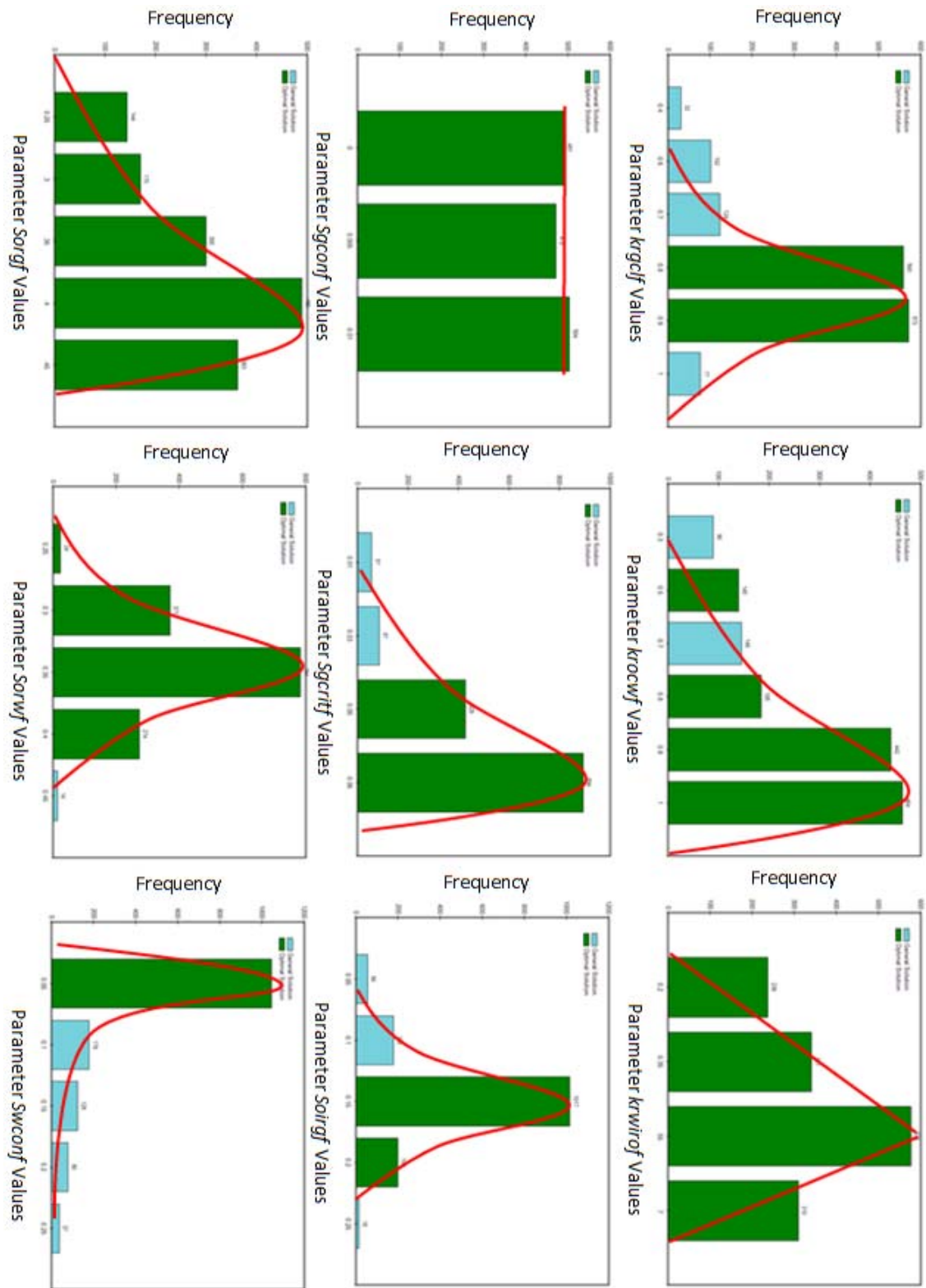


Figure 109. Fitting probability distribution function to *Rel.Perm.Table_NatFrac* by history matching

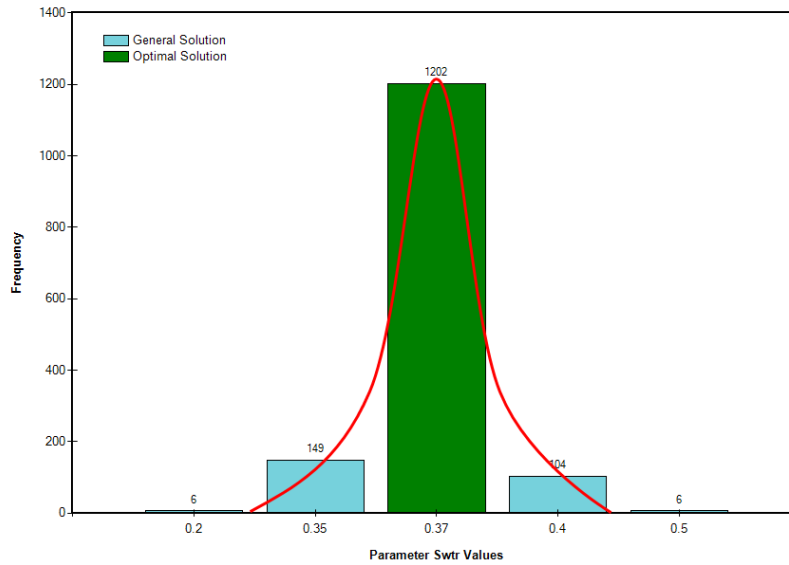


Figure 110. Fitting a probability distribution function to *Swtr* by history matching— Normal Distribution Function fits the data.

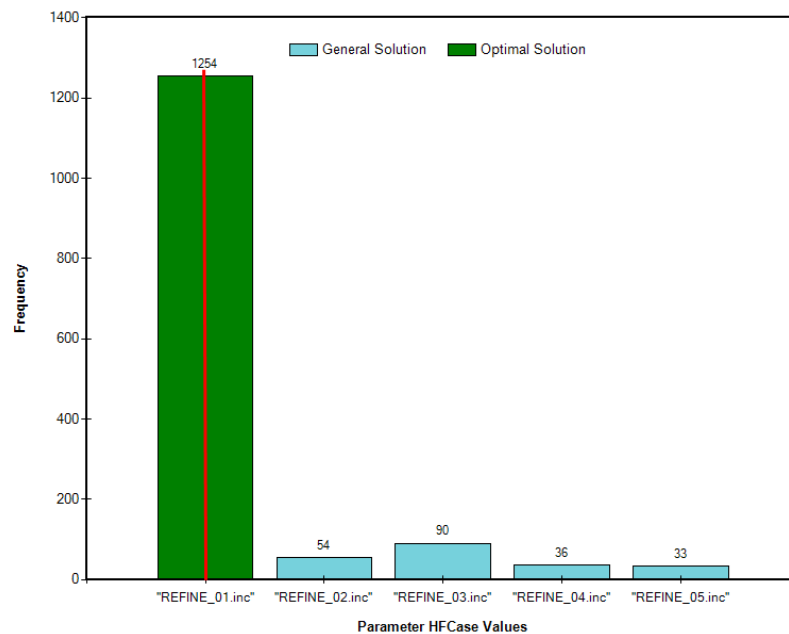


Figure 111. Fitting a probability distribution function to *HFCase* by history matching— Fixed-value Distribution Function fits the data.

- 4) Performing the calculations. The Monte Carlo simulation involves repeated random sampling from the input distributions and subsequent calculation of a set of sample values for the output distributions. This process is repeated over

several iterations. In this study, the Monte Carlo simulation was repeated 65,000 times, each time taking a new set of input parameters. In Monte Carlo sampling each random variable remains as an element of the distribution, thus leaving the entire statistical range available for sampling in subsequent iterations. Hence, this would result in clustering of sampling in some parts of the distribution while other parts are not sampled [Mian, 2011]. For avoiding such a problem in our sampling, we have used *Latin hypercube sampling (LHS)* in which the cumulative distribution function is first partitioned into non-overlapping intervals of equal probability. LHS is a better sampling method because it guarantees that all probabilities are present in the calculations, thus giving equal weight to all probabilities on the CDF (cumulative distribution function) (Figure 112). Using LHS greatly reduces the number of required iterations in a simulation case with a large number of input parameters.

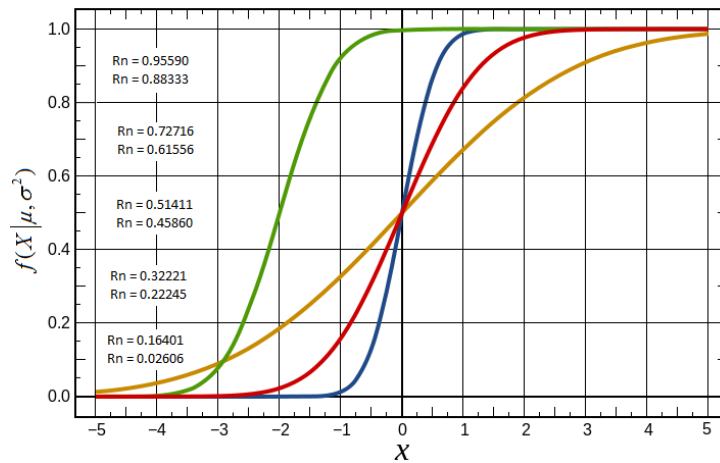


Figure 112. Latin hypercube sampling

RSM for NPV Calculations using Monte Carlo Simulation

The final step of the uncertainty assessment was utilizing the concept of response surface method (RSM) to develop proxy models being used to perform thousands of Monte Carlo simulations. The goal at this stage was to describe in detail the relationship between the uncertain factors and the response, i.e. the NPV. A full quadratic model was used to both predict the whole sample space and identify the optimal cases. The general quadratic model for k independent variables is given by:

$$\hat{Y} = b_0 + \sum_{i=1}^k b_i X_i + \sum_{i=1}^k b_{ii} X_i^2 + \sum_{i=1}^{k-1} \sum_{j=i+1}^k b_{ij} X_i X_j \quad (59)$$

Where b 's are the coefficients to be obtained by regression analysis. Note that in the model used to fit the data (Eq.59), the higher order interaction terms (higher than 2) were neglected, as are usually ignored in the experimental design [Lawson and Erjavec, 2001]. Hence, the experimental design method used in this research (LHS) helped us to estimate all main effects, squared terms, and two-factor interaction terms.

Comparing the actual data (from simulations) versus the predicted values (from Eq.59), we can identify the outliers (if any) and check the validity of the response surface model (Figures 113, 114, and 116). In these figures, the blue dots are training jobs for creating the response surface model, and the red dots are the verification jobs used to check if the response surface model is a good proxy to the actual simulation results.

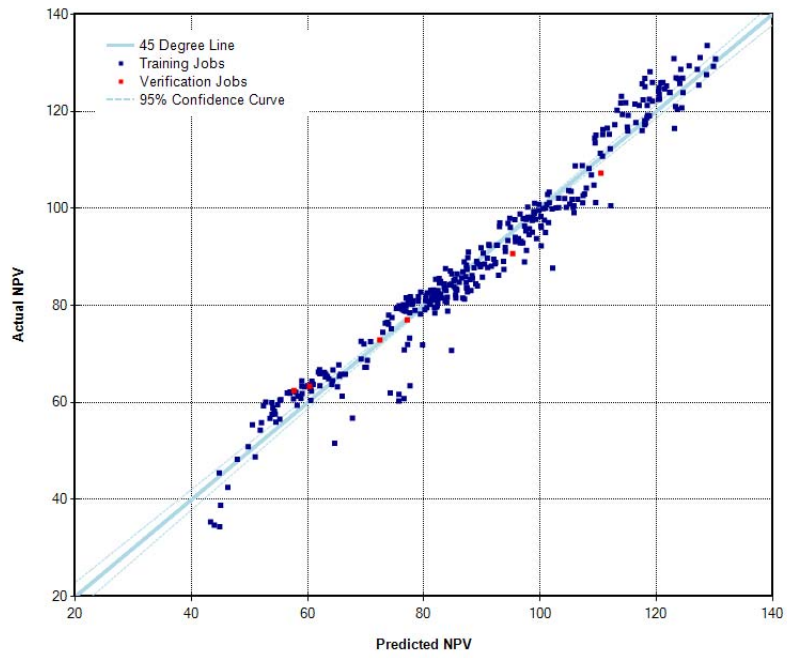


Figure 113. The verification plot (actual vs. prediction)— linear model

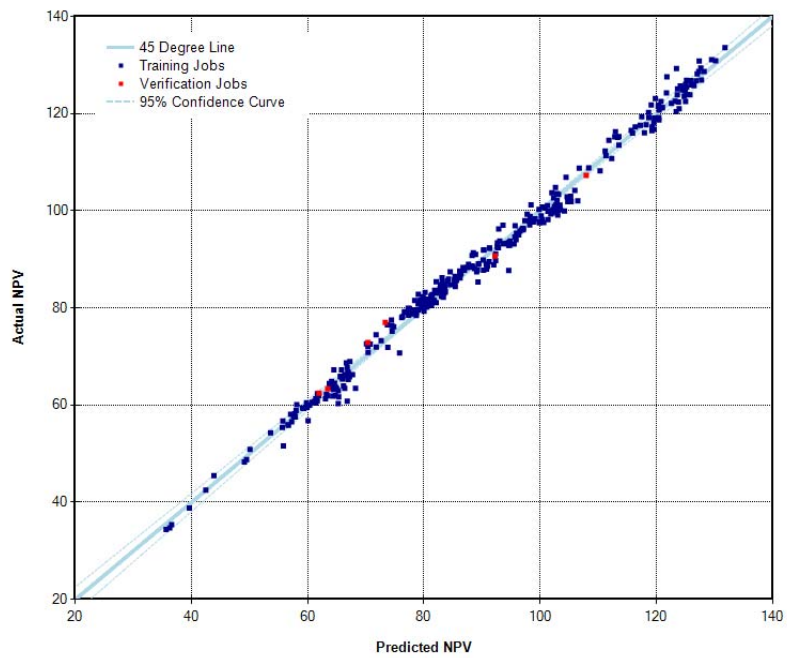


Figure 114. The verification plot (actual vs. prediction)— quadratic model

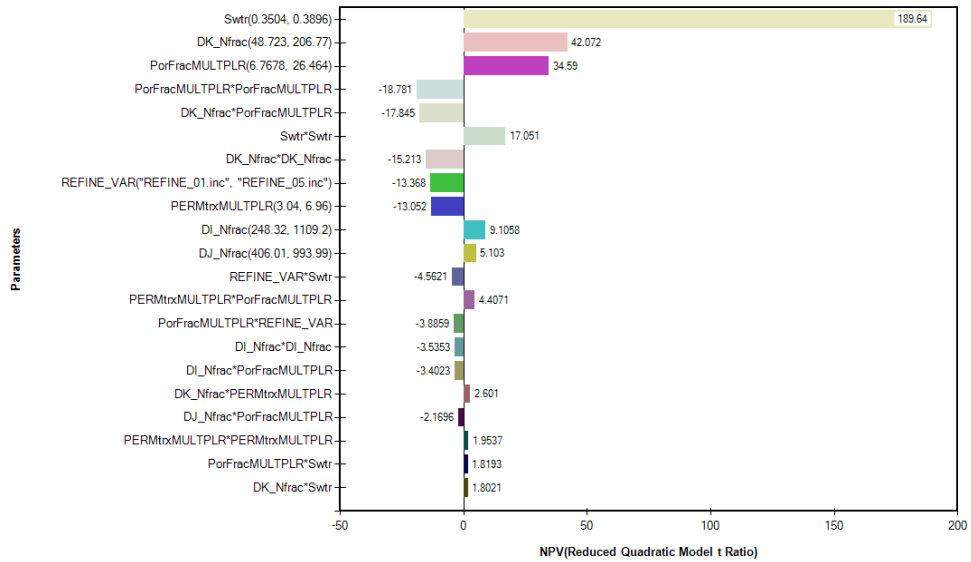


Figure 115. Tornado plot of NPV function (reduced quadratic model)

The tornado plot in Figure 115 displays the terms which have the greatest effect on the objective function (NPV). The statistical significance of each term (linear, squared, or interaction) is characterized by its corresponding $prob > |t|$ value shown in Table 22. If such probability values of some terms were larger than $\alpha / 2$ (for a 2-tailed t-test) or larger than α (for a 1-tailed t-test), the corresponding terms would not be significant and they can be ignored in the proxy model regressions. Finally, only the significant terms were used to develop the response surface proxy model as shown in Figure 115.

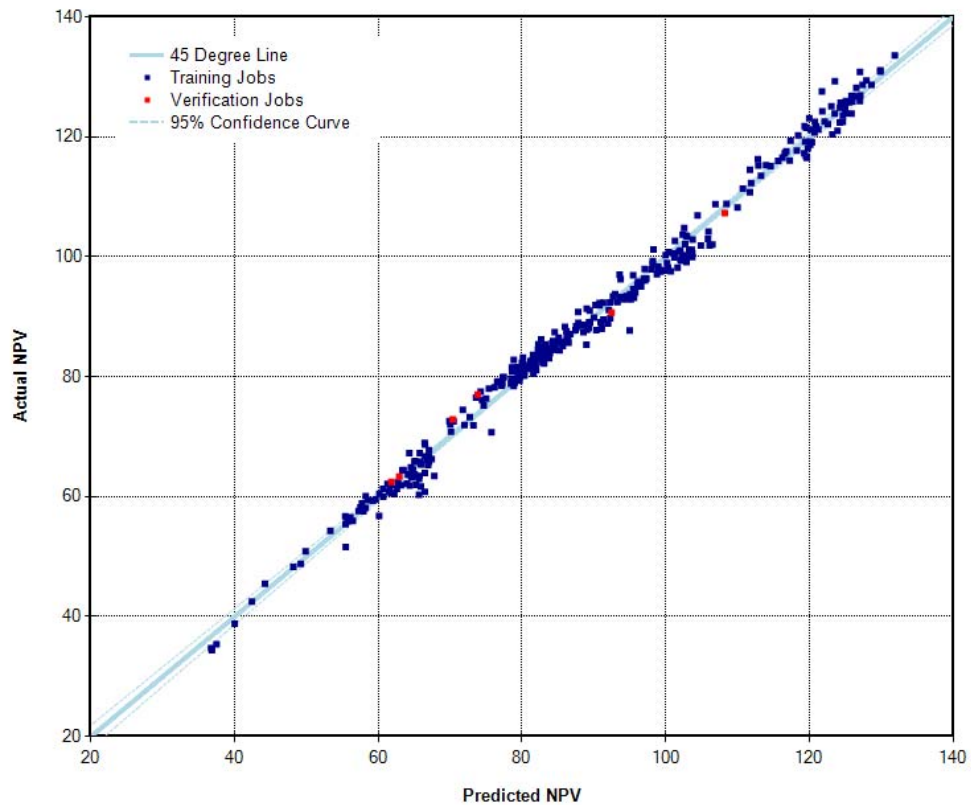


Figure 116. The verification plot (actual vs. prediction)— reduced quadratic model

The plots shown above depict how closely the response surface predictions match the actual values from the simulations. The 45 degree line represents a perfect match between the equation and actual simulation results. The closer the points are to the 45 degree line, the more precise the developed response surface model. The points that are far away from the 45 degree are considered as outliers. In the case of too many outliers, we need to figure out the cause of the outliers before using the response surface model. The lower and upper 95% confidence curves are also drawn to show whether the model is statistically significant [Sall, 1990]. It is clear from Figure 116 that the reduced quadratic model is the most accurate proxy model (among the three)

for the actual simulation runs. The details of the equation-fit to the training data are shown in Table 22.

Table 22. Effect screening using normalized parameters (-1, +1)

Term	Coefficient	Standard Error	t Ratio	Prob > t	VIF
Intercept	89.9867	0.263308	341.755	<0.00001	0.00
DI_Nfrac(248.32, 1109.2)	1.4179	0.155713	9.10585	<0.00001	1.14
DJ_Nfrac(406.01, 993.99)	0.782536	0.153349	5.10297	<0.00001	1.06
DK_Nfrac(48.723, 206.77)	6.24367	0.148405	42.0718	<0.00001	1.07
PERMtrxMULTPLR(3.04, 6.96)	-2.07736	0.159156	-13.0523	<0.00001	1.08
PorFracMULTPLR(6.7678, 26.464)	5.17362	0.149569	34.5903	<0.00001	1.06
REFINE_VAR("REFINE_01.inc", "REFINE_05.inc")	-1.91103	0.142954	-13.3682	<0.00001	1.07
Swtr(0.3504, 0.3896)	29.4367	0.155226	189.637	<0.00001	1.05
DI_Nfrac*DI_Nfrac	-0.837544	0.236909	-3.53529	0.00046	1.06
DI_Nfrac*PorFracMULTPLR	-0.731168	0.214904	-3.4023	0.00075	1.09
DJ_Nfrac*PorFracMULTPLR	-0.463064	0.213436	-2.16957	0.03073	1.05
DK_Nfrac*DK_Nfrac	-3.73748	0.245685	-15.2125	<0.00001	1.09
DK_Nfrac*PERMtrxMULTPLR	0.602929	0.231808	2.60098	0.00970	1.09
DK_Nfrac*PorFracMULTPLR	-3.85676	0.21612	-17.8455	<0.00001	1.11
DK_Nfrac*Swtr	0.38776	0.215175	1.80207	0.01242	1.10
PERMtrxMULTPLR*PERMtrxMULTPLR	0.442924	0.226709	1.95371	0.02156	1.04
PERMtrxMULTPLR*PorFracMULTPLR	1.00943	0.229048	4.40708	0.00001	1.06
PorFracMULTPLR*PorFracMULTPLR	-4.59523	0.244679	-18.7806	<0.00001	1.08
PorFracMULTPLR*REFINE_VAR	-0.807905	0.207906	-3.88592	0.00012	1.06
PorFracMULTPLR*Swtr	0.418312	0.229934	1.81927	0.01975	1.07
REFINE_VAR*Swtr	-0.967904	0.212161	-4.56213	<0.00001	1.05
Swtr*Swtr	3.92957	0.230463	17.0508	<0.00001	1.08

The parameters shown in the table are described as follows:

- a) “***t-Ratio***” is a statistic that tests whether the true parameter (coefficient) is zero. It is also called the signal-to-noise t-ratio which is a tool to judge the significance of each effect and interaction by comparing its t-ratio to the critical t-value (or standard error) and has a *Student’s T-distribution* under the hypothesis, given the normal assumptions about the model [CMG, 2012].
- b) “ $prob > |t|$ ” is the probability of getting a great t-statistic (in absolute value), given the hypothesis that the parameter (coefficient) is zero. If such probability values of some terms were larger than $\alpha/2$ (for a 2-tailed t-

test) or larger than α (for a 1-tailed t-test), the corresponding terms would not be significant and they can be ignored in the proxy model regressions.

- c) “**VIF**” or variance inflation factor quantifies the severity of multicollinearity in an ordinary least-square regression analysis. It provides an index that measures how much the variance (the square of standard deviation) of an estimated regression coefficient is increased because of collinearity. Multicollinearity is a statistical phenomenon in which two or more predictor variables in a multiple regression model are highly correlated, meaning that one can be linearly predicted from the others with a non-trivial degree of accuracy. In this situation the coefficient estimates may change erratically in response to small changes in the model or the data. Multicollinearity does not reduce the predictive power or reliability of the model as a whole, at least within the sample data themselves; it only affects calculations regarding individual predictors. That is, a multiple regression model with correlated predictors can indicate how well the entire bundle of predictors predicts the outcome variable, but it may not give valid results about any individual predictor, or about which predictors are redundant with respect to others. A high degree of multicollinearity can also prevent computer software packages from performing the matrix inversion required for computing the regression coefficients, or it may make the results of that inversion inaccurate. For analyzing the magnitude of multicollinearity, we should consider the size of each $VIF(i)$. A common rule of thumb is that if $VIF(i) > 5$, then multicollinearity is high [*Lipovestky and Conklin*, 2001; *Van den Poel et al.*, 2004].

Note that in statements of the assumptions underlying regression analysis, such as ordinary least-square method, the phrase "no multicollinearity" is sometimes used to mean the absence of perfect multicollinearity, which is an exact (non-stochastic) linear relation among the regressors. The final equation of NPV for the investigated hydraulic fracturing treatment was then obtained as follows:

$$\begin{aligned}
 NPV = & 824.017 + 0.0122967(DI_Nfrac) + 0.00531932(DJ_Nfrac) \\
 & + 0.202175(DK_Nfrac) - 3.57907(PERMtrxMULTPLR) \\
 & + 2.30887(PorFracMULTPLR) + 0.0886187(REFINE_VAR) \\
 & - 5888.66(Swtr) - 4.52046 \times 10^{-6} (DI_Nfrac \times DI_Nfrac) \\
 & + 0.250352(DK_Nfrac \times Swtr) + 2.16716(PorFracMULTPLR \times Swtr) \\
 & - 0.000172485(DI_Nfrac \times PorFracMULTPLR) \\
 & - 0.00015994(DJ_Nfrac \times PorFracMULTPLR) \\
 & - 0.000598503(DK_Nfrac \times DK_Nfrac) \\
 & + 0.00389273(DK_Nfrac \times PERMtrxMULTPLR) \\
 & - 0.00495581(DK_Nfrac \times PorFracMULTPLR) \\
 & + 0.115297(PERMtrxMULTPLR \times PERMtrxMULTPLR) \\
 & + 0.0522959(PERMtrxMULTPLR \times PorFracMULTPLR) \\
 & - 0.0473808(PorFracMULTPLR \times PorFracMULTPLR) \\
 & - 0.000410183(PorFracMULTPLR \times REFINE_VAR) \\
 & - 0.246914(REFINE_VAR \times Swtr) + 10229(Swtr \times Swtr)
 \end{aligned} \tag{60}$$

with the coefficients shown in Table 23.

Table 23. Coefficients in terms of actual parameters

Term	Coefficient
Intercept	824.017
DI_Nfrac	0.0122967
DJ_Nfrac	0.00531932
DK_Nfrac	0.202175
PERMtrxMULTPLR	-3.57907
PorFracMULTPLR	2.30887
REFINE_VAR	0.0886187
Swtr	-5888.66
DI_Nfrac*DI_Nfrac	-4.52E-06
DI_Nfrac*PorFracMULTPLR	-0.000172485
DJ_Nfrac*PorFracMULTPLR	-0.00015994
DK_Nfrac*DK_Nfrac	-0.000598503

DK_Nfrac*PERMtrxMULTPLR	0.00389273
DK_Nfrac*PorFracMULTPLR	-0.00495581
DK_Nfrac*Swtr	0.250352
PERMtrxMULTPLR*PERMtrxMULTPLR	0.115297
PERMtrxMULTPLR*PorFracMULTPLR	0.0522959
PorFracMULTPLR*PorFracMULTPLR	-0.0473808
PorFracMULTPLR*REFINE_VAR	-0.000410183
PorFracMULTPLR*Swtr	2.16716
REFINE_VAR*Swtr	-0.246914
Swtr*Swtr	10229

Once the least-square model has been fit to the data, generally the first question of interest would be: “How well does the equation fit?”

The minimized sum of squared errors is a direct measure of how well the model fits the data:

$$SSE = \sum_{i=1}^k (Y_i - \hat{Y}_i)^2 \quad (61)$$

This measure has to be normalized to the total variability in the data (SST) for being used to compare the model for different situations.

$$SST = \sum_{i=1}^k (Y_i - \bar{Y})^2 \quad (62)$$

The ratio of SSE to SST represents the fraction of the total variability in the data that is not explained by the model [Lawson and Erjavec, 2001].

The summary of the model statistics (fit table) quantifies the quality of the regressions which indeed shows the details of the developed response surface model (Table 24).

Table 24. The summary of fit

R-Square	0.986108
R-Square Adjusted	0.985078
R-Square Prediction	0.983747
Mean of Response	86.9627
Standard Error	2.15332

In this table the following numeric parameters are summarized:

R-Squared: In statistics, we normally use the complementary statistic (R^2), which describes the fraction of the total variability in the data that is explained by the model:

$$R^2 = 1 - \frac{SSE}{SST} \quad (63)$$

R-Squared adjusted: Adjusted R^2 is used to compensate for the addition of variables to the model. As more independent variables are added to the regression model, unadjusted R^2 will generally increase but there will never be a decrease. This will occur even when the additional variables do little to help explain the dependent variable. To compensate for this, adjusted R^2 is corrected for the number of independent variables in the model. The result is an adjusted R^2 that can go up or down depending on whether the addition of another variable adds or does not add to the explanatory power of the model. Adjusted R^2 will always be lower than unadjusted [Lothar, 1984].

$$R_{adjusted}^2 = 1 - \left(\frac{n-1}{n-p} \right) (1 - R^2) \quad (64)$$

Where n is the number of observations (training simulation jobs) and p is the number of terms in the response model, including the intercept.

R-Squared prediction: Predicted R-squared is used in regression analysis to indicate how well the model predicts responses for new observations, whereas R-squared indicates how well the model fits the simulation data. Predicted R-squared can prevent overfitting the model and can be more useful than adjusted R-squared for comparing models because it is calculated using the observations not included in model estimation. Overfitting refers to models that appear to explain the relationship

between the predictor and response variables for the data set used for model calculation but fail to provide valid predictions for new observations.

$$R^2_{prediction} = 1 - \frac{\sum_{i=1}^n (y_i - \hat{y}_i)^2}{SST} \quad (65)$$

Where y_i is an observation point in the sample space, \hat{y}_i is the predicted value using the developed response surface, and SST is the total sum of squares. This parameter ($R^2_{prediction}$) gives some identification of the predictive capability of the regression model. For example, if $R^2_{prediction}$ was 0.97 for a regression model, we would expect that the response surface model may explain almost 97% of the variability in predicting new observations.

Mean of Response: In regression “mean of response” is the value of the dependent variable calculated from the regression parameters and a given set of the values of independent variables. It is important as a base model for prediction because all other models are compared to it.

Standard Error: The standard error is the standard deviation of an effect or interaction, or, it is the sampling distribution of a statistic [Lawson and Erjavec, 2001; Everitt, 2003]. It is the square root of variance and is denoted by s_E .

ANOVA— Analysis of Variance

In general, the purpose of analysis of variance (ANOVA) is to test for significant differences between means. In its simplest form, ANOVA provides a statistical test of whether or not the means of several groups are all equal, and therefore generalizes t-test to more than two groups. The calculations of ANOVA can be characterized as

computing a number of means and variances, dividing two variances and comparing the ratio to a handbook value to determine statistical significance. Calculating a treatment effect is then trivial, "the effect of any treatment is estimated by taking the difference between the mean of the observations which receive the treatment and the general mean [Cochran and Cox, 1992]. The ANOVA table obtained from the response surface fit is outlined in Table 25.

Table 25. ANOVA (Analysis of Variance)

Source	Degrees of Freedom	Sum of Squares	Mean Square	<i>F</i> Ratio	Prob > <i>F</i>
Model	31	137582	4438.13	957.161	<0.00001
Error	418	1938.17	4.63677		
Total	449	139520			

In this output, the test statistic, *F*, is obtained as 957.161. The p-value for this statistic is *prob* < 0.00001. This means that there is evidence that there are differences in the means across groups. In the ANOVA table the following numeric parameters are summarized:

Degree of Freedom: This is the number of values in the final calculation of a statistic that are free to vary.

Sum of Squares: It accounts for the variability measured in the response. It is the sum of squares of the differences between the fitted response and the actual response.

Mean Square: It is the sum of squares divided by its associated degrees of freedom. This computation converts the sum of squares to an average (mean square). The Error mean square estimates the variance of the error term.

***F* Ratio:** This ratio is the mean square of the model divided by error mean-square. This parameter tests the hypothesis if all the regression parameters (except the intercept) are zero. Under this whole-model hypothesis, the two mean squares have

the same expectation. If the random errors are normal, then under this hypothesis the values reported in the *Sum of Squares* column are two independent Chi-squares. The ratio of these two Chi-squares divided by their respective degrees of freedom (reported in the *Degrees of Freedom* column) has an F-distribution. If there is a significant effect in the model, the F-Ratio is higher than the one expected by chance alone [Cochran and Cox. 1992; Cox, 2006].

Prob > F: This is the probability of obtaining a greater F-value (by chance alone) if the specified model fits not better than the overall response mean. Significance probabilities of 0.05 or less are often considered evidence that there is at least one significant regression factor in the model. This significance is also shown graphically by the “*Actual vs. Predicted*” plot described in the “*Response Model Verification*” section.

- 5) Analyzing the output. The information obtained from simulation runs can be critically analyzed in light of the output distributions achieved. Two types of Monte Carlo distributions were made: *Unconditional* and *Conditional Distributions*. An unconditional distribution graph depicts the distribution of the values of objective functions (e.g. *NPV* or *Cum_OIL*) with all the uncertain parameters sampled from the input probability density functions (Figure 117).

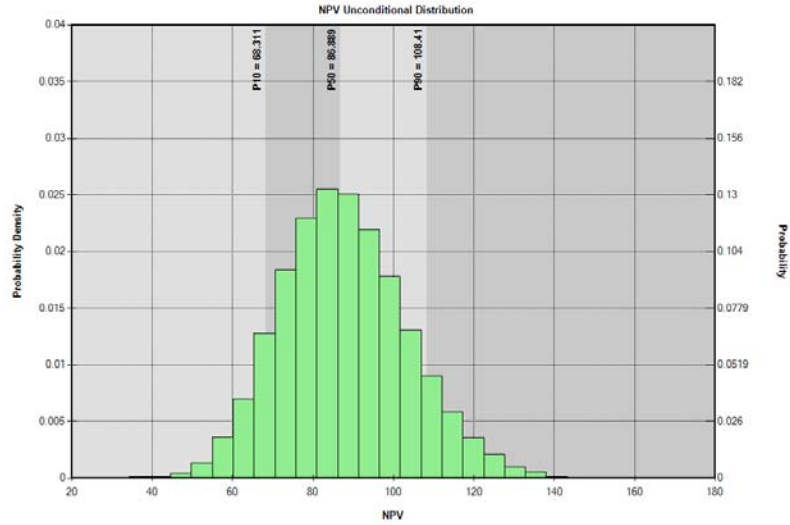


Figure 117. Monte Carlo results—unconditional distributions (PDF plot)

The histograms shown in Figure 117 illustrate the shape of the objective function distribution, which is NPV (net present value) in this case. Figure 117 also shows that the NPV varies between \$44.8 million and \$145.78 million with a standard deviation being \$18.38 million. The values of P_{10} (likelihood of real NPV being less than \$68.311 million), P_{50} (likelihood of real NPV being less than or greater than \$86.889 million), and P_{90} (likelihood of real NPV being less than \$108.41 million) are also shown on the PDF and CDF plots, presented in Figures 117 and 118.

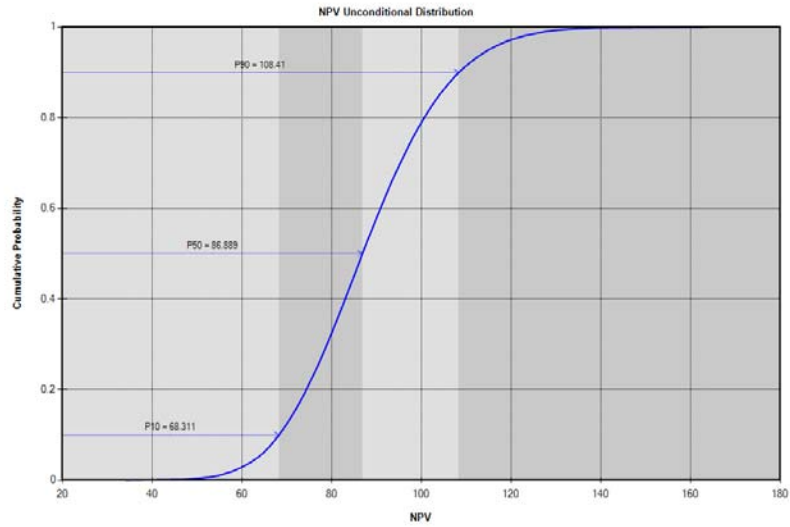


Figure 118. Monte Carlo results—unconditional distributions (CDF plot)

On the other hand, a conditional distribution shows different distributions for the objective function given that a certain parameter is held constant. In other words, a conditional probability distribution is a probability with some conditions imposed. The conditional probability distributions of the NPVs for all the uncertain parameters are shown in Figures 119 to 134.

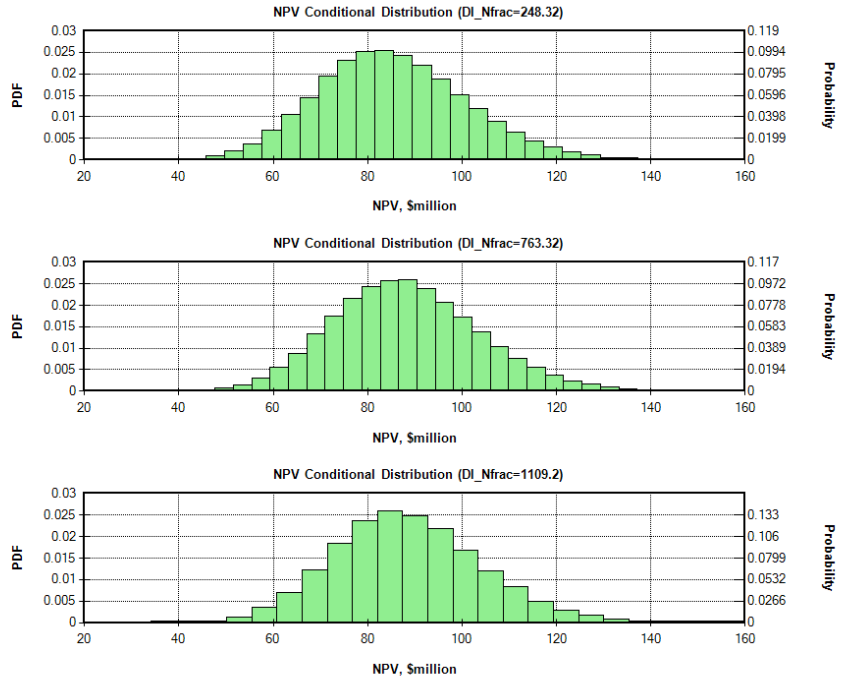


Figure 119. Monte Carlo results for DI_Nfrac —conditional distributions (PDF plot)

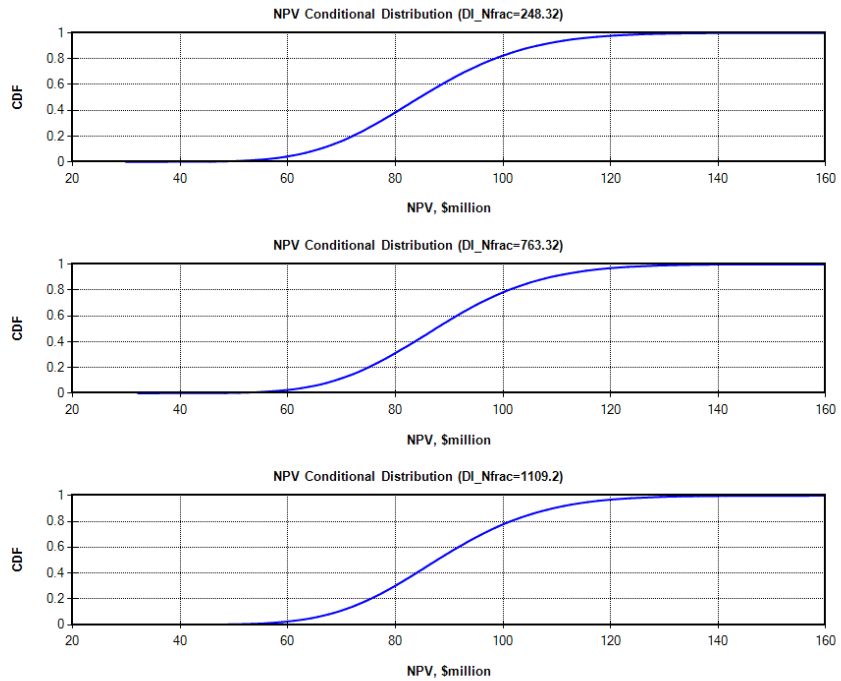


Figure 120. Monte Carlo results for DI_Nfrac —conditional distributions (CDF plot)

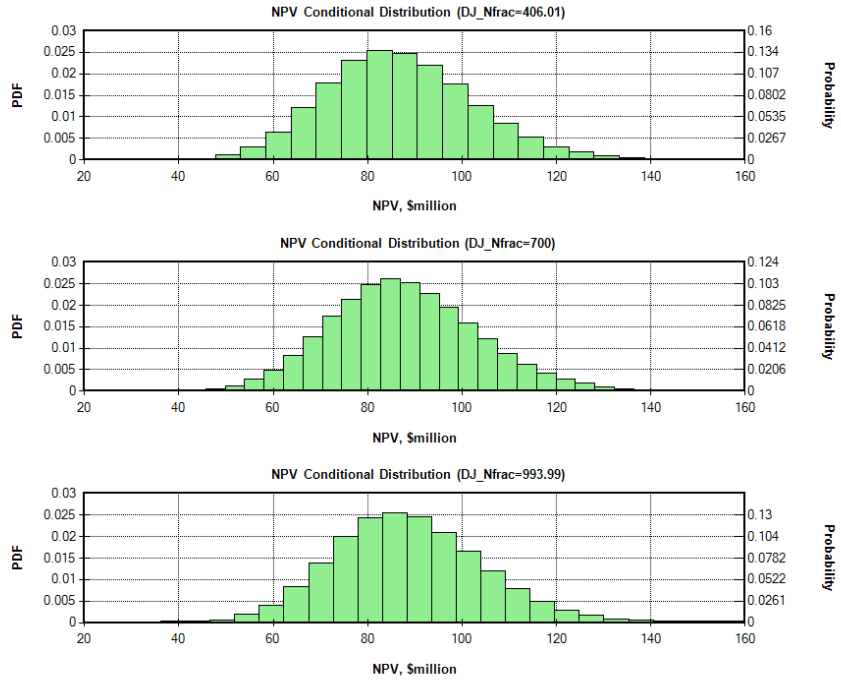


Figure 121. Monte Carlo results for DJ_Nfrac —conditional distributions (PDF plot)

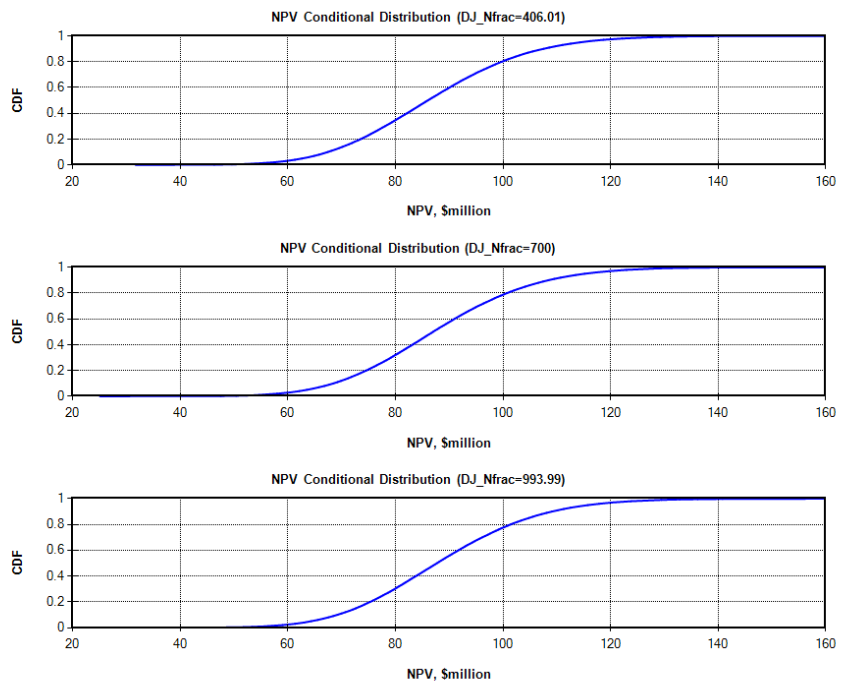


Figure 122. Monte Carlo results for DJ_Nfrac —conditional distributions (CDF plot)

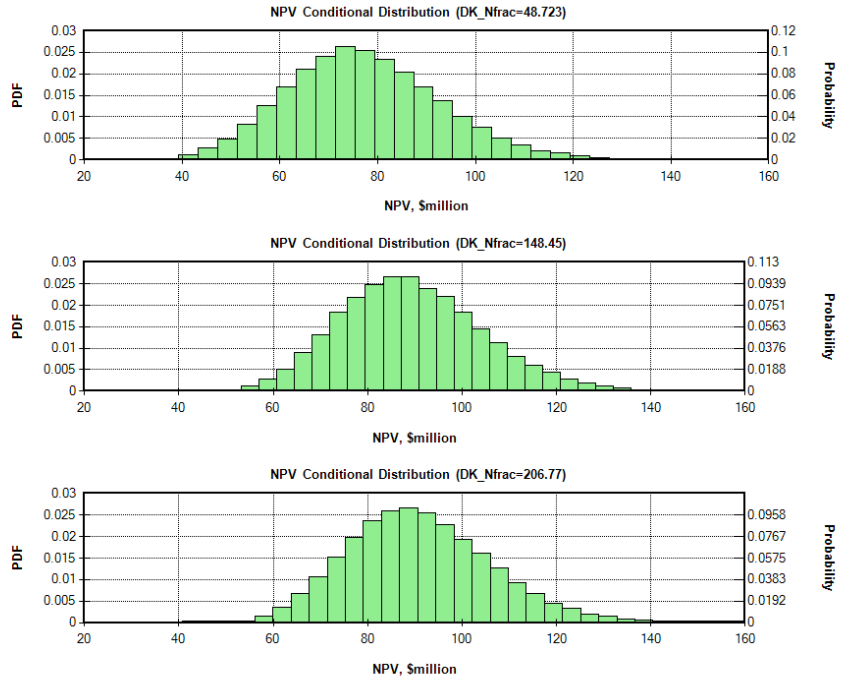


Figure 123. Monte Carlo results for DK_Nfrac —conditional distributions (PDF plot)

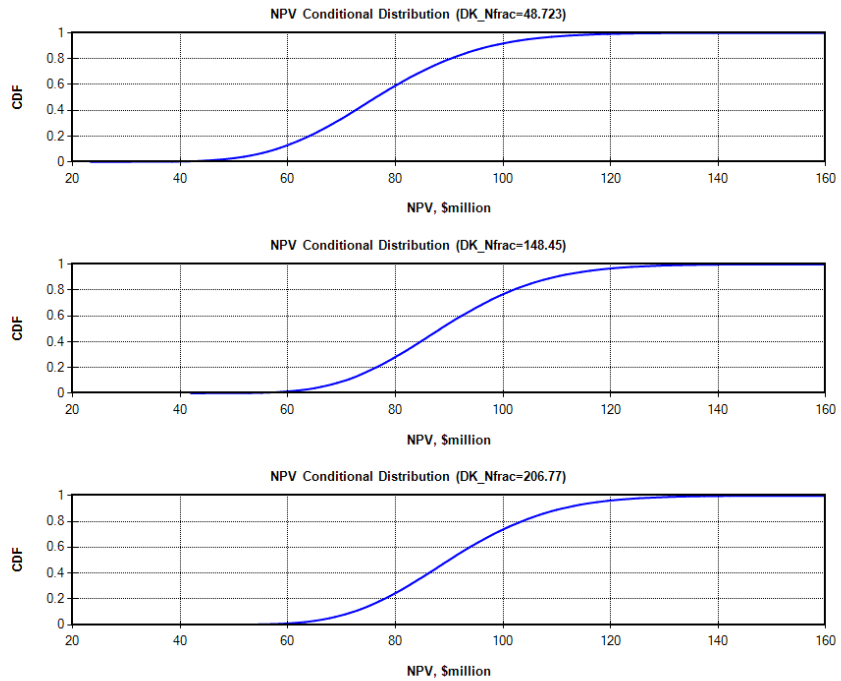


Figure 124. Monte Carlo results for DK_Nfrac —conditional distributions (CDF plot)

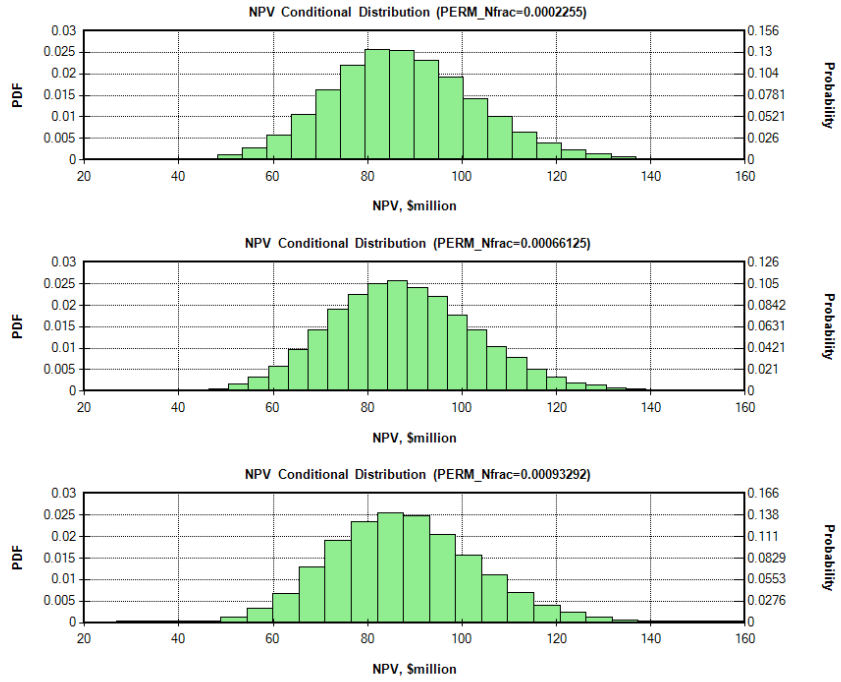


Figure 125. Monte Carlo results for $PERM_Nfrac$ —conditional distributions (PDF plot)

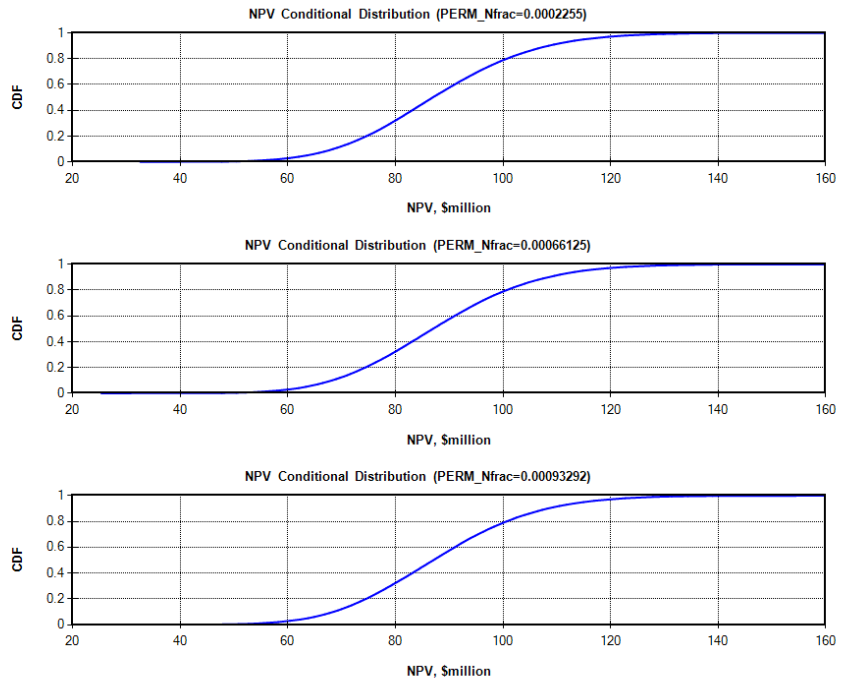


Figure 126. Monte Carlo results for $PERM_Nfrac$ —conditional distributions (CDF plot)

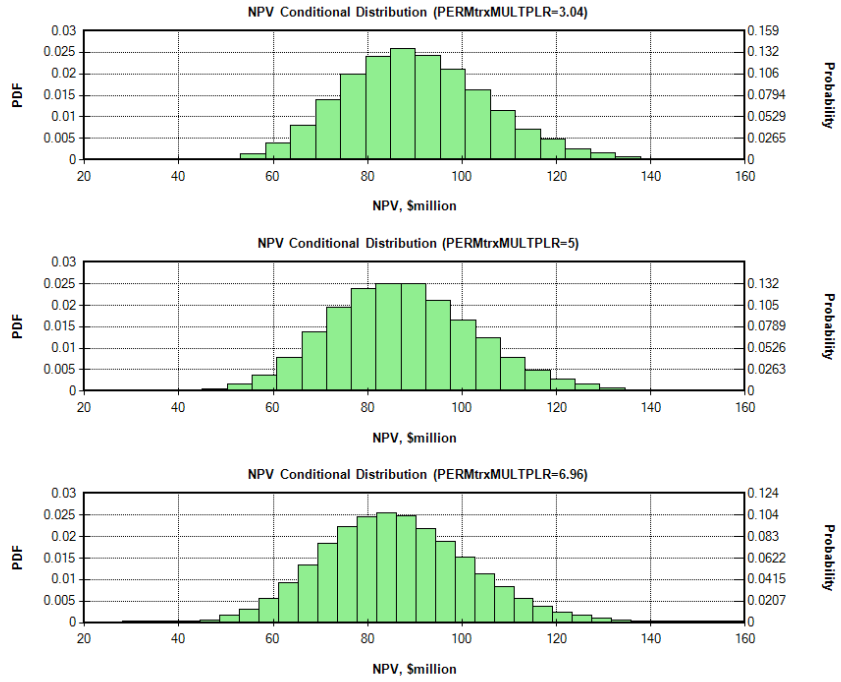


Figure 127. Monte Carlo results for $PERM_{trx}MULTPLR$ —conditional distributions (PDF plot)

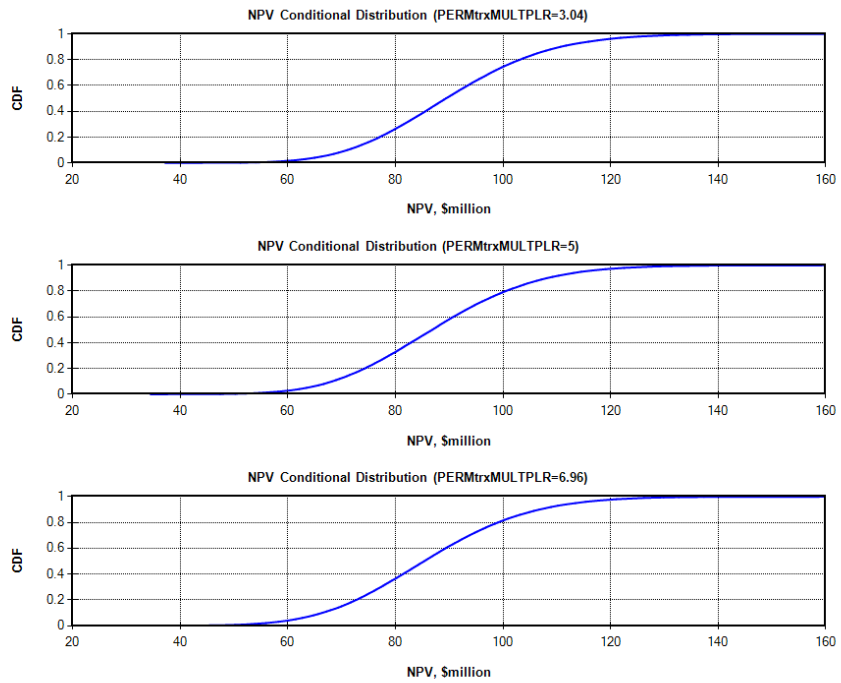


Figure 128. Monte Carlo results for $PERM_{trx}MULTPLR$ —conditional distributions (CDF plot)

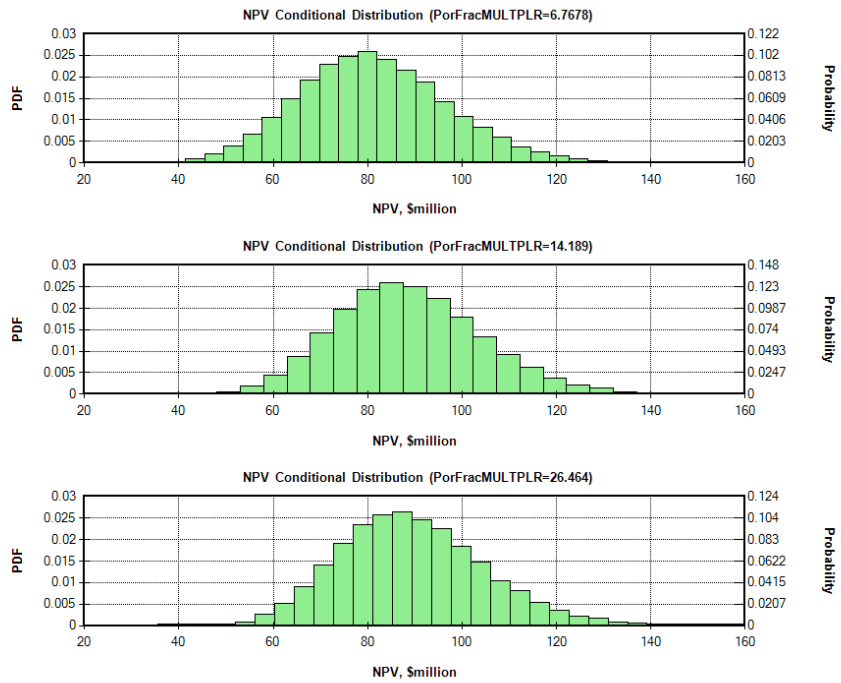


Figure 129. Monte Carlo results for *PorFracMULTPLR*—conditional distributions (PDF plot)

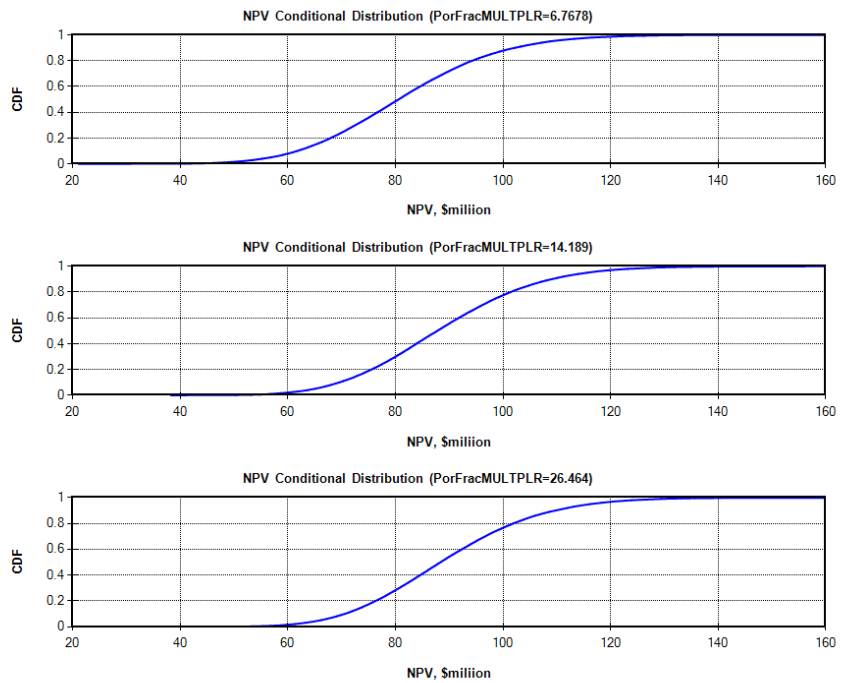


Figure 130. Monte Carlo results for *PorFracMULTPLR* —conditional distributions (CDF plot)

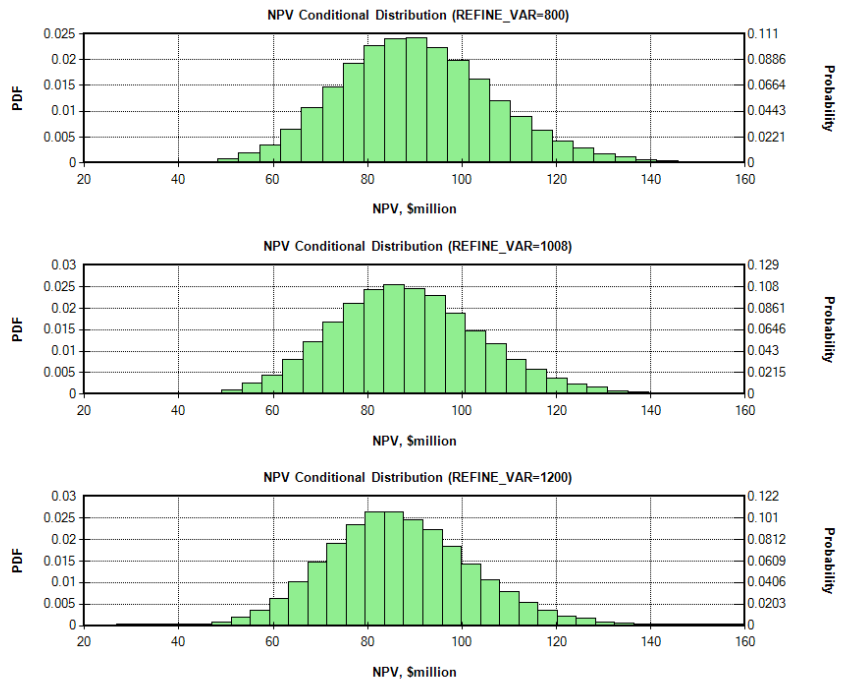


Figure 131. Monte Carlo results for *REFINE_VAR*—conditional distributions (PDF plot)

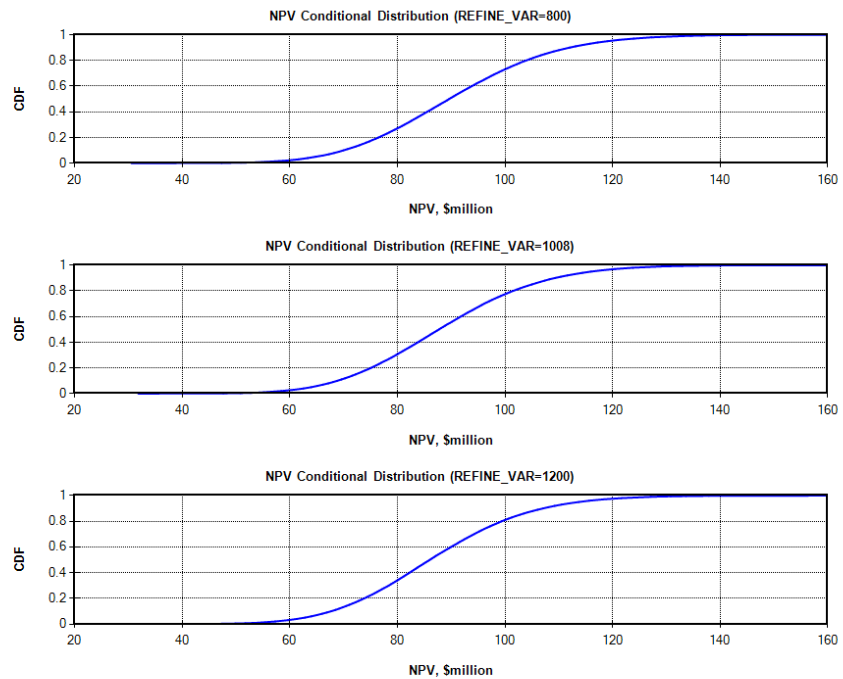


Figure 132. Monte Carlo results for *REFINE_VAR*—conditional distributions (CDF plot)

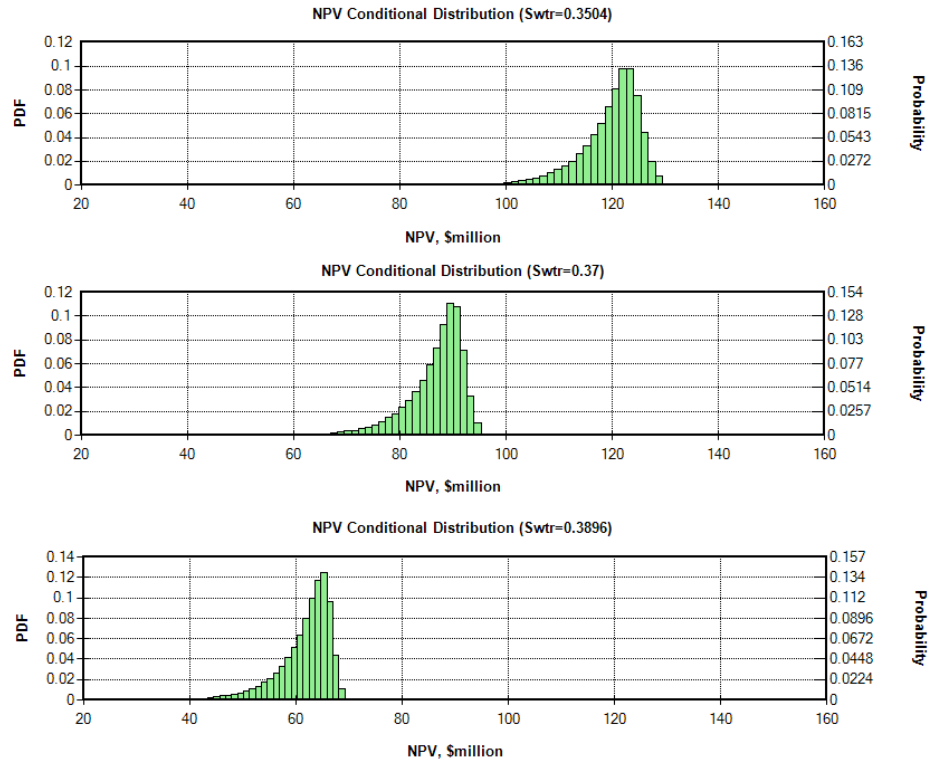


Figure 133. Monte Carlo results for $Swtr$ —conditional distributions (PDF plot)

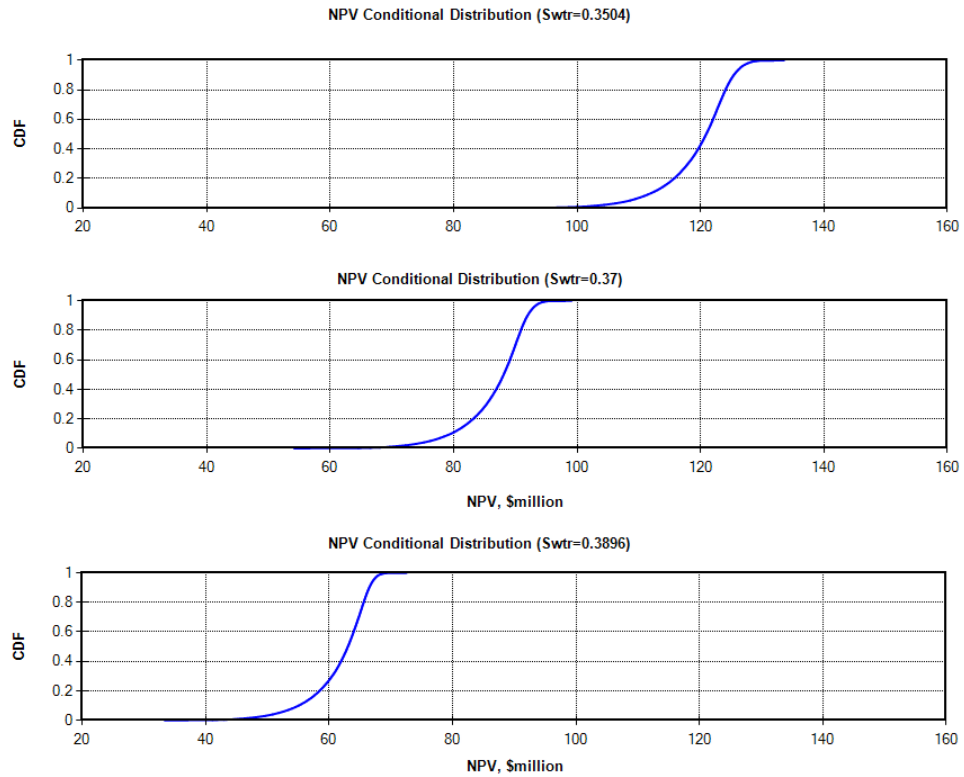


Figure 134. Monte Carlo results for $Swtr$ —conditional distributions (CDF plot)

6) Analyzing the simulated alternatives. In most decision- and policy-making processes the main goal is to make choices between alternatives. Therefore, all the alternatives under consideration should be simulated consistently to generate individual distributions and statistical information [Allaire, 2009; Mian, 2011]. The results from the alternatives are displayed in Figures 119 to 134. The cross plots in Figures 135-142 also show the results of the post-process analysis for the uncertainty assessment task. These figures display the relationships between NPV and the uncertain parameters.

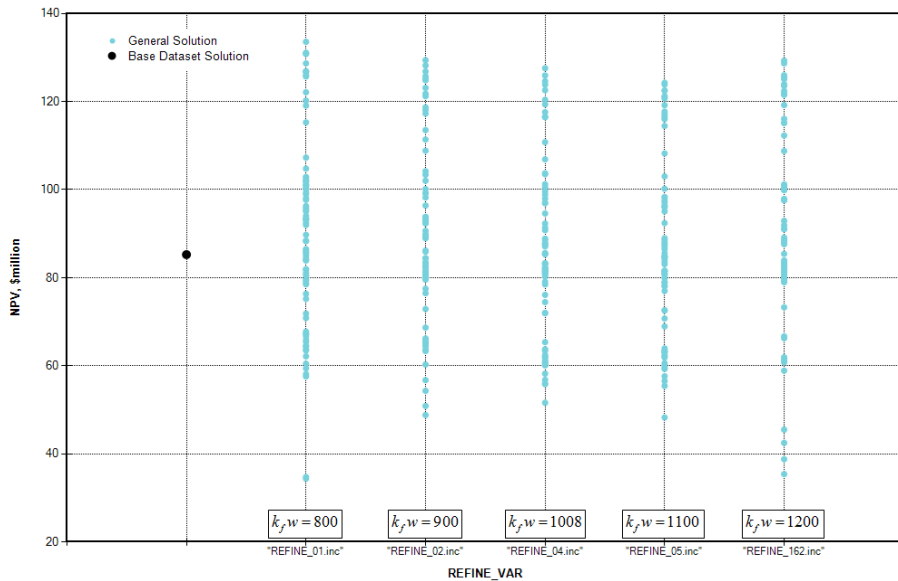


Figure 135. Cross plot of NPV versus fracturing treatment scenarios

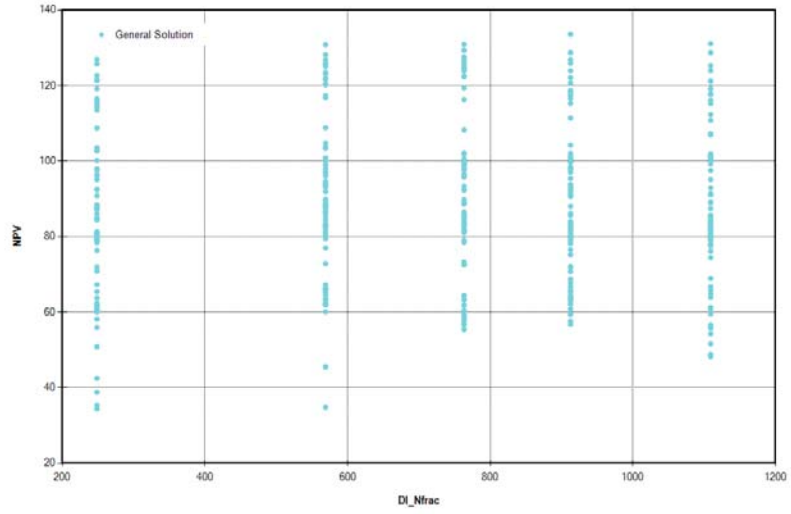


Figure 136. Cross plot of NPV versus DI_Nfrac

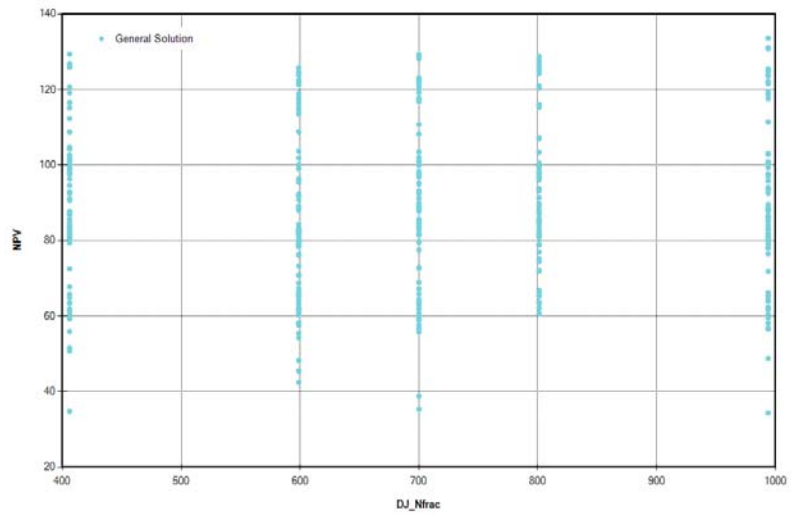


Figure 137. Cross plot of NPV versus DJ_Nfrac

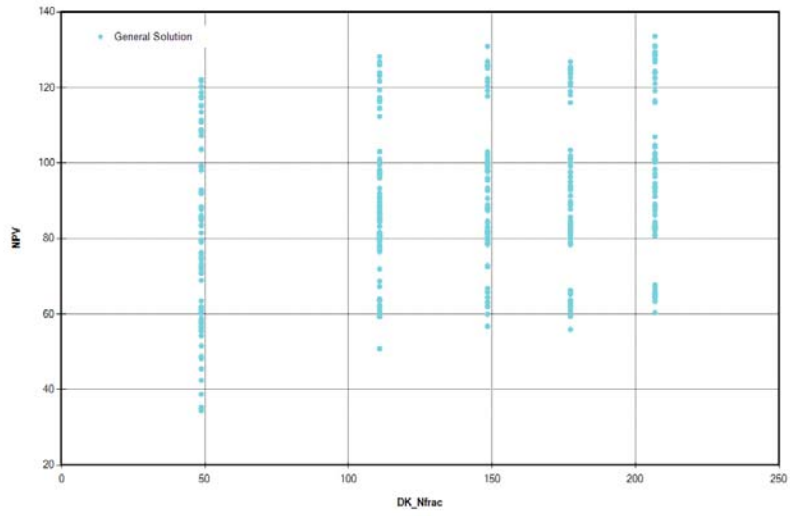


Figure 138. Cross plot of NPV versus DK_Nfrac

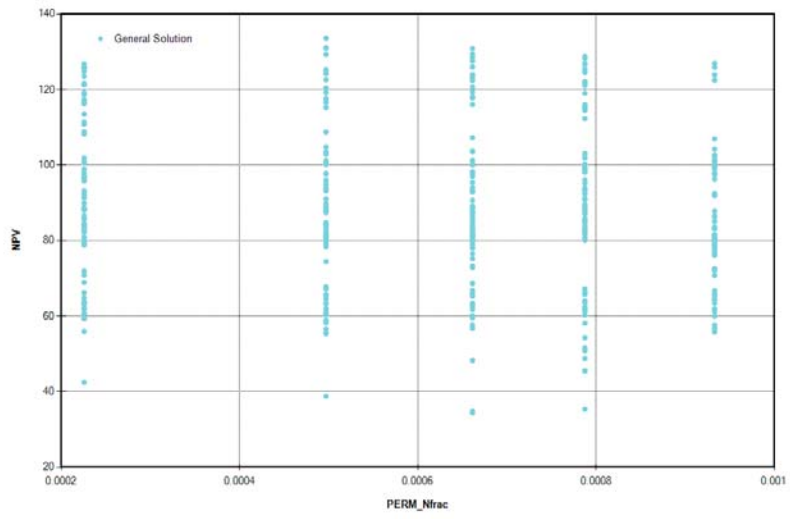


Figure 139. Cross plot of NPV versus $PERM_Nfrac$

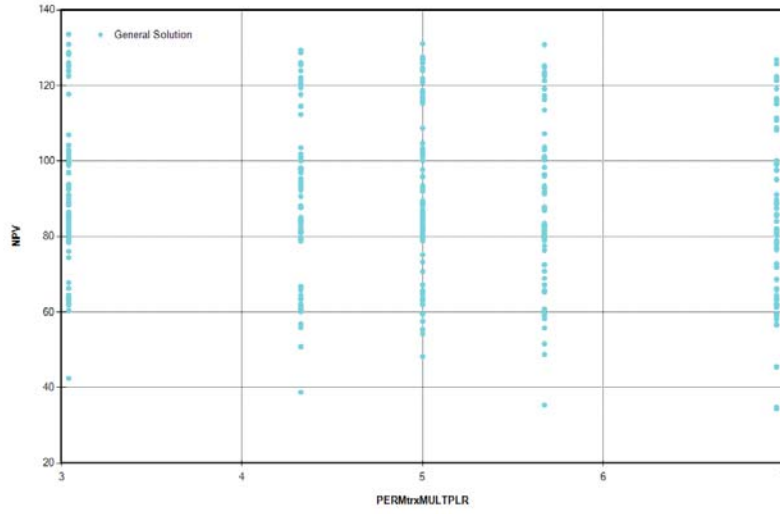


Figure 140. Cross plot of NPV versus *PERMtrxMULTPLR*

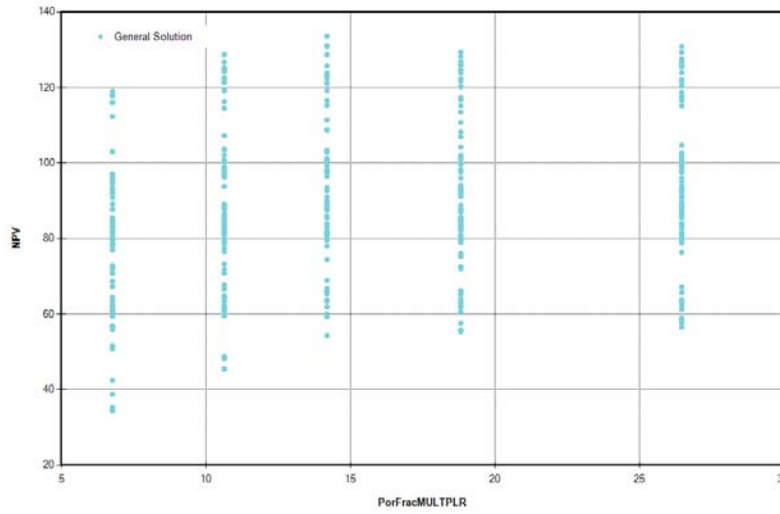


Figure 141. Cross plot of NPV versus *PorFracMULTPLR*

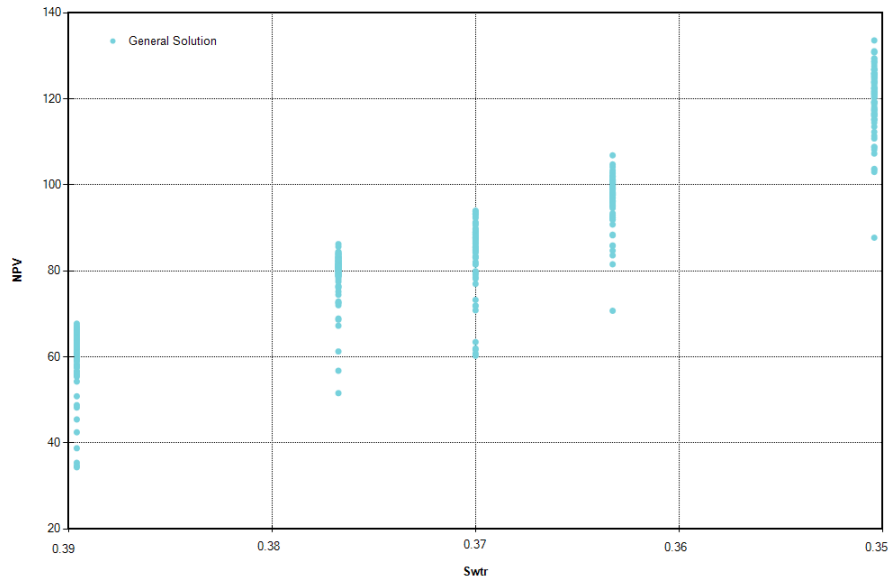


Figure 142. Cross plot of NPV versus $Swtr$

Uncertainty of Oil Price in the NPV Calculations—Engineering vs. Politics

In the optimization and uncertainty tasks, discussed above, the price of oil was considered to be constant within the 5-year time period over which the NPV calculations were made. However, due to the economic and political uncertainties in the world these days, the decision rules based on the calculated NPVs with a constant oil price would be subject to error. Hence, we may need to conduct our monetary calculations (NPV) based on variable oil prices.

The price of oil is volatile and extremely difficult to predict, which is affected by many factors. For example, assuming an oil shock in the market in 2014, the price of oil would soar in the years ahead. For making the NPV calculations under such a virtual condition, we have considered six scenarios for the price of oil to conduct more realistic NPV calculations (Figure 143). The likelihood of each scenario (event “B”) in case of an oil shock, which leads to a volatile oil prices, would be as those shown in Table 26 [*Financial Times*, 2012].

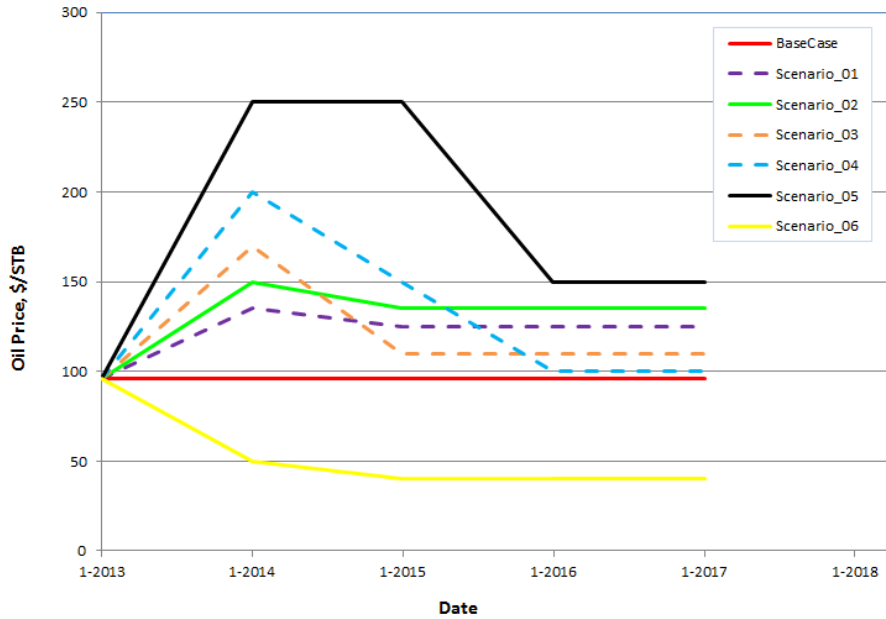


Figure 143. Average annual world oil prices in six scenarios— WTI[§] crude oil

For conducting the NPV calculations on an annual basis, we have defined the prices by step-functions as shown in Figure 144.

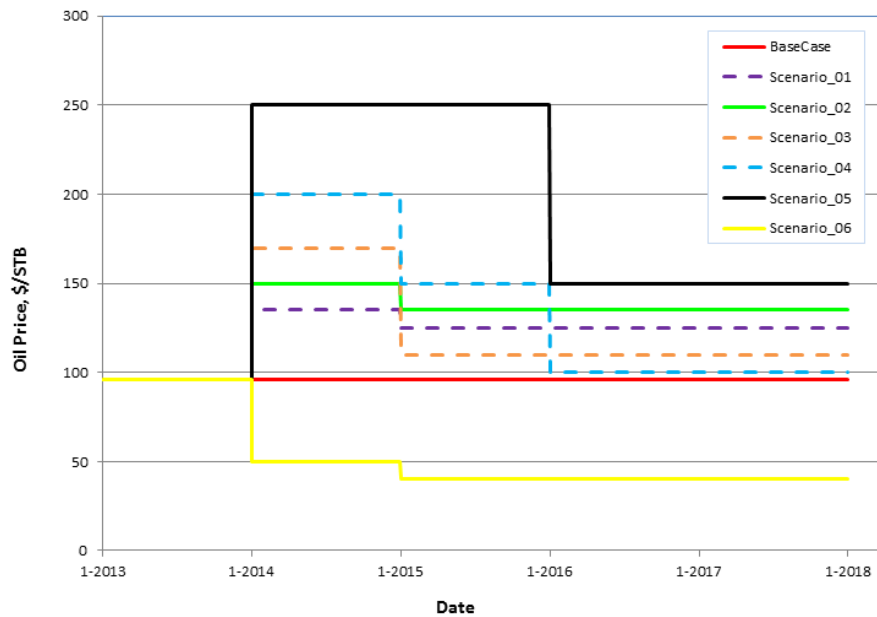


Figure 144. Average annual world oil prices in six scenarios— prices are in WTI (in step-function form)

§ West Texas Intermediate

Table 26. The probability of occurrence of the oil price events (event B) [*Financial Times*, 2012]

Scenarios	P(B)
BaseCase	-
Scenario_01	50%
Scenario_02	40%
Scenario_03	30%
Scenario_04	60%
Scenario_05	30%
Scenario_06	5%

Due to the uncertainties from random or chance caused by such variability, we can never expect to be right 100% of the time. However, we can formulate the objective rules that will minimize the chance of error if we base our calculations on the understanding of probability theory. This will let us calculate the chances of being wrong when we make decisions.

The probability-based NPV calculations were constructed in the following way. We hypothesize different situations to be the usual, expected, or likely to occur. Proper cash flow models were constructed with consideration of each oil-price scenario, and their corresponding net present values (NPV) were obtained, accordingly. Two types of probabilities were developed using Monte Carlo simulations: *conditional probability curves* and *joint probability curves*.

In the conditional probability type, the likelihoods of the calculated NPVs for each trend of oil-price were determined. In the joint probability type, the probability of the situation under which the specified price trend would be likely was also considered (Eq.66). Given two events A and B with $P(B) > 0$, the joint probability of A and B is defined as the product of the conditional probability of A given B and the probability of B :

$$P(A \cap B) = P(A|B) \cdot P(B) \quad (66)$$

Given two jointly distributed random variables A and B , the conditional probability distribution of A given B is the probability distribution of A when B is known to be a particular value. If the conditional distribution of A given B is a continuous distribution, then its probability density function is known as the conditional density function (Figures 100-111). The distribution of the NPVs of different oil-price scenarios, with all the uncertain parameters (well, reservoir, etc.), sampled from the input probability density functions were calculated as shown in Figure 145.

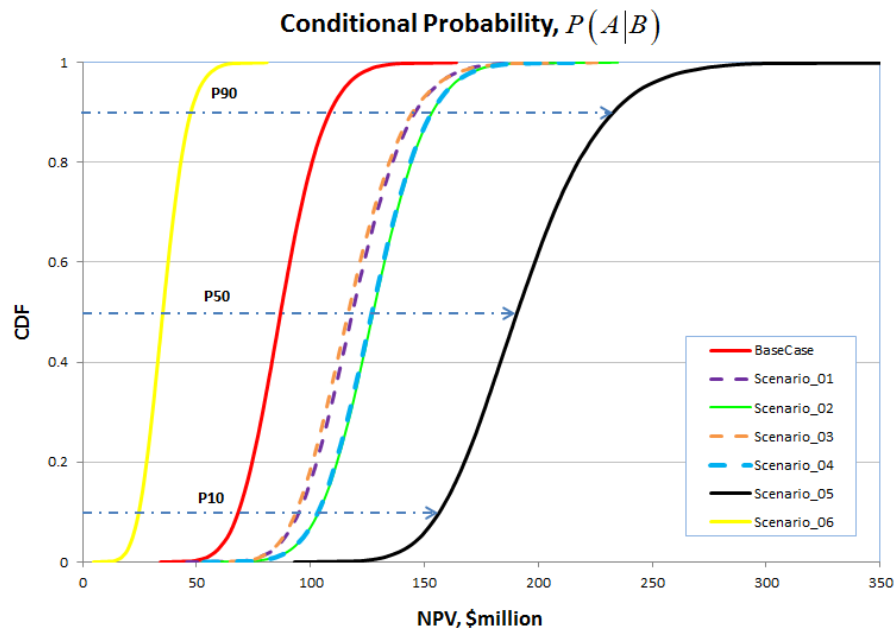


Figure 145. Conditional probability curves for six oil-price scenarios

The joint probability distribution curves for the six oil-price scenarios are also depicted in Figure 146. This figure describes how the revenues earned from a hydraulic fracturing treatment in the Bakken Formation could depend upon the potential oil-price scenarios in the market.

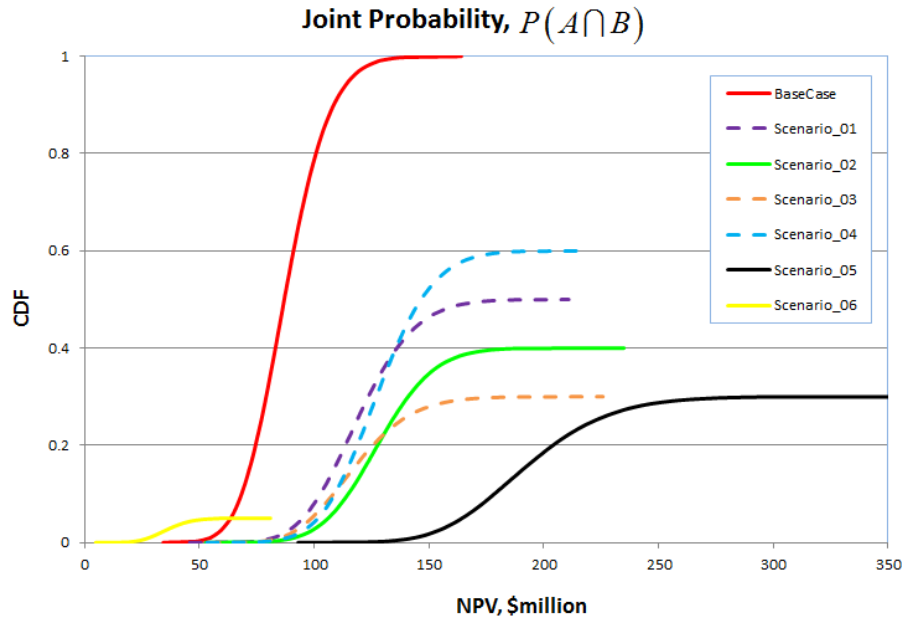


Figure 146. Joint probability curves for six oil-price scenarios

Anticipated value for a given investment

In statistics and probability analysis, expected value is calculated by multiplying each of the possible outcomes by the likelihood that each outcome will occur, and summing all of those values. By calculating expected values, investors can choose the scenario that is most likely to give them their desired outcome. In probability theory, the expected value (or expectation, mathematical expectation, EV, mean, or the first moment) of a random variable is the weighted average of all possible values that this random variable can take on. The weights used in computing this average correspond to the probabilities in case of a discrete random variable, or densities in case of a continuous random variable. From a rigorous theoretical standpoint, the expected value is the integral of the random variable with respect to its probability measure [Hamming, 1991; Ross, 2007].

If x is a discrete random variable taking values x_1, x_2, x_3, \dots with probabilities p_1, p_2, p_3, \dots , respectively. Then, the expected value of this random variable is the finite sum [Hamming, 1991]:

$$E[x] = \sum_{i=1}^{\infty} x_i p_i \quad (67)$$

If the probability distribution of the random variable (x) admits a probability density function $f(x)$, then the expected value can be computed by:

$$E[x] = \int_{-\infty}^{\infty} x f(x) dx \quad (68)$$

The scenario analysis performed on the price of oil in this research is one technique for calculating the expected value of an investment opportunity for a well stimulation plan in the Bakken Formation. It uses estimated probabilities with multivariate models (from Monte Carlo simulation), to examine possible outcomes for a proposed investment. Scenario analysis also may help investors determine whether they are taking on an appropriate level of risk, given the likely outcome of the investment. Figure 147 presents the expected value of each oil-price scenario considered in the simulations, based on the conditional probabilities displayed in Figure 145.

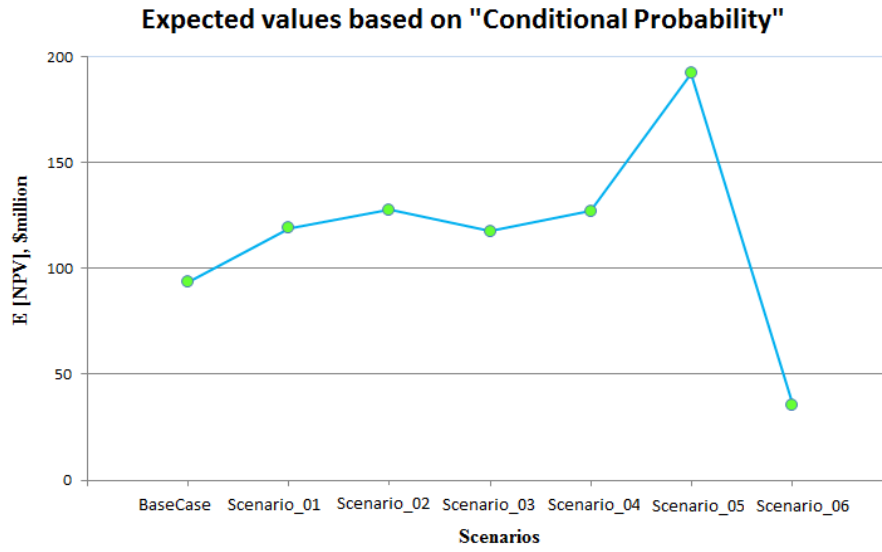


Figure 147. Expected values of NPV for six oil-price scenarios

CHAPTER V

CONCLUSIONS AND RECOMMENDATIONS

The objectives of this research were fourfold: a) to make a reliable reservoir model for the Bakken Formation through a comprehensive study including sensitivity analysis and history matching, b) to come up with best fracturing materials and develop preliminary pump schedules based on the selected design parameters, such as fracture half-length, pump rate, and maximum proppant concentration (obtained from optimization), c) to perform fully-3D hydraulic fracture simulation for modeling the created fracture geometry and for pump schedule refinement to place the right amount of proppant in the right place along the fracture, and d) to conduct an uncertainty assessment of the complex numerical simulations, which was intended to support decision- and policy-making processes in well stimulation planning.

A summary of the work performed to meet each of the objectives is given below. It is followed by general conclusions from this research as well as a discussion of future research scopes.

Summary of the research

The first part of this research was devoted to developing a reliable reservoir model for the Bakken Formation. As a next step of fracturing design, the main parameters controlling the fracture stimulation in Bakken horizontal wells were

evaluated. The main goal was to investigate opportunities to optimize hydraulic fracturing and production of horizontal Williston Basin Bakken Formation wells. To design a successful hydraulic fracture treatment, four main tasks were carried out.

First, a reservoir simulation to evaluate the response of the reservoir to fracture stimulation and to calibrate the reservoir model was performed through two steps involving: a) sensitivity analysis (SA) to determine the significant well/reservoir properties and parameters and b) history matching (HM) the simulation results to the production data from a stimulated horizontal well in the study area. Note that the history matching and reservoir calibration was conducted based on the data from only one well. This was because the microseismic data (used for the estimation of SRV) was available for only one well in the study area over the Bakken Formation. Second, the amount of fracturing materials was estimated and preliminary pump schedules were developed based on selected design parameters including: fracture half-length, pump rate, and maximum proppant concentration.

Then, design parameters screening was conducted using 2D fracture geometry solutions for fracture treatment parameters. An optimization task was then performed to identify optimal stimulation treatment(s) that together with optimal operating conditions would return a maximum value for the objective function (i.e. Net Present Value).

Next, fully-3D/FEM fracture modeling was utilized to perform implicit, coupled, finite difference/finite element solutions to basic conservation equations. The pump schedule— obtained from the scoping design— was changed in terms of the pad volume and proppant schedule for treatment optimization. The overall goal of such a schedule refinement was to place the right amount of proppant in the right place along the fracture.

Finally, a comprehensive approach to the uncertainty assessment of the complex numerical simulations was performed that is applicable to support decision- and policy-making processes in a well stimulation planning. The approach was comprised of several steps to establish the assessment goals. A surrogate modeling technique together with Monte Carlo simulation was utilized for the uncertainty assessment of a hydraulic fracturing treatment plan, obtained from the optimization task. Factor uncertainties were presented probabilistically, which were characterized by the principle of probability theory, and propagated via Monte Carlo simulation methodology.

In this research, a new approach to hydraulic fracturing design for Bakken horizontal wells was demonstrated. The comprehensive study showed that use of combined deterministic and probabilistic modeling is applicable to well stimulation planning aimed at decision-making processes.

Conclusions

As mentioned at the outset, hydraulic fracturing and horizontal drilling are needed to exploit a low-permeability shale formation as the Bakken. The use of numerical simulation led to answer such questions as: What type of fracturing fluid we should use? What type of proppant we should choose? How can we decide upon the amount of pad, fracturing fluid, proppants, and injection rate, and how can we come up with an optimal pump schedule?

In this research by integrating reservoir and hydraulic fracture simulations, we have concluded that a proper use of hybrid fracture treatments in the Bakken Formation would return optimal well stimulation results. The conductivity and

fracture height growth contour plots, obtained from fully 3D/FEM fracture simulation, showed that a fracturing treatment with injecting slickwater as the pad followed by crosslinked gel together with either ceramic or resin-coated sand would guarantee that most proppants would stay within the Bakken layers. The results from this study would also suggest that in a Bakken well with 10,000-ft lateral length, a fracturing strategy that leads to a high fracture half-length (e.g. 1000 ft) and with high number of fractures (36 or more) would return an efficient balance between the operating charges, fracture treatment costs, drilling expenses, and the benefits earned from the incremental oil production.

On the basis of the numerical simulations conducted in this research, the following conclusions can also be drawn:

- Fully-3D hydraulic fracture simulation can help us to come up with an optimal pump schedule that would not yield height growth into an unwanted zone, being the LodgePole in this case.
- We have used a robust workflow to evaluate all the plausible combinations of fracturing materials (i.e. fluids and proppants) and well/fracture parameters (i.e. lateral length, SRV, fracture spacing, and fracture half-length), to find the best candidates for well stimulation plans.
- We have used a comprehensive approach to uncertainty assessment using sampling-based probabilistic methods for an optimal hydraulic fracture treatment where such uncertainty assessment analysis could be computationally tedious. For this reason, surrogate models were used in the uncertainty assessment. We have also used the concept of response surface method (RSM) to develop such proxy models being used to perform thousands of Monte Carlo

simulations. The goal at this stage was to describe, in detail, the relationship between the uncertain factors and the response (NPV). A full quadratic model was used to both predict the whole sample space and identify the optimal cases. Two types of probability distributions were then developed for the calculated NPVs from the Monte Carlo simulations: *Unconditional* and *Conditional Distributions*. An unconditional distribution graph depicts the distribution of the values of NPVs with all the uncertain parameters sampled from the input probability density functions, and a conditional distribution shows different distributions for the objective function (i.e. *Cum_OIL* or *NPV*) given that a certain parameter is held constant.

- NPV calculations can be influenced by the volatility of the oil market. More realistic estimates were made through the use of the probability theory by considering different scenarios for the price of oil. Two types of probabilities were developed using Monte Carlo simulations: *Conditional Probability Curves* and *Joint Probability Curves*. Finally, the expected values from each scenario were calculated from their corresponding probability distributions. By calculating the expected values using such methodology, investors can observe the level of investment from the different scenario(s), and they can realize which one(s) is (are) more likely to return their desired outcome(s).

Future work

Although the objectives of this research were met, there will be some other aspects of the hydraulic fracturing design for Bakken horizontal wells that should be considered in future research. In designing a successful hydraulic fracturing, it is vitally important to know the in-situ stress field, reservoir properties, natural fracture

parameters, and fundamental geomechanical parameters for selecting the adequate orientation of horizontal wells. Hence, we suggest a comprehensive quantitative analysis of the Bakken petroleum system be conducted in terms of reservoir responses to the available tests and logs that have been conducted in the field. This will help us to conduct more accurate modeling of hydraulic fracturing design in the Bakken Formation.

Regarding the hydraulic fracture simulation, the use of other fracture modeling techniques, such as the displacement discontinuity method (DDM) should also be considered in the optimization workflow, which we used in this research. This would help us to model out-of-plane propagation of fractures that was not considered in our 3D fracture simulations in this study.

With regard to the general approach to the uncertainty assessment, using other uncertainty methods, such as possibility method, Dempster Shafer evidence theory, and interval analysis could be considered given their ability to represent epistemic uncertainties in the reservoir properties. The application of uncertainty assessment and probability theory can be useful in the optimization of hydraulic fracturing design in developing unconventional reservoirs, such as the Bakken Formation.

NOMENCLATURE

CPor_Mtrx	: matrix compressibility, $1/psi$
CPor_NatFrac	: natural fracture compressibility, $1/psi$
DI_NatFrac	: natural fracture density in x-direction (used in DualPOR model), ft
DJ_NatFrac	: natural fracture density in y-direction (used in DualPOR model), ft
DK_NatFrac	: natural fracture density in z-direction (used in DualPOR model), ft
<i>HHP</i>	: hydraulic horsepower, hp
KvKhRatio	: ratio of vertical to horizontal permeability of matrix
k_{rocw}	: k_{ro} at connate water
k_{rwiro}	: k_{rw} at irreducible oil
k_{rogcg}	: k_{rog} at connate gas
k_{rgcl}	: k_{rg} at connate liquid
m_p	: Proppant mass, lb
n	: run number
n_w	: exponent for calculating k_{rw}
n_{ow}	: exponent for calculating k_{row}
n_{og}	: exponent for calculating k_{rog}
n_g	: exponent for calculating k_{rg}
PermMtrxMultiplier	: matrix permeability modifier (used in HM), md
PermNatFrac	: natural fracture permeability, md
PorMtrxMultiplier	: matrix porosity modifier (used in HM)
PorFracMultiplier	: natural fracture porosity modifier (used in HM)
s_p	: pooled estimate of standard deviation of individual responses
S_w	: water saturation
S_{wcrit}	: critical water saturation
S_{oirw}	: irreducible oil for water-oil table
S_{orw}	: residual oil for water-oil table
S_{wcon}	: connate water saturation
S_{orw}	: residual oil for water-oil table
S_l	: liquid saturation
S_{org}	: residual oil for gas-liquid table
S_{gcon}	: connate gas saturation
S_{wtr}	: connate water saturation
t_e	: time at end of pumping, min
t_i	: time of injection, min
t_E	: signal-to-noise t-ratio
t^*	: critical t-ratio
V_i	: volume of injection into one wing, $cu\ ft$

- V_f : volume of fracturing fluid, *cu ft*
 w : hydraulic fracture width, *in*
 X_f : fracture half-length, *ft*
 \bar{Y} : sample average
 μ : mean
 ε : proppant schedule exponent, *dimensionless*
 η_e : fluid efficiency at end of pumping, *dimensionless*

REFERENCES

- Ackermann, N.L. and H.T. Shen. 1979. Rheological characteristics of solid-liquid mixtures. *AICHE 1. () 25*, No. 2, 327-32.
- Adachi, J., E. Siebrits, A. Peirce, and J. Desroche. 2007. Computer simulation of hydraulic fractures. *International Journal of Rock Mechanics & Mining Sciences* 44 (2007) 739–757.
- Advani, S.H., T.S. Lee, and J.K. Lee. 1990. Three dimensional modeling of hydraulic fractures in layered media: Finite element formulations, *J. Energy Res. Tech.*, 112, p. 1-18.
- Agarwal, M.K., B.R. Patterson, and P.E. Clark. 1990. Rheology of metal powder slurries used in powder injection molding, paper presented at the 1990 Annual Meeting of the Soc. of Rheology, Santa Fe, Oct. 21-25.
- Al-Ghazal, M.A. S. Al-Driweesh, and F. Al-Shammari. 2013. First successful application of an environment friendly fracturing fluid during on-the-fly proppant fracturing. 6th International Petroleum Technology Conference, Mar 26 - 28, Beijing, China.
- Alkhatami, M.D. 2007. Investigation of proppant transport in hydraulic fractures. BS Thesis. Petroleum Eng Dept.
- Allaire, D.L. 2009. Uncertainty assessment of complex models with application to aviation environmental systems. PhD dissertation submitted to the Dept. of Aeronautics and Astronautics, Massachusetts Institute of Tech., MA, USA.
- Almond, S.W. 1982. Factors affecting gelling agent residue under low temperature conditions, paper SPE 10658 presented at the 1982 SPE Formation Damage Control Symposium, Lafayette, LA.
- Anderson, H.L. 1986. Metropolis, Monte Carlo and the MANIAC. *Los Alamos Science* 14: 96–108.
- Ang, A. and W. Tang. 2007. Probability concepts in engineering: emphasis on applications to civil and environmental engineering. John Wiley & Sons, Inc., Hoboken, New Jersey, second edition.
- Ardalan, A. 2000. Economic & financial analysis for engineering & project management. Technomic Publishing Company, Inc. Lancaster, Pennsylvania, USA.
- Ayyub, B.M. and G.J. Klir. Uncertainty modeling and analysis in Engineering and the Sciences. Taylor & Francis Group, Boca Raton, Florida, 2006.
- Bahat, D. 1991. Tecton-fractography. Springer-Verlag Publishers.
- Barrenblatt, G.I. 1962. Mathematical theory of equilibrium cracks. *Advances in Applied Mechanics*, 7, 55.
- Barsom, J.M. 1987. Fracture Mechanics Retrospective. American Society for Testing and Materials, Philadelphia.

- Barree, R.D. 1983. A practical numerical simulator for three-dimensional hydraulic fracture propagation in heterogeneous media, SPE Paper 12273, SPE Symp. Reservoir Simulation, San Francisco, Nov. 15-18.
- Barree R. D. and M. W. Conway. 1994. Experimental and numerical modeling of convective proppant transport, SPE 28564 presented at the 1994 SPE Annual Technical Conference and Exhibition, Louisiana, New Orleans, Sept. 25-28.
- Bartosek, M., A. Mennella, and E. Causin. 1994. Polymer gels for conformance treatments: propagation on Cr(III) crosslinking complex in porous media. Paper SPE/DOE 27828 presented at the SPE/DOE ninth symposium on improved oil recover, Tulsa, Oklahoma, USA.
- Besler, M. R; J.W. Steele, T. Egan, and J. Wagner. 2007. Improving Well Productivity and Profitability in the Bakken--A Summary of Our Experiences Drilling, Stimulating, and Operating Horizontal Wells, presented at the SPE Annual Technical Conference and Exhibition, 11-14 November, Anaheim, California, U.S.A.
- Bohrer, M., S. Fried , L. Helms , B. Hicks , B. Juenker, D. McCusker , F. Anderson, J. LeFever, E. Murphy, and S. Nordeng. 2008. North Dakota Bakken Formation Resource Study: North Dakota Department of Mineral Resources, 1 CD.
- Brannon, H., B. Wood, and R. Wheeler. 2005. The quest for improved proppant placement: investigation of the effects of proppant slurry component properties on transport. SPE Annual Technical Conference and Exhibition, 9-12 October, Dallas, Texas.
- BRC report (Bakken Research Consortium). 2008. Hydraulic fracturing and microseismic monitoring project, a report submitted by Headington Oil Co. and XTO Energy Inc. on behalf of the Bakken Research Consortium: Brigham Exploration, Continental Resources, Encore Operating, Hess Corporation, Petro-Hunt LLC, Whiting Petroleum, Schlumberger Oilfield Services, MicroSeismic Inc., TerraScience, DOE National Energy Technology Laboratory, and Lawrence Berkeley National Laboratory.
- Breit, V.S., Stright Jr., D.H., and Dozzon, J.A. 1992. Reservoir Characterization of the Bakken Shale from Modeling of Horizontal Well Production Interference Data. Paper SPE 24320, presented at the SPE Rocky Mountain Meeting, Casper, Wyoming, USA, 18-21 May.
- Brooks, R.H. and A.T. Corey. 1964. Hydraulic properties of porous media. Hydraulic paper No.3, Colorado State University.
- Brooks, R.H. and A.T. Corey. 1966. Properties of porous media affecting fluid flow, J. of the Irrigation and Drainage Division, Proc. Of ASCE, 92, No.1R2, 61-88.
- Cacuci, D. 2003. Sensitivity and Uncertainty Analysis: Volume I, Theory. Chapman & Hall/CRC, Boca Raton, Florida.
- Carter, B.J., J. Desroches, A.R. Ingraffea, and P.A. Wawrzynek. 1998. Simulation of fully 3D hydraulic fracturing. Cornell University, Schlumberger Well Services, TX.
- Chatterji, J., and J.K. Borchardt. 1981. Application of water-soluble polymers in the oil field. JPT2042-56.

- Che, M., Y. Wang, X. Cheng, Y. Lu, Y. Li, F. Zhang, J. Peng, K. Zou, R. Zhu. 2013. Study and application of shallow water fracturing fluid in high temperature deep carbonate reservoir. 6th International Petroleum Technology Conference, Mar 26 - 28, Beijing, China.
- Chhabra, R. P. and J.F. Richardson. 1999. Non-Newtonian flow in the process industry—fundamentals and applications. Butterworth-Heinemann, Oxford.
- Cioppa, T.M. 2002. Efficient nearly orthogonal and space-filling experimental designs for high-dimensional complex models. Naval Postgraduate School PhD Dissertation, Sep.
- Clifton, R.J. and A.S. Abou-Sayed. 1979. On the computation of the three-dimensional geometry of hydraulic fractures. SPE 7943.
- Cleary, M.P. 1994. Critical Issues in Hydraulic Fracturing of High-Permeability Reservoirs, paper SPE 27618 presented at the Aberdeen, United Kingdom, 15-17 March, European Production Operations Conference and Exhibition.
- Cohen, C.E., C. Abad, X. Weng, K. England, A. Phatak, O. Kresse, O. Neuvonen, V. Lafitte, P. Abivin. 2013. Optimum fluid and proppant selection for hydraulic fracturing in shale gas reservoirs: a parametric study based on fracturing-to-production simulations. SPE Hydraulic Fracturing Technology Conference, Feb 04 - 06, The Woodlands, TX, USA.
- Cochran, W.G. and G. Cox. 1992. Experimental designs (2nd ed.). New York: Wiley. ISBN 978-0-471-54567-5.
- Collins, J.A. 1981. Failure of Materials in Mechanical Design. Wiley.
- Conway, M.W. and L.E. Harris. 1982. A laboratory and field evaluation of a technique for hydraulic fracturing stimulation of deep wells. SPE paper 10964.
- Cox, D. R. 2006. Principles of statistical inference. Cambridge New York: Cambridge University Press. ISBN 978-0-521-68567-2.
- Cox, X.A., D.M. Cook, K. Dunek, R. Daniels, C. Jump, and B. Barree. 2008. Unconventional Resource Play Evaluation: A Look at the Bakken Shale Play of North Dakota. Paper SPE 114171 presented at the SPE Unconventional Reservoirs Conference, Keystone, Colorado, USA, February 10-12.
- Dabak, T. and O. Yucel. 1986. Shear viscosity of dense-Phase slurries at varying shear-rates. IntI. Symposium on Slurry Flows, American Soc. of Mechanical Engineers, New York 38, 31-39.
- Daneshy. A.A. 1973. On the design of vertical hydraulic fractures, J. Pet. Tech., pp. 83-97.
- Daneshy. A.A. 1978. Hydraulic fracture propagation in ayered formations. Soc. Pet. Eng., pp. 33-41.
- Deutsch, C. and A. Journel. 1998. GSLIB: Geostatistical software library and user's guide, second edition, Oxford University Press, New York.
- Dodge, D. W., and A. B. Metzner. 1959. Turbulent flow of non-Newtonian systems. AICHE Journal, 5(2), 189-204.

- Dow, W.G. 1974. Application of oil-correlation and source-rock data to exploration in Williston Basin: American Association of Petroleum Geologists Bulletin, Vol. 58, No. 7, p. 1253-1262.
- Druyff, L. 1991. Reservoir properties of the Bakken Shale (abs): in Geology and Horizontal Drilling of the Bakken Formation, Montana Geological Society, p. 91.
- Dubois, D. 2006. Possibility theory and statistical reasoning. Computational Statistics and Data Analysis, 51:47-69.
- Dunek, K.L. and D.W. Walser, and D.K. Astakhov. 2009. Far-field volumetric distribution of fracturing fluids away from an uncemented horizontal liner in the Bakken Formation. SPE Rocky Mountain Petroleum Technology Conference, 14-16 April, Denver, Colorado, USA.
- Economides, M.J. and A. Demarchos. 2008. Benefits of a p-3D over a 2D model for Unified Fracture Design, SPE International Symposium and Exhibition on Formation Damage Control, 13-15 February, Lafayette, Louisiana, USA.
- Economides, M.J., R.E. Oligney, and P. Valko. 2002. Unified Fracture Design. Orsa Press, Alvin, TX.
- Einstein, A. 1956. Investigation of the theory of brownian movement. Dover Publications Inc., New York City.
- Ely, J.W. 1981. Fracturing fluid systems state of the art. Proc., South-western Petroleum Short Course, Lubbock, TX.
- England, A.H. and A.E. Green. 1963. Some two-dimensional punch and crack problems in classical elasticity. Proc. Camb. Phil. Soc., Vol. 59. 59, pp.489-500.
- Everitt, B.S. 2003. The Cambridge Dictionary of Statistics, CUP. ISBN 0-521-81099-X.
- Fang, P., M. R. Manglik, and A. M. Jog. 1997. Characteristics of laminar viscous shearthinning fluid flows in eccentric annular channels. J. of Non-Newt. Fluid Mech, ,84, 1-17.
- Faulkner, D.L., and L.R. Schmidt. 1977. Glass Bead-Filled Polypropylene Part 1: Rheological and Mechanical Properties. Polymer Eng. And Sciences, , 17, No.9, 657-665.
- Fisher, M.K. J.R. Heinze, C.D. Harris, B.M Davidson, C.A. Wright, K.P. Dunn. 2004. Optimizing horizontal completion techniques in the Barnett shale using microseismic fracture mapping, SPE Annual Technical Conference and Exhibition, 26-29 September, Houston, Texas.
- Flannery, J., and J. Kraus. 2006. Integrated analysis of the Bakken petroleum system, U.S. Williston basin: American Association of Petroleum Geologists Search and Discovery Article #10105.
- Frankel, N.A., and A. Acrivos. 1987. On the viscosity of a concentrated suspensions of solid spheres. Chem. Eng. Science, 1987, 22, 847-853.
- Geertsma, J. 1978. Some rock mechanical aspects of oil and gas well completions. Paper EUR-38 presented at SPE European Offshore Petroleum Conference and Exhibition, Dallas, Sept. 21-24.

- Gidley, J.L., S.A. Holditch, D.E. Nierode, and R.W. Jr. Veatch. 1990. Recent advances in hydraulic fracturing. SPE Monograph, Vol. 12, SPE, Richardson, TX, USA.
- Ghassemi, A. 1996. Three dimensional poroelastic hydraulic fracture simulation using the displacement discontinuity method. PhD dissertation, University of Oklahoma, Norman, OK.
- Gomez, S. and A. Patel. 2013. Shale Inhibition: What Works? SPE International Symposium on Oilfield Chemistry, Apr 08 - 10, 2013 2013, The Woodlands, TX, USA.
- Gonzales, V.M. and J. Callard. 2011. Optimizing horizontal stimulation design utilizing reservoir characterization from decline curve analysis, SPE Production and Operations Symposium, 27-29 March, Oklahoma City, Oklahoma, USA.
- Graham, A. L. 1980. On the viscosity of suspensions of solid spheres. Technical Report RRC 62, U. of Wisconsin Rheology Research Center, Madison, June.
- Grattoni, C. 2001. Rheology and permeability of crosslinked polyacrylamide gel. J. of Colloid and Interface Science, 240, 601-6.
- Griffith, A.A. 1921. The phenomena of rupture and flows in solids, Phil. Trans. Royal Soc., 221, 163-167.
- Griffith, A., and Nichols, N., 1996, Accounting for model error in data assimilation using adjoint methods, in Computational Differentiation: Techniques, Applications and Tools, Proceedings.
- Gu, H. and K.H. Leung. 1993. 3D numerical simulation of hydraulic fracture closure with application to mini-fracture analysis, JPT, March, p. 206-211.
- Guo, B., W.C. Lyons, and A. Ghalambor. 2007. Petroleum production engineering, a computer assisted approach. Gulf Prof. Publishing, MA 10803, USA.
- Gupta, D.V. and R.G. Pierce. 1998. A new concept for on-the-fly hydration of water-based fracturing fluids. SPE Gas Technology Symposium, 15-18 March, Calgary, Alberta, Canada.
- Hassen, B. Y. Zotskine, and D. Gulewicz. 2012. Hydraulic fracture containment in the Bakken with a synthetic polymer water based fracture fluid. SPE Canadian Unconventional Resources Conference, 30 October-1 November, Calgary, Alberta, Canada.
- Hannah, R. R., L. J. Harrington, and L. C. Lance. 1983. The real-time Calculation of accurate bottomhole fracturing pressure from surface measurements using measured pressure as a base, SPE 12062 presented at the 1983 SPE Annual Technical Conference and Exhibition, San Francisco, Oct. 5-8.
- Hamming, R.W. 1991. The art of probability for scientists and engineers. Addison-Wesley. p.64 ff. ISBN 0-201-40686-1.
- Harris, P.C. 1985. Influence of temperature and shear history on fracturing fluid efficiency, paper SPE 14258, presented at the 1985 ATCE, Sep.

- Heck, T.J., R.D. LeFever, D.W. Fischer, and J. LeFever, 2002. Overview of the petroleum geology of the North Dakota Williston Basin. North Dakota Geological Survey, Bismarck, ND.
- Herschel, W.H. and R. Bulkley. 1926. Konsistenzmessungen von Gummi-Benzollösungen. *Kolloid Zeitschrift* 39: 291–300.
- Holditch, S.A. 2011. Hydraulic fracturing: Overview, trends, issues, Texas A&M University.
- Honarpour, M., L. Koederitz, and A.H. Harvey. 1986. Relative permeability of petroleum reservoirs. *Boca Raton, Fla. Publishing, C.R.C. Press*, ©1986.
- Howard, G. C., and C. R. Fast. 1970. Hydraulic Fracturing. Monograph Volume 2 of SPE.
- Hutchinson, M., 1989, A stochastic estimator of the trace of the influence matrix for Laplacian smoothing splines. *Communication in Statistics – Simulation and Computation*, v. 19, no. 2, p. 433–450.
- Inglis, C.E. 1913. Stresses in a plate due to the presence of cracks and sharp corners. *Trans. Institute of Naval Architecture*, 55, 219-241.
- Jabbari H. and Z. Zeng. 2011. A Three-Parameter Dual Porosity model for Naturally Fractured Reservoirs. SPE-144560, presented at the Western Regional Meeting held in Anchorage, Alaska (7-11 May).
- Jabbari H., Z. Zeng, and M. Ostadhassan. 2011. Impact of In-Situ Stress Change on Fracture Conductivity in Naturally Fractured Reservoirs. ARMA 11-239, presented at the 45th ARMA held 26-29 June 2011 in San Francisco, CA.
- Jabbari H., Z. Zeng, and M. Ostadhassan. 2011. Incorporating Geomechanics into the Decline-Curve Analysis of Naturally Fractured Reservoirs. SPE-147008, presented at the SPE ATCE 2011, Denver, Co. (Oct.30- Nov.2).
- Jabbari, H., Z. Zeng, S.F. Korom, and M. Khavanin. 2012. Well test analysis in dual-porosity aquifers with stress-dependent conductivity. *Res. J. of Env. and Earth Sci.* 4(11): 962-981, 2012, ISSN: 2041-0492.
- Jeffrey, D. J., and A. Acrivos. 1976. The rheological properties of suspensions of rigid particles. *AIChEJ.*, May, 22, No.3, 417-32.
- Johnson, D. 1997. The triangular distribution as a proxy for the beta distribution in risk analysis. *The Statistician*, 46(3):387–398.
- Jones, F.O. Jr. Influence of chemical composition of water on clay blocking or permeability, JPT 441-46, *Trans. AIME*, 231.
- Kalos, M. and P. Whitlock. 1986. Monte Carlo Methods Volume 1: Basics. John Wiley & Sons, Inc., New York.
- Kim, G.H. and J.Y Wang. 2011. Interpretation of hydraulic fracturing pressure in low-permeability gas formations. SPE 141525, presented at the SPE Production and Operations Symposium, 27-29 March 2011, Oklahoma City, Oklahoma, USA.
- King, M. 1969. Static and dynamic moduli of rocks under pressure, in Somerton, W., and H. Ed. *Rock mechanics-theory and practices*. In proceedings of 11th symposium of rock mechanics. University of Calif., Berkeley, 329-351.

- Khristianovic, S.A. and Y.P. Zheltov. 1955. Formation of vertical fractures by means of highly viscous fluid. Proc. 4th World Petroleum Congress, Rome, Paper 3, p. 579-586.
- Kresse, O., X. Weng, , R. Wu, , H. Gu. 2012. Numerical modeling of hydraulic fractures interaction in complex naturally fractured formations. 46th U.S. Rock Mechanics/Geomechanics Symposium, June 24 - 27, Chicago, Illinois.
- Landel, R. F., B. T. Moser, and A. J. Bauman. 1965. Rheology of concentrated suspensions: Effect of a Surfactant,” Proc., 4th international Congress on Rheology, U.S.A. Part 2, 663-692.
- Landa, J.L. and B. Güyagüler. 2003. A Methodology for History Matching and the Assessment of Uncertainties Associated with Flow Prediction, presented at the SPE Annual Technical Conference and Exhibition, 5-8 October 2003, Denver, Colorado.
- Lantz, T., D. Greene, M. Eberhard, S. Norrid, and R. Pershall. 2007. Refracture Treatments Proving Successful In Horizontal Bakken Wells. Rocky Mountain Oil & Gas Tech. Symp., Denver, Colorado, USA, April 16-18.
- Lawson, J. and J. Erjavec. 2001. Modern statistics for engineering and quality improvements. Duxbury, USA.
- LeDimet, F., Ngodock, H., and Navon I., 1995, Sensitivity analysis in variational data assimilation: Supercomputer Computations Research Institute Technical Report, FSU-SCRI-95T-103, The Florida State University, Tallahassee, Florida
- LeFever, J.A., and L. Helms. 2006. Bakken Formation reserve estimates: North Dakota Geological Survey website, 6 p.
- Lehman, L.V., L. Weijers, M. Mayerhofer, C. Wright, K. Fisher, E. Davis, D. Fulton. 2002. Calibrating fracture models with direct diagnostics: A necessary but humbling experience, SPE Asia Pacific Oil and Gas Conference and Exhibition, 8-10 October, Melbourne, Australia.
- Lipovestky and Conklin. 2001. Analysis of regression in game theory approach. Applied Stochastic Models and Data Analysis 17 (2001): 319-330.
- Lolon, E.P., C.L. Cipolla, L. Weijers, R.E. Hesketh, and M.W. Grigg. 2009. Evaluating horizontal well placement and hydraulic fracture spacing/conductivity in the Bakken Formation, North Dakota. SPE Annual Technical Conference and Exhibition, 4-7 October , New Orleans, Louisiana, USA.
- Lothar, S. 1984. Applied Statistics: A Handbook of Techniques (Springer Series in Statistics). Springer-Verlag, Second Story Books, ABAA Rockville, MD, U.S.A.
- Manno, I. 1999. Introduction to the Monte-Carlo Method. Akademiai Kiado, Budapest.
- Marais, K. S. Lukachko, M. Jun, A. Mahashabde, and I. Waitz. 2008. Assessing the impact of aviation on the climate. Meteorologische Zeitschrift, 17(2):157–172.
- Marie Deza, M. and E. Deza. 2009. Encyclopedia of Distances. Springer, ISBN: 9783642002335.

- Marongiu-Porcu, M., M.J. Economides, and S.A. Holditch. 2008. Economic and physical optimization of hydraulic fracturing, SPE 111793.
- Mayerhofer, M.J. and N.D. Meehan. 1998. Waterfracs – Results from 50 Cotton Valley Wells, paper SPE 49104 presented at the 1998 SPE Annual Technical Conference and Exhibition, New Orleans, 27-30 September.
- Mayerhofer, M.J., E.P. Lolon, J.E. Youngblood, and J.R. Heinze. 2006. Integration of microseismic-fracture-mapping results with numerical fracture network production modeling in the Barnett shale. SPE Annual Technical Conference and Exhibition, 24-27 September 2006, San Antonio, Texas, USA.
- Mayerhofer, M.J., E.P. Lolon, N.R. Warpinski, C.L. Cipolla, D. Walser, and C.M. Rightmire. 2010. What Is Stimulated Reservoir Volume?, *J. of SPE Production & Operations*, Volume 25, Number 1, pp. 89-98.
- Mckay, M.D., R.J. Beckman, and W.J. Conover. 1979. A comparison of three methods for selecting values of input variables in the analysis of output from a computer code, *Technometrics*.
- Meissner, F. F. 1978. Petroleum geology of the Bakken Formation Williston Basin, North Dakota and Montana, in the economic geology of the Williston Basin: The Montana Geological Society 24th Annual Conference, 1978 Williston Basin Symposium, p. 207-227.
- Menjivar, J. 1986. Use of gelation theory to characterize metal crosslinked polymer gels in water soluble polymers; glass, J. E. Ed. American chemical society, Washington DC, pp. 209-26.
- Mian, M.A. 2011. Project economics and decision analysis, Volume 1: Deterministic Models, PennWell Corp., Tulsa, Oklahoma, USA.
- Mian, M.A. 2011. Project economics and decision analysis, Volume 2: Probabilistic Models, PennWell Corp., Tulsa, Oklahoma, USA.
- Montgomery, C.T. and R.E. Steanson. 1985. Proppant selection: The key to successful fracture stimulation. *Journal of Petroleum Technology*, Volume 37, Number 12.
- Montgomery, C.T. and M.B. Smith. 2010. Hydraulic fracturing; history of an enduring technology. *J. of Pet. Tech.*
- Morales, R.H. 1989. Microcomputer analysis of hydraulic fracture behavior with a pseudo-three dimensional simulator, SPEPE, Feb., p. 69-74.
- Morita, N., D.L. Whitfill, and H.A. Wahl. 1988. Stress-intensity factor and fracture cross sectional shape predictions from a three-dimensional model for hydraulically induced fractures, *JPT*, Oct., p. 1329-1342.
- Murray, G. H. 1968. Quantitative fracture study-sanish pool, McKenzie County, North Dakota: American Association of Petroleum Geologists Bulletin, Vol. 52, No. 1, p. 57-65.
- Nicodemo, L., L. Nicolais, and R.F. Landel. 1974. Shear rate dependent viscosity of suspensions in Newtonian and non-Newtonian liquids, *Chem Eng. Sciences*, 29, 729-35.

- Nijenhuis, K. 2001. Crosslink nature in Cr(III)-polyacrylamide gels. *Macromol. Symp.* 171, pp 189-200.
- Nijhuis, M. 2006. How Halliburton Technology is Wrecking the Rockies. *onearth Summer Web.* 12 Jul.
- Nolte, K.G. 1986. Determination of Proppant and Fluid Schedules From Fracturing-Pressure Decline. *SPE Production Engineering*, Vol.1, NO.4 (SPE 13278-PA).
- Nordgren, R.P. 1972. Propagation of a vertical hydraulic fracture. *SPEJ* 306-14; *Trans.*, AIME, 253.
- Perez, N. 2004. *Fracture Mechanics*. Kluwer Academic Publishers. Boston.
- Perkins, T.K. and L.R. Kern. 1961. Widths of hydraulic fractures. *JPT*, 937-49; *Trans.*, AIME, 222.
- Philipp P. Kuhn, R. di Primio, R. Hill, James R. Lawrence, and Brian Horsfield. 2012. Three-dimensional modeling study of the low-permeability petroleum system of the Bakken Formation. *AAPG Bulletin*, Vol. 96, NO. 10.
- Phillips, A.M. and R.W. Anderson. 1985. Use of proppant selection models to optimize fracturing treatment designs in low-permeability reservoirs. *SPE/DOE Low Permeability Gas Reservoirs Symposium*, 19-22 March 1985, Denver, Colorado, USA.
- Phillips, Z.D., R.J. Halverson, S.R. Strauss, J.M. Layman, and T.W. Green. 2007. A case study in the Bakken Formation: changes to hydraulic fracture stimulation treatments result in improved oil production and reduced treatment costs, paper SPE 108045 presented at the 2007 Rocky Mountain Oil and Gas Symposium, Denver, April 16-18.
- Pitakbunkate, T., M. Yang, P.P. Valkó, and M.J. Economides. 2011. Hydraulic fracture optimization with a p-3D model. *SPE Production and Operations Symposium*, 27-29 March, Oklahoma City, Oklahoma, USA.
- Pitman, J.K., L.C. Price, and J.A. LeFever. 2001. Diagenesis and fracture development in the Bakken Formation, Williston Basin: Implications for Reservoir Quality in the Middle Member. *US Geological Survey, professional paper* 1653.
- Pober, K.W. et al. 1983. Water-insoluble residue following acid hydrolysis of water-soluble polysaccharides, *JPT* 2185-91.
- Rahim, Z., H. Al-Anazi, and A. Al-Kanaan. 2013. Selecting optimal fracture fluids, breaker system, and proppant type for successful hydraulic fracturing and enhanced gas production - case studies. 2013 *SPE Middle East Unconventional Gas Conference & Exhibition*, Jan 28 - 30, 2013, Muscat, Sultanate of Oman.
- Rajcopal, V. 2006. Selection of Fracturing Fluid for Stimulating Tight Gas Reservoirs. *MS thesis*, Texas A&M U., College Station, Texas.
- Raysoni, N. and J. Weaver. 2012. Selection of proppants for long-term stability. *SPE Hydraulic Fracturing Technology Conference*, 6-8 February, The Woodlands, Texas, USA.

- Reed, M.G. 1972. Stabilization of formation clays with hydroxyl aluminum solutions, JPT 860-864, Trans. AIME, 253.
- Romero-zeron, L., F. Manalo, and A. Kantzas. 2004. Characterization of crosslinked gel kinetics and gel strength using NMR. SPE 86547, presented at the SPE International Symposium and Exhibition on Formation Damage Control held in Lafayette, LA, USA.
- Ross, S.M. 2007. Introduction to probability models (9th Ed.). Academic Press. p.38 ff. ISBN 0-12-598062-0.
- Roylance, D. 2001. Introduction to Fracture Mechanics. Massachusetts Institute of Technology, Cambridge, MA 02139.
- Sall, J. 1990. Leverage plots for general linear hypotheses. American Statistical Association, Vol.44, NO.4.
- Saltelli, A., S. Tarantola, and F. Campolongo, M. Ratto. 2004. Sensitivity Analysis in Practice: A Guide to Assessing Scientific Models. John Wiley & Sons Inc. USA.
- Satchwell, R.M., M.P. Sharma, and R.L. Miller. 1988. A mathematical model for predicting concentration profiles in liquid-solid fine slurry pipe flows. Energy Resources Tech. () 110, 141-45.
- Schmoker, J. W., and T. C. Hester. 1983. Organic carbon in Bakken Formation, United States Portion of Williston Basin: American Association of Petroleum Geologist Bulletin Vol. 67, No. 12, p. 2165-2174.
- Settari, A. and M.P. Cleary. 1986. Development and testing of a pseudo-three-dimensional model of hydraulic fracture geometry, SPE, Trans. AIME, 281, p.449-466.
- Shah, S.N. 1993. Rheological characterization of hydraulic fracturing slurries. SPE Production & Facilities, Volume 8, Number 2.
- Shah, S.N., Lord, D.L. Tan, H.C. 1992. Recent advances in the fluid mechanics and rheology of fracturing fluids. International Meeting on Petroleum Engineering, 24-27 March 1992, Beijing, China.
- Shanqiang, L., M. Wolff, J. Ciosek, F. Rasdi, L. Neal, P. Arulampalam, and S. Willis. 2011. Probabilistic Reservoir Simulation Workflow for Unconventional Resource Play: Bakken Case Study. Paper SPE 142896 presented at the SPE EUROPEC/EAGE Annual Conference and Exhibition, Vienna, Austria, May 23-26.
- Smith, C.F., J.P. Pavlich, and R.L. Solvinsky. 1964. Potassium, calcium treatments inhibit clay swelling, Oil & Gas J., 80.
- Sneddon, I.N. 1949. The distribution of stress in the neighborhood of a crack in an elastic solid. Proc. Royal Soc. London, Vol.187. Ser. A. pp.229-260.
- Sturm, S.D. and E. Gomez. 2009. Role of natural fracturing in production from the Bakken Formation, Williston Basin, North Dakota, AAPG 50199, Adapted from poster presentation at AAPG Annual Convention and Exhibition, Denver, Colorado, USA, June 7-10

- Terracina, J.M., J.M. Turner, D.H. Collins, and S.E. Spillars. 2010. Proppant selection and its effect on the results of fracturing treatments performed in shale formations. SPE Annual Technical Conference and Exhibition, 19-22 September, Florence, Italy.
- Tiab, D. E.C. Donaldson. 2012. *Petrophysics, Third Edition: Theory and Practice of Measuring Reservoir Rock and Fluid Transport Properties*. Gulf Profess. Publishing, MA, USA.
- Tiner, R. 1976. Polymers and their use in the oilfields. Proc., South-western Petroleum Short Course, Lubbock, TX.
- Thomas, D. G. 1965. Transport characteristics of suspension: VIII: A Note on the viscosity of Newtonian suspension of uniform spherical particles. *J. Colloid Science*, 20, 267-277.
- Tsai, S., D. Botts, and B. Viers. 1989. Effects of liquid viscosity on rheology of concentrated suspensions. *Particulate Sci. & Tech.* 7, 87-95.
- Tschirhart, N.R. 2005. The Evaluation of Waterfrac Technology in Low-Permeability Gas Sands in the East Texas Basin. MS thesis, Texas A&M U., College Station, Texas.
- Van den Poel, Dirk, and Larivière, Bart. 2004. Attrition analysis for financial services using proportional hazard models. *European Journal of Operational Research*, 157 (1), 196-217.
- Van Gijtenbeek, K., A. Neyfeld, and A. Prudnikova. 2006. One molar salt solutions used for clay control in waterbased frac fluids in west Siberia. SPE Russian Oil and Gas Technical Conference and Exhibition, 3-6 October 2006, Moscow, Russia.
- Vassilios, C.K. 2003. Terminal velocity of solid spheres falling in Newtonian and non-Newtonian liquids. *Tech. Chron. Sci. J. TCG*, V, No 1-2.
- Veatch, R.W., Moschovidis, Z.A. and Fast, C.R. 1989. An overview of hydraulic fracturing", in *Recent Advances in Hydraulic Fracturing*; SPE Monograph, 12, pp 2-38.
- Volk, L.J. et al. 1983. A method for evaluation of formation damage due to fracturing fluids, paper SPE 11638.
- Warpinski, N.R., R.A. Schmidt, and D.A. Northrop. 1982. Insitu stresses: the predominant influence on hydraulic fracture containment. *J. of Pet. Tech.*, 653-664, March.
- Warpinski, N.R., Z.A. Moschovidis, C.D. Parker and I.S. Abou-Sayed. 1994. Comparison study of hydraulic fracturing models—Test case: GRI staged filed experiment No. 3, *SPE Production & Facilities*, Feb., p. 7-16.
- Warpinski, N.R., M.J. Mayerhofer, M.C. Vincent, C.L. Cipolla, and E.P. Lonon. 2008. Stimulating unconventional reservoirs: maximizing network growth while optimizing fracture conductivity. *SPE Unconventional Reservoirs Conference*, 10-12 February 2008, Keystone, Colorado, USA.
- Webster, R. L. 1984. Petroleum source rocks and stratigraphy of the Bakken Formation in North Dakota: in J. Woodward, F.

- White, G.L. and D.L. Free. 1976. Properties of various frac fluids as compared to the ideal fluid, Proc., AGA Symposium on Stimulation of low permeability reservoirs, 1-14.
- Wieland, D.R. 1971. Recent trends in hydraulic fracturing. SPE Eastern Regional Meeting, 4-5 November 1971, Charleston, West Virginia, USA.
- Williams, T.M. 1992. Practical use of distributions in network analysis. *J. Opl Res. Soc.*, 43(3):265–270.
- Wiley, C., B. Barree, M. Eberhard, and Tom Lantz. 2004. Improved horizontal well stimulations in the Bakken Formation, Williston Basin, Montana. SPE Annual Technical Conference and Exhibition, 26-29 September 2004, Houston, Texas.
- Woodroof, R.A., Asadi, M., Leonard, R.S., Rainbolt, M. 2003. Monitoring fracturing fluid flowback and optimizing fracturing fluid cleanup in the bossier sand using chemical frac tracers. SPE Annual Technical Conference and Exhibition, 5-8 October, Denver, Colorado, USA.
- Yang, C., L. Nghiem, , C. Card, and M. Bremeier. 2007. Reservoir model uncertainty quantification through computer-assisted history matching: SPE 109825 Annual Technical Conference and Exhibition, Anaheim, California, November 11–14.
- Yang, M. 2011. Hydraulic fracture optimization with a P3D model in multi-layered lithology. MS thesis, Texas A&M University.
- Youness, El. F. 2005. Drag coefficient model for single particle settling in non-Newtonian pseudoplastic fluids. Msc.Thesis, Norman, University of Oklahoma.
- Zadeh, L. 1965. Fuzzy sets. *Information and Control*, 8(3):338–353.
- Zander, D., R. Seale, and D.J. Snyder. 2011. Well completion strategy and optimization in a North Dakota Bakken oilfield. SPE Middle East Unconventional Gas Conference and Exhibition, 31 January-2 February, Muscat, Oman.